IV

Effect of Fire on the Capacity of Reinforced Concrete Columns

L'effet du feu sur la résistance des colonnes en béton armé

Der Einfluss des Feuers auf die Tragfähigkeit von Stahlbetonstützen

R.G. DRYSDALE
Associate Professor
Department of Civil Engineering
and Engineering Mechanics
McMaster University
Hamilton, Ontario, Canada

E.F. VICKERS
Structural Design Engineer
Robertson-Irwin Ltd.
Hamilton, Ontario, Canada

1. INTRODUCTION

Even without considering the effects of fire the behaviour of reinforced concrete columns is complex. The effects of fire are rarely taken into account in design except by satisfying standard requirements for concrete cover over the reinforcing steel. High temperatures change the stress-strain properties of the concrete and steel as functions of the temperature. Therefore areas of cross sections which are close to exposed surfaces are more effected than areas near the centre. Similarly fire causes non-uniform expansion related to the variation of temperature over the cross section.

The effects of fire can be evaluated theoretically provided that sufficient information about the properties of steel and concrete at high temperatures is available. However the previously accepted basis for evaluating strengths of columns based on section capacity and equivalent pinned end lengths may not be accurate or safe. In fires the "softening" of the stiffnesses of exposed columns can allow substantial redistributions of bending moment which will increase their axial load capacity. Conversely the expansion of columns exposed to fire can result in large increases in axial load as a result of the restraining influence of the remainder of the structure.

This study is based on theoretical predictions for strength of individual columns, column sections and columns in frames.

2. THEORETICAL ANALYSIS

2.1 Material Properties

The material properties which directly affect the capacity and behaviour of reinforced concrete sections subjected to fire are discussed below. Unless otherwise specified these properties are based on information from references 1, 5, 6, 7 and 8.

2.1.1 Concrete Stress-Strain Relationships

The concrete stress-strain curve at normal temperatures is shown as the upper curve in Figure 1(a). A continuous equation for this curve has been found[4] based on test data for 27.5 MN/m^2 strength concrete. Concrete is assumed to have no tensile strength.

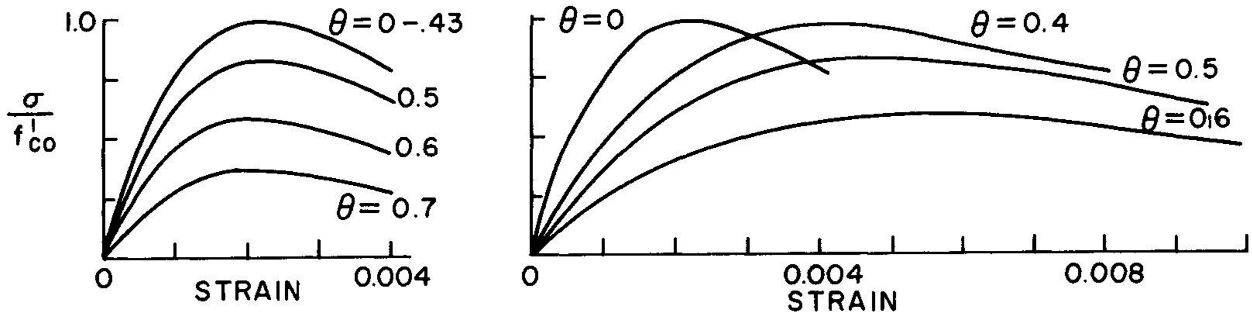

a) NO EXPANSION, ϵ_u CONSTANT b) EXPANSION ALLOWED, ϵ_u VARIES

Fig. 1 Concrete Stress-Strain Relations

If the effects of thermal expansion are neglected it was thought reasonable to maintain the failure strain of concrete at a constant value. Therefore it was decided to change the stress for a given strain in proportion to the change in concrete strength, f'_c, which is a function of temperature. The expression for concrete strength as a ratio of the strength, f'_{co}, at normal temperatures is:

$$f'_c/f'_{co} = 1.0 \quad \text{if } \theta < 0.429 \tag{1}$$

$$\text{and } f'_c/f'_{co} = 2.011 - 2.353\theta \quad \text{if } \theta > 0.429 \tag{2}$$

$$\text{where } \theta = \frac{T-20}{1000}$$

The curves corresponding to different values of θ are shown in Figure 1(a).

A more realistic model for the changes in the stress-strain relationship at high temperatures involves increasing the failure strain of the concrete. The equation for failure strains, ε_{cu}, is:

$$\varepsilon_{cu} = 0.002724 + 0.01276\theta > 0.004 \tag{4}$$

The curves in Figure 1(b) show the effect of proportionally modifying the stresses as concrete strength changes and proportionally increasing strains corresponding to a given stress by multiplying the strain by the ratio of failure strains. When these curves are used the effects of thermal expansion should be included.

Use of both of the constitutive relations shown graphically in Figure 1 yield very similar stress distributions and section capacities. However very different deformations result. These differences will have significant effects on the structural analysis.

Creep of the concrete at high temperatures can have a significant effect for long columns and for columns with large eccentricities of loading. No attempt was made to include the effect of creep in this study. The relations for ε_{cu}, however, do contain some creep since they are based on tests carried out over a short period. The effects of temperature history and load history are neglected in the analysis due to lack of information.

2.1.2 Steel Stress-Strain Relationships

An idealized elastic-plastic stress-strain curve for steel having a yield stress of 412.5 MN/m^2 was used in this study. Figure 2 contains the graphical representation of the reduction in yield stress and modulus of elasticity with increased temperature.

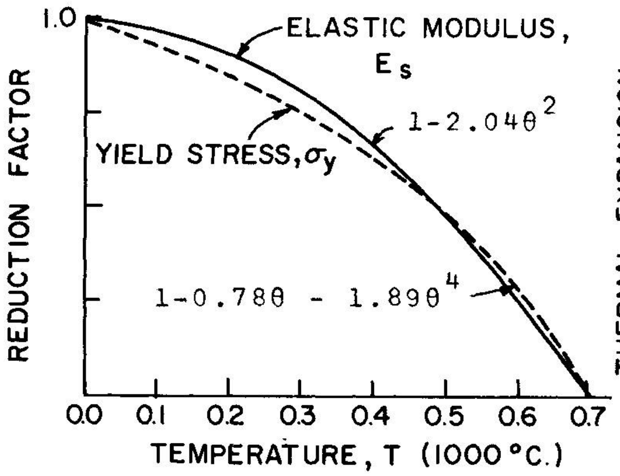

Fig. 2 Effect of Temperature on Steel Stress-Strain Relations

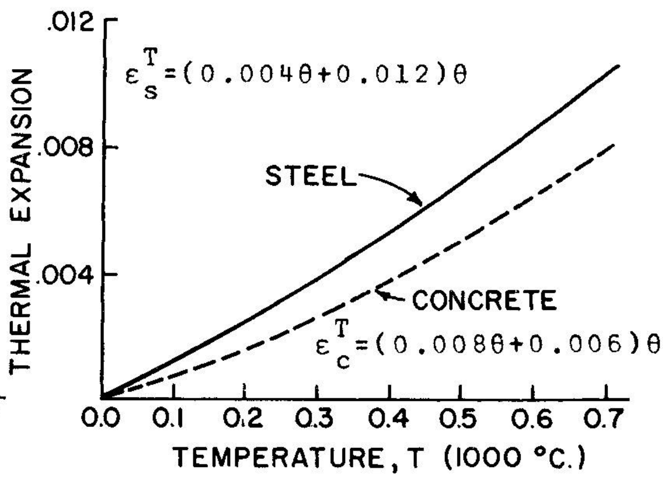

Fig. 3 Thermal Expansion of Concrete and Steel

2.1.3 Thermal Expansion

The coefficients of thermal expansion for concrete and steel are not constant at high temperatures. The curves for thermal expansion are shown in Figure 3.

2.1.4 Temperature Distribution in Cross Sections

The temperature distribution in concrete sections were obtained from T.T. Lie[8] of the National Research Council of Canada. Temperatures at the centres of 2.5 cm square elements of a grid were provided for various sizes of square columns. These columns were assumed to be exposed on all sides to a fire which produces temperatures coinciding with the temperature course for the standard fire test described in ASTM E119-71[3]. The temperature in the reinforcing steel was taken to be the same as that for concrete at the same position in the cross section.

2.2 Analysis of Cross Sections

The temperature at the centre of each 2.5 cm square element of the cross section and each reinforcing bar were calculated for any desired period of exposure to the assumed fire. Then for any plane strain distribution on the section the stress at the centre of each element can be found using the constitutive relations for the concrete and steel. The effect of fire on the resistance of the section can be calculated by transforming the area of each element according to the change in elastic modulus for that element.

By cross section mechanics the forces on each element and the moments of these forces about mid depth are summed to give the total internal forces. These are then compared to the applied forces. Successive corrections are made to the magnitude and slope of the plane strain distribution until the calculated internal forces balance the applied forces to within 1 percent. Failure of the section is defined when the internal forces cannot be increased to balance the applied forces.

2.3 Analysis of Individual Columns

Columns with eccentric load applied at pinned ends are analysed to provide information on the $P\Delta$ effect. The column is divided into a number of sub-member lengths. The axial deformation and curvature for each sub-member are taken as the average of the calculated values of its end sections. Using an iterative sequence the additional bending moments due to column deflection are included in the analysis.

2.4 Analysis of Frames

For the structural analysis of frames exposed to fire, it is convenient to be able to model section properties in a way which is common to normal analytical methods. For a specific set of forces and duration of fire, the relationships between these forces and the resulting deformations on the section can be represented by equivalent stiffnesses EA and EI. The axial stiffness, EA, of the section is the sum of the stiffness of each of the elements where the modulus of elasticity is the secant modulus for stresses which occur on each element when internal forces balance the applied forces. The flexural stiffness, EI, is found by summing the product of the moment of inertia of each element about the centroid of the section multiplied by the corresponding secant modulus of elasticity.

A computer program for elastic stiffness matrix analysis was modified to permit member stiffnesses to be changed as a result of calculation of the effects of high temperatures. Members selected to be exposed to fire are divided into sub-members to improve the accuracy of the calculation of equivalent stiffnesses for different combinations of axial load and bending moment.

Where thermal expansion is included, the forces due to expansion must be applied at the ends of each affected member. These forces are re-calculated after each iterative cycle for calculation of EA and EI values. Application of these forces to the frame at the ends of the expanding members causes the expected increase in length and depending upon the stiffness of the frame can cause significant redistribution of forces. The structural analysis program is said to have converged when the forces and stiffnesses in every sub-member do not change with successive iterations. Failure is defined by cross section failure as described in section 2.2.

3. ANALYTICAL RESULTS

3.1 Cross Section Capacities

A 40 cm square column with 3.5% reinforcement is used to study the influence of fire on failure load. Figure 4 contains values of predicted capacities for different durations of fire. Load is applied at eccentricities of 0.1h, 0.4h and 0.7h for nominal covers over the reinforcement of 1.90 cm, 3.80 cm, and 6.35 cm (corresponding to depths to the centroid of reinforcing bars of 4.75 cm, 6.65 cm and 9.20 cm).

At like eccentricities and like concrete covers the decreases of cross section capacity with increased exposure to fire are similar for other percentages of steel. The capacities approached the same values at the time when the strength of the steel approached zero. Expansion is neglected in the results shown in Figure 4. Inclusion of expansion gave nearly the same results.

3.2 Individual Column Capacities

Results for pinned end columns for the same eccentricities as above are shown in Figure 5 for different slendernesses. Only the results for 3.5% steel and 3.80 cm nominal cover are shown. The differences in capacity for the two times of exposure to fire found by comparing these results with corresponding section capacities in Figure 4 provide a measure of the secondary moment effect.

3.3 Capacities of Columns in Frames

Several frames have been analysed[9] for various combinations of loading and columns exposed to fire. Figure 6 contains a sketch of a building with design levels of gravity load and wind load. Only columns 1 and 2 are exposed to fire. Analytic results are shown both with and without the effect of thermal expansion. Without expansion, the axial loads remain nearly constant and the moments in columns exposed to fire decrease substantially.

Inclusion of expansion causes some modification to the redistribution of moments. However the main effect is change in axial load on the columns. With expansion the capacity of column 2 is exceeded just prior to 3 hours exposure.

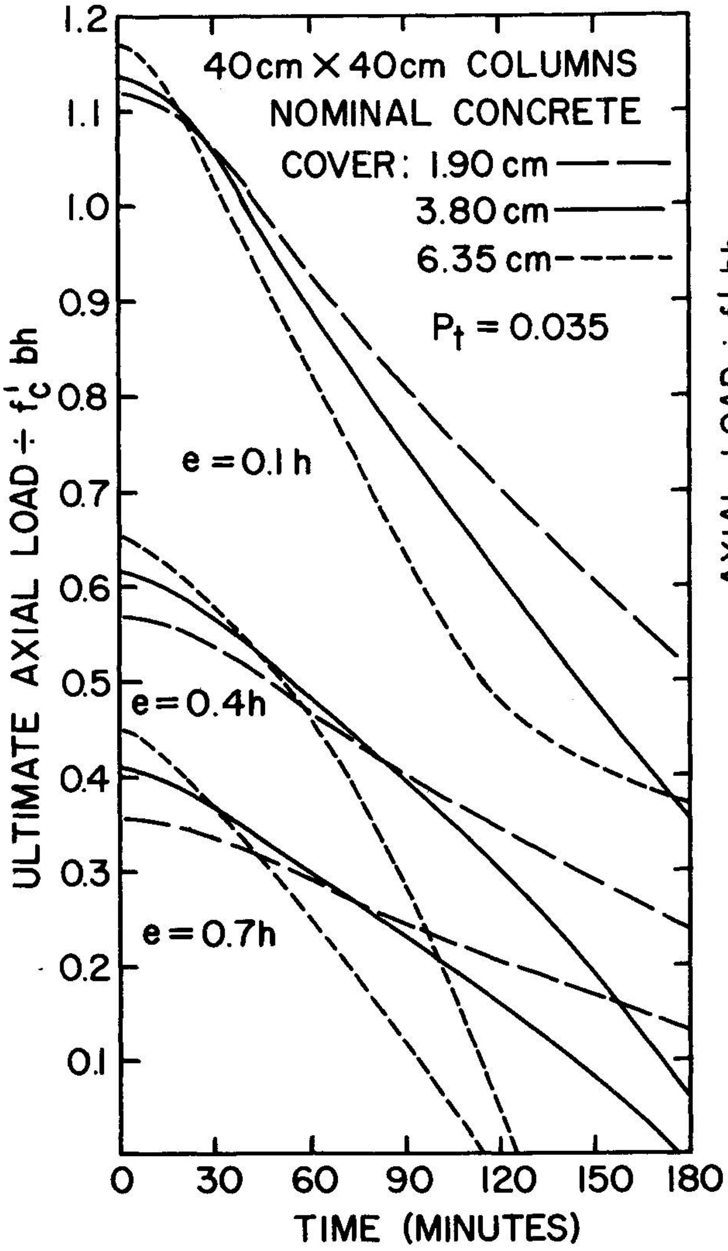

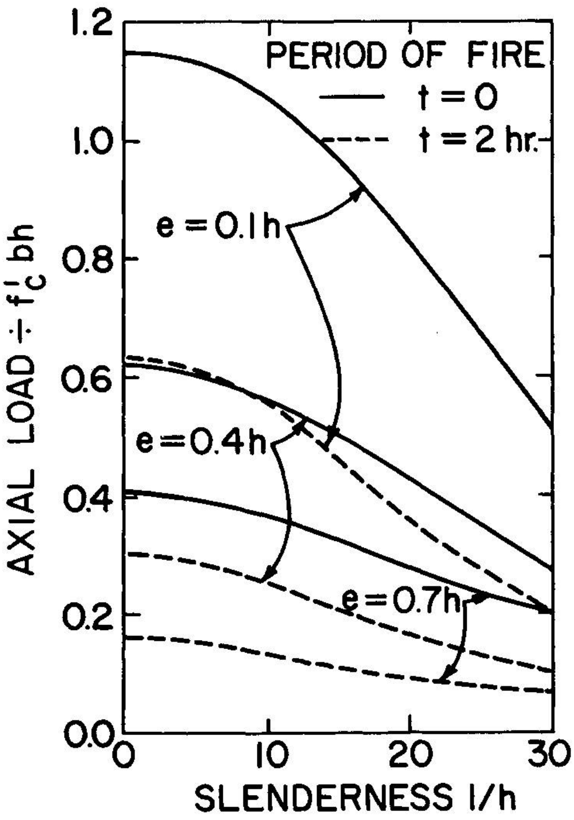

Fig. 5 Effect of Fire on Capacity of Individual Columns

Fig. 4 Effect of Fire on Cross Section Capacity

4. CONCLUSIONS

The capacity of column cross sections is most affected by concrete cover over the reinforcement. Except for small eccentricities, no capacity remains at 3 hours exposure for the standard nominal cover of 3.80 cm. For all cases the 40 cm square section retains less than half of the original capacity after 3 hours exposure.

Analyses of individual long columns show the influence of increased secondary bending resulting from reduced stiffness due to fire. If the forces on a column can be assumed to be unaffected by thermal expansion or by changes in the stiffnesses of members, capacities can be adequately predicted using this type of analysis. It is suggested that the above assumptions are not normally valid.

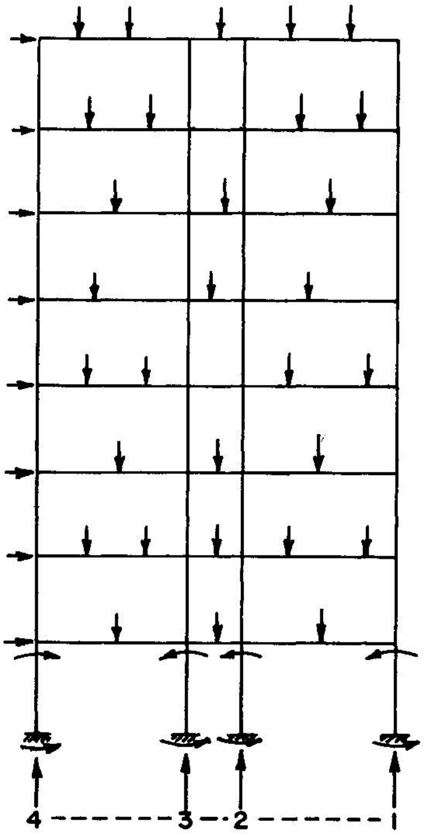

Column Force		Period of Exposure to Fire (hrs)						
			Without Expansion			With Expansion		
		0	1/2	2	3	1	2	3
1	P	25.5	25.5	25.7	26.0	23.8	24.8	
	M_L	4.5	4.3	2.8	1.7	1.6	1.3	
	M_u	4.9	4.7	3.2	2.0	3.1	2.2	
2	P	36.0	35.9	34.5	32.5	51.2	44.4	failure
	M_L	1.3	1.2	0.8	0.5	0.7	0.7	
	M_u	1.3	1.2	0.4	0.2	1.5	0.7	
3	P	34.3	34.4	35.7	37.7	18.5	25.0	
	M_L	4.4	4.5	5.4	6.2	4.4	5.3	
	M_u	4.9	4.9	5.4	5.6	9.0	8.2	
4	P	27.3	27.3	27.0	26.8	29.7	28.8	
	M_L	0.1	0.1	1.0	1.9	1.9	0.4	
	M_u	3.7	3.6	3.1	2.7	3.3	2.8	

P = (*Vertical Reaction* $\div f'_c bh$) x100
M_L = (*Base Moment* $\div f'_c bh^2$) x100
M_u = (*Upper Column Moment* $\div f'_c bh^2$) x100

Fig. 6 Column Forces in a Building Exposed to Fire

The ability of columns in frames to support the structure are dependent on the restraining effect of the structure, the loading combinations and the portion exposed to fire. In many cases moments in exposed columns decrease thereby increasing the axial load capacity. However expansion causes substantial increases in axial load on some exposed columns which increases the likelihood of failure.

It is the authors' opinion that analyses or standard tests(3) of individual columns exposed to fire can only provide an approximate and not necessarily safe estimate of the effect of fire. Design provisions must be based on consideration of the behaviour of columns in structures.

It is important to note that much more research is required to better define the affect of fire on the material properties.

5. NOTATION

The notation used corresponds to that specified in the Introductory Report for this Symposium. Additional symbols are defined where they first appear in the text.

6. REFERENCES

1. Abrams, M.S., "Compressive Strength of Concrete at Temperatures to 1600F", Temperature and Concrete, ACI Publication SP25, 1968, p. 33-58.
2. ACI Committee 318, "Building Code Requirements for Reinforced Concrete", ACI 318-71, American Concrete Institute, 1971.
3. ASTM, "Standard Methods of Fire Tests of Building Construction and Materials", American Society for Testing and Materials, Designation E119-71, 1971.
4. Drysdale, R.G. and Huggins, M.W., "Sustained Biaxial Load on Slender Concrete Columns", Journal of the Structural Division, ASCE, May 1971, p. 1423-1443.
5. Harmathy, T.Z., "Thermal Properties of Concrete at Elevated Temperatures", ASTM Journal of Materials, Vol. 5, No. 1, March 1970, p. 47-74, (NRC 11266).
6. Lie, T.T., "Fire and Buildings", London, Applied Science Pub. Ltd., 1972.
7. Lie, T.T. and Allen, D.E., "Calculation of the Fire Resistance of Reinforced Concrete Columns", National Research Council of Canada, Division of Building Research, NRC 12797, August 1972, p. 44.
8. Lie, T.T. and Harmathy, T.Z., "A Numerical Procedure to Calculate the Temperature of Protected Steel Columns Exposed to Fire", National Research Council of Canada 12535, 1972.
9. Vickers, E.F., "Fire Endurance of Reinforced Concrete Structures", M.Eng. Thesis, McMaster University, Hamilton, Ontario, 1974.

SUMMARY

Numerical analyses have shown that strengths of individual reinforced concrete columns are dramatically reduced when exposed to fire. However the redistribution of forces in frames is shown to partially offset the loss of strength. This evidence and analyses of the effects of thermal expansion raise questions about the validity of present day evaluations of columns exposed to fire.

RESUME

Les résultats d'analyses numériques ont révélé que la résistance de colonnes individuelles en béton armé est de façon critique lorsque celles-ci sont exposées au feu. Cependant la redistribution de forces dans la structure compense partiellement cette perte de résistance. Ce phénomène ainsi que l'analyse d'effets de dilatation thermique conduisent à certaines questions sur la validité du calcul actuel des colonnes exposées au feu.

ZUSAMMENFASSUNG

Numerische Berechnungen haben gezeigt, dass eine kritische Verminderung der Tragfähigkeit von einzelnen bewehrten Betonsäulen stattfindet, sobald diese dem Feuer ausgesetzt werden. Jedoch wird dieser Verlust an Tragfähigkeit bis zu einem gewissen Grade kompensiert durch eine Umlagerung der Kräfte in Rahmentragwerken. Diese Tatsache und Untersuchungen über den Einfluss der Wärmedehnungen stellen die üblichen Vorschriften für Bemessung bewehrter Betonsäulen in Frage.

Tragverhalten brandbeanspruchter Stahlbetonstützen

Fire Resistance of Reinforced Concrete Columns

Comportement des colonnes en béton armé soumises au feu

K. KORDINA W. KLINGSCH
Institut für Baustoffkunde und Stahlbetonbau
TU Braunschweig, BRD

1. Einleitung

In den letzten Jahren ist die Klärung des Tragverhaltens von Bauteilen unter hohen thermischen Belastungen verstärkt in den Mittelpunkt der Forschung gerückt. Nachdem bisher größtenteils durch Brandversuche experimentell gewonnene Ergebnisse zur Verfügung standen, wird heute auf internationalem Gebiet eine intensive Forschung mit dem Ziel betrieben, verallgemeinerungsfähige Aussagen auf der Grundlage mathematisch-physikalischer Gesetzmäßigkeiten zu erarbeiten. In Deutschland ist zu diesem Zweck im Jahre 1972 an der Technischen Universität Braunschweig mit Unterstützung der Deutschen Forschungsgemeinschaft ein Sonderforschungsbereich "Brandverhalten von Bauteilen" (SFB 148) gegründet worden. Die hier vorgetragenen Ergebnisse stellen einen Teil der im Teilprojekt "Stützen" bis jetzt erarbeiteten Ergebnisse dar [1].

2. Temperaturverteilung

Die instationäre, zeit- und ortsabhängige Temperaturverteilung eines homogenen und isotropen Körpers wird durch die Fouriersche Differentialgleichung

$$c \cdot \rho \cdot \frac{\partial \Theta}{\partial t} = \operatorname{div} \lambda \, (\operatorname{grad} \Theta) \qquad (1)$$

beschrieben. Ihre Anwendung auf Stahlbeton stellt jedoch nur eine Näherung dar, da infolge thermo-chemischer Prozesse sich örtliche Wärmequellen und -senken ausbilden und neben der Wärmeleitung eine Feuchtigkeitsdiffusion mit gegenseitiger Beeinflussung abläuft. Für die praktische Berechnung muß die Beziehung (1) daher noch modifiziert werden. Des weiteren werden auch die thermischen Randbedingungen durch eine zeitabhängige Funktion beschrieben, und schließlich sind die Stoffwerte c, ρ, λ keine Konstanten, sondern temperaturabhängige Variable. Die Auswertung der Funktion (1) kann daher i.d.R. nur numerisch erfolgen wobei bestimmte thermische Übergangsbedingungen (Brandraum-Bauteiloberfläche) in Zeit- und Ortsabhängigkeit zu beachten sind [3].
Für die hier vorliegenden Untersuchungen wird ein zeitabhängiger Verlauf der Umgebungstemperatur (Brandraumtemperatur) entsprechend der "Einheitstemperaturkurve" (ETK) nach DIN 4102 angenommen. Weiterhin soll hier nur der Fall einer allseitig erwärmten Recheckstütze mit quarzitischen Zuschlägen behandelt werden.
Bild 1 zeigt den Verlauf der ETK und die Temperaturentwicklung für zwei ausgewählte Querschnittspunkte.

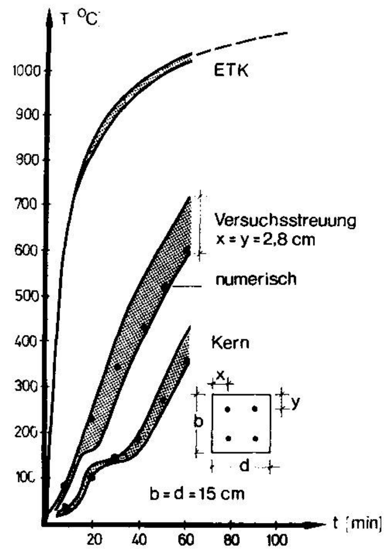

Abbildung 1

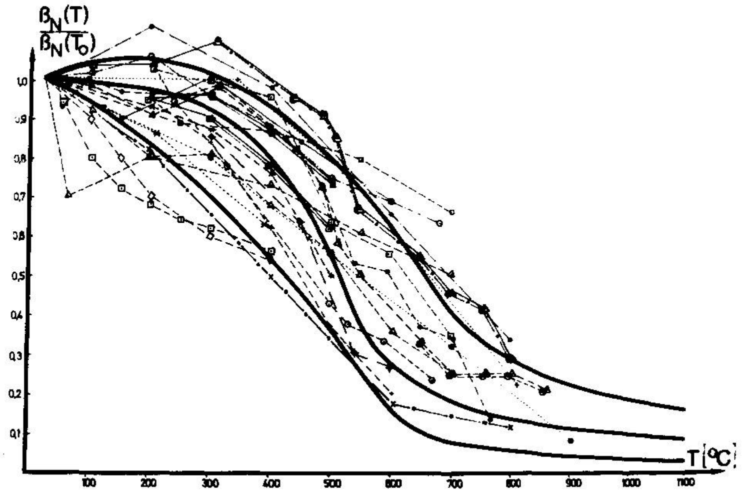

Abbildung 2

3. Temperaturabhängiges Materialverhalten

Die Formulierungen der temperaturabhängigen Spannungs-Dehnungsbeziehungen für Beton und Stahl werden so gewählt, daß sie zum Zeitpunkt t = 0 gegen die entsprechenden Werte der DIN 1045 konvergieren.

Der funktionale Zusammenhang $\sigma = \sigma(\varepsilon)$ muß verschiedenen Randbedingungen genügen, die durch die mechanischen Materialeigenschaften angegeben werden ($ß_N$, ε_u, ε_F usw). Diese Materialdaten zeigen sehr unterschiedliche, i. d. R. nichtlineare Temperaturabhängigkeiten. Es ist daher erforderlich, sämtliche Einzelparameter, die den Verlauf der σ-ε-Beziehung bestimmen, als temperaturabhängige Funktionen zu entwickeln.

Bild 2 zeigt die Temperaturabhängigkeit der Betondruckfestigkeit, bezogen auf den "kalten" Ausgangszustand (t = 0, T = T_0=20°C). Der Schwankungsbereich der Meßwerte hat verschiedene Gründe, auf die hier nicht näher eingegangen werden kann. Die Analyse einer Vielzahl von international vorhandenen Versuchsergebnissen zeigte jedoch, daß durch die Rechenwert-Funktion in guter Näherung jenes Verhalten wiedergegeben werden kann, das für einen baupraktischen Fall von Interesse ist (Aufheizgeschwindigkeit, Erwärmung unter Last, heißer Zustand u. a.).
Für den Verlauf dieser Funktion wurde folgender Ansatz gewählt:

$$ß_N(T) = ß_N(T_0) \begin{Bmatrix} \sum\limits_{n=0}^{4} A_n \cdot T^n \\ B \cdot (T - T_2)^{-1} \end{Bmatrix} \text{ für } \begin{cases} T_0 \le T \le T_1 \\ T > T_1 \end{cases} \qquad (2)$$

Alle anderen Materialdaten wurden in ähnlicher Art entwickelt. Dabei läßt sich für alle mechanischen Materialdaten folgende qualitative Temperaturabhängigkeit feststellen:

1. Festigkeitsabnahme bei zunehmender Temperatur,
2. Zunahme des Plastizierungsvermögens bei zunehmender Temperatur.

Diese so erhaltenen Funktionen treten an die Stelle der konstanten Materialdaten in den Gleichungen der Spannungs-Dehnungs-Beziehungen für Beton bzw. Stahl.

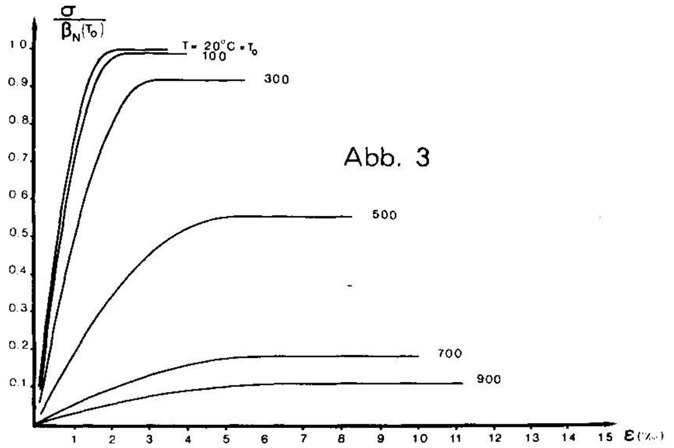

Abb. 3

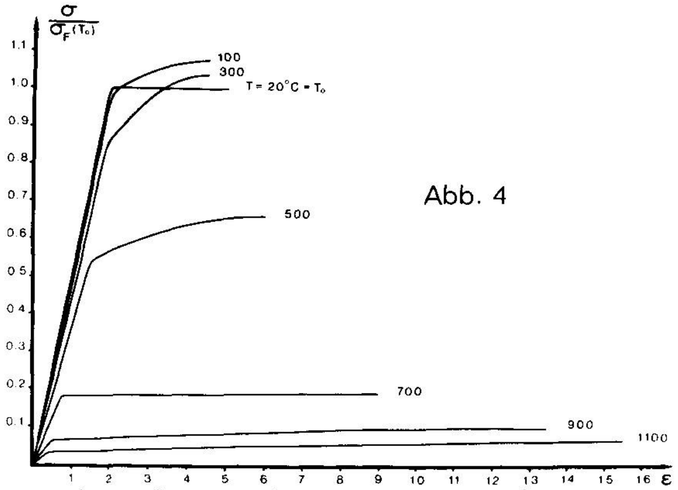

Abb. 4

Die Abbildungen 3 (Beton) und 4 (Stahl) zeigen die Verläufe dieser Funktionen. Es ist zu erkennen, daß die physikalische Nichtlinearität mit steigender Temperatur zunimmt ($\dot{T}$ = 2°C/min). Eine umfassende experimentelle Bestätigung dieser Gesetze steht noch aus. Erste Messungen von Arbeitslinien, die allerdings nicht in allen Punkten den o. g. Versuchsbedingungen entsprechen, scheinen den hier postulierten Verlauf jedoch prinzipiell zu bestätigen [2].

4. Rechenverfahren

Die Anwendung der temperaturabhängigen Spannungs-Dehnungs-Gesetze auf einen instationär thermisch belasteten Querschnitt führt zu der Aufgabe, jeder Isotherme das ihr eigene Materialverhalten zuzuordnen. Damit wird das Problem der Berechnung eines Verbundquerschnitts aus zwei Materialien, Beton und Stahl, erweitert zur Berechnung eines Vielstoffquerschnitts, Beton und Stahl in Zeit- und Ortsabhängigkeit. Dies geschieht am sinnvollsten durch eine Diskretisierung des Querschnitts. Jetzt lassen sich für jedes Element die Temperatur berechnen und die entsprechenden Materialwerte zuordnen. Damit erhält jedes Element ein eigenes Spannungs-Dehnungs-Gesetz, das in Beziehung steht zur vorgewählten Aufheizgeschwindigkeit. Diese zweidimensionale Diskretisierung erlaubt zunächst jedoch nur die Berechnung von Bauteilen, bei denen eine geometrische Nichtlinearität nicht zu berücksichtigen ist. Das Traglastproblem für Stützen bedingt jedoch i.d.R. die Berechnung der Schnittgrößen nach Theorie II. Ordnung, also am verformten System. Diese zusätzliche geometrische Nichtlinearität wird durch eine weitere Diskretisierung in Richtung der Stabachse erreicht.

5. Dehnungs-Spannungs-Zustände im Querschnitt

Die Ermittlung der Dehnungs-Spannungsverteilung eines thermisch belasteten Querschnitts wird wesentlich von der Größe der thermischen Dehnung beeinflußt, die affin zur Temperaturverteilung verläuft. Während bei der "kalten" Stahlbetonberechnung die Dehnungen linear über den Querschnitt verlaufen, sind bei instationärer thermischer Belastung diese spannungserzeugenden Dehnungen selbst nichtlinear (Bild 5). Dieser Sachverhalt muß bei der Ermittlung der zu einer vorgegebenen Lastkombination N, M zugehörigen Grenzdehnungen ε_1, ε_2 beachtet werden. Diese Berechnung geschieht, wie üblich, mit Hilfe des totalen Differentials der beiden Funktionen

$$N = N\ (\varepsilon_1, \varepsilon_2) \qquad (5.1)$$

$$M = M\ (\varepsilon_1, \varepsilon_2) \qquad (5.2)$$

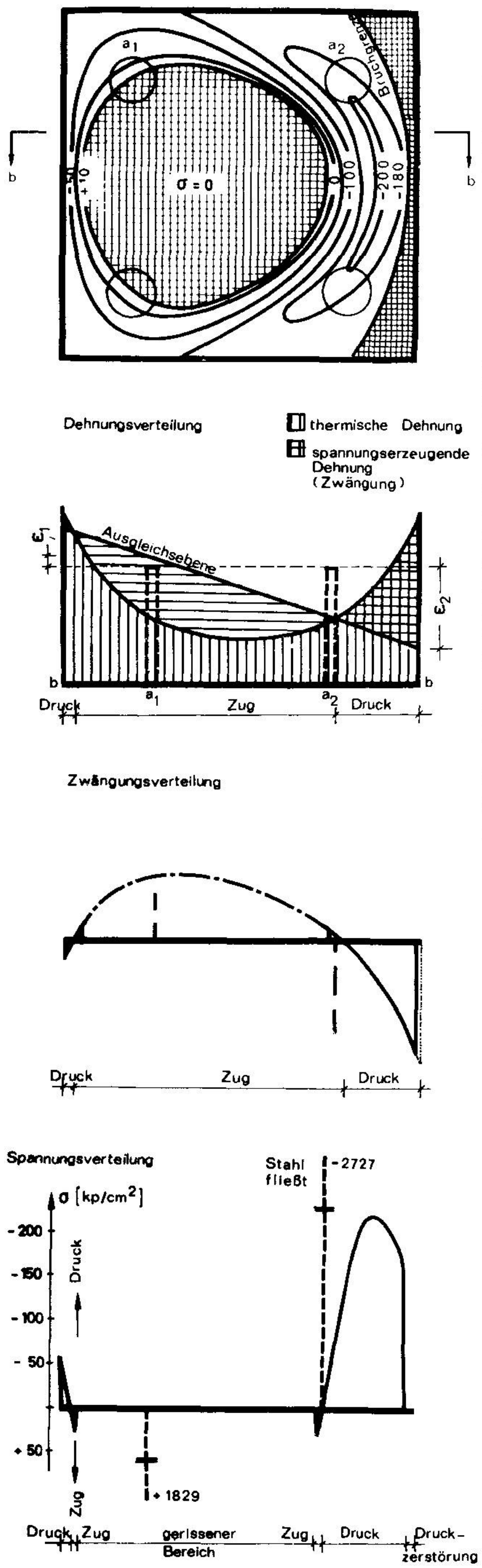

Abbildung 5

Infolge der nichtlinearen Zwängungsverteilung und der zum Rand hin abnehmenden Materialfestigkeit ergeben sich jedoch zwei wesentliche Änderungen. Die normalerweise gültigen Grenztragfähigkeitskriterien

$$\max P_{zentr.} = \sigma(\varepsilon = \varepsilon_{0,2}) \cdot F_{ideell} \qquad (6.1)$$

$$\max M = M(\varepsilon_1 = \delta_5, \varepsilon_2 = \varepsilon_u) \qquad (6.2)$$

lassen sich nur modifiziert auf den "heißen" Traglastfall übertragen. Die Anwendung der Gleichung (6.1) ist a priori wegen der nichtlinearen ε-Verteilung über den Querschnitt ausgeschlossen. Zudem gilt außerdem für jede Isotherme ein anderer $\varepsilon_{0,2}$-Wert. Die zentrische Tragfähigkeit eines Querschnittes kann dadurch nur bestimmt werden, indem man das Maximum der $P(\varepsilon)$-Funktion ermittelt. In Abhängigkeit von der Temperaturverteilung kann sich u. U. $\max P_{zentr}$ erst für einen ε-Wert ergeben, bei dem die kälteren und damit in ihrer Festigkeit weniger reduzierten Kernbereiche aktiviert und die heißen Randbereiche infolge Druckzerstörung (Zermürbung) bereits ausgefallen sind (Bilder 6 bis 8).

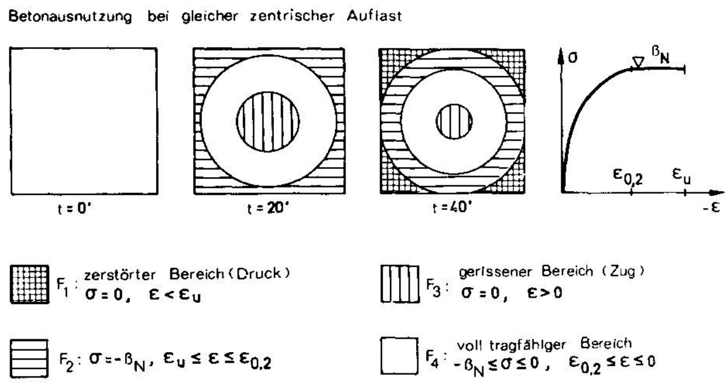

Abbildung 6

Ein ähnlicher Effekt zeigt sich bei der Bestimmung von maxM nach (6.2). Am Betondruckrand kann sich als maßgebender Dehnwert für die Randelemente $\varepsilon_2 > \varepsilon_u$ ergeben.

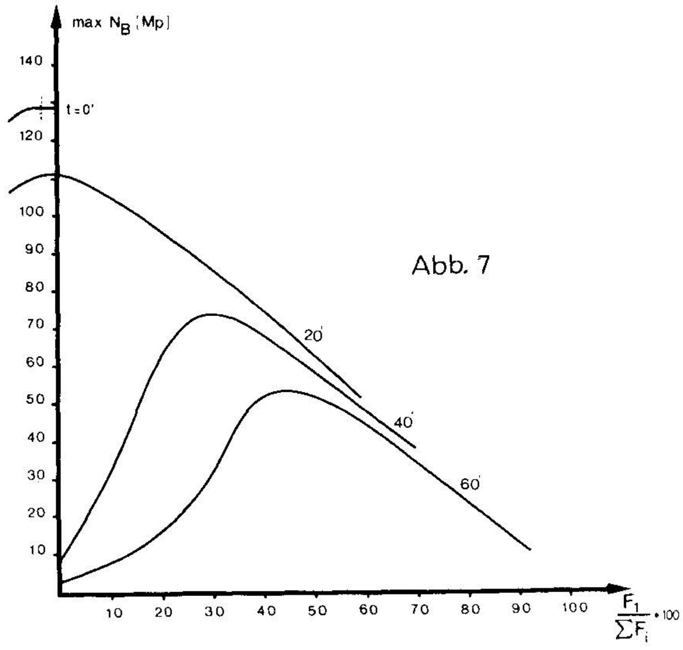

Abb. 7

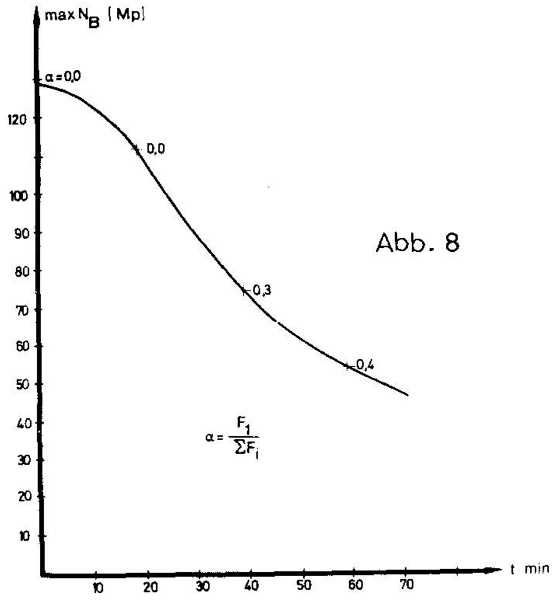

Abb. 8

6. Tragfähigkeit nicht stabilitätsgefährdeter Stahlbetonbauteile

Bei Stahlbetonquerschnitten, die i.d.R. ohne Rücksicht auf Bauteilverformungen berechnet werden (Balken, Rahmenriegel, gedrungene Stützen u. a.) läßt sich deren Grenztragfähigkeit bei Biegedruckbeanspruchung durch das M_u-N_u-Interaktionsdiagramm angeben.

Mit Hilfe der in den Abschnitten 3 und 4 aufgezeigten zweidimensionalen Diskretisierung und Grenztragfähigkeitsbestimmung können jetzt entsprechende Diagramme für thermisch belastete Querschnitte berechnet werden, deren Scharparameter bei konstanten Querschnittswerten die Zeit ist (Bild 9).

7. Tragfähigkeit stabilitätsgefährdeter Stahlbetonbauteile

Stabilitätsgefährdete Bauteile sind dadurch gekennzeichnet, daß ein Versagen vor Eintritt der Grenzschnittgrößen nach Abschnitt 5 eintritt. Infolge der Zusatzverformungen nach Theorie II.Ordnung kann das äußere Moment schneller anwachsen als das innere Moment. Die Folge ist ein Stabilitätsversagen ohne Gleichgewichtsverzweigung. Zur Berechnung solcher Systeme wird, wie unter Punkt 3 beschrieben, eine dreidimensionale Diskretisierung benutzt.

Greifen an einem Stabelement j der Länge Δl_j die beiden Endmomente M_i und M_{i+1} an, so ergibt sich über die zugehörigen Krümmungen mit ausreichender Genauigkeit die Stabauslenkung, d. h. Verformung nach Theorie II. Ordnung zu

$$\Delta w_j = \frac{\Delta l_j}{6}(2\varkappa_i + \varkappa_{i+1}) \qquad (7)$$

Mit einer rekursiven Iteration kann dann bei einem vorgegebenen Anfangswert von M_i das Moment M_{i+1} so bestimmt werden, daß die Kopplungen

$$M_{II} = P \cdot w \qquad (8.1)$$

$$M_i = M_{i+1} + M_{II} \qquad (8.2)$$

erfüllt werden.

Da die Beziehung Moment-Krümmung (M-$\varkappa$) in direkter Form die Steifigkeit repräsentiert, läßt sich aus Bild 10 deren fortschreitender Abbau bei zunehmender Temperaturbeanspruchung erkennen. Unter Beachtung der Gleichungen (7) und (8) wird der zunehmende Einfluß der Verformungsmomente nach Theorie II. Ordnung und damit der zu erwartende Traglastverlust deutlich.

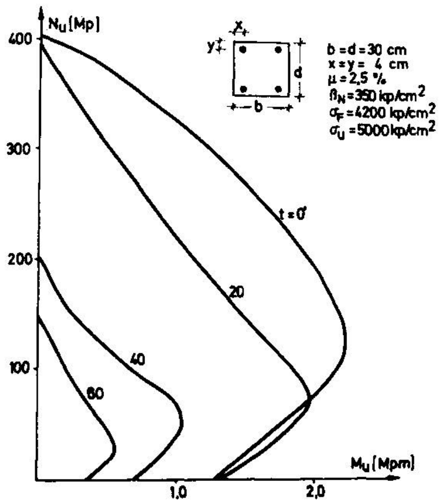

Abbildung 9

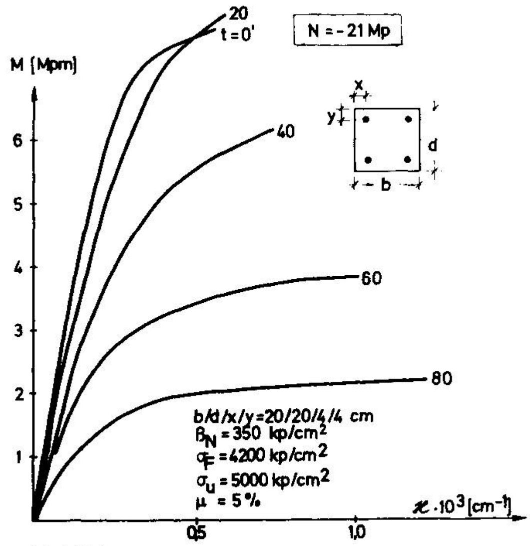

Abbildung 10

Die praktische Bemessung schlanker Stahlbetondruckglieder erfolgt in der BRD nach DIN 1045 i.d.R. mit Hilfe des sogenannten "Ersatzstabverfahrens". Um einen Vergleich zwischen "heißer" und "kalter", also der üblichen Traglast zu ermöglichen, soll den folgenden Betrachtungen auch das statische Modell dieses "Ersatzstabverfahrens" zugrunde gelegt werden (s. Bild 11).

Definiert man als Traglast die Kombination aus N und zugehörigem Maximalmoment $M_u(N) = N \cdot e_u$, so läßt sich der Abbau der Traglast bei konstanter Auflast N durch die Verkleinerung der maximal aufnehmbaren Exzentrizität e_u darstellen. Abb. 11 zeigt diesen so definierten Abbau der Traglast für einen Querschnittstyp bei verschiedenen Bewehrungsprozentsätzen und Stablängen. Der Zeitpunkt, zu dem kein planmäßiges Moment mehr aufnehmbar ist, wird erreicht mit $e_u \leq \bar{e}_o$, wobei hier $\bar{e}_o$ die sicherheitstheoretisch bedingte "ungewollte" Ausmitte darstellt ($\bar{e}_o \cong s_k/300$).

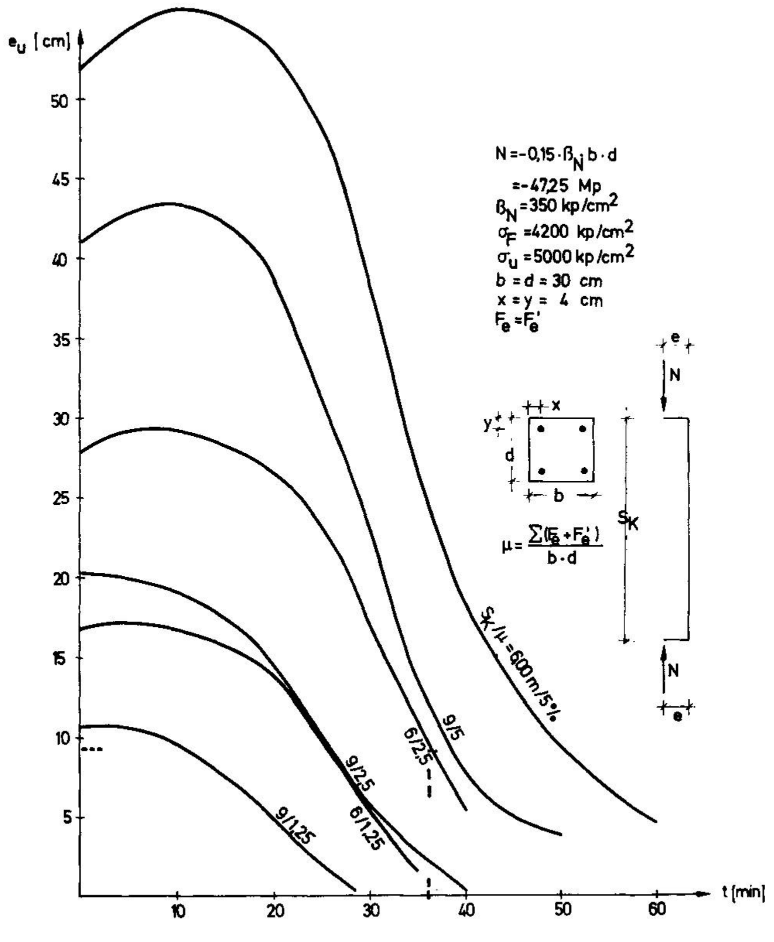

Abbildung 11

8. Längsdehnungsbehinderte Stützen

Die Dehnung einer thermisch belasteten Stahlbetonstütze wird in vielen Fällen durch Unterzüge, Wandscheiben oder andere Stützen mehr oder weniger stark behindert. Eine Beurteilung des Versagenszeitpunktes ist ohne Kenntnis der daraus resultierenden Zwängungskräfte nicht möglich.

Neuere experimentelle Untersuchungen über das Verformungsverhalten von belastetem Beton bei instationärer Temperaturbeanspruchung zeigen eine der aktuellen Festigkeitsausnutzung überproportionale Zunahme der Stauchungen . Diese Verformungen sind wesentlich größer als die den Lastspannungen zugeordneten Dehnwerte $\varepsilon_p = \varepsilon(\sigma)$. Die Gesamtstauchungen einer unter Last stehenden Betonprobe gegenüber einer unbelasteten Probe setzt sich additiv aus folgenden Einzeldehnungen zusammen:

$$\Delta\varepsilon = \varepsilon_p + \varepsilon_z + \varepsilon_\varphi \qquad (9)$$

Der Anteil ε_φ stellt einen reinen viskoelastischen, temperatur- und spannungsabhängigen Kriechanteil dar, der jedoch i.d.R. vernachlässigt werden kann. Der verbleibende Anteil ε_z resultiert aus einer fortschreitenden Gefügezerstörung infolge innerer Mikrorißbildung. Bild 12 zeigt das temperaturabhängige Verhalten dieser Einzelverformungen. Überträgt man diesen Sachverhalt auf einen Stützenquerschnitt, so gilt es, jedem Punkt das ihm eigene funktional gekoppelte Wertetripel

$$\left\{ \sigma, T, \varepsilon_z \right\}$$

zuzuordnen und gleichzeitig gewisse physikalische Randbedingungen des Gesamtquerschnitts zu erfüllen. Bild 13 zeigt die so ermittelte zeitliche Entwicklung der Zwängungskräfte für einen Querschnittstyp bei vollständiger Längsdehnungsbehinderung.

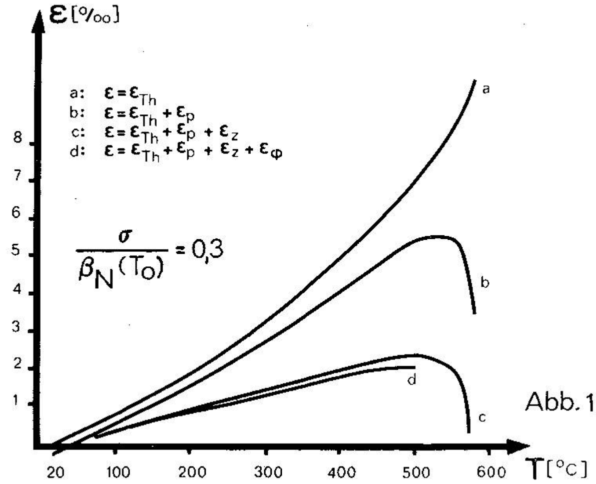

Abb. 12

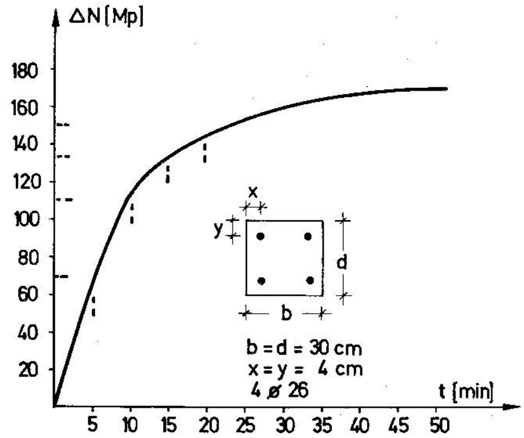

Abbildung 13

9. Beispiel

Es soll die Sicherheit einer Stahlbetonstütze im Brandlastfall mit folgenden geometrischen Daten untersucht werden: b = d = 30 cm, x = y = 4,0 cm, s_K = 6,00 m. Die Werkstoffe werden entsprechend DIN 1045 gewählt: Bn 350, BSt 42/50. Die Stütze sei, einer Beanspruchung im Gebrauchszustand von N_O = - 47,25 Mp und M_O = 4,55 Mpm (e_O = 4,55/47,25 = 9,63 cm) entsprechend, mit Fe+Fe' = 4.5,6 cm2 (2,5 %) bewehrt. Die Traglast dieser Stütze im "kalten" Zustand errechnet sich zu

$$M_u = 17{,}0 \text{ Mpm und } e_u = 28{,}0 \text{ cm.}$$

Für eine thermische Belastung entsprechend der ETK (Abb. 1) soll der Zeitpunkt ermittelt werden, zu dem die Stütze unter Gebrauchslast versagt. Unterliegt die Stütze keiner Längsdehnungsbehinderung, so kann der Traglastabbau Bild 11 entnommen werden. Der Versagenszeitpunkt ergibt sich zu $_{krit}$ t = 36 Minuten. Bei vollständiger Längsdehnungsbehinderung werden Zwängungskräfte geweckt, deren Verlauf Bild 13 wiedergibt. Der Einfluß auf die Traglast kann nur erfaßt werden, indem e_u-Verläufe entsprechend Bild 11 für diskrete Zeitpunkte t mit der Gesamtlast P(t) = N+ ΔP(t) berechnet werden (Bild 14). Es zeigt sich, daß infolge der starken Normalkraftzunahme die gleichzeitig mögliche Momentenbelastung stark zurückgeht und ein Versagen bereits nach $_{krit}$ t = 14 Minuten eintritt.

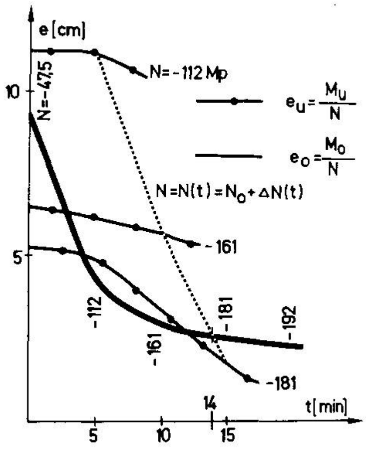

Abbildung 14

Literatur:

[1] Klingsch, W.: "Traglastberechnung thermisch beanspruchter Stahlbetondruckglieder mit zwei- und dreidimensionaler Diskretisierung"
- Dissertation, TU Braunschweig, 1974 -

[2] Schneider, U.: "Zur Kinetik festigkeitsmindernder Reaktionen in Normalbetonen bei hohen Temperaturen"
- Dissertation, TU Braunschweig, 1973 -

[3] Ehm, H.: "Ein Beitrag zur rechnerischen Bemessung von brandbeanspruchten balkenartigen Stahlbetonbauteilen"
- Dissertation, TU Braunschweig, 1967 -

ZUSAMMENFASSUNG

Eine zwei- und dreidimensionale Diskretisierungsmethode zur Traglastberechnung von brandbeanspruchten Stahlbetonstützen unter Beachtung eines wirklichkeitsnahen Festigkeits- und Verformungsverhaltens wird erläutert. Es werden sowohl physikalische als auch geometrische Nichtlinearitäten berücksichtigt. Es wird gezeigt, dass ein Bauteilversagen bereits unter Gebrauchslasten zu erwarten ist und dass bei Längsdehnungsbehinderung dieser Versagenszeitpunkt sehr früh eintreten kann.

SUMMARY

A 2- and 3-dimensional discretization process is discussed for the ultimate-load calculation of reinforced concrete columns under fire conditions, considering the stiffness and deformation behavior close to reality. Not only the physical but also the geometric non-linearities are taken into consideration. It is shown that failure of a structural element may be expected under service loading, and that the instant of failure can be very early if the longitudinal expansion is restrained.

RESUME

On indique une méthode de discrétisation bi- et tridimensionnelle pour le calcul de la charge ultime des colonnes en béton armé soumises au feu, en tenant compte d'un comportement tension - déformation proche de la réalité. On tient compte des comportements non-linéaires aussi bien physiques que géométriques. On démontre que la ruine d'un élément soumis à sa charge utile peut se produire, et qu'en cas d'empêchement de déformation longitudinale, cette ruine peut intervenir très tôt.

Leere Seite
Blank page
Page vide

IV

Fire Resistance of Reinforced Concrete Columns

Résistance au feu des colonnes en béton armé

Feuerwiderstand von Stahlbetonstützen

T.T. LIE D.E. ALLEN
Division of Building Research
National Research Council of Canada
Ottawa, Canada

In the past, the fire resistance of structural members could only be determined by subjecting them to standard fire tests. Now it is possible to determine the fire resistance of various structural members by calculation.

A numerical procedure has been developed (1) to calculate the fire resistance of square reinforced concrete columns and has been checked with the results of actual fire tests. The procedure has been used to calculate fire resistance under both standard ASTM test conditions (1) and under conditions that more closely resemble those encountered in practice (2).

Under standard test conditions, the fire resistance, expressed in time to failure, is calculated as a function of type of aggregate, column size, cover thickness to steel, amount of steel, eccentricity of loading, design safety factor and equivalent buckling length.

The standard ASTM test conditions (3) assume that the column is free to expand, whereas in fact a column is often restrained by the surrounding structure and thereby attracts more load than assumed. To examine the influence of restraint on the behaviour of the columns, calculations of fire resistance have been made for columns under various degrees of axial restraint.

Another condition in which test and practice differ is the temperature course of the fire to which the column is exposed (in practice fire severities can vary over a wide range). To study this, fire-resistance calculations have been made for columns exposed to heating according to various temperature curves that are characteristic of those of actual fires.

Material Properties

The temperature rise in a column is determined for the heat flow equations as a function of two properties of the concrete, thermal conductivity and thermal capacity. These properties are strongly dependent on the type of aggregate. Quartz aggregate, which has the highest thermal diffusivity of all concretes, was selected for determining these properties for normal weight; crystalline expanded shale aggregate was chosen for lightweight concrete. Values of the properties are given in reference (4).

The most important mechanical properties that determine the strength of reinforced concrete are the compressive strength and modulus of elasticity of the concrete, and the yield strength and modulus of elasticity of the steel reinforcing. Approximate analytical relations, which give these properties as a function of temperature, have been derived for normal weight concrete, lightweight concrete and steel using existing data (5-7). The relationships are shown in Figure 1.

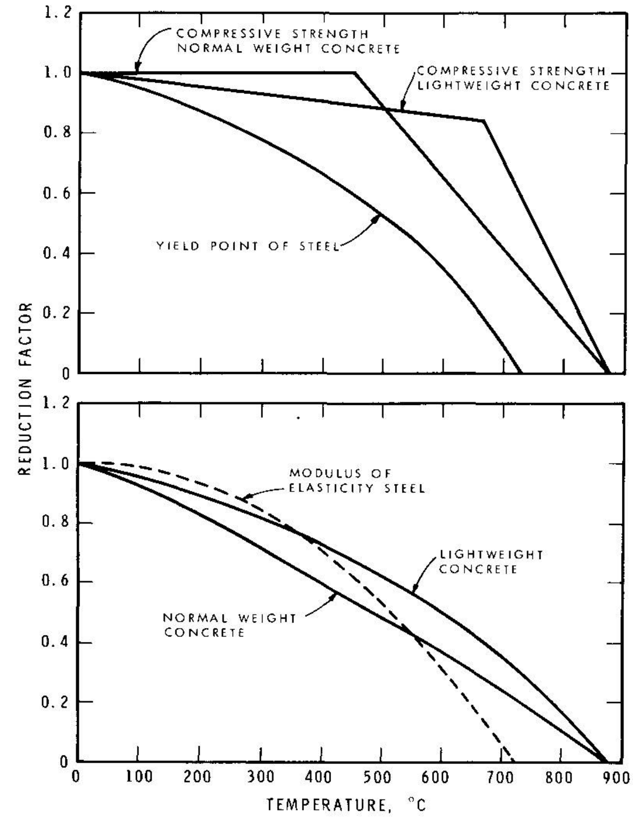

Figure 1: Effect of Temperature on Material Properties

In those parts of the studies that included a period of decaying fire temperature, the following assumptions were made regarding the change of material properties as they cool down. For concrete it was assumed that the material properties are unchanged during cooling and are equal to those corresponding to the maximum temperature reached. For steel it was assumed that the same relationships hold for cooling as well as for heating.

Deformations of concrete and steel due to temperature change were assumed (2) based on existing information. Quartz aggregate concrete was chosen because other aggregates, especially lightweight aggregates, expand less with increasing temperature.

Calculation of Fire Resistance

Column temperatures are calculated by a numerical method (8). The method assumes radiative heat transfer from the fire to the surface of the column. In the column the heat transfer proceeds by conduction. The temperature dependence of the thermal properties of the material are taken into account in the calculation.

During a fire, large temperature gradients, hence large stress gradients, occur in the column cross-section. Figure 2, based on an analysis of the stresses and strains occurring in the column during fire (2), shows how stress distribution changes in a column section during a fire. Early in a fire, very high stresses occur near the outside of the section and cracks appear in the inner area, which is under tensile strain. As the fire progresses, the outer concrete loses its strength, the temperature gradients become less steep, and the extent of cracking in the inner area is reduced. As failure is approached, the cracks in the central area disappear as the reduced effective cross-section becomes stressed to capacity throughout. This demonstrates that fire resistance can be calculated on the basis of ultimate capacity of the cross-section, which assumes full stress redistribution at failure.

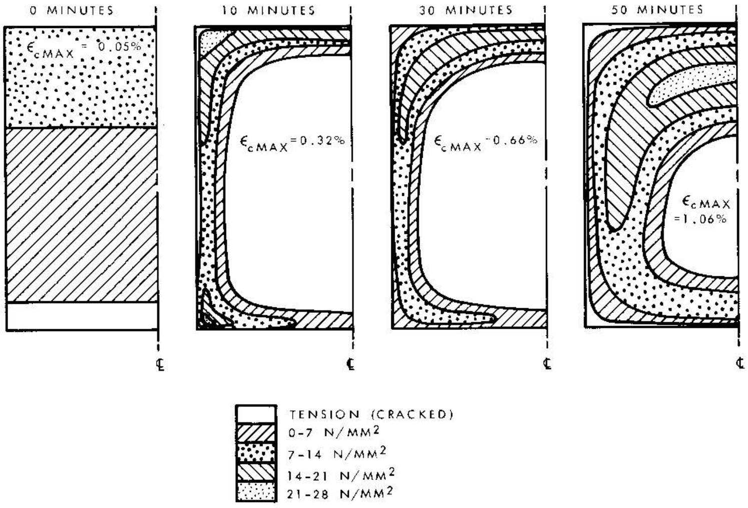

Figure 2: Stress Distribution in Concrete Section During Fire (20 cm Square, 4.9% Steel, 1.25 cm Cover, Calculated Fire Resistance 54 min.)

The strength of reinforced concrete columns at elevated temperatures has been determined by the same method as the ACI method (9) for room temperature, by replacing the relevant material properties by their temperature-dependent values given in Figure 1. To do this the cross-section was divided into small elements, the properties for each element determined for the corresponding temperature, and the effects integrated over the section. Figure 3, a typical interaction diagram of axial and bending strength, shows how fire reduces the section strength with time.

In the case of long columns, the resistance also depends on the buckling load, which is a function of the stiffness. The stiffness is likewise determined by integrating the temperature-dependent stiffness of elements. The stiffness of the concrete, however, is reduced due to cracking and this is approximated by means of a reduction factor. Figure 3 shows how buckling effects during fire reduce the strength of an intermediate column and that of a short column.

In Table I the calculation method is compared to actual test results of axially loaded quartz aggregate columns (10); these tests were carried out under well defined heating and loading conditions. It is seen that the calculation procedure gives a consistent, although somewhat conservative, estimate of the fire resistances of reinforced concrete columns under known load conditions over a considerable range of slenderness ratios. The differences, which are in the order of 10 to 20 per cent, are probably mainly due to conservativeness in the material properties used and in the calculation assumptions.

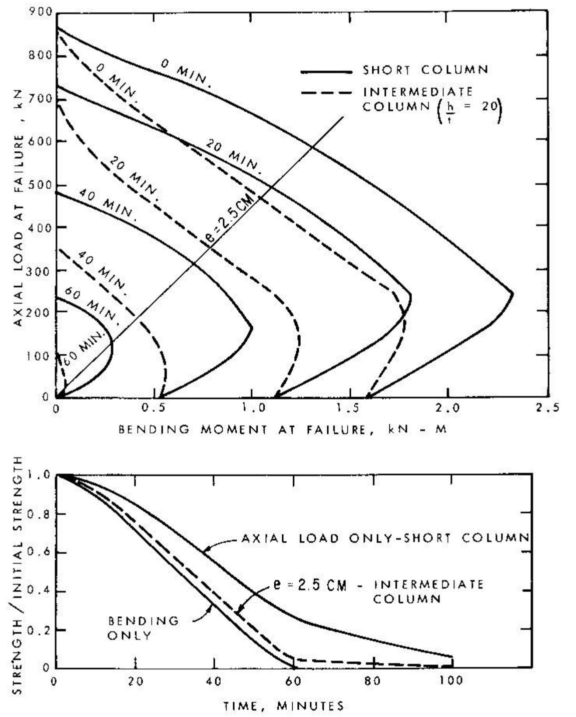

Figure 3: Effect of Fire on Column Strength (15 cm x 15 cm, Normal Weight Concrete 3.5% Reinforcing, 1.25 cm Cover)

<u>Standard Fire Resistance of Square Columns</u>

Figure 4 shows the calculated fire resistance of square columns under ASTM fire test conditions (3) for a standard

TABLE I - COMPARISON OF CALCULATED FIRE RESISTANCES WITH TEST RESULTS

Specimen	Compressive strength of concrete, N/mm^2	Test load, kN	Time to failure, minutes		Ratio time to failure,
			Test	Calculated	Test/Calc.
(i) 15 cm x 15 cm - 4 corner bars 2 cm dia., cover 1.2 cm					
2	38	273	64	57	1.12
3	31	273	69	55	1.25
4	31	273	63	55	1.15
5	31	273	66	55	1.20
(ii) 20 cm x 20 cm - 4 corner bars 2 cm dia., cover 2.9 cm					
3	32	464	107	89	1.20
4	32	464	105	89	1.18
5	43	598	107	88	1.22
6	43	598	107	88	1.22
(iii) 30 cm x 30 cm - 4 corner bars 2.1 cm dia., 4 mid-face bars 2.2 cm dia., cover 3 cm					
11	46	1708	165	147	1.12

case described as follows. The column, designed according to ACI 318-63 (adopted for the National Building Code of Canada), was pin-ended, 3 m long, and subjected to full design dead load plus live load. It was also subjected to the minimum eccentricity specified in ACI-318 (0.1 of the size of the column or 2.5 cm, whichever is the greater); this corresponds to a typical interior lower storey column.

The main parameters affecting fire resistance are column size, cover and type of aggregate. Figure 4 shows that an increase of cover increases the fire resistance, as expected, owing to thermal protection. This increase, however, levels off when the cover reaches 1/4 of column size (t). It is followed by a decrease, caused by a decrease in the moment-resisting lever arm due to a weakening of the outer layers of concrete. For large, lightly reinforced sections and small cover, the influence of the cover is negligible because the concrete carries the entire load at failure.

Other factors that affect the fire resistance of a column are the length of the column, eccentricity (or moment) and the safety factor. Studies (1) showed that an increase of safety factor or a live load less than the full design live load, may significantly increase the fire resistance. The results also show that an increase in eccentricity decreases the fire resistance, especially when the percentage of steel is small (1 to 2%). The decrease, however, is generally not of practical importance because eccentricity in a column under fire will be

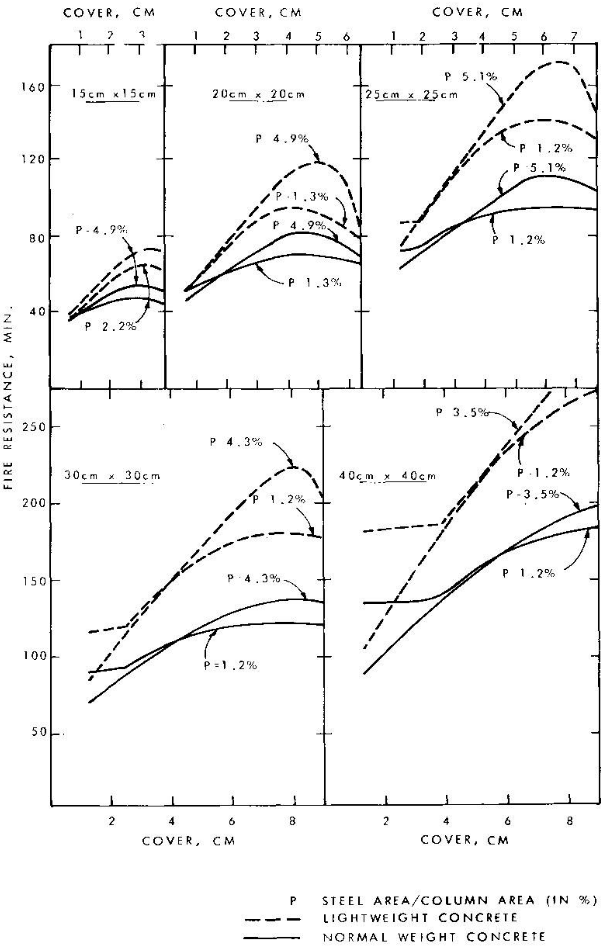

Figure 4: Fire Resistance of Reinforced Concrete Columns as a Function of Cover Thickness to Steel for Various Column and Steel Sizes (Column Length: 3 m; Min Eccentricity: 2.5 cm or 0.1t; Full Live Load)

greatly reduced from the design eccentricity assumed for calculation (1). It was also found that the fire resistance decreases with increase of slenderness ratio; this generally affects only tall slender columns with a small percentage of steel.

The results given in Figure 4 and in Reference 1 for square columns can be expressed in the following simple design rules for minimum column size (t_{min}, cm) and cover* (C_{min}, cm) in terms of required fire resistance (R, hr):

$$
\begin{aligned}
t_{min} &= 10f(R + 1) && \text{for normal weight concrete} \\
t_{min} &= 7.5f(R + 1) && \text{for lightweight concrete} \\
C_{min} &= 2.5\,R && \text{for } R \leq 2 \text{ hr} \\
C_{min} &= 1.25\,R + 2.5 && \text{for } R > 2 \text{ hr}
\end{aligned}
\qquad (1)
$$

where f, a factor that takes into account over-design, equivalent buckling length (kh) and percentage of steel (p), is given as follows:

Over-design factor	Values of f		
	kh $\leq$ 3 m	kh = 6 m	
		t $\leq$ 30 cm p < 3%	All other cases
1.00	1.0	1.2	1.0
1.25	0.9	1.1	0.9
1.50	0.8	1.0	0.8

* Wire mesh in cover is recommended if cover is greater than 3.75 cm

These results indicate lower ratings on dimensions for normal weight concretes than existing ratings cited in the National Building Code of Canada, and about the same for lightweight concretes. The lower ratings are attributed to a decrease in design safety factor (existing ratings were based on tests carried out in 1920 - 1921), a consideration of minimum eccentricity that occurs in practice, and a more accurate simulation of the heat transfer conditions in a fire.

Interaction With Building Structure

Determination of fire resistance, whether by standard fire test or by the above calculations, is based on the assumption of a pin-ended column with no interaction with the surrounding building structure. Actually, a column expands during fire and, because of the resistance of the surrounding structure to this expansion, more than the assumed dead load plus live load is attracted to the column. It therefore appears, for the single column exposed to fire, that the standard procedure errs on the unsafe side.

Figure 5 shows the results of an interaction study of a column with a typical reinforced concrete building structure. The curves in the top graph show how the applied load, including the effect of interaction, compares with the calculated column strength. The different curves labelled "n slabs" refer to the number of floor slabs above the column that resist expansion of the column; "0 slab" corresponds to no interaction. Curves in the bottom graph show the corresponding column lengthening and lateral deflection of the column at mid-height.

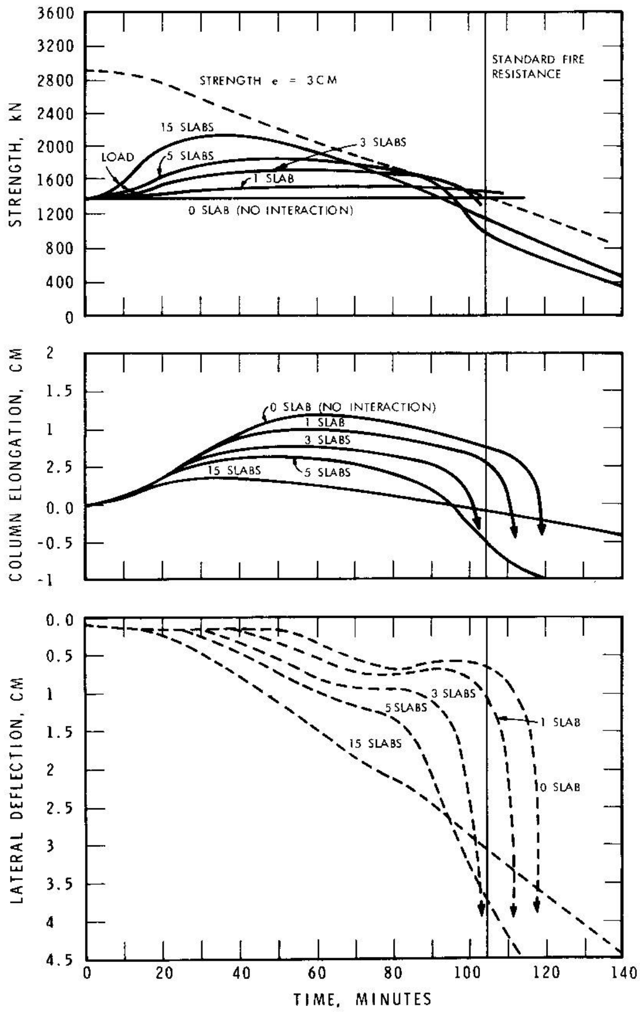

Figure 5: Column-Structure Interaction During Fire (30 cm x 30 cm Square Column, 4.3% Steel, 3.75 cm Cover, 3 m long.)

As the vertical stiffness of the surrounding structure increases from 0 to 3 storeys (or slabs), the applied load increases and the fire resistance is decreased, as seen by comparing column movements. The decrease, however, is not large and the resulting fire resistance is never much less than that calculated from Equation (1). This is because a reduction in end moments due to increased column flexibility compensates for the increased column load due to interaction.

As the vertical stiffness is increased further to 5 storeys, however, a change takes place. What happens is that the increased applied load causes lateral bending to take place, followed by chord shortening between the column ends and relief of the applied load, so that failure does not take place. Eventually, the column becomes shorter than it was initially and, owing to load transfer to adjacent supports, the fire resistance is increased beyond that for an isolated column. For very stiff resistance (15 storeys), the column bends or buckles quite early, but the column does not fail. If the structure can transfer the total load to other supports, the column will never fail.

The results in Figure 5, therefore, indicate that interaction effects with the surrounding structure due to column expansion are not likely to reduce the fire resistance of isolated columns, and in some cases may increase it substantially. Another more critical interaction effect, revealed in the recent St. Louis fire, however, is the effect of large lateral expansion of the slab above the fire floor causing shear failure of columns. This requires further investigation.

Fire Resistance Under Actual Fire Conditions

The standard fire temperature curve initially rises at a prescribed rate and then drops suddenly to ambient temperature (3). In actual fires the temperature reached in the period of temperature rise can be much higher or lower than the standard temperatures. In addition, instead of a sudden drop to ambient temperature, there is, in actual practice, a gradual decrease of the fire temperature after the period of temperature rise.

A wide variety of temperature courses are possible, depending on the fire load, ventilation and other characteristics of the enclosure (1). The most severe are the ventilation controlled fires, i.e., the rate of burning of the combustible materials in the enclosure is determined by the dimensions of the openings through which the air necessary for combustion can be supplied. Formulae describing the temperature course of ventilation-controlled fires (11) have been adopted to calculate fire resistance of reinforced concrete columns (2).

As shown in Figure 6, two major parameters determine the temperature course of ventilation-controlled fires -- the window opening and the fire load (Q), as defined in Figure 6. The larger the opening factor (F) the greater the temperature rise and the shorter the duration. The fire load affects only the duration of the fire -- the higher the fire load the longer the duration of the fire. In studies at DBR/NRC (2), three characteristic temperature curves, corresponding to F = 0.02, F = 0.05 (standard case), and F = 0.1, were chosen.

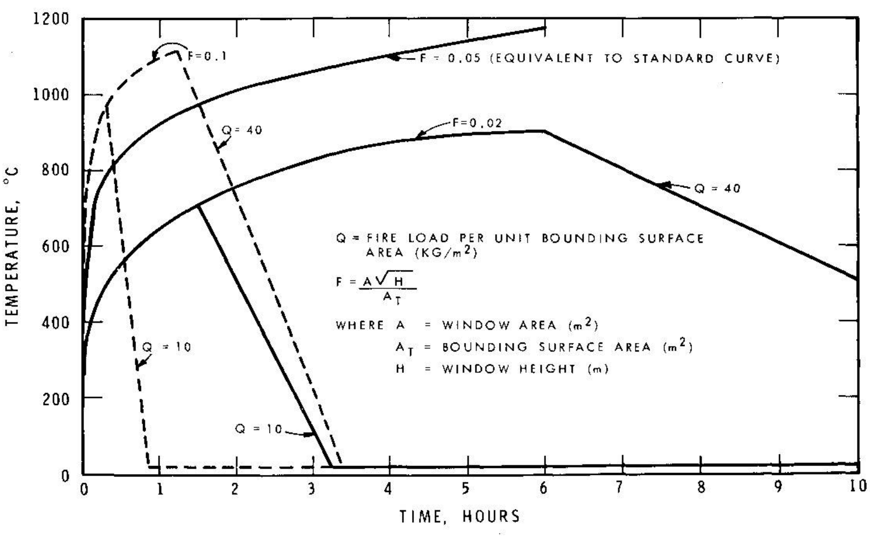

Figure 6: Characteristic Temperature Curves For Various Fire Loads Q and Opening Factors F (Heavy Bounding Walls)

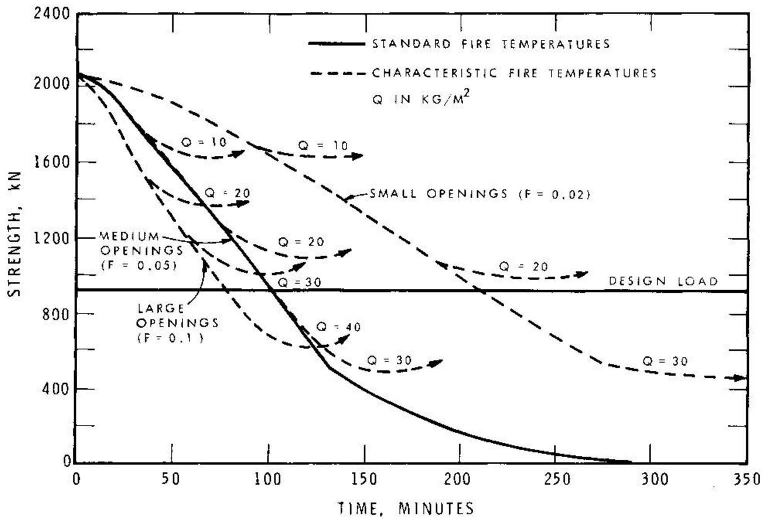

Figure 7: Strength-Time Curves for 30 cm x 30 cm Column (2.2% Steel 3.75 cm Cover)

Figure 7 compares, for a typical case, column strength vs time for different characteristic temperature curves with that for the standard curve. The curves show that for a fire load less than a critical value, Q_{crit}, no failure of the column takes place; in other words below a certain critical value of the fire load there is insufficient combustible content to heat the column to failure. Above the critical fire load, i.e., when $Q > Q_{crit}$, the time to failure very quickly approaches a constant value, R, obtained by assuming an unlimited fire load. The time to failure, R, is a function of the opening factor: the greater the openings, the greater the rate of heat rise, and the shorter the time to failure. On the other hand, Q_{crit} increases with an increase of opening factor since more of the heat escapes the fire compartment.

Figure 8 shows the relationship between Q_{crit}, R, and dimensions for a cover of 3.75 cm. The major variables affecting critical fire load were found (2) to be column size, cover and opening factor; percentage of steel has only a minor effect. The following approximate relationship between critical fire load, Q_{crit}, and fire resistance based on the standard fire test (time to failure for F = 0.05), R_s, was determined from the results for normal weight square concrete columns:

$$\begin{aligned} Q_{crit} &= 4 + 10\,R_s \quad \text{(small, medium openings)} \\ &= 4 + 16\,R_s \quad \text{(large openings)} \end{aligned} \qquad (2)$$

This relationship is helpful in assessing Code fire resistance requirements since Q_{crit} can be related to mean fire load for a given occupancy, Q_m, as follows:

$$Q_{crit} = k\,Q_m \qquad (3)$$

where k is a design safety factor. The design fire safety factor is related to the risk of failure which can be determined as a function of the basic requirements of life safety and economic loss (5); for example, a greater value

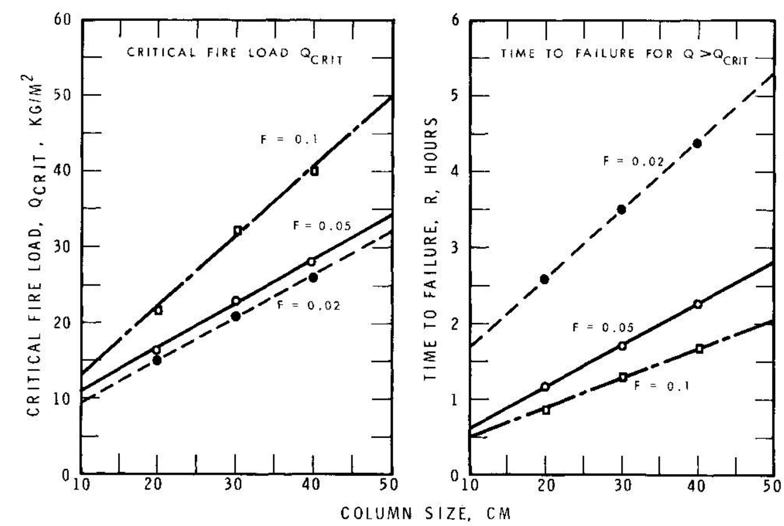

Figure 8: Fire Resistance Parameters For Square Columns (3.75 cm Cover)

of k is required for tall buildings for reasons of life safety and economic loss than for low buildings. Thus, by using Equations (2) and (3) the required fire resistance, R_s, can be related to the basic requirements of life safety and economic loss.

Summary and Conclusions

The fire resistance of square, reinforced concrete columns has been studied under both standard ASTM test conditions and under conditions that more closely resemble those met in practice. Fire resistances are determined by numerical calculation based on the thermal and structural properties of materials at high temperatures. Comparisons with furnace tests of columns show that the calculated fire resistances are consistent with those measured but are about 10 to 20 minutes less, the difference being attributable mainly to conservativeness in the material properties used.

Under standard ASTM test conditions, the fire resistance in time to failure is calculated as a function of type of aggregate, column size, cover, percentage of steel, eccentricity of load, design safety factor and buckling length. Based on calculated results, simple design rules are given (Equation (1)).

The standard ASTM test conditions assume that a column is free to expand, whereas in fact a column is restrained by the surrounding structure and thereby attracts more load than assumed. A numerical study of a restrained column during fire (Fig. 5) indicates, however, that the assumption of no restraint is generally conservative.

Based on the use of more realistic fire temperature curves than the standard ASTM curve, fire resistance was calculated in terms of critical fire load (amount of combustibles) below which no failure takes place, and time to failure if the fire load is greater than critical. Although the critical fire load increases with increased ventilation, the time to failure decreases considerably with increased ventilation. Equations (2) and (3) provide an approximate relationship between standard fire resistance of concrete columns and critical fire load; this is useful in relating Code fire resistance requirements to the fundamental requirements of life safety and economic loss.

This paper is a contribution from the Division of Building Research of the National Research Council of Canada and is published with the approval of the Director of the Division.

References

(1) Lie, T.T. and D.E. Allen. Calculation of the Fire Resistance of Reinforced Concrete Columns. National Research Council of Canada, Division of Building Research, Tech. Paper No. 378 (NRCC 12797), 1972.

(2) Allen, D.E. and T.T. Lie. Further Studies of the Fire Resistance of Reinforced Concrete Columns. In press.

(3) Standard Methods of Fire Tests of Building Construction and Materials. ASTM Designation E110-71, 1971 Book of ASTM Standards, Part 14, p. 431-448.

(4) Harmathy, T.Z. Thermal Properties of Concrete at Elevated Temperatures. ASTM Journal of Materials, Vol. 5, No. 1, March 1970, p. 47-74 (NRC 11266).

(5) Lie, T.T. Fire and Buildings. London, Applied Science Pub. Ltd., 1972.

(6) Abrams, M.S. Compressive Strength of Concrete at Temperatures to 1000 F. Temperature and Concrete, ACI Publication Sp 25, 1968, p. 33-58.

(7) Harmathy, T.Z. and J.E. Berndt. Hydrated Portland Cement and Lightweight Concrete at Elevated Temperatures. Journal, American Concrete Institute, Vol. 63, No. 1, 1966, p. 93-112. (NRC 8847)

(8) Lie, T.T. and T.Z. Harmathy. A Numerical Procedure to Calculate the Temperature of Protected Steel Columns Exposed to Fire. National Research Council of Canada, Division of Building Research, (NRC 12535), 1972.

(9) ACI Building Code Requirements for Reinforced Concrete. American Concrete Institute, ACI Standard 318-71, 1971.

(10) Becker, W. and J. Stanke. Brandversuche an Stahlbetonfertigstutzen. Deutscher Ausschuss für Stahlbeton, Heft 215, Berlin, 1970.

(11) Lie, T.T. Characteristic Temperature Curves for Various Fire Severities. In press.

SUMMARY

The fire resistance of square, reinforced concrete columns has been studied under both standard fire test conditions and under conditions that more closely resemble those encountered in practice, including column-structure interaction effects and realistic fire conditions. Based on calculated results, simple design rules are given for the fire resistance as a function of type of aggregate, column size, cover thickness to steel, amount of steel, design safety factor and equivalent buckling strength.

RESUME

On a procédé à l'étude de la résistance au feu des colonnes en béton armé soumises d'une part aux conditions généralement définies par les normes, d'autre part à des conditions qui correspondent mieux à celles rencontrées dans la pratique, en tenant compte des effets d'interaction entre la colonne et la structure, et des conditions d'incendie réalistes. En se basant sur les résultats du calcul, on indique des règles de dimensionnement simples donnant la résistance au feu en fonction du type d'agrégats, de la taille de la colonne, du recouvrement des aciers d'armature, du pourcentage d'armature, du facteur de sécurité et de la résistance équivalente au flambement.

ZUSAMMENFASSUNG

Der Feuerwiderstand quadratischer Stahlbetonstützen wurde sowohl für normierten Brandverlauf, als auch für praxisnahe Bedingungen unter Einschluss der Wechselwirkung zwischen Stützen und Tragwerk und realistischer Brandbedingungen untersucht. Gestützt auf die Berechnungsergebnisse werden einfache Bemessungsregeln gegeben für den Feuerwiderstand in Abhängigkeit der Zuschlagstoffe, der Stützengrösse, der Stahlüberdeckung, des Bewehrungsgehalts, des rechnerischen Sicherheitsfaktors und der äquivalenten Knickfestigkeit.

Effect of Axial Compression on Flexural Hinge Rotation Capacity

Influence de l'effort normal sur la capacité de rotation des rotules plastiques

Der Einfluss der Normalkraft auf die Rotationsfähigkeit von plastischen Biegegelenken

M. Saeed MIRZA
Associate Professor of Civil Engineering
and Applied Mechanics and Dean of Students

John O. McCUTCHEON
Professor of Civil Engineering
and Applied Mechanics

McGill University
Montreal, Canada

INTRODUCTION

All limit design methods are based on the assumption that some sections of a statically indeterminate structure can attain a certain limiting moment value (M_u) dependent on the structure and loading geometry, cross-section details, reinforcement ratio, concrete strength, etc. When this maximum value of bending moment is approached, curvatures at this section and in its immediate vicinity increase very significantly and lead to the formation of the so-called "flexural hinge". It has been established by several investigators that complete redistribution of bending moments in a statically indeterminate structure occurs only if the hinging sections are capable of undergoing sufficient rotation. The rotation capacity of a flexural hinge decreases with an increase in the tension reinforcement and it has been shown to increase significantly if the concrete at the flexural fringe is confined by closely spaced lateral ties. Presence of axial compressive or tensile forces is known to modify the behaviour of a flexural hinge. However very little research work has been undertaken in this area of limit design.

This paper presents the results of an analytical experimental investigation (1) on twenty specimens with symmetrically reinforced square sections to examine the influence of longitudinal steel percentage and axial compression on rotation capacity of the so-called flexural hinges in beams and columns in statically indeterminate systems. These beams and eccentrically loaded columns had a constant cross-section of 4 in. by 4 in. and a constant moment zone was maintained over a minimum length of 10 ins. in both types of specimens (Fig.1). Two reinforcing steel percentages ($p = p' = 1.37$ per cent for Series S1 and $p = p' = 2.06$ per cent for Series S2) were used in this investigation and two identical specimens were tested for each loading combination to verify the reproduc bility of results. The eccentric column loading brackets and the beam ends were heavily reinforced to eliminate any possibility of shear failures in these regions. The concrete strength and the lateral reinforcement were kept constant in all specimens which were tested under varying eccentricities giving a wide range of loadings from pure axial compressive loads to the case of pure bending.

ANALYTICAL METHOD

Once the curvature distribution along a member is established the rotation between any two sections can be evaluated by simple integration. The relationship between the bending moment and the curvature at a section is principally a function of the cross-section characteristics. Variation of the flexural rigidity along the span on account of cracking complicates the curvature calculations in cracked reinforced concrete members. For a member subjected to a constant bending moment the curvature varies from a maximum value at the cracked section to a mimimum at a point between the cracks.

Existing research data on cracking of concrete lead the assumption that the average spacing of cracks ΔL_{av} is 1.8 times the minimum spacing ΔL_{min} and the following expression was derived in Reference 1:

$$\Delta L_{av} = \frac{3\phi}{\gamma}\left(1 + 0.1\,\frac{B_f}{A_s}\right) \qquad (1)$$

where ϕ = the bar diameter
γ = a coefficient. For plain bars $\gamma = 1$ and for deformed bars = 1.6
A_s = cross-sectional area of tension reinforcement
and B_f = twice the area of the concrete cover.

Average crack spacing, evaluated using equation (1), was noted to be 2.5 in. for Series S1 and 2.0 in. for Series S2, which agreed well with the experimental results (Ref.1).

The following assumptions were made in evaluating the moment-curvature relationships:

1. At any load level, the compressive strain at the extreme fibre is assumed to be uniform along the reference length of 10 inches at a maximum concrete strain value. Strain distribution across a section was assumed to be linear.

2(a) The maximum compressive stress fc" was assumed to be (Ref.2)

$$f_c'' = 0.85\ fc' \qquad (2)$$

where f_c' = 28-day concrete compressive strength obtained from tests on 6 x 12 in. cylinders.

(b) As recommended by Hognestad (2), the maximum concrete compressive strain was assumed to be 0.0038.

3. The minimum curvature at a section between two cracks

$$\varepsilon_u/(^d/_2)$$

4. The maximum curvature over a crack can be determined using the method to be described later.

5. Knowing the maximum and minimum curvatures, the curvature distribution along the reference length can be established for rotating evaluation.

The concrete stress-strain curve shown in Fig.2 is given by the following equations:

(i) For $\varepsilon<\varepsilon_o = 0.002$

$$f_c = f_c''[2^{\varepsilon}/\varepsilon_o - (^{\varepsilon}/\varepsilon_o)^2] \qquad (3)$$

(ii) For $0.002<\varepsilon< 0.0038$

$$f_c = f_c'' - \frac{250}{3} fc''(\varepsilon - 0.002) \qquad (4)$$

The compressive force C at any stress level f_c (Fig.) is given by

$$C = K_1 \varepsilon f_c'' \qquad (5)$$

with the resultant located at a distance $K_2\varepsilon$ from the extreme compression fibre.

For $\varepsilon< 0.002$,

$$K_1 = \frac{\varepsilon}{\varepsilon_o}\left(1 - \frac{\varepsilon}{3\varepsilon_o}\right) \qquad (6)$$

and

$$K_2 = \frac{4 - {^{\varepsilon}/\varepsilon_o}}{12\left(1 - \frac{\varepsilon}{3\varepsilon_o}\right)} \qquad (7)$$

For $\varepsilon = \varepsilon_u = 0.0038$, Obeid (1) derived the following values for K_1 and K_2:

$$K_1 = 0.79 \qquad \text{and} \qquad K_2 = 0.40 \qquad (8)$$

The ultimate compressive force C_u is given by

$$C_u = K_1 b\ f_c''\ n_u \qquad (9)$$

where n_u = depth of the neutral axis at ultimate load.

The ultimate curvature ϕ_u is given by

$$\phi_u = \frac{\varepsilon_u}{n_u} \tag{10}$$

Substituting from equation (10) into equation (9), the ultimate axial compressive load P_u is given by

$$P_u = C_u = K_1 b f_c'' \varepsilon_u \left(\frac{1}{\phi_u}\right) \tag{11}$$

Substituting values of K_1, b, ε_u and f_c'', equation (11) becomes

$$P_u = \frac{1}{20}\left(\frac{1}{\phi_u}\right) \text{ kips} \tag{12}$$

and $$M_u = P_u e = \frac{1}{20}\left(\frac{e}{\phi_u}\right) \text{ kip-in.} \tag{13}$$

Similar equations have been derived in Reference 1 for the conditions at yielding of tension reinforcement and for the case of pure flexure. Curvature and rotation values for the different specimens at yielding of tension steel and at ultimate load, calculated using the above method are detailed and compared with experimental results in Table 1 and are presented graphically in Figures 3 through 5.

EXPERIMENTAL PROCEDURE

Strain gauges were installed at the top and at the side of the concrete compressive zone and on the steel bars. Strains and deflections were recorded continuously using an automatic recorder. Curvature was calculated from the strain values using the equation

$$\phi = \frac{\varepsilon_c + \varepsilon_s}{d}$$

where ε_c is the compressive strain on the extreme concrete fibre and ε_s is the tensile strain in steel reinforcement. Rotation over a reference length of 10 inches was measured using rotation arms and two DCDT's (direct current differential transducers). Rotation values were also calculated by an integration of the experimental curvature values over the reference length.

All specimens were tested either in a 400,000 lb. capacity Baldwin - Lima - Hamilton universal testing machine or in a 60,000 lb. capacity Riehle universal testing machine. The load was applied in suitable increments at preselected eccentricity values (Table 1) through a ball and socket arrangement.

The following three distinct failure modes were observed in this investigation:

(i) Compression failures: (e.g. Specimen S1-1):Failure occurred during the crushing and spalling of the concrete cover on the compression side after compression steel had yielded. Tension steel did not show any signs of yielding. Signs of distress in concrete were initially observed at loads ranging between 80 and 95 per cent of the ultimate load. Spalling of concrete was immediately followed by buckling of the compression steel.

(ii) Balanced failure mode (Specimen S2-3):
This mode of failure consisted generally of the yielding of the compression reinforcement, accompanied almost immediately by the yielding of the tension reinforcement and followed by a crushing of concrete in compression zone as the applied deformations were increased without any further increase of load.

(iii) Flexural mode of failure (Specimen S1-4):
General behaviour of these specimens was typical of under-reinforced beams due to yielding of the tension reinforcement. These specimens showed significantly larger deformations and ductility than those in cases (ii) and (i) above. Beam specimens tested under pure flexure (axial force P=0) showed the largest ductility which was observed to increase as the applied compressive loads were decreased from the pure axial compression capacity (at zero eccentricity) to zero for the case of pure flexure.

Comparison of Computed and Experimental Data:

The computed axial load and bending moments at ultimate load are compared with the experimental values in Table 1. A generally good agreement can be noted. Comparison of calculated curvature values at yield show good agreement with the experimental data. The curvature values at ultimate load were obtained from the last reading from the strain gauges before they become inoperational and therefore the calculated values are generally larger than the experimental ones. It may be noted that near ultimate load, strain values of the order of 0.006 were recorded which makes conservative the maximum strain value of 0.003 specified by the various codes.

Rotation and deflections were recorded continuously up to the ultimate load using DCDT's. Good correlation can be noted in the calculated and experimental values detailed in Table 1.

An examination of test data on all 20 test specimens shows that the available rotation capacity was not dependent on the steel percentages used. The rotation capacity was a maximum for the case of pure flexure and it decreased gradually by approximately 25 per cent as the applied axial compression load was increased to a point where a balanced failure condition was obtained. Further increase in the applied compression loads decreased the available rotation capacity at the hinge more rapidly to zero for the case of pure axial compression (eccentricity = 0). This trend was also noted in the computed results which show satisfactory agreement with the experimental data.

CONCLUSIONS

The results of this investigation can be summarized as follows:

1. Suitable equations have been developed to accurately predict axial force - bending moment - curvature characteristics. Good agreement was obtained between the calculated strength and deformation values and the corresponding experimental data.
2. Maximum compressive strains of the order of 0.006 existed at extreme fibres near ultimate load, suggesting that larger deformations can be sustained at the so-called "flexural hinges". This would lead to a higher degree of moment redistribution in statically indeterminate reinforced concrete systems, which constitutes the basis of limit design.
3. Rotation capacity of the "flexural hinge" was not significantly influenced by the longitudinal steel percentage and was a maximum for the case of pure flexure.
4. Analytical and experimental results show that the available rotation capacity decreased by approximately 25 per cent as the axial compressive load was increased from zero to a point where balanced column failure resulted. Beyond the balance point, available hinge rotation diminished gradually becoming zero for the case of pure axial compression.

AGKNOWLEDGMENTS

This investigation formed a part of the M.Eng. Thesis of Mr. E. Obeid under the direction of the authors. The financial assistance of the National Research Council of Canada, the Canada Emergency Measures Organization and the Department of Education, Government of Quebec to continuing research programs at McGill University is gratefully acknowledged.

REFERENCES

1. E. Obeid, "Compression Hinges in Reinforced Concrete Elements", M.Eng. Thesis, McGill University, September 1969.
2. E. Hognestad, "A Study of Combined Bending and Axial Load in Reinforced Concrete Members", Research Bulletin Series No. 399, University of Illinois, November 1951.

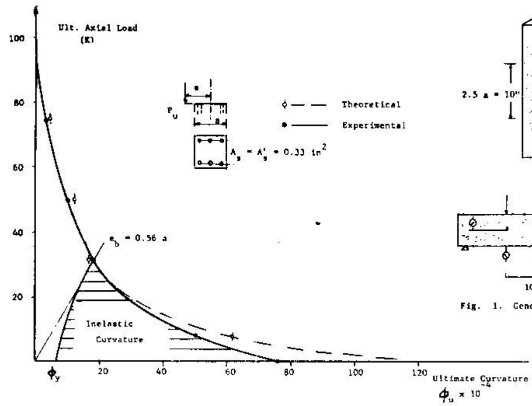

Fig. 4. Comparison of Calculated and Measured Ultimate Curvature versus Ultimate Axial Load.

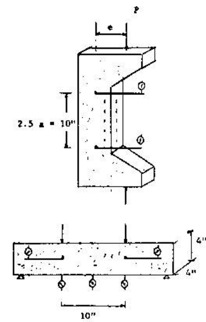

Fig. 1. General Arrangement.

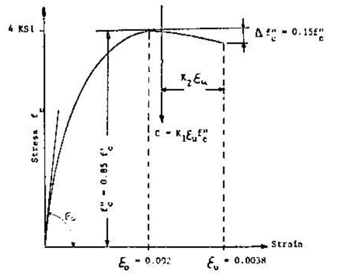

Fig. 2. Assumed Stress-Strain Diagram of Concrete in Combined Axial Load and Bending.

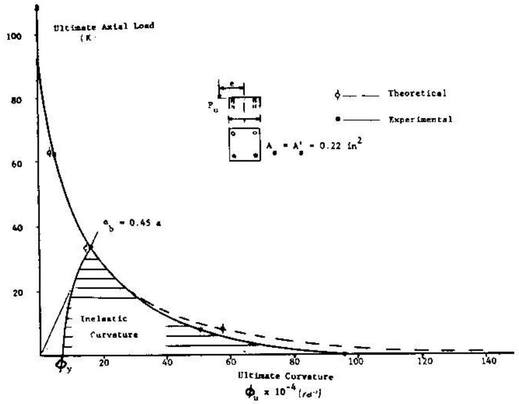

Fig. 3. Comparison of Calculated and Measured Ultimate Curvature versus Ultimate Axial Load.

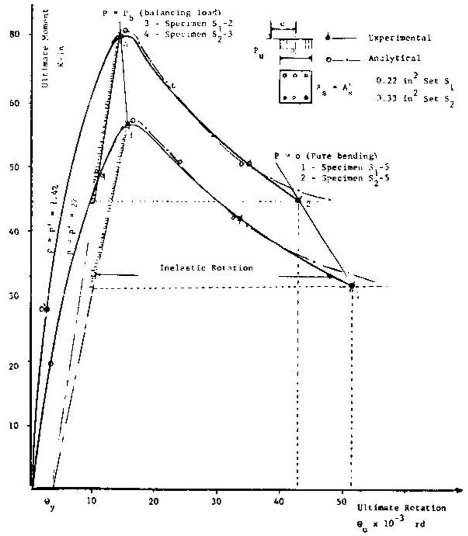

Fig. 5. Comparison of Calculated and Measured Ultimate Rotation, Axial Load and Moment.

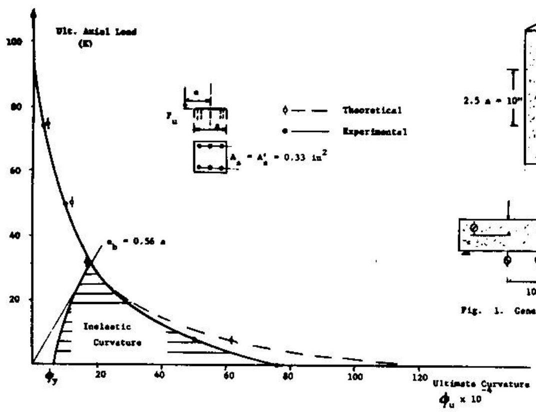

Fig. 4. Comparison of Calculated and Measured Ultimate Curvature versus Ultimate Axial Load.

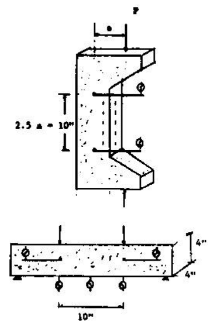

Fig. 1. General Arrangement.

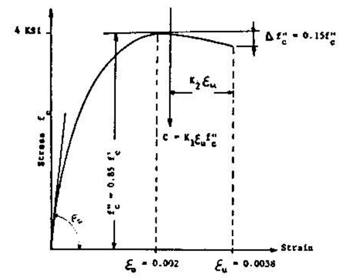

Fig. 2. Assumed Stress-Strain Diagram of Concrete in Combined Axial Load and Bending.

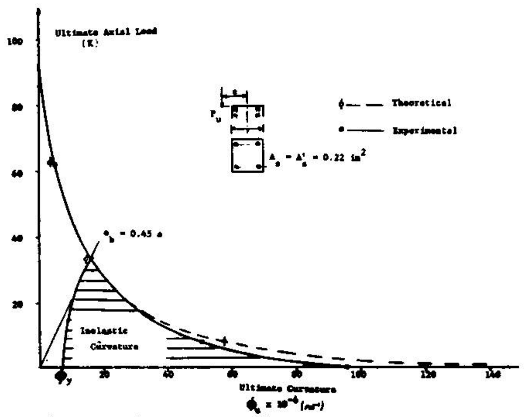

Fig. 4b. Comparison of Calculated and Measured Ultimate Curvature versus Ultimate Axial Load.

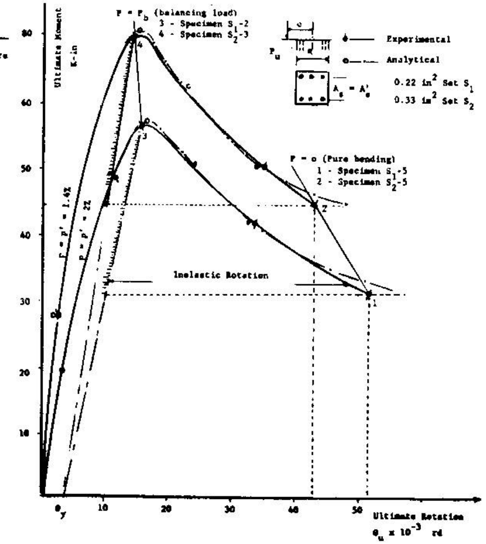

Fig. 5. Comparison of Calculated and Measured Ultimate Rotation, Axial Load and Moment.

TABLE 1

Sp.No	$\frac{M_u}{P_u}=e_u$ in.	Curvature at Yield $\phi_y \times 10^{-4}$ (1/in) Exp.	Anal.	Curvature at Ultimate $\phi_u \times 10^{-4}$ (1/in) Exp.	Anal.	Inelastic Curvature 10^{-4} (1/in) Exp.	Anal.	Rotation at Yield $\theta_y \times 10^{-3}$ (rad) Exp.	Anal.	Rotation at Ultimate $\theta_u \times 10^{-3}$ (rad) Exp.	Anal.	Inelastic Rotation 10^{-3} (rad) Exp.	Anal.	Axial Load Ult. P_u (K) Exp.	Anal.	Moment Ult. M_u (K-in) Exp.	Anal.
Series S1 $p = p' = 0.0137$																	
S_1-1	0.40	-	-	6.5	6.0	-	-	-	-	6.5	6.0	-	-	62.0	60.0	24.8	24.0
S_1-2	1.83	17.0	15.3	17.0	16.0	0.0	0.0	16.0	15.3	16.0	15.3	0.0	0.0	31.3	31.0	57.5	57.0
S_1-3	2.50	14.0	13.0	26.0	23.8	12.0	13.8	12.0	13.0	22.0	20.0	10.0	9.74	21.75	21.0	54.4	52.5
S_1-4	5.60	12.0	7.0	48.0	71.5	36.0	64.0	8.0	7.0	36.0	34.6	28.0	27.05	7.3	7.0	39.2	38.8
S_1-5	∞	7.0	6.5	90.0	183.0	83.0	17.64	7.0	6.5	52.0	70.0	43.0	61.0	0.0	0.0	32.5	31.0
Series S2 $p = p' = 0.0206$																	
S_2-1	0.4	-	-	3.9	4.0	-	-	-	-	4.1	4.0	-	-	71.0	70.0	28.4	28.0
S_2-2	1.2	-	-	9.2	10.0	-	-	-	-	10.2	10.0	-	-	52.0	50.0	62.4	60.0
S_2-3	2.3	10.5	14.0	16.5	16.0	0.0	0.0	14.2	14.0	14.2	15.3	0.0	0.0	31.5	31.0	72.5	71.5
S_2-4	7.0	7.0	7.6	50.0	68.5	43.0	60.8	9.0	7.60	34.0	33.0	25.0	26.2	7.5	7.3	52.5	51.1
S_2-5	∞	6.0	7.0	70.0	148.0	64.0	141.0	7.0	7.0	43.0	60.0	36.0	50.5	0.0	0.0	46.0	44.0

SUMMARY

The results of this investigation can be summarized as follows:

1. Suitable equations have been developed to accurately predict axial force - bending moment - curvature characteristics. Good agreement was obtained between the calculated strength and deformation values and the corresponding experimental data.

2. Maximum compressive strains of the order of 0.006 existed at extreme fibres near ultimate load, suggesting that larger deformations can be substained at the so-called "flexural hinges". This would lead to a higher degree of moment redistribution in statically indeterminate reinforced concrete systems, which constitutes the basis of limit design.

3. Rotation capacity of the "flexural hinge" was not significantly influenced by the longitudinal steel percentage and was a maximum for the case of pure flexure.

4. Analytical and experimental results show that the available rotation capacity decreased by approximately 25 per cent as the axial compressive load was increased from zero to a point where balanced column failure resulted. Beyond the balance point, available hinge rotation diminished gradually becoming zero for the case of pure axial compression.

RESUME

Les résultats de cette étude peuvent se résumer de la façon suivante:

1. On a développé des équations permettant de prévoir avec précision les interactions force axiale - moment de flexion - courbure. On a obtenu une bonne concordance entre les charges ultimes et les déformations calculées et les résultats expérimentaux.

2. On a constaté, à l'approche de la charge ultime, des déformations de compression maximales de l'ordre de 0.006 dans les fibres extérieures, ce qui conduit à penser qu'on peut obtenir de plus grandes déformations aux rotules plastiques. Cela conduirait à un plus haut degré de redistribution des moments pour les systèmes hyperstatiques en béton armé, ce qui constitue la base du dimensionnement à la limite.

3. La capacité de rotation des rotules plastiques n'a pas été influencée de façon décisive par la quantité d'armature longitudinale, et s'est avérée maximale dans le cas de la flexion pure.

4. Les résultats analytiques et expérimentaux montrent que la capacité de rotation diminue d'environ 25% quand on fait varier la compression axiale de zéro jusqu'au point d'écoulement simultané des armatures tendues et comprimées. Au delà de ce point, la capacité de rotation diminue graduellement jusqu'à atteindre zéro pour le cas de la compression pure.

ZUSAMMENFASSUNG

Die Ergebnisse der vorliegenden Untersuchung lassen sich wie folgt zusammenfassen:

1. Einfache Ausdrücke gestatten die genaue Voraussage der Beziehungen zwischen Normalkraft, Biegemoment und Krümmung. Eine gute Uebereinstimmung zwischen Rechnung und Versuch besteht.

2. Randbruchstauchungen der Grössenordnung 0.006 waren in der Nähe der Bruchlast zu beobachten und lassen den Schluss zu, dass grössere Verformungen im Bereich der sog. plastischen Gelenke ertragen werden können. Diese Tatsache lässt eine stärkere Momentenumlagerung in statisch unbestimmten Stahlbetontragwerken erwarten (Traglastverfahren).

3. Die Rotationsfähigkeit plastischer Gelenke war nicht spürbar beeinflusst durch den Längsbewehrungsgehalt und zeigte ein Maximum bei reiner Biegung.

4. Rechnerische und Versuchstechnische Ergebnisse zeigen, dass die verfügbare Rotationsfähigkeit nur etwa 25% zurückgeht, wenn die Normalkraft von Null bis zu derjenigen Last anwächst, bei welcher gleichzeitig sowohl die Druck- als auch die Zugbewehrung fliesst. Oberhalb dieser Last ging die Rotationsfähigkeit stetig zurück bis auf Null für zentrischen Druck.

Leere Seite
Blank page
Page vide

Effect of Confining Reinforcement on the Flexural Ductility of Rectangular Reinforced Concrete Column Sections with High Strength Steel

Influence des armatures en acier à haute résistance situées au bord de la section sur la ductilité à la flexion des colonnes rectangulaires en béton armé

Der Einfluss hochfester Bewehrung in rechteckigen Stahlbetonstützen auf das Verformungsvermögen infolge Biegung

R. PARK
University of Canterbury
Christchurch

J.A. NORTON
Ministry of Works
Wellington

New Zealand

INTRODUCTION

The need to design structures capable of undergoing large post-elastic deformations is of considerable importance if very severe earthquakes are to be survived. Current seismic design codes rely on this energy dissipating characteristic as a major factor in justifying the present levels of seismic design load.

The ductility of compressed concrete can be significantly increased by the presence of closely spaced transverse steel in the form of steel spirals or hoops. Such steel confines the concrete and significantly improves the stress-strain characteristics of the concrete at high strains.

This paper is based on a theoretical study (1) into the effect of transverse confining steel on the flexural ductility of short reinforced concrete columns with rectangular cross sections. Moment-curvature characteristics of column sections under eccentric monotonic loading are determined from the stress-strain curves of concrete confined with rectangular steel hoops and of longitudinal steel including the effects of strain hardening. The degree of flexural ductility available from sections is indicated by the moment-curvature curves and the effect of transverse steel is assessed. This leads to a method for detailing columns for flexural ductility. A range of square column sections containing longitudinal steel with a yield strength of 60,000 psi (414 N/mm^2) is examined. This paper extends a previous study in which columns containing steel with a yield strength of 40,000 psi (276 N/mm^2) were examined (2).

2. DETAILING FOR DUCTILITY

2.1 Ductility Demands During Seismic Loading

A measure of the post-elastic performance of structures is given by the displacement ductility factor defined as Δ_u/Δ_y where Δ_u is the lateral deflection at the end of the post-elastic range and Δ_y is the lateral deflection at first yield. Several dynamic analyses of structures using recorded ground motion response from severe earthquakes have indicated that displacement ductility factors of the order 3 to 5 should provide structures designed to the SEAOC (3) and ICBO (4) code loading with sufficient energy dissipation capacity. Those codes, and the ACI code (5), make detailing recommendations for design which are aimed at achieving adequate ductility. The post-elastic deformation of reinforced concrete frames is concentrated in regions of plastic hinging and to achieve a given displacement factor much larger local rotational ductilities are required within the hinging region. The rotation capacity of sections can be expressed by the curvature ductility factor φ_u/φ_y, where φ_u is the section curvature at the end of the post-elastic range and φ_y is the curvature at first yield. This assumes that flexural deformations predominate. An approximate procedure for assessing the likely demands, based on a static collapse mechanism of frames under lateral loading (6), has indicated that for a collapse mechanism involving plastic hinges in the beams and at the column bases, the φ_u/φ_y demands at the column bases could be in the order of three times the Δ_u/Δ_y value. For a collapse mechanism involving plastic hinges only in the columns, inducing an inter-storey sidesway collapse mechanism, the φ_u/φ_y demands may be much higher.

2.2 Capacity of Reinforced Concrete Column Sections for Ductile Behaviour

The moment-curvature relationship provides a measure of the plastic rotation capacity of sections. One problem in assessing this in relation to the φ_u/φ_y demand is the definition of the ultimate curvature φ_u. It has been pointed out previously (2) that many sections maintain considerable capacity for plastic rotation beyond the peak of the moment-curvature curve and that it would be reasonable to recognise this and define φ_u as the curvature when the moment capacity of the section has reduced to 80-90% of the maximum moment. A criterion for satisfactory ductile performance of columns can thus be established on the basis of reaching a curvature ductility φ_u/φ_y of at least 15, with φ_u defined as above. This should ensure structures achieving a displacement ductility factor Δ_u/Δ_y of at least 4 with a limited reduction in strength provided sidesway mechanisms with plastic hinging concentrating in the columns of one storey, and brittle shear and anchorage failures, are avoided. The derivation of moment-curvature relationships from the stress-strain curves of confined concrete and longitudinal steel allows this criterion to be applied and enables the required amount of transverse steel to be determined.

Such an approach is more rational than existing seismic code procedures for determining transverse steel requirements in columns. The shortcomings of the existing code (3), (4), (5) requirements have been discussed previously (2), (7). These existing code requirements are based on the increase in concrete strength observed in tests on axially loaded columns with confined concrete. The code approach involves a philosophy of maintaining the axial load carrying capacity of the column. Sufficient transverse steel is provided to enhance the strength of the core concrete so that when the cover concrete spalls the axial load strength is not reduced. In deriving the requirements to meet this philosophy for columns with rectangular hoops, the hoop steel is assumed to be 50% as effective as circular spirals as confining reinforcement. The philosophy itself is assumed to produce structures with sufficient ductility. This code approach may maintain the axial load strength of columns but fails to relate the detailing requirements to the required rotational capacities of eccentrically loaded sections. The approach based on the moment-curvature relationships obtained from stress-strain curves outlined previously could form a rational basis of detailing columns for ductility.

3. DERIVATION OF MOMENT-CURVATURE CHARACTERISTICS

3.1 Factors Taken Into Account

In deriving the moment-curvature characteristics of eccentrically loaded rectangular reinforced concrete column sections the following factors are taken into account: the level of axial load on the column, the proportion of column section confined, the longitudinal steel content, and the material strength characteristics. Ideally the effects of cyclic loading should also be considered but the complexity of a cyclic analysis makes it difficult to study a large range of cases. In this study monotonic loading will be analysed and it is felt that this should give a reasonable assessment in the first instance.

3.2 Assumptions

The analysis of the moment-curvature characteristics is derived on the basis of the following assumptions:

(i) Plane sections remain plane after flexure.

(ii) The stress-strain curve of steel reinforcement in tension or compression follows the curve of Fig. 1a. There are three regions as follows:

Region AB $\quad \varepsilon_s \leq \varepsilon_y \;,\quad f_s = \varepsilon_s E_s$ ... (1)

Region BC $\quad \varepsilon_y \leq \varepsilon_s \leq \varepsilon_{sh} \;,\quad f_s = f_y$ ... (2)

Region CD $\quad \varepsilon_{sh} \leq \varepsilon_s \leq \varepsilon_{su} \;,$

$$f_s = f_y \left\{ \frac{m(\varepsilon_s - \varepsilon_{sh}) + 2}{60(\varepsilon_s - \varepsilon_{sh}) + 2} + \frac{(\varepsilon_s - \varepsilon_{sh})(60 - m)}{2\,(30r + 1)^2} \right\} \quad \ldots (3)$$

where $m = \left\{ \frac{f_{su}}{f_y} (30r + 1)^2 - 60r - 1 \right\} / \; 15r^2$ and $r = \varepsilon_{su} - \varepsilon_{sh}$

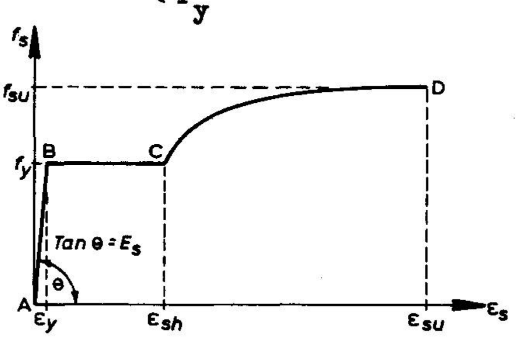

(a) Steel in tension or compression

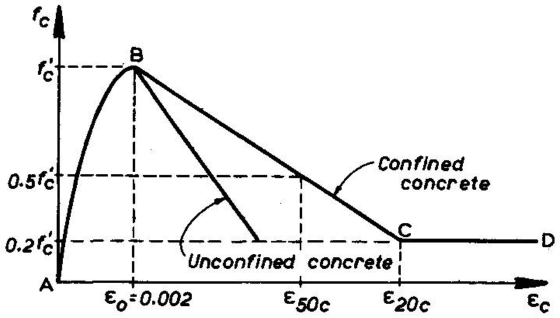

(b) Concrete in compression confined by rectangular hoops

Fig. 1 Assumed Stress-Strain Curves.

This curve follows that reported previously (2).

For columns with high yield (f_y = 60,000 psi = 414 N/mm^2) longitudinal steel studied in this paper, the following steel parameters are used: $\varepsilon_{sh} = 4\,\varepsilon_y$, $\varepsilon_{su} = 0.12$, $f_{su} = 1.58 f_y$. These values were obtained from a series of tests conducted by Norton (1) on New Zealand produced reinforcing steel of this grade.

(iii) The tensile strength of concrete is ignored.

(iv) The stress-strain curve for confined concrete in compression follows the curve of Fig. 1b. There are three regions as follows:

Region AB $\quad \varepsilon_c \leq 0.002$

$$f_c = f_c' \left\{ \frac{2\varepsilon_c}{0.002} - \left(\frac{\varepsilon_c}{0.002}\right)^2 \right\} \quad \ldots (4)$$

Region BC $\quad 0.002 \leq \varepsilon_c \leq \varepsilon_{20c}$

$$f_c = f_c' \left\{ 1 - Z\left(\varepsilon_c - 0.002\right) \right\} \quad \ldots (5)$$

where $Z = 0.5 \Big/ \left(\frac{3}{4} \rho_s \sqrt{\frac{b''}{s_h}} + \frac{3 + 0.002 f_c'}{f_c' - 1000} - 0.002 \right)$ with f_c' in psi ...(6)

Region CD $\quad \varepsilon_{20c} \leq \varepsilon_c \;,\quad f_c = 0.2 f_c'$ ...(7)

This curve follows that proposed previously (8). From Eq. (6) and Fig. 1b it can be seen that the parameter Z defines the slope of the falling of the stress-strain curve in non-dimensional terms. It describes the effect of the transverse rectangular confining steel on the stress carried by the concrete at high strains.

(v) The stress-strain curve for the cover concrete (outside the hoops) in compression is identical to that of the confined concrete core up to a strain of 0.004. The cover concrete at strains greater than 0.004 is considered to have spalled and to have zero strength.

3.3 Calculation of the Parameter Z for Arrangements of Transverse Steel

In practice, various arrangements of transverse steel involving overlapping hoops, or hoops with supplementary cross ties, may be required in columns to provide lateral support to the longitudinal bars in the section. The column section of Fig. 2 shows one possible arrangement. The stress-strain relationship for confined concrete given by Eqs. (5) and (6) was obtained from test results for small concrete specimens with hoops only

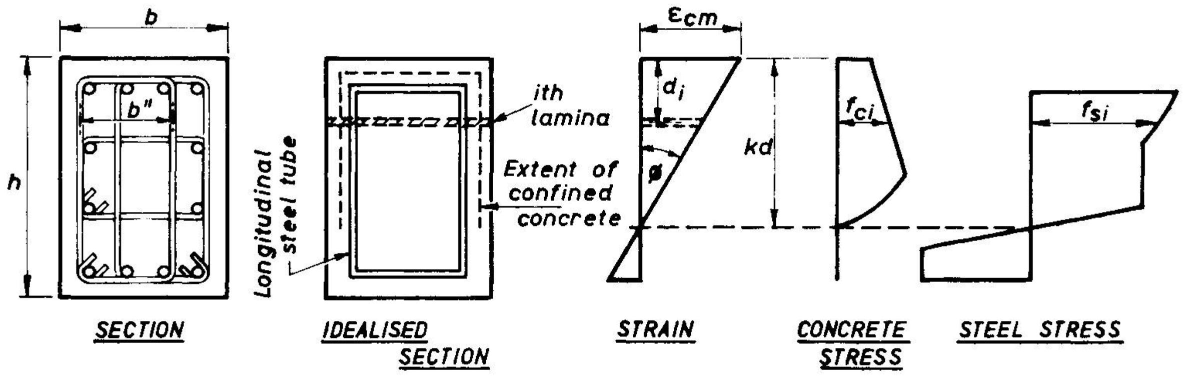

Fig. 2 Section With Stress and Strain Distribution.

around the perimeter of the specimen. Additional transverse bars across the section will help confine the concrete and need to be taken into account. To include the effect of such additional transverse bars the parameter Z in the stress-strain relationship may be calculated for the partitioned concrete section. For example, for the section with overlapping hoops shown in Fig. 2, Z may be calculated using b" = width of side of one hoop, s_h = spacing of sets of overlapping hoops and ρ_s = ratio of volume of one hoop to volume of concrete core within that hoop. This definition of ρ_s is more conservative than the alternative of taking ρ_s as the ratio of the total volume of hoops to total volume of concrete core, but in view of the lack of test data on the efficiency of overlapping hoops it is probably wise to use the more conservative definition. It is also to be noted that Eqs. (5) and (6) were derived from test results in which the whole of the concrete core was in compression, whereas in a column part of the concrete section will be in tension. However the lowly stressed concrete near the neutral axis will help confine the highly stressed concrete and hence the fact that the hoop terminates in the tension zone is of no great significance. It is suggested that ρ_s be defined as above by ratio of volume of hoop to volume of concrete enclosed, rather than by any new definition which considers an effective hoop volume and the compressed concrete volume.

3.4 Moment-Curvature Analysis

The procedure for evaluating the moment-curvature relationship of a section has been described in detail elsewhere (2), (1). Briefly, the bending moments and curvatures associated with an axial load and a range of deformations are determined from the requirements of strain compatibility and equilibrium of stress resultants. The section is divided into a number of discrete laminae each having the orientation of the neutral axis. The longitudinal steel is replaced with an equivalent thin tube so that each lamina contains a particular amount of cover concrete, core concrete and longitudinal steel at a strain consistent with the strain profile. Fig. 2 shows a cross section with strain and stress distribution. For a value of extreme compression fibre strain ϵ_{cm} the neutral axis depth kd, for which the sum of the internal forces found from the laminae stress resultants equals the axial load P, is determined by an iterative process. The internal moment M corresponding to that value of ϵ_{cm} and P is then calculated and the corresponding curvature φ is determined from ϵ_{cm}/kd. The theoretical moment-curvature relationship is obtained by successively incrementing the value of ϵ_{cm}.

3.5 Variables Studied

Using the analysis procedure outlined above, a series of square column sections with high strength longitudinal reinforcement were studied (1) with the following range of variables:

(i) Axial load intensity, $\frac{P}{f'_c A_g}$ = 0.1, 0.2, 0.3 and 0.5.

(ii) Cover ratio, c_v/b = 0.1, 0.075 and 0.05 corresponding to square column sections of 15 in (381 mm), 20 in (508 mm) and 30 in (762 mm) dimensions with concrete cover thickness to the outside of the transverse steel of 1.5 in (38 mm).

(iii) Concrete strength, f'_c = 4000 psi (27.6 N/mm^2) and 6000 psi (41.4 N/mm^2).

(iv) Longitudinal steel strength, f_y = 60,000 psi (414 N/mm^2), with E_s = 29 x 10^6 psi (200,000 N/mm^2).

(v) Longitudinal steel content uniformly distributed around the four sides of the section, ρ_t = 0.02, 0.04 and 0.06, where $\rho_t = A_{st}/A_g$.

(vi) Transverse steel content, various arrangements of transverse rectangular hoops as defined by a range of Z values. For a given arrangement of transverse hoops the corresponding Z value may be calculated using Eq. (6) as discussed in Section 3.3. For example, for the arrangement of three overlapping hoops shown in the column section of Fig.2, if the hoop diameter is ½ in (12.7 mm), the spacing of each set of hoops is s_h = 4 in (102 mm), column dimensions are b = h = 20 in (508 mm), cover thickness c_v = 1.5 in (38 mm), concrete strength f'_c = 4000 psi (27.6 N/mm^2), and assuming that b" = ⅔ (b-2c_v), Eq. (6) gives

$$Z = \frac{0.5}{0.75 \times \frac{2(17+11.33)0.2}{17 \times 11.33 \times 4}\sqrt{\frac{11.33}{4}} + \frac{3 + 8}{3000} - 0.002} = 24.8$$

Table 1 gives some values of Z calculated as above for the arrangement of three overlapping hoops shown in Fig. 2 for various hoop diameters and spacing of hoop sets. The Z values for other spacings can also be calculated. The Z values corresponding to the ACI code (5) requirements for special transverse steel using the above arrangement when $P > P_b$ are also shown in the note under the table.

Table 1 Z Values for Square Sections With Three Overlapping Rectangular Hoops with Unsupported Length of Hoop Side = ⅔ x dimension of confined core, f'_c = 4000 psi (27.6 N/mm^2) and c_v = 1.5 in (38 mm).

Transverse Steel	Section size		
	15 in (381 mm)	20 in (508 mm)	30 in (762 mm)
⅜ in(9.5 mm) dia. at 12 in (305 mm)centres	125	138	155
⅜ in(9.5 mm) dia. at 4 in (102 mm)centres	36	42	51
½ in(12.7 mm) dia. at 4 in(102 mm)centres	21	25	31
⅝ in(15.9 mm) dia. at 4 in(102 mm)centres	14	16	20
¾ in(19.1 mm) dia. at 4 in(102 mm)centres	9.9	12	15

Note: ACI 318-71 (5) requires for $P > 0.4P_b$ ⅝ in (15.9 mm) dia. hoops with f_y = 40,000 psi (276 N/mm^2) spaced as follows:
For 15 in (381 mm) section, spacing = 3.1 in (79 mm), giving Z = 9.6
For 20 in (508 mm) section, spacing = 3.2 in (81 mm), giving Z = 12
For 30 in (762 mm) section, spacing = 2.9 in (74 mm), giving Z = 13

3.6 Moment-Curvature Results

Typical moment-curvature curves from the analysis for bending about a principal axis of the section are shown in Figs. 3, 4 and 5. On each curve, A denotes the onset of spalling of the cover concrete (ϵ_{cm} = 0.004),

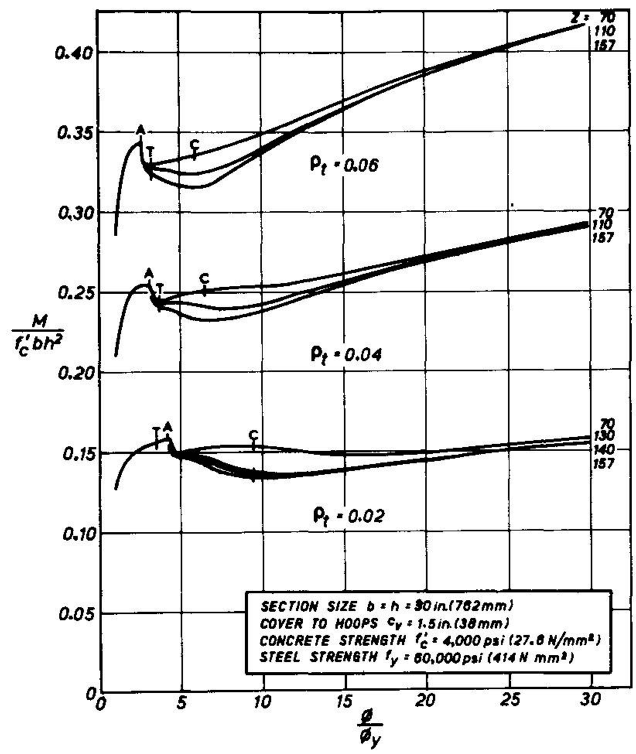

Fig. 3 Moment-Ductility Curves for $P = 0.1f'_cA_g$

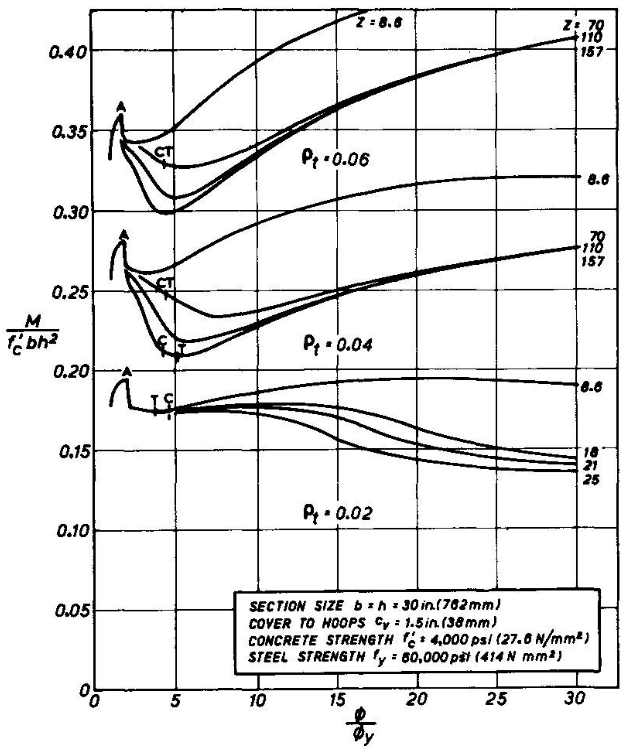

Fig. 4 Moment-Ductility Curves for $P = 0.3f'_cA_g$

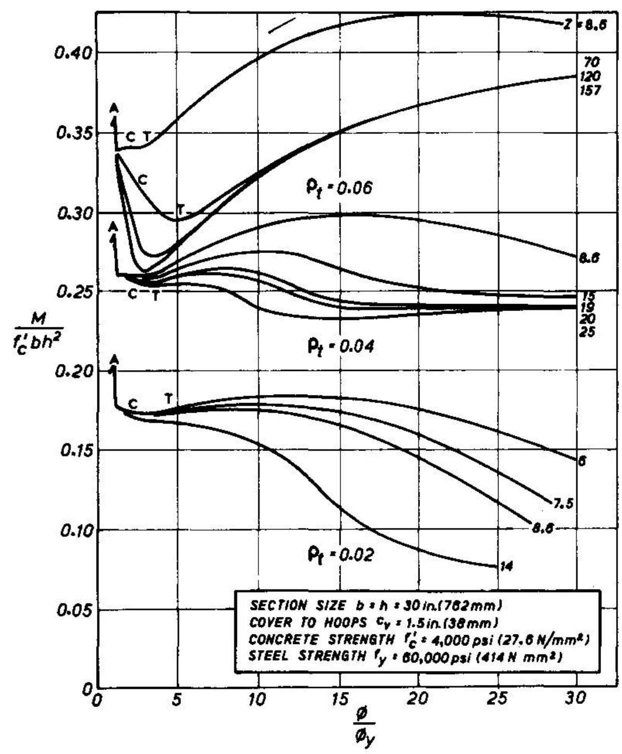

Fig. 5 Moment-Ductility Curves for $P = 0.5f'_cA_g$

and C and T denote the onset of strain hardening of the compression and tension steel, respectively. The curves are drawn from first yielding of the tension steel. Curves for other column sections are available elsewhere (1). The influence of the variables on the moment capacity at high strains may be summarized as follows:

Transverse Steel Content: A large transverse steel content leads to better concrete stress-strain characteristics and therefore the moment capacity is better maintained at large strains.

Longitudinal Steel Content: Sections with large longitudinal steel content rely less on the concrete capacity and therefore the moment capacity is better maintained at large strains.

Axial Load Intensity: A large axial load means a large proportion of the load is carried by the concrete and therefore the moment capacity is reduced at higher strains.

Steel Strength: High strength steel with early strain hardening maintains the moment capacity better than mild steel in which strain hardening does

not commence until higher strains.
Concrete Strength: High strength concrete results in a greater reduction in moment capacity at spalling of the cover concrete.
Cover Ratio: The larger proportion of cover concrete in smaller sections results in a greater reduction in moment capacity at spalling of the cover concrete.

4. APPROACH FOR DETAILING COLUMNS FOR DUCTILITY

The transverse steel requirements for columns can be assessed from the moment-curvature curves by establishing the Z value required to achieve adequate ductility. For seismic design, as discussed in Section 2, the requirement could be a curvature ductility factor φ_u/φ_y of 16 at a moment capacity of not less than 0.85 of the maximum moment capacity. Table 2 shows the Z values meeting this criterion for the sections considered. Where this criterion could not be met with reasonable amounts of transverse steel no Z value is indicated in the table. The Z values corresponding to the ACI code (5) requirements for an axial load level greater than $0.4P_b$ are in the note under Table 1. An axial load level $0.4P_b$ corresponds to approximately 0.12 to $0.18f'_cA_g$ for the sections studied. In general the ACI requirements appear to be conservative for most cases in contrast with results obtained for sections containing mild steel reported previously (2) and by Norton(1). The early onset of strain hardening of high strength longitudinal steel allows the moment capacity to be maintained without such high transverse steel contents.

The Z values shown in Table 2 and Eq. (6) can be used to design the transverse steel of ductile columns. It must be noted however, that the analysis assumes the compression steel does not buckle. The calculated strain in the compression steel at $\varphi_u/\varphi_y = 16$ for each case is included in brackets in Table 2. This is an area of considerable concern since little experimental evidence on the buckling of compression steel is available. Some tests have indicated that in sections with closely spaced hoops strain hardening of mild compression steel can take place without

Table 2 Approximate Z Values Required for a Moment Capacity of 85% of the Maximum Moment Capacity at $\varphi/\varphi_y = 16$ for Concrete $f'_c = 4000$ psi (27.6 N/mm²), Longitudinal Steel $f_y = 60{,}000$ psi (414 N/mm²), $c_v = 1.5$ in (38 mm).

Section Size	Longitudinal Steel Content, ρ_t	Axial Load Level, $\frac{P}{f'_c A_g}$			
		0.1	0.2	0.3	0.5
15 in square (381 mm)	0.02	55(0.019)	16(0.023)	5(0.030)	-
	0.04	127(0.025)	127(0.033)	25(0.037)	9(0.074)
	0.06	127(0.027)	127(0.034)	127(0.040)	127(0.073)
20 in square (508 mm)	0.02	90(0.021)	28(0.025)	14(0.032)	-
	0.04	140(0.026)	140(0.033)	70(0.041)	13(0.067)
	0.06	140(0.027)	140(0.033)	140(0.040)	140(0.068)
30 in square (762 mm)	0.02	157(0.023)	39(0.028)	21(0.034)	7.5(0.057)
	0.04	157(0.025)	157(0.033)	157(0.042)	19(0.059)
	0.06	157(0.027)	157(0.033)	157(0.041)	157(0.061)

buckling occurring. The high Z values in Table 2 should be modified to limit the spacing of hoops to a maximum of 4 in (102 mm) but not greater than 6 longitudinal bar diameters. Serious doubts may exist as to whether some of the large compression steel strains associated with the high axial load levels indicated in Table 2 can be achieved without steel buckling.

It should also be noted that transverse steel is also required in columns to resist shear forces. The transverse steel can play a simultaneous role of confining the concrete, restraining buckling of bars and resisting shear force, but it should always be checked that the transverse steel content is sufficient to resist the shear force induced at the flexural capacity of the column.

5. CONCLUSIONS

The results of this study lead to the following conclusions:

1. The capacity of column sections for post-elastic behaviour is dependent on the level of axial load, the concrete cover to steel ratio, the longitudinal and transverse steel contents and the material strengths. Procedures for detailing transverse steel for ductility should take these factors into account.

2. Columns containing high strength longitudinal reinforcement and sufficient transverse steel can exhibit good ductile characteristics. The required quantity of transverse steel may be obtained from the moment-curvature relationships.

3. The transverse steel required to prevent buckling of the compression steel and shear failure may override the requirements for concrete confinement in some cases.

6. NOTATION

A_g = gross area of column section, A_{st} = total area of longitudinal steel, b = width of section, b" = width of confined core measured to the outside of hoops, c_v = thickness of cover concrete, E_s = modulus of elasticity of steel, f_c = stress in concrete, f'_c = compressive cylinder strength of concrete, f_s = stress in steel, f_{su} = ultimate strength of steel, f_y = yield strength of steel, h = overall depth of member, kd = neutral axis depth, M = moment of resistance, P = axial load on section, P_b = axial load capacity at simultaneous attainment of $\epsilon_{cm} = 0.003$ and yielding of the tension steel, s_h = spacing of transverse hoops, Z = constant defined by Eq. (6), ρ_s = ratio of volume of transverse reinforcement to volume of concrete core, ρ_t = ratio of total area of longitudinal steel to gross area of column section, ϵ_c = strain in concrete, ϵ_{cm} = strain in concrete at extreme compression fibre, ϵ_s = strain in steel, ϵ_{sh} = steel strain at commencement of strain hardening, ϵ_{su} = steel strain at ultimate steel stress, ϵ_y = strain in steel at onset of yielding, φ = section curvature, φ_u = curvature at end of post-elastic range, φ_y = curvature at commencement of yielding of tension steel, Δ_y = lateral deflection at first yield, Δ_u = lateral deflection at end of post-elastic range.

7. REFERENCES

1. Norton, J.A., "Ductility of Rectangular Reinforced Concrete Columns", Master of Engineering Report, University of Canterbury, Christchurch, New Zealand, 1972.
2. Park, Robert., and Sampson, Richard A., "Ductility of Reinforced Concrete Column Sections in Seismic Design", ACI Journal, Proceedings V.69, No. 9, Sept. 1972.
3. "Recommended Lateral Force Requirements and Commentary", Seismology Committee, Structural Engineers' Association of California, San Francisco, 1968 (with 1970 amendment).
4. Uniform Building Code, International Conference of Building Officials, Pasadena, V.1, 1970.
5. ACI Committee 318, "Building Code Requirements for Reinforced Concrete (ACI 318-71)", American Concrete Institute, Detroit, 1971.
6. Park, R., "Ductility of Reinforced Concrete Frames Under Seismic Loading", New Zealand Engineering (Wellington), V.23, No.11, Nov.1968.
7. Park, Robert., Discussion of "Proposed Revision of ACI 318-63, Building Code Requirements for Reinforced Concrete", by ACI Committee 318, ACI Journal, Proceedings V.67, No. 9, Sept. 1970.
8. Kent, D.C. and Park, R., "Flexural Members with Confined Concrete", Proceedings, ASCE, V.97, ST7, July 1971.

SUMMARY

The ductility required of eccentrically loaded reinforced concrete column sections in seismic design is discussed. A theoretical method for the determination of the amount of transverse steel required for flexural ductility is described. The method is based on assumed stress-strain curves for confined concrete and steel, and takes into account the required ultimate curvature, the level of axial load, the longitudinal steel content, and material strengths. Moment-curvature curves for columns reinforced longitudinally by high strength steel are derived and transverse steel contents for such columns suggested.

RESUME

On traite de la ductilité des colonnes en béton armé à charge excentrée qui doivent résister aux séismes. On décrit une méthode théorique pour déterminer la quantité d'armature transversale nécessaire pour obtenir la ductilité requise. Cette méthode se base sur l'hypothèse de courbes tension-déformation pour le béton et les armatures, et tient compte également de la courbure ultime exigée, de la grandeur de la charge axiale, du pourcentage d'armature longitudinale et de la résistance des matériaux. On obtient des diagrammes moment - courbure pour les colonnes avec armature longitudinale en acier à haute résistance, et on propose des pourcentages pour les armatures transversales.

ZUSAMMENFASSUNG

Im vorliegenden Beitrag wird das erforderliche Verformungsvermögen exzentrisch belasteter Stahlbetonstützen-Querschnitte bei Erdbebeneinflüssen diskutiert. In der Folge wird eine theoretische Methode zur Bestimmung des Bewehrungsgehalts beschrieben, welcher ausreichendes Verformungsvermögen gewährleistet. Die Methode beruht auf angenommenen Spannungs-Dehnungs-Diagrammen für Beton und Stahl und berücksichtigt die erforderliche maximale Krümmung, die Grösse der Normalkraft, den Längsbewehrungs-Gehalt und die Materialfestigkeiten. Es werden Moment/Krümmungs-Diagramme für in der Längsrichtung mit hochfestem Stahl bewehrte Stützen abgeleitet und der Anteil an Querbewehrung für solche Stützen vorgeschlagen.

Leere Seite
Blank page
Page vide

Experimental Research on Ductility of Reinforced Concrete Short Columns under Cyclic Lateral Loads

Recherche expérimentale sur la ductilité de colonnes courtes en béton armé soumises à des charges latérales répétées

Experimentelle Untersuchungen über das Verformungsvermögen von kurzen Stahlbetonstützen unter wiederholten Querbelastungen

Yoichi HIGASHI
Professor of Structural Engineering
Department of Architecture
Tokyo Metropolitan University

Masaya HIROSAWA
Research Member of Structural Division
Building Research Institute
Ministry of Construction

Tokyo, Japan

1. INTRODUCTION

In such a country as Japan where severe earthquakes occur so often, structural safety of buildings is dominated distinguishly by earthquake. It is gradually becoming apparent by many strong motion earthquake observations, response analyses and earthquake damage observations that the influence of earthquake to structures is fairly superior to the simulated earthquake load which is usually regulated as design seismic force coefficient in many countries. Actually, at the Tokachi-Oki earthquake, 1968, several buildings, whose yield shear coefficients are more than 0.5, were destroyed.

It is generally impossible and uneconomical to make all buildings so strong as to resist severe shocks only by their strength. However, it also became apparent by many response analyses that the buildings with adequate strength and full ductility can survive even at a severe shock.

As it is said that the reinforced concrete buildings with short length columns are considered to fail in brittle way, synthetic experimental research was started with the objective, how to make the short columns ductile. This research is sponsored by Ministry of Construction of Japan and a committee was organized for the execution of this big project. This committee was consisted from not only official researchers but also ones belonging to technical branches of general constructions companies. The members are refered to §7 ACKNOWLEDGEMENT.

About the results on 125 specimens, failure mode and factors which affect ductility are discussed in this report.

2. EPITOME OF EXPERIMENT

2.1 Master Plan for Experiment

Mean unit axial stresses of the columns at the first story due to permanent load in usual reinforced concrete low stories buildings in Japan, are about 40 kg/cm^2. Assuming 0.4 as yield shear coefficient, mean unit shear stresses at a severe shock are generally less than 20 kg/cm^2. The web reinforcements required for such a stress condition as above will not become excessively much and it will be not so difficult to execute them well.

Accordingly, combinations of tensile reinforcement ratio and shear span ratio were selected at first so that their maximum flexural capacities do not become excessively large under constant axial stresses 40 kg/cm^2. Next such reinforcing details as quantity, spacing and shape of web reinforcement and arrangement of axial reinforcement were selected.

2.2 Outline of Tested Series and Specimens

1) Variable Factors

Based on the past experimental research results, the committee selected ten factors affecting ductility. They are shown in Table 1 as from F1 to F10. Further, after investigations for these factors of many existing reinforced concrete buildings, standard values and characteristics for several variables were decided as shown in Table 1.

Out of them, how to decide the standard size of cross section related to scale effect, web reinforcement ratio, loading cycling and loading apparatus are described in the followings.

2) Scale Effect

There seems not to be the reliably available data concerning scale effect. And further, due to the limited budget and facilities, it is practically impossible to carry out all the tests in full scale. So, the standard size of cross section was decided to be 25 cm square and one series were carried out using 50 cm square cross section to discuss scale effect.

3) Web Reinforcement Ratio

The method to calculate reasonable web reinforcement ratio for ductile column has not been established up to date. So, it was decided to use tentatively the Arakawa's minimum equation (Cf. § 4.2, eq. (1)) to set the standard web reinforcement ratio. This equation is the experimental one showing the minimum shear strength of reinforced concrete members without axial force and was used as a back datum to decide the regulations of A.I.J. standard in Ref. 1) for shear reinforcement. One of the standard value of web reinforcement ratio was set as P_{w1} which can be obtained by equating the flexural capacity ${}_{C}Q_{FU}$ (Cf. § 4.2, eq. (2)) to the Arakawa's minimum equation. This aimed to raise the shear strength of the column up to the flexural strength, because the flexural yielding shows good ductility. And, the half of P_{w1} was adopted as another standard value as the example of poor shear strength.

TABLE 1 LIST OF FACTORS COMMON TO SPECIMEN

	COMMON FACTORS	NOTE
F1	Section: b x D = 25 x 25 cm, d_t=d_c=3.5 cm	SE Series: b x D = 50 x 50 cm, d_t=d_c=7.0 cm
F2	Concrete: Normal concrete, F_c=210 kg/cm^2 (Design)	FC Series: F_c = 350 kg/cm^2 (Design)
F3	Shape of web reinforcement: Rectangular hoop with a standard hook at each end	PILOT Series: Welded rectangular hoops used in the half of specimens
F4	Web bar: SR24 Round bar	Specified yield point of 2400 kg/cm^2
F5	Axial bar: SD35 Deformed bar	Specified yield point of 3500 kg/cm^2
F6	Tensile reinforcement ratio: p_t=0.34% (3-D10), 0.61% (3-D13), 0.95% (3-D16)	PILOT Series: p_t= 0.41% (2-D13), 1.24% (2-D22) AF Series: p_t=1.38% (3-D19)
F7	Shear span ratio M/QD: M/QD = 1 and 2	PILOT and LS Series: M/QD = 1.5 and 3.0
F8	Axial stress: N/bD = 210/4 and 210/8 kg/cm^2	30 kg/cm^2 (PILOT S.), 0 and -210/10 kg/cm^2 (AF S.)
F9	Web reinforcement ratio: by Arakawa's min. Equation	PILOT Series: by A.I.J. Equation
F10	Loading method: Restrained column type, reversal loading of multi cycles	WAKABAYASHI-type (PILOT S.), Inverse-Symmetrical-type (LM1, SE S.), B.R.I.-type (other series)

4) Loading Excursion

Until a certain rational dynamic method is established for estimating seismic properties of structural members, it seems difficult to discuss them by some special vibration test results. Accordingly we must adopt a certain rational, static, cyclic loading method. In this research, such a multi-cyclic alternate loading method as shown in Fig. 1 was adopted as standard loading excursion. This mainly depends on the following reasons.

a) Ductility factors μ obtained through response analyses of not so highrized buildings at severe shocks are about 3 or 4 at most, if their strength and ductility are not excessively small.

b) The number of acceleration responses corresponding to more than 80% of the maximum value has been reported to be about 10 times in some cases.

c) Structural behavior of members under cyclic loading at constant deflection tends to become apparent within 10 cycles.

5) Loading System

In most of past experiment, simple beam systems are used world-widely as the loading system for structural members. However, this method is not so good to discuss seismic behavior of reinforced concrete column, because of the following reasons.

a) When discussing shear and bond problems of members, restrained column type is more similar to the real condition of columns in actual buildings during an earthquake than simple beam is.

b) It is more similar to the real condition that both sections at column ends keep pararel to each other than that they have some inclinations.

c) Discussing behaviors under large deflection, it is preferable that the influence of additional moment due to eccentric axial load can be easily estimated.

d) It is preferable that many cycles of load reversals can be easily carried out and that developing of cracks can be easily observed and recorded.

So, such a new loading apparatus as shown in Fig. 2 was developed and was used to test many series. Still more, in order to discuss the influence of loading systems, two series were carried out by continuous beam system.

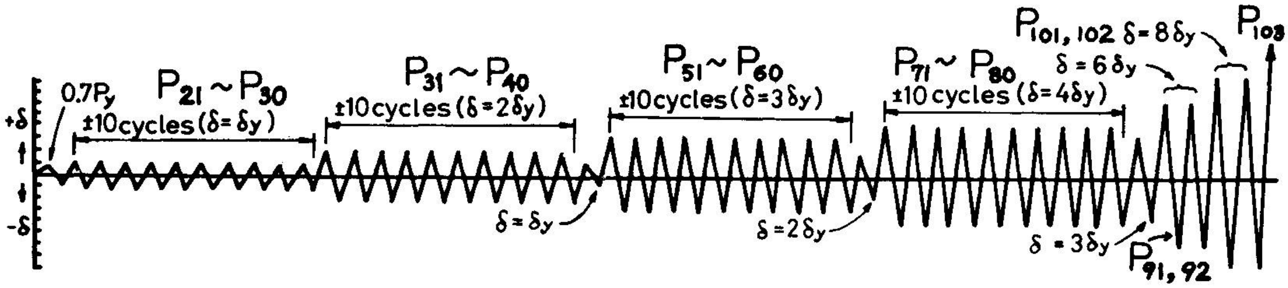

P_{mn}: Load at test equals shear force Q of specimen, (mn; loading number).

P_y: Load when tensile reinforcement yields at test, ($P_y = P_{21}$).

δ_y : Measured horizontal displacement at yielding.

FIG. 1 LOADING PROCEDURE USED IN ALL SPECIMENS

2.3 Constitution of Typical Series and Specimens

On the basis of the previous discussions, it was decided that a typical series is constituted from 15 specimens taking 3 kinds of tensile reinforcement ratio p_t, 2 kinds of shear span ratio M/QD, 2 kinds of axial compression stress σ_0 and 2 kinds of web reinforcement ratio p_w as variable factors. A list of specimens belonging to a typical series is shown in Table 2. In other series, each common factors, for example $c\sigma B$ or size of section etc., was changed one by one. Fig. 3 shows an example of specimen details.

Ten series, including 165 specimens in total, as shown in Table 3 had been tested already and the results on the upper seven series in the table are discussed in this report. In Fig. 4, frequency distributions of σ_0, M/QD, p_t and p_w of the 125 specimens are shown with their failure modes and classified ductilities which are described as follows.

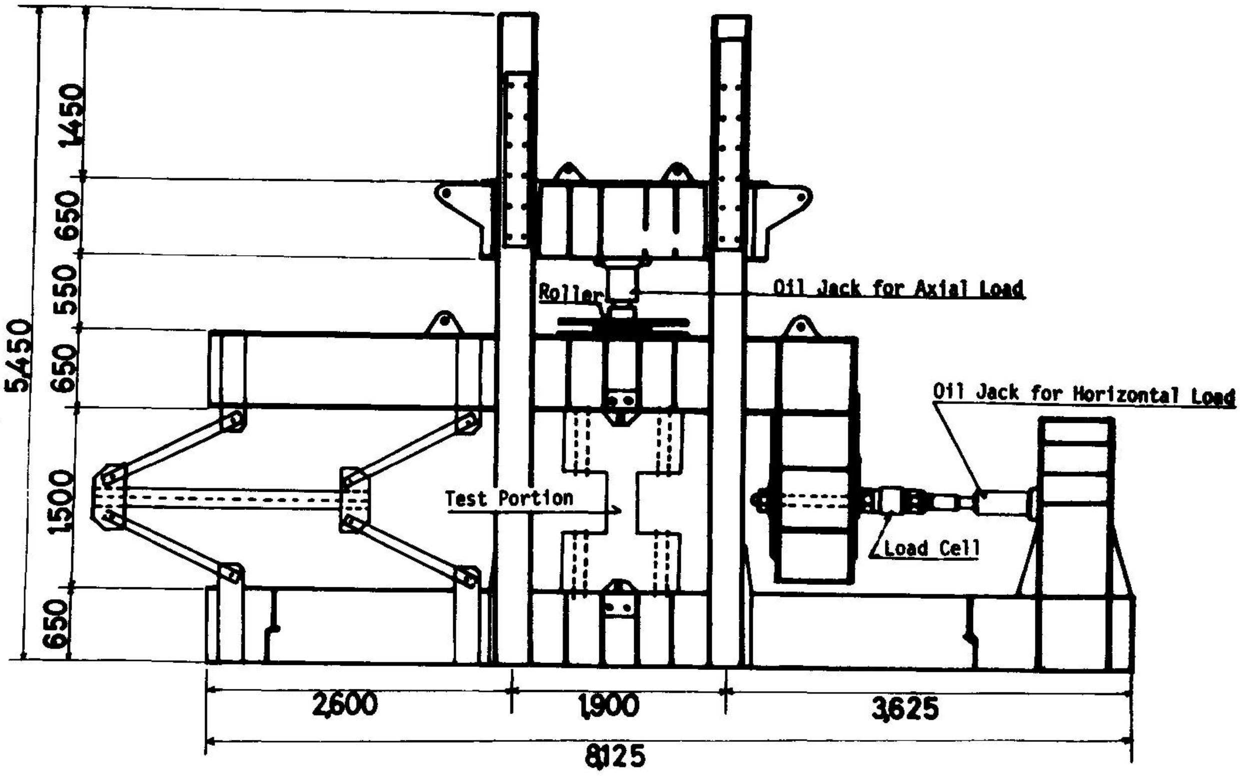

FIG. 2 B.R.I.-TYPE LOADING APARATUS

TABLE 2 LIST OF SPECIMENS BELONG TO A TYPICAL SERIES

Mark	Tensile Reinforcement	Tensile Reinforcement Ratio	Shear Span Ratio	Web Reinforcement	Web Reinforcement Ratio	Axial Unit Stress
	Number-Size	$p_t = a_t/bD$ (%)	$\frac{M}{QD}$	Number-Size-Spacing (mm)	$p_w = a_w/bs$ (%)	$\sigma_0 = N/bD$ (kg/cm²)
1B	3-D10	0.34	1	16- 9 - 33.3	1.53	210/4
2A	3-D10	0.34	2	15- 9 - 71.5	0.71	210/4
2B	3-D10	0.34	2	17- 6 - 62.5	0.36	210/4
3A	3-D10	0.34	1	10- 9 - 55.5	0.92	210/8
3B	3-D10	0.34	1	11- 6 - 50.0	0.45	210/8
4A	3-D10	0.34	2	10- 4 - 55.5	0.18	210/8
4B	3-D10	0.34	2	10- 4 - 111.1	0.09	210/8
5A	3-D13	0.61	1	12-13 - 45.5	2.33	210/8
5B	3-D13	0.61	1	12- 9 - 45.5	1.12	210/8
6A	3-D13	0.61	2	24- 6 - 43.5	0.51	210/8
6B	3-D13	0.61	2	28- 4 - 37.0	0.27	210/8
7A	3-D16	0.95	2	24- 4 - 43.5	2.44	210/4
7B	3-D16	0.95	2	25- 9 - 41.7	1.22	210/4
8A	3-D16	0.95	2	26- 9 - 40.0	1.27	210/8
8B	3-D16	0.95	2	28- 6 - 37.0	0.61	210/8

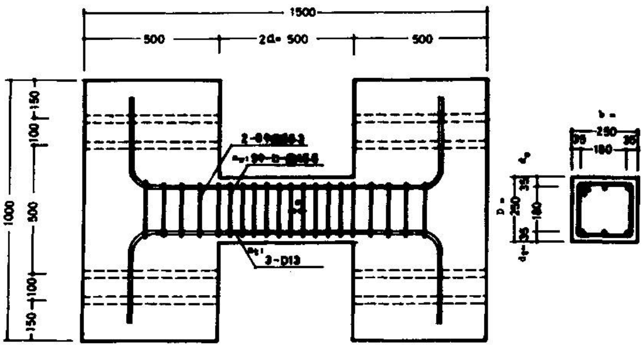

FIG. 3 AN EXAMPLE OF SPECIMEN DETAILS (Unit in mm)

TABLE 3 LIST OF TEST SERIES

Name of Series	Section of Specimen (cm x cm)	Shear Span Ratio (M/QD)	Loading *1 System	Institution *2 in Charge	Year	Main Objective	Number of Specimens
Pilot	25 x 25	1.5, 3.0	W - Type	B.R.I.	1971	Welded Hoop	36
LM1	25 x 25	1.0, 2.0	R,B - Type	T.I. of Takenaka Komuten	1972	Loading System Scale Effect	15
LM2	25 x 25	1.0, 2.0	BRI - Type	Tokyo Institue of Technology	1972	Loading System	15
SE	50 x 50	1.0, 2.0	R,B - Type	Meiji Univ. and B.R.I.	1972	Scale Effect	15
FC	25 x 25	1.0, 2.0	BRI - Type	T.I. of Taisei Const. Co., Ltd.	1972	Concrete Strength	14
WS	25 x 25	1.0, 2.0	BRI - Type	T.I. of Obayashi-Gumi Co., Ltd.	1973	Welded Hoop of Deformed Bar	15
AF	25 x 25	1.0, 2.0	BRI - Type	T.I. of Fujita Kogyo	1973	Axial Force	15
CW	25 x 25	1.0, 2.0	BRI - Type	Tokyo Metropo-litan Univ.	1973	Columns with Side Wall	10
WS2	25 x 25	1.0, 2.0	BRI - Type	T.I. of Kajima Const. Co., Ltd.	1973	Spiral Hoop	15
LS	25 x 25	1.5, 3.0	BRI - Type	T.D.C. of Toda Const. Co., Ltd.	1973	Shear Span Ratio	15

*1 W - Type : Loading System devised by Dr. Wakabayashi
R,B - Type : Restrained Beam Type
BRI - Type : Loading System newly developed in B.R.I.

*2 T.I. : Technical Institute
T.D.C. : Technical Development Center

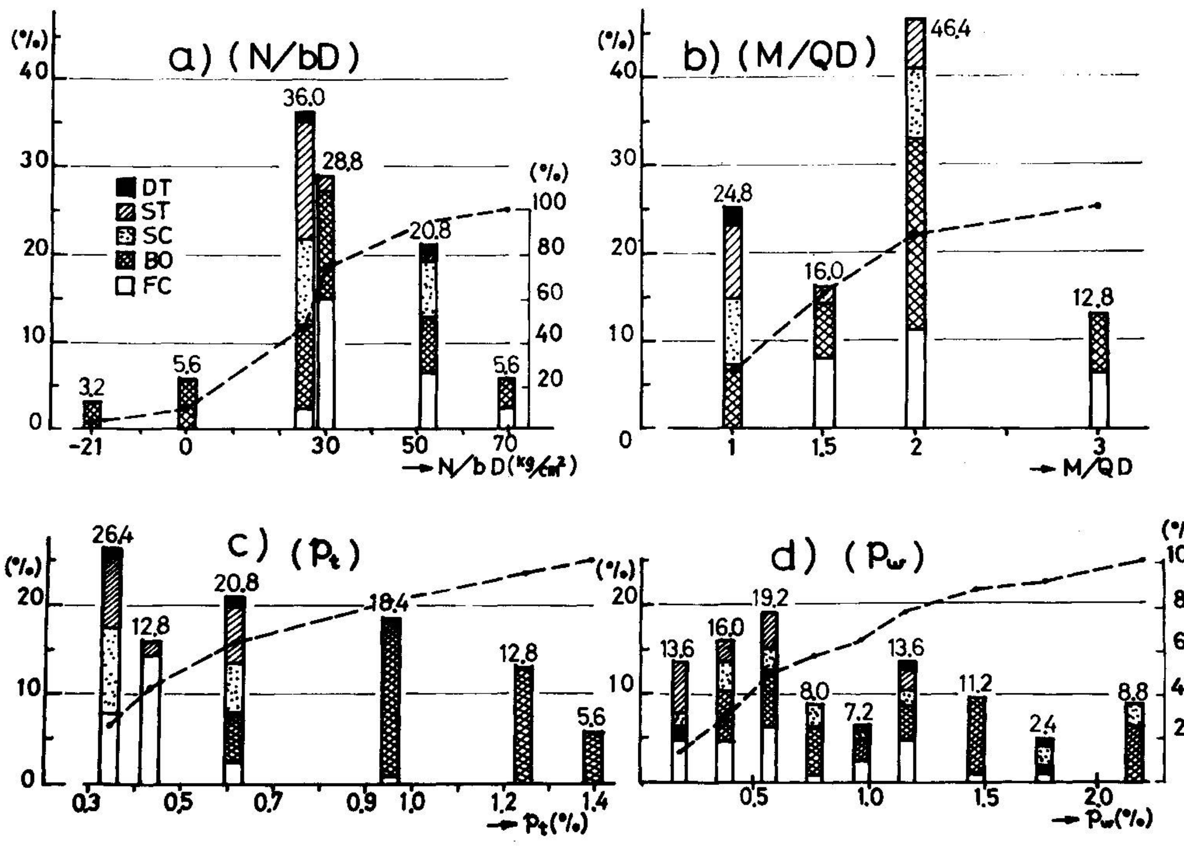

FIG. 4 FREQUENCY DISTRIBUTION OF σ_0, M/QD, p_t and p_w

3. OUTLINE OF TEST RESULTS

3.1 Failure Mode of Tested Specimens

Followings are the typical failure modes observed in the test.

1) Compression failure of concrete after flexural tensile yielding with or without compression steel buckling. - F (flexural yielding), F•C (after flexural yielding, failed by crushing of concrete), F•C•Bu (after flexural yielding and crushing, failed by buckling of compression bar).
2) Shear failure before or after flexural yielding. - S•DT (after shear cracking, failed by diagonal tension), S•ST (after shear cracking, failed by shear tension), F•ST (after flexural yielding, failed by shear tension), S•SC (after shear cracking, failed by shear compression), F•SC (after flexural yielding, failed by shear compression).
3) Bond split failure before or after flexural yielding. - B•BO (after bond cracking, failed by bond split), F•BO (after flexural yielding, failed by bond split).

3.2 Classified Ductility

In this report, test results were classified by the ductilities defined in Table 4, based on their critical deflections δ and their ductility factors δ/δ_y, (δ_y shows yeilding deflection).

3.3 Relationship between Failure Modes and Classified Ductilities

Test results of 125 specimens were classified by their failure modes and classified ductilities, and their relationships and their frequencies are shown in Fig. 5. As observed in these figures, the most ductile failure mode is F•C type and next one is S•C type. Many specimens which were failed in ST type and BO type showed poor ductilities. Accordingly, it becomes one of the important subjects how to prevent such brittle failure modes as SC type, ST type and B type.

TABLE 4 CLASSIFIED DUCTILITY

DUCTILITY	CHARACTERISTICS
A	Very ductile columns which failed by shear or by buckling of compression bars at horizontal large deflection. ($P_{21} \sim P_{91} \geqq 0.8{}_cQ_{FU}$, ${}_cQ_{FU}$: Flexural strength obtained by A.I.J. formula)
B	Ductile columns, whose deterioration of shear capacity were small untill $\mu = 4$, ($\mu = \delta / \delta_y$), but which failed by shear or by bond or by buckling of bar before $\mu = 6$. ($P_{21} \sim P_{71} \geqq 0.75{}_cQ_{FU}$)
C	Columns yielded by flexure at first, but deteriorated remarkably due to shear or bond failure or buckling of bars before they reached to large deflection. ($P_{21} \sim P_{31} \geqq 0.75{}_cQ_{FU}$)
D	Columns failed by shear or by bond before flexural yielding. (Others than A, B and C)

Also, load-deflection relationships, cracking patterns and shear force capacity deteriorations of the typical specimens are shown in Fig. 6, 7 and 8 respectively.

4. DISCUSSION ON TEST RESULTS

4.1 Axial Reinforcement Buckling

Out of 32 specimens which failed in F·C typed mode, bucklings of axial compression reinforcements were observed in 24 specimens. In 10 specimens, buckling occurred at the ductility factors $\mu = 2\sim4$ and caused the strength deterioration. Discussing these results, are as follows.

1) Lengths of buckling ℓ_k were around 1 ~ 2 times spacings of web reinforcement s. But in case of spiral hoops and welded square hoops, ℓ_k was nearly equal to s.
2) The relationship between slenderness ratio λ calculated assuming ℓ_k equals s, and the rotation angle ($R = \delta/2a$) of the member at buckling R_{BU} was investigated about all specimens. By this result, when λ is more than 34, R_{BU} becomes between 1/100 and 1/50, but when λ is less than 34, buckling did not occur until fairly large deflection.
3) The above results are expressed $s \leqq 8\phi$ where ϕ shows the diameter of compression reinforcement. Namely, it is preferable to space the web reinforcements at column ends less than 8 times diameter of axial reinforcement.

4.2 Shear Failure Mode

41 specimens failed by shear before or after flexure yielding. They can be divided to 10 specimens failed by diagonal tension, 12 by shear tension and 19 by shear compression.

1) General Discussion by means of Arakawa's Formula

As there is no quantitative equation concerning the relationship between ductility of members and web reinforcement ratio, general discussion was at first done by Arakawa's formula which was used as the ground to calculate web reinforcement of our specimens.

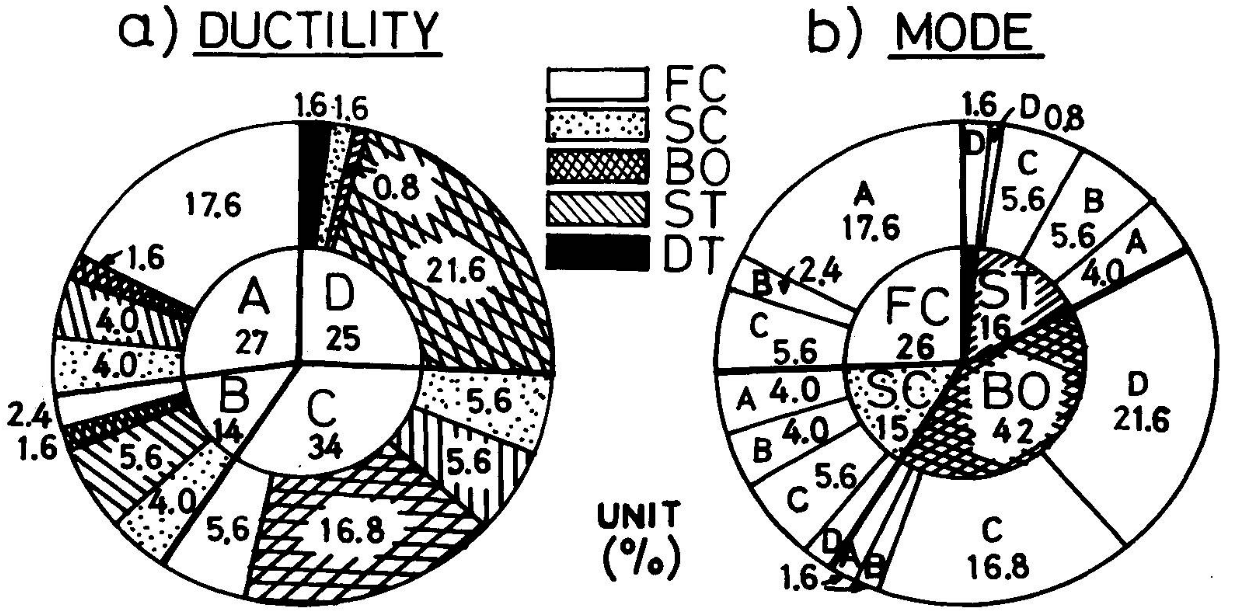

FIG. 5

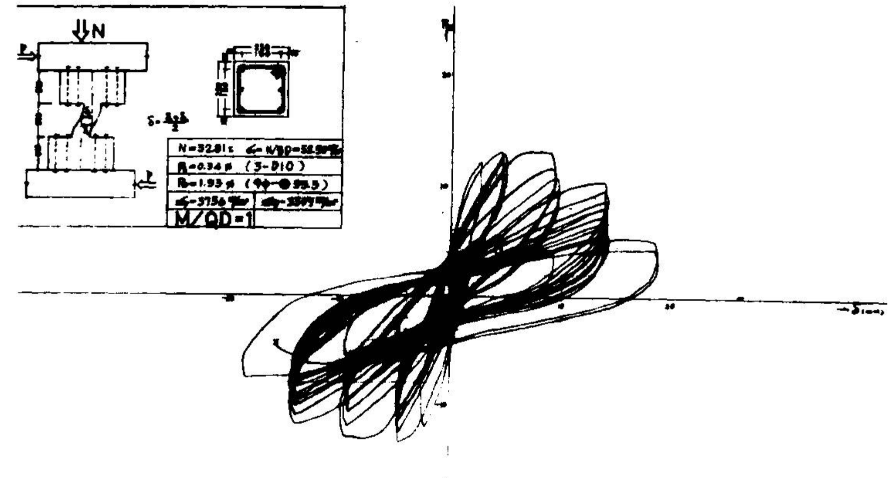

a) LM2-1B (S•DT, Ductility D)

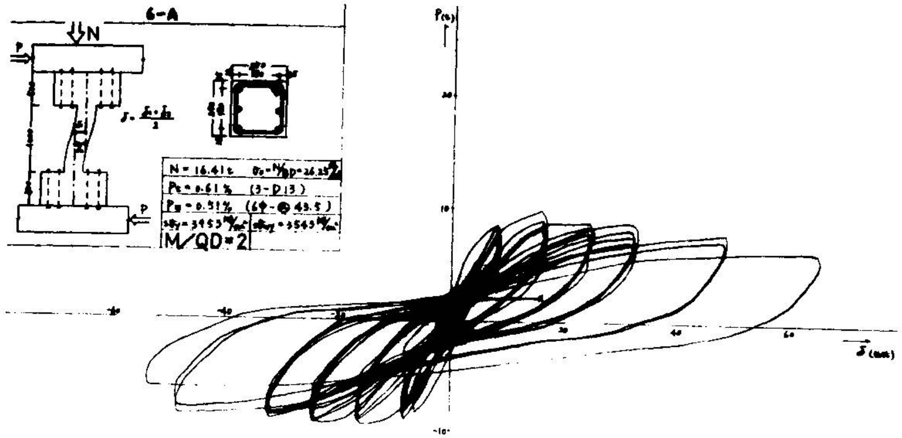

b) LM2-6A (F•SC, Ductility A)

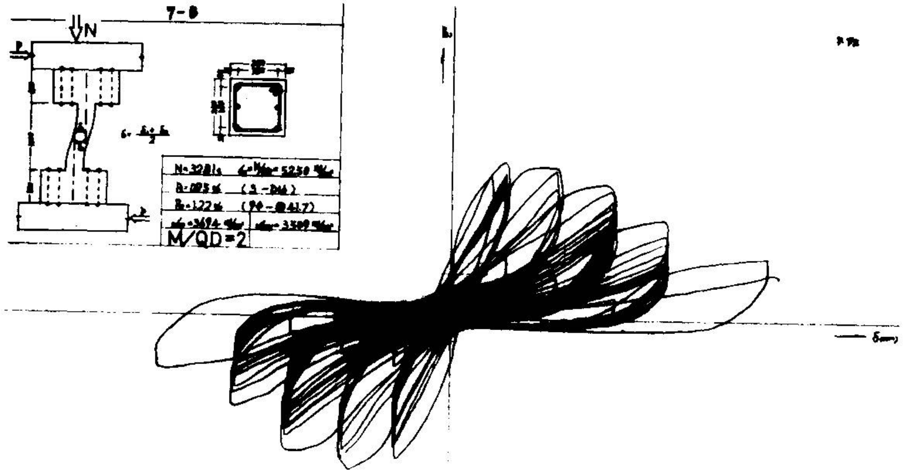

c) LM2-7B (F•BO, Ductility D)

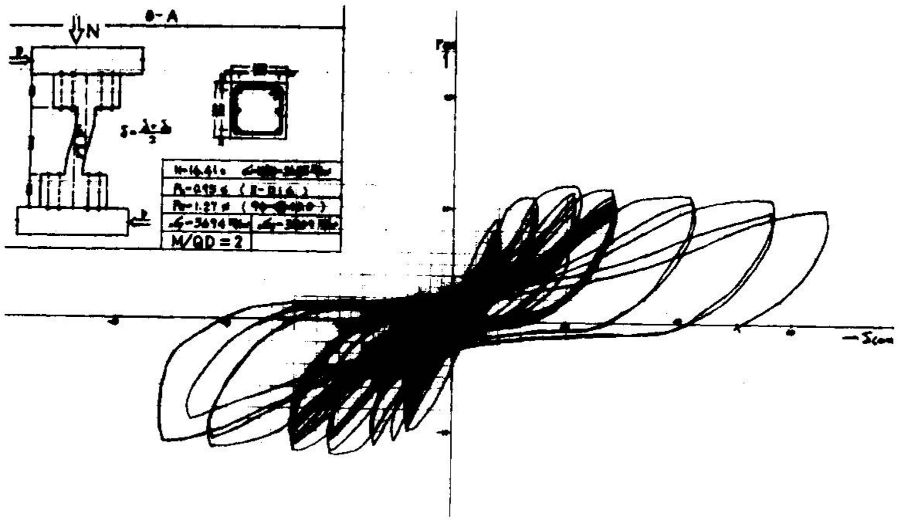

d) LM2-8A (FC, Ductility B)

FIG. 6 LOAD - DEFLECTION CURVES

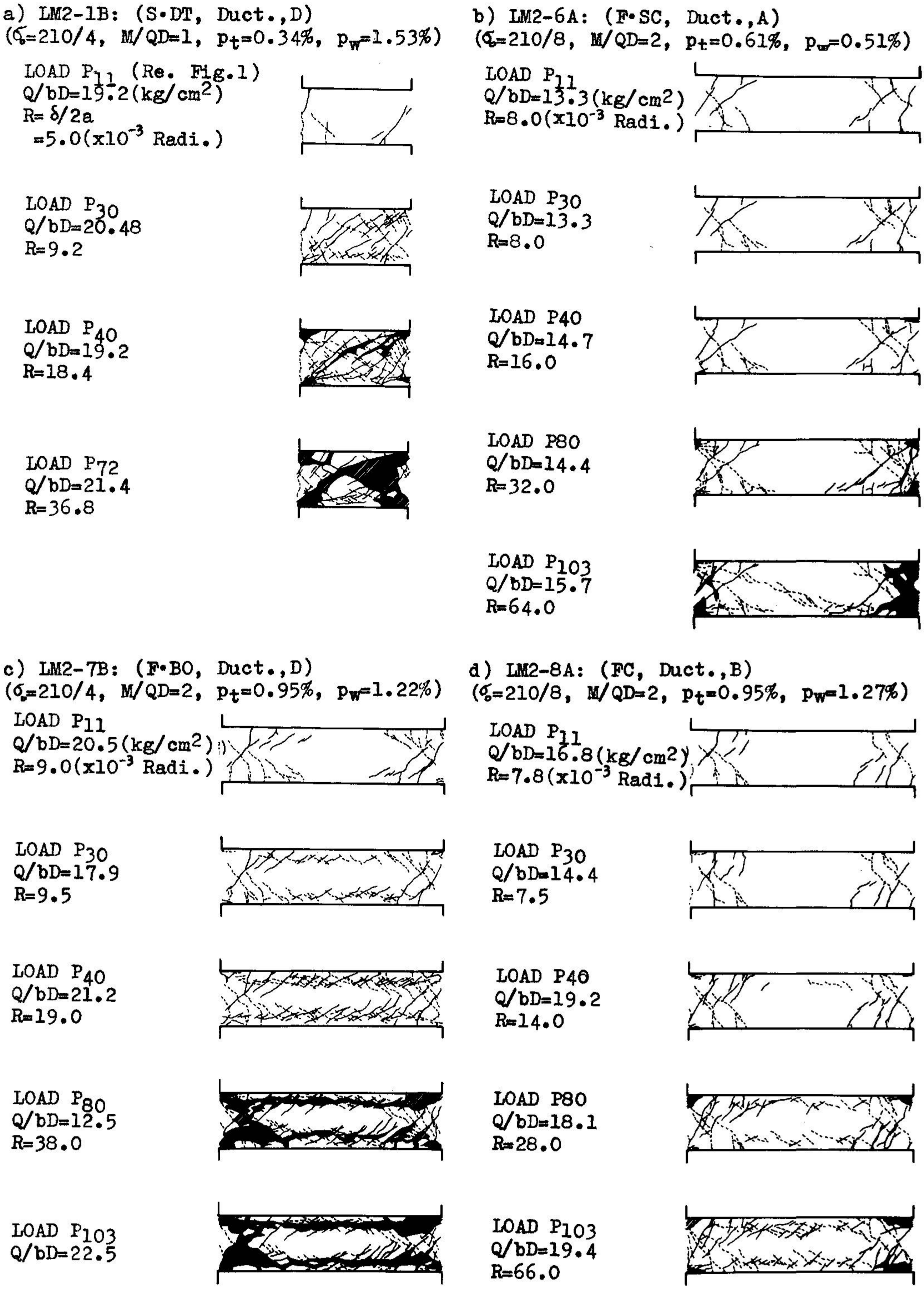

FIG. 7 CRACKING PATTERNS

Namely, we investigated the relationship between the classified ductility and ratio of calculated shear strength $_cQ_{ARA}$, to calculated flexure strength when the column yield at both ends $_cQ_{FU}$. The formulae used to calculate $_cQ_{ARA}$ and $_cQ_{FU}$ are shown in the followings. The notations used in the formulae are refered to §8.

$$_cQ_{ARA} = \frac{0.0754\ P_t^{0.23}\ K_U(_c\sigma_B + 180)}{M/Q_d + 0.12} + 2.7\sqrt{p_w \cdot {_s\sigma_{wy}}} \times \frac{7}{8}\ bd \qquad (1)$$

here $K_U = 0.80$ (d = 21.5 cm), 0.72 (d = 43 cm); scale factor

$$_cQ_{FU} = a_t \cdot {_s\sigma_y} \cdot g + 0.5ND\left(1 - \frac{N}{bD \cdot {_c\sigma_B}}\right) / a \qquad (2)$$

The results except 52 specimens which failed by bond-split are shown in Fig. 9. As observed, when the ratio $_cQ_{ARA}/_cQ_{BU}$ is larger than unit, the classified ductility is A or B except several cases, and when the ratio is less than unit, the ductility is almost C or D. However, as Qmax/bd becomes larger, the ductility tended to become poor.

2) Diagonal Tension Failure

At first, initial diagonal tension cracking load Q_{DTC}, was investigated. The theoretical value $_cQ_{DTC}$ was obtained to put the tensile principal stress, which was calculated on the center of the section neglecting the appearance of

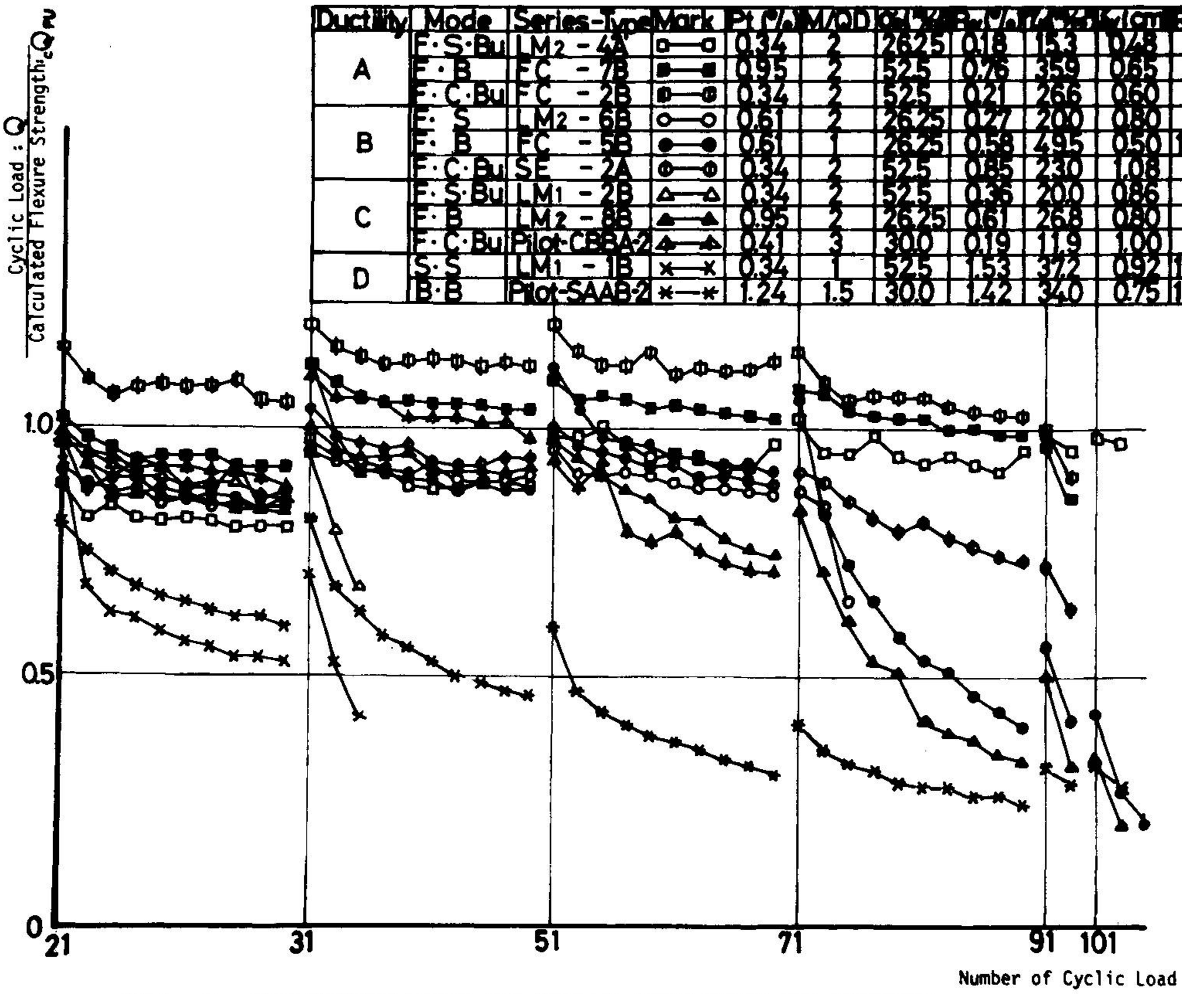

Ductility	Mode	Series-Type	Mark	Pt (%)	M/QD	[illegible]	[illegible]	[illegible]	[illegible]	[illegible]
A	F·S·Bu	LM2 - 4A	□—□	0.34	2	26.25	0.18	15.3	0.48	4.8
	F·B	FC - 7B	■—■	0.95	2	52.5	0.76	35.9	0.65	6.5
	F·C·Bu	FC - 2B	⊕—⊕	0.34	2	52.5	0.21	26.6	0.60	6.0
B	F·S	LM2 - 6B	○—○	0.61	2	26.25	0.27	20.0	0.80	8.0
	F·B	FC - 5B	●—●	0.61	1	26.25	0.58	49.5	0.50	10.0
	F·C·Bu	SE - 2A	Φ—Φ	0.34	2	52.5	0.85	23.0	1.08	5.4
C	F·S·Bu	LM1 - 2B	△—△	0.34	2	52.5	0.36	20.0	0.86	8.6
	F·B	LM2 - 8B	▲—▲	0.95	2	26.25	0.61	26.8	0.80	8.0
	F·C·Bu	Pilot-CBBA-2	∆—∆	0.41	3	30.0	0.19	11.9	1.00	6.67
D	S·S	LM1 - 1B	×—×	0.34	1	52.5	1.53	37.2	0.92	18.4
	B·B	Pilot-SAAB-2	✱—✱	1.24	1.5	30.0	1.42	34.0	0.75	10.0

FIG. 8 DETERIORATION OF SHEAR CAPACITY BY CYCLIC LOADING IN TYPICAL SPECIMENS

other cracks and the influence of axial reinforcements, equals to the tensile strength of concrete ${}_{c}\sigma_t$ which was assumed equal to $1.8\sqrt{{}_{c}\sigma_B}$. Here, ${}_{c}\sigma_B$ shows the compressive strength of concrete. The result is as follow.

$$ {}_{c}Q_{DTC} = \frac{{}_{c}\sigma_t}{1.5} bD\sqrt{1 + \frac{\sigma_o}{{}_{c}\sigma_t}} \tag{3}$$

The ratios of test results ${}_{T}Q_{DTC}$ to calculated values concerning 23 specimens in which diagonal tension cracks appeared, were deviated from 0.66 to 1.13 and the average was 0.87.

Next, the critical web reinforcement p_{WDTC} was calculated assuming that web reinforcements carry the diagonal tension lost by the appearance of this crack. The result is as follow.

$$ p_{WDTC} = \frac{{}_{c}\sigma_t}{\cos\theta \cdot {}_{s}\sigma_{wy}} \tag{4}$$

$$ \text{here} \qquad \theta = \frac{1}{2}\tan^{-1}\left\{2\sqrt{\frac{{}_{c}\sigma_t}{\sigma_o} + \left(\frac{{}_{c}\sigma_t}{\sigma_o}\right)^2}\right\} \tag{4.1}$$

Taking the values of p_w/p_{WDTC} and ${}_{T}Q_{max}/{}_{C}Q_{DTC}$ as the ordinate and the abscisa respectively, test results except bond-split failured specimens were plotted in Fig. 10 with their failure mode. Here, ${}_{T}Q_{mas}$ and p_w mean the tested maximum shear strength and web reinforcement ratio, respectively.

It is observed in this figure that the specimens, in which ${}_{T}Q_{max}$ are more than about 0.8 ${}_{C}Q_{DTC}$ and p_w are less than p_{wDTC}, show the diagonal tension failure mode.

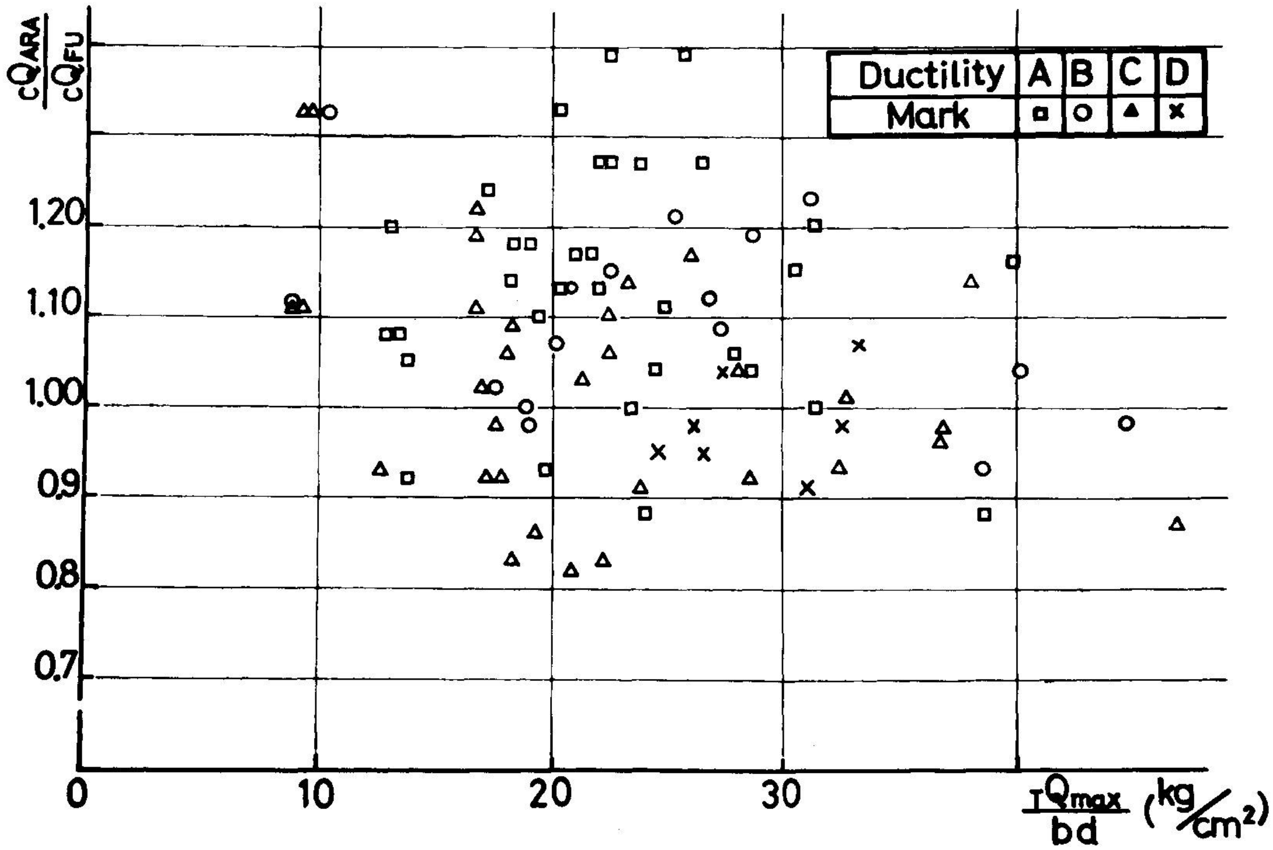

FIG. 9

3) Shear Tension Failure

At first, initial shear tension cracking load Q_{STC} was investigated. The theoretical value ${}_cQ_{STC}$ was calculated by the following formula which was derived semi-theoretically with some assumptions.

$$ {}_cQ_{STC} = 0.589\, K_0 \cdot {}_c\sigma_t \cdot bD \qquad (5.1)$$

When $a_1 = M/Qd < 0.75 + 0.283\, K_0$

$$ {}_cQ_{STC} = \left\{ 0.78 - 1.04a_1 + \sqrt{(0.78 - 1.04a_1)^2 + 0.694K_0^2} \right\} {}_c\sigma_t \cdot bD \qquad (5.2)$$

When $a_1 \geqq 0.75 + 0.283\, K_0$

here $K_0 = \sqrt{\dfrac{{}_c\sigma_t + \sigma_0}{{}_c\sigma_t}}$

The ratios of ${}_TQ_{STC}$ to ${}_cQ_{STC}$, concerning 119 specimens in which shear tension cracks appeared, were deviated from 0.62 to 1.59 and the average was 0.91.

Next, the following equation of critical web reinforcement ratio p_{WST} which will be required for the specimens to reach flexure strength after shear tension cracking was derived with some assumptions.

$$ p_{WST} = \frac{1.6\, j x l \cdot p_t \cdot {}_s\sigma_y}{a_1^{\,1.25} \cdot {}_s\sigma_{wy}} \qquad (6)$$

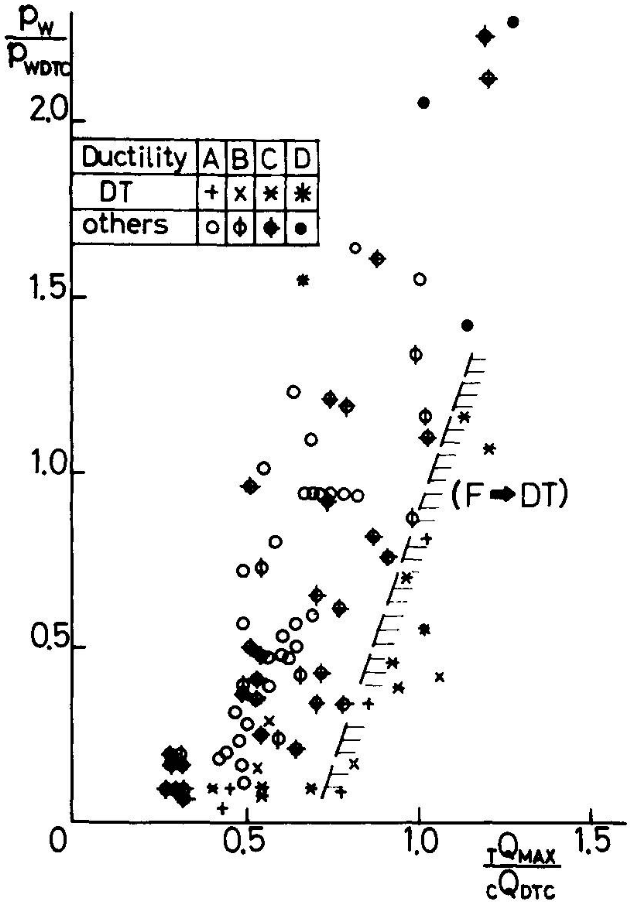

FIG. 10

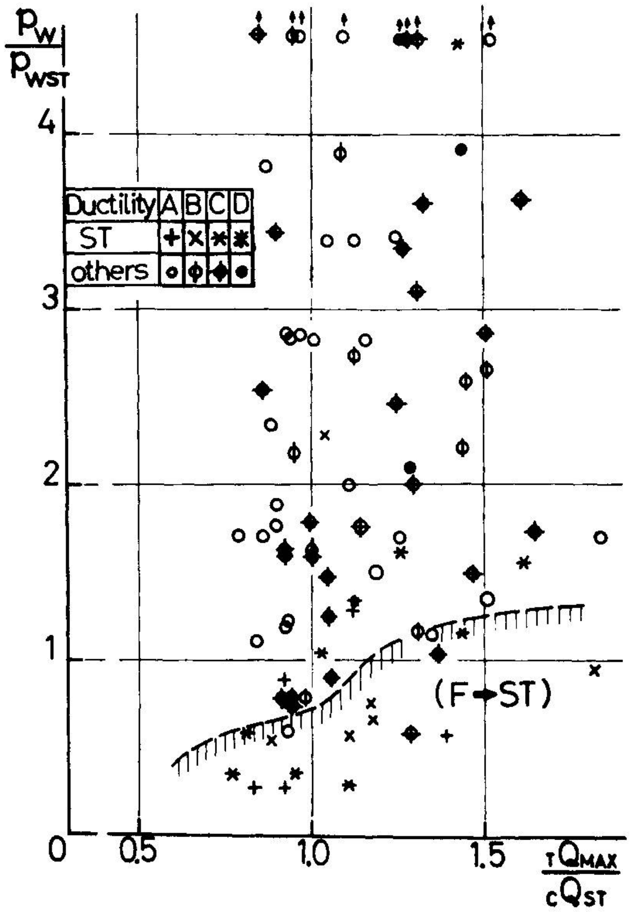

FIG. 11

here $$j_{x1} = \frac{d - x_n}{D} = d_1 - \frac{\sigma_o + p_t \cdot {}_s\sigma_y \cdot a_1{}^{-0.75}}{0.85_c\sigma_B} \tag{6.1}$$

Taking the values of p_w/p_{wST} and ${}_TQ\max/{}_cQ_{STC}$ as the coordinates, test results except bond-split failured specimens were plotted in Fig. 11 with their failure mode. As shown, there are many specimens whose values of ${}_TQ\max$ are more than ${}_cQ_{STC}$, however the specimens with ${}_TQ\max$ more than about 0.8 ${}_cQ_{STC}$ but p_w less than p_{wST} show shear-tension failure mode.

4) Shear Compression Failure

As shear compression failure mode is caused essentially by collapse of compression concrete, it is easily presumed that there will be some conditions where adequate ductility cannot be expected even with much web reinforcements. In this report, we could not succeed to show the conditions definitely. However, we could find out some tendencies as follows.

First, it is necessary to get good ductility that axial stress is not so high and influence of shear stress is not so large. Accordingly, the distance from neutral axis to compression fiber Xn was roughly calculated neglecting compression reinforcement as shown in the following and the ratio of tensile principal stress to concrete tensile strength $\sigma_1/{}_c\sigma_t$ was calculated assuming that all of shear force is carried only by compression concrete at the critical section.

$$Xn1 = \frac{Xn}{D} = \frac{N + a_t \cdot {}_s\sigma_t}{0.85 \cdot {}_c\sigma_B \cdot bD} \tag{7.1}$$

$$\sigma_1 = -0.425\ {}_c\sigma_B + \sqrt{(0.425\ {}_c\sigma_B)^2 + \tau^2} \tag{7.2}$$

here $$\tau = \frac{{}_TQ\max}{bXn} \tag{7.3}$$

Further, the critical web reinforcement ratio p_{wz} was calculated by the so-called truss-analogy which is used as one of the shear strength theories for beam.

$$p_{wz} = \frac{{}_TQ\max}{b \cdot j \cdot {}_s\sigma_{wy}} \tag{7.4}$$

here $j = 0.875\ d$

Taking the values of $\sigma_1/{}_c\sigma_t$ and Xn1 as the coordinate, test results except 52 bond-split failured specimens were plotted in Fig. 12. As observed, many of the specimens satisfying the following limitation show good ductility regardless that p_w is more than p_{wz} or not.

$$\frac{\sigma_1}{{}_c\sigma_t} + 6\frac{Xn}{D} \leqq 3 \tag{8}$$

Basing on this result, the relations of the calculated values corresponding to the left side of eq. (8) and p_w/p_{wz} were plotted in Fig. 13. The zones which show the shear-tension failure mode, the shear-compression failure mode

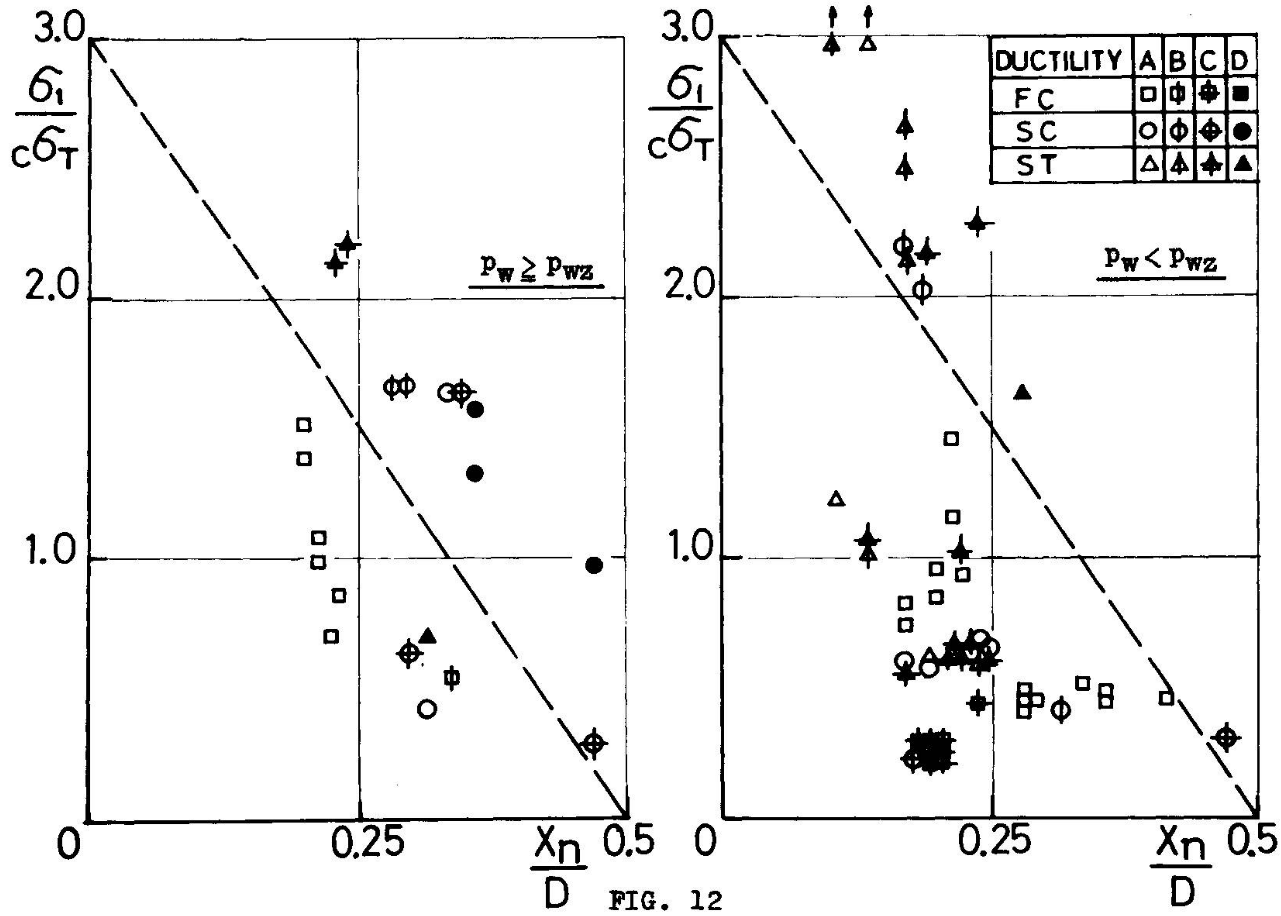
3.0
2.0
1.0
0
0.25
0.5
$\frac{\sigma_1}{c\sigma_T}$
$\frac{X_n}{D}$
$p_w \geqq p_{wz}$
$p_w < p_{wz}$
DUCTILITY A B C D
FC
SC
ST

FIG. 12

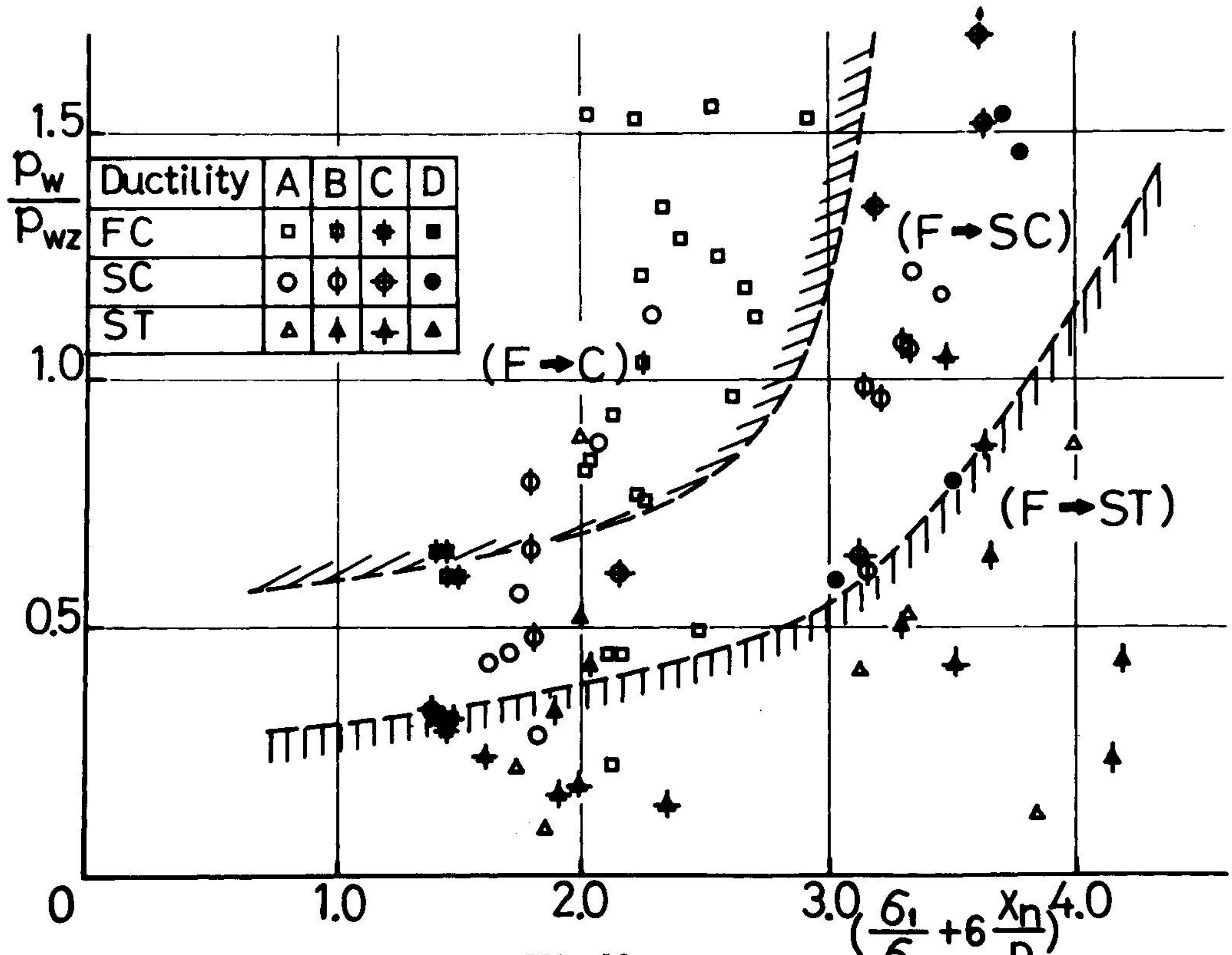
1.5
1.0
0.5
0
1.0
2.0
3.0
4.0
$\frac{p_w}{p_{wz}}$
Ductility A B C D
FC
SC
ST
(F → C)
(F → SC)
(F → ST)
$\left(\frac{\sigma_1}{c\sigma_T} + 6\frac{X_n}{D}\right)$

FIG. 13

and flexure-compression failure mode can be understood relatively apparently from this figure.

Accordingly, if such a limitation as shown in eq. (8) can be refined more theoretically and rigorously by accumulating test results, it will be possible to decide the limitation for effective web reinforcement ratio related to the combination of pt, σ_o and M/QD.

4.3 Bond-Split Failure

The distinction of this experimental result is that many specimens failed in the bond-split failure mode. 52 specimens showed this mode and this mode was observed in the specimens with high tensile reinforcement ratio p_t. Especially, 46 specimens showed this failure mode, out of 47 specimens with p_t more than 0.95%.

In the specimens failed in this mode, a small inclined crackings appeared initially at the position of tensile reinforcements apart by the effective depth d from the ends of the column. As the number of cyclic loadings increased or as horizontal deflection enlarged, many similar cracks progressed along the tensile reinforcements toward the center of the specimen. And, gradually, concrete cover exfoliated and shear capacity of the speciman deteriorated. Thus, the bond failures in this test are different from usual bond slip in massive concrete and this initial small inclined crack-called bond-split crack here after--is considered as a trigger for this failure mode.

So, after calculating the principal tensile stress caused by bending moment, shear force and bond stress at the point on tensile reinforcement apart by d from the end of the column, the shear force corresponding to this initial crack ${}_cQ_{BO}$ was obtained by putting the principal stress equals to ${}_c\sigma_t$.

The result is as follows.

$$ {}_cQ_{BO} = \frac{-{}_c\sigma_t \cdot B + \sqrt{{}_c\sigma_t{}^2 \cdot B^2 + 4C^2\,({}_c\sigma_t{}^2 + {}_c\sigma_t \cdot \sigma_0)}}{2C^2} \quad \text{(kg)} \qquad (9) $$

here $B = \dfrac{(M/Q - d)\cdot(D/2 - d_t)}{I_e}$, ${}_c\sigma_t = 1.8\sqrt{{}_c\sigma_B}$

$$ C = \frac{1}{1.75 \cdot n' \cdot b' \cdot d} + \frac{6 \cdot I \cdot d \cdot d_t}{I_e \cdot b \cdot D^3} $$

I, Ie: Moment of inertia without and with the effect of axial reinforcements, respectively

b': smaller one of $(2\sqrt{2}\ dt - \phi_o)$ or $\dfrac{b - \Sigma\phi_o}{n'}$

n': number of tensile reinforcements

ϕ_o, $\Sigma\phi_o$: Diameter of a tensile reinforcement and the summation, respectively

Comparison of the calculated results ${}_cQ_{BO}$ with the test results ${}_TQ_{BO}$ are shown in Fig. 14. As shown, ${}_TQ_{BO}$ becomes generally more than ${}_cQ_{BO}$ as M/QD and pt decrease, and as σ_o increase. However, influence of web reinforcement ratio can not be observed.

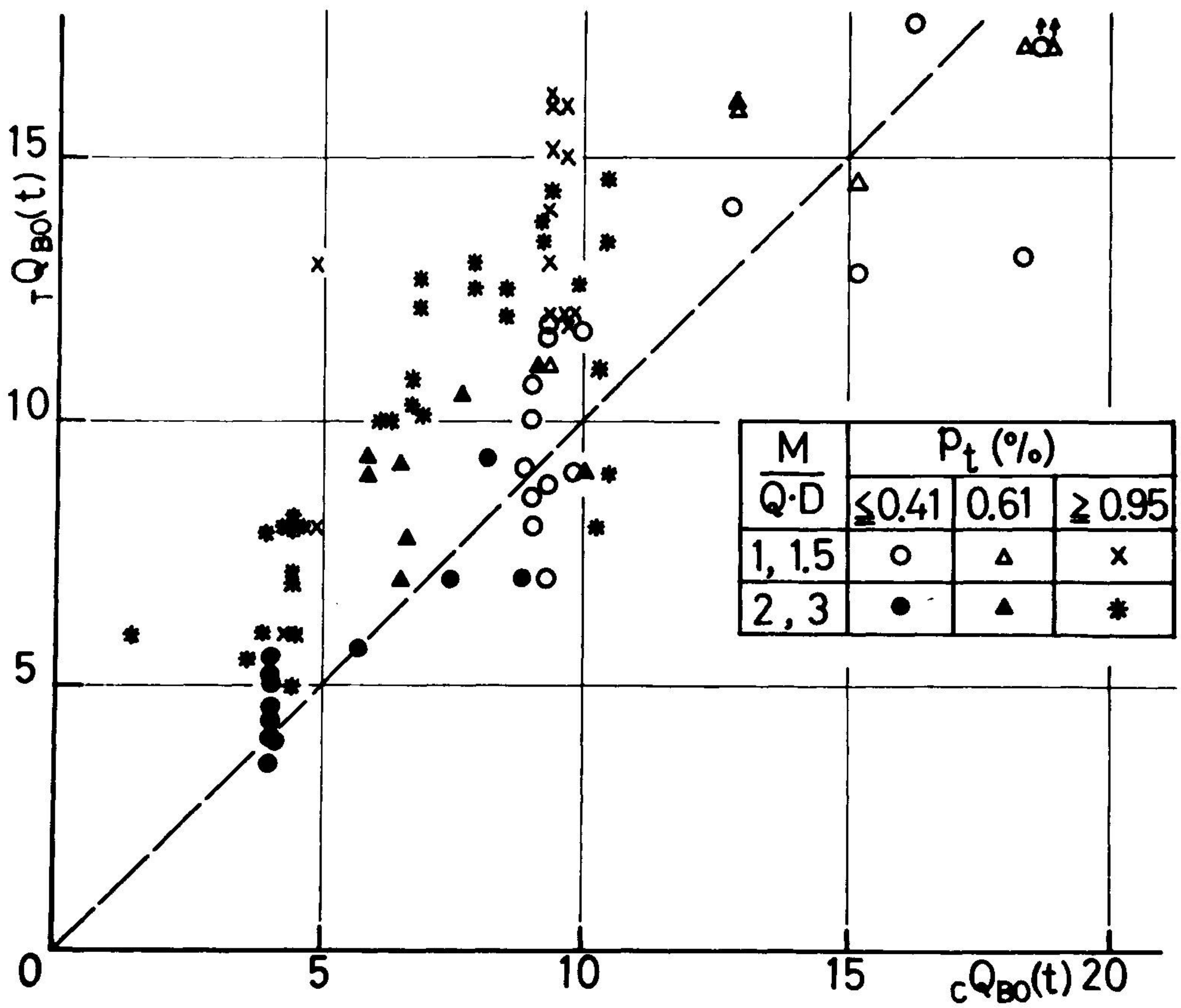

FIG. 14

Next taking the values of ${}_{T}Q_{max}/{}_{C}Q_{BO}$ and ${}_{T}F_{max}/F_{al}$ as the coordinates, all of the test results were plotted in Fig. 15 with their failure mode and classified ductilities. Here, ${}_{T}Q_{max}$ means the maximum shearing force at the test, and ${}_{T}F_{max}$ and F_{al} mean the maximum test results of mean bond stress and the allowable bond stress in the A.I.J. Standard(in Ref. 1) respectively. As shown, the value of ${}_{T}Q_{max}/{}_{C}Q_{BO}$ has more influence to the bond-split failure than ${}_{T}F_{max}/F_{al}$ has.

Fig. 16 shows the relationship between the value of p_w/p_{wz} and the classified ductilities of the specimens failed in bond-split failure. As shown, these ductilities could not be improved so much even by increasing web reinforcement. However, in such specimens with ${}_{C}\sigma_{B}$ more than 270 kg/cm^2, when ${}_{C}Q_{FU}$ is less than 1.4 times ${}_{C}Q_{BO}$ and p_w nearly equal to p_{wz}, good ductilities could be obtained. Further, it is presumed from their cracking patterns that the confinement of the concrete within the core with spiral hoops etc. will be effective.

5. CONCLUSION

Flexure-shear tests under constant axial compression and multi-cyclic lateral forces were carried out on 125 short column specimens and following items on ductility were obtained.

1) As the factors which control ductility of columns, buckling of compression reinforcements, shear failure and bond failure are considered important.

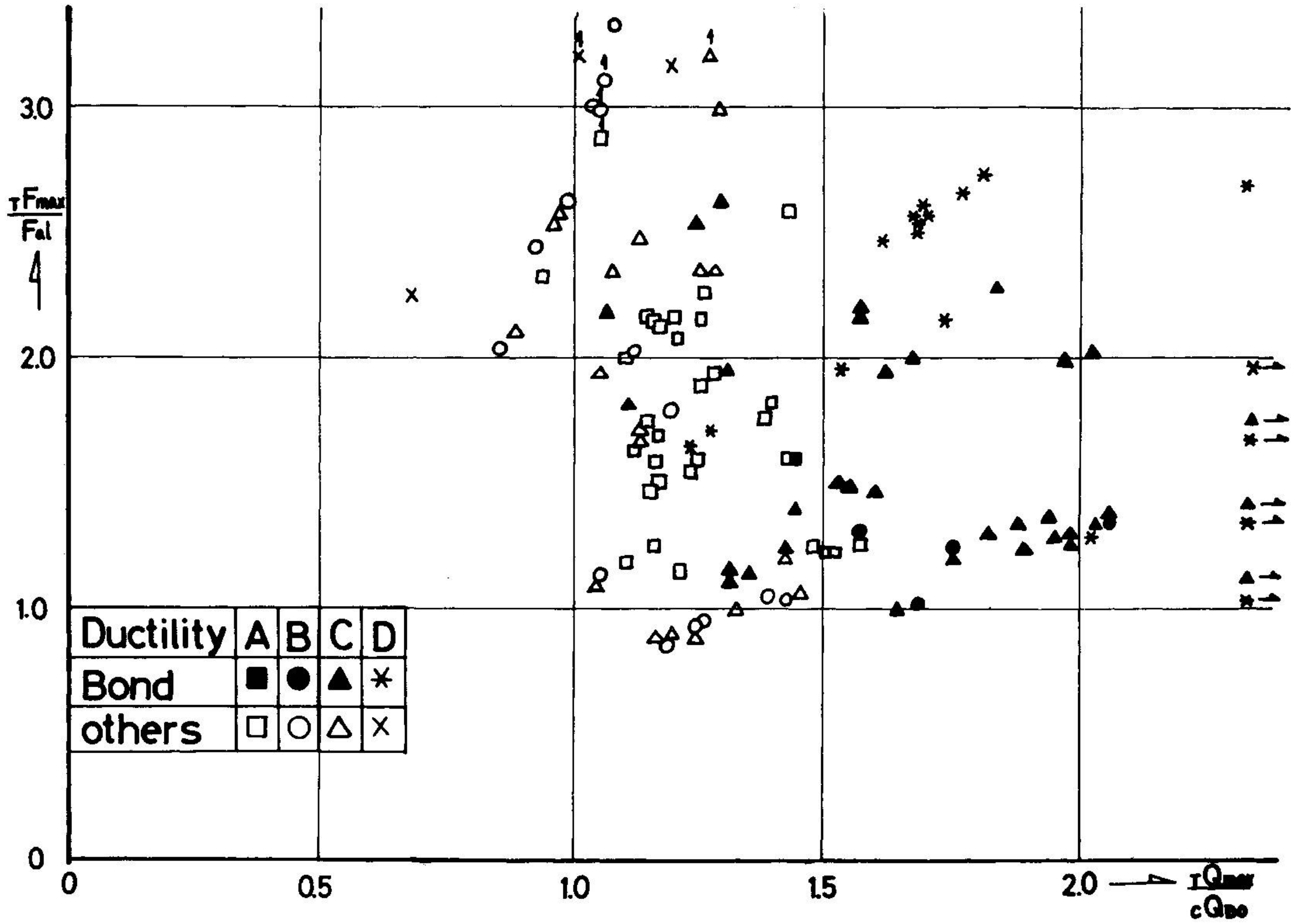

FIG. 15

2) To prevent compression reinforcements buckling until large deflection of column, it will be effective to keep spacing of web reinforcements less than 8 times diameter of the axial reinforcement.

3) When the flexure capacity ${}_CQ_{FU}$ shown by eq. (2) is more than about 0.8 times diagonal tension cracking load ${}_CQ_{DTC}$ shown by eq. (3), it is effective for preventing members from diagonal tension failure to put the web reinforcements much more than that calculated by eq. (4).

4) When the flexure capacity ${}_CQ_{FU}$ is more than about 0.8 times shear tension cracking load ${}_CQ_{STC}$ calculated by eq. (5), it is effective to put more web reinforcements than that shown in eq. (6).

5) There are certain conditions for the combination of pt, σ_o and M/QD where shear compression failure can not be avoid even with much web reinforcements. This conditions could not be made so apparent, but eq. (8) is considered to be one approach. When the combination of pt, σ_o and M/QD of specimens satisfy eq. (8) and when their p_w are more than p_{wz} shown in eq. (7.4), good ductilities could be recognized. However, there is a possibility that this value p_{wz} may be decreased still more.

6) Discussion by bond stress is not effective to prevent bond-split failure of the column. It seems effective to keep the flexure capacity ${}_CQ_{FU}$ within about 1.4 times of the initial bond-split cracking load ${}_CQ_{BO}$ shown by eq. (8). It is not effective to increase rectangular-typed hoops but it will be effective to put spiral hoop closely.

6. ADDITIONAL REMARKS

Analitical works about the following items are scheduled by the committee (Cf. § 7), and authors wish to present these results and the experimental results about the columns with side walls in the near future.

1) Influence of scale effect, loading excursion etc. to ductility of structural members.
2) Quantification of the rational web reinforcement ratio to make structural members ductile.
3) Persuit of structural device for preventing the split-bond failure.
4) Estimation of hysteresis damping of test results.
5) Method for estimating the seismic properties of the members from the results due to certain static cyclic loadings.

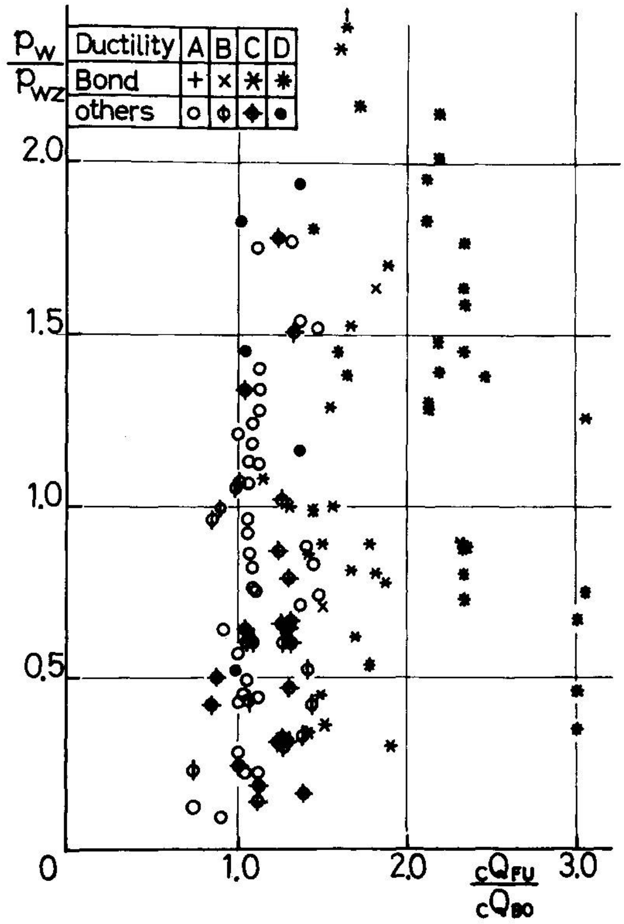

FIG. 16

7. ACKNOWLEDGEMENT

The authors wish to thank the following members of the committee on Reinforced Concrete Structures in B.R.I. for carrying out this experimental research and Mr. M. Ohkubo, assistant, Tokyo Metroporitan Univ. and Mr. K. Yamamoto, research member, Fujita Kogyo for helping to finish this report.

The Committee Members

Chairman:

Y. Higashi: Tokyo Metropolitan University

General Secretary:

M. Hirosawa: Building Research Institute, Ministry of Construction

Members:

H. Aoyama, University of Tokyo; Y. Kanoh, Meiji University; M. Fukuhara, Tokyo Institute of Technology; O. Chiba, Toda Construction Co., Ltd.; Y. Fukada, Shimizu Const. Co., Ltd.; T. Takahashi, Kajima Const. Co., Ltd.; T. Takeda, Obayashigumi Const. Co., Ltd.; K. Yamamoto, Fujita Kogyo Co., Ltd.; I. Yamaguchi, Takenaka Komuten; S. Yoshizaki, Taisei Const. Co., Ltd.; N. Yanagisawa, Secretary of the committee.

8. NOTATION

b, D ; width and overall depth of speciman respectively (cm)

d_t (or d_c); distance from extreme tension (or compression) fiber to centroid of tension (or compression) reinforcement (cm)

d ; $= D - d_t$, effective depth (cm)

g ; $= d - d_t - d_c$ (cm) S; spacing of web reinforcement (cm)

p_t ; $= a_t/bD$, tensile reinforcement ratio

p_w ; $= a_w/bs$, web reinforcement ratio

$s\sigma y$; yield stress of tensile reinforcement (kg/cm^2)

$s\sigma wy$; yield stress of web reinforcement (kg/cm^2)

$c\sigma B$, $c\sigma t$; compressive and tensile strength of concrete, respectively (kg/cm^2)

Q ; shear force (kg) P; $= Q$, Lateral cyclic load (kg)

σ_o ; $= N/bD$ (kg/cm^2) N; constant axial force (kg)

M ; bending moment at critical section (kg•cm)

a ; $= M/Q$, half of the column length in this test (cm)

a_1 ; $a/D = M/QD$, shear span ratio

δ ; displacement δ_y; displacement at yielding

μ ; $= \delta/\delta_y$ ductility factor R; $= \delta/2a$, Rotation angle of member

REFERENCES

1) "The 1971 AIJ Standard for Structural Design of Reinforce Concrete Construction," Architectural Institute of JAPAN (AIJ).

2) Ozaki, M., Wakabayashi, M. and Hirosawa, M., "Experimental Study on Large Models of Reinforced Concrete Columns," Proceedings of the Fifth World Conference on Earthquake Engineering in Roma, 1973.

3) Hirosawa, M., "Synthetic Research on Preventing Reinforced Concrete Columns from Total Collapse (in Japanese)," Building Research Constitute, BRI Transactions of Main Research in 1972.

4) Hirosawa, M., "A List of Past Experimental Results of Reinforced Concrete Columns," Kenkyu Shiryo No. 2, Building Research Institute, 1973.

5) Higashi, Y. and other committee members, "Synthetic Research on Preventing the Collapse of Reinforced Concrete Short Column, No. 1 ~ No. 8," Synopses of Reports at Annual Meeting of AIJ (1973), pp. 1413 ~ 1428.

SUMMARY

Experimental research on ductility of reinforced concrete columns under constant axial compression and multi-cyclic lateral forces, and the results are reviewed. 165 short column specimens with many variable factors were tested. The important factors which influence ductility of column were buckling of axial compression bars at the ends of column, shear failure and bond split failure along axial tension bars. The behaviour and the analysis of the above failures and crackings, and the method to obtain good ductility are discussed about the results of 125 specimens.

RESUME

Ce rapport présente la recherche expérimentale sur la ductilité de colonnes en béton armé soumises à une compression axiale constante et à des forces latérales multicycliques ainsi que les résultats obtenus. 165 colonnes courtes ont été essayées sous de nombreuses conditions diverses. Les facteurs importants influençant la ductilité des colonnes étaient le flambage des barres d'acier comprimées aux extrémités des colonnes, la rupture au cisaillement et la rupture de l'ancrage des barre longitudinales. Le comportement et l'analyse des différentes formes de rupture indiquées ci-dessus ainsi que les mesures à prendre pour atteindre une bonne ductilité sont discutées en s'appuyant sur les résultats de 125 essais.

ZUSAMMENFASSUNG

Experimentelle Untersuchungen über das Verformungsvermögen von kurzen Stahlbetonstützen unter konstanter Normalkraft und wiederholter seitlicher Belastung werden mitgeteilt. 165 kurze Stützen wurden unter Variation vieler Einflussgrössen geprüft. Die Verformbarkeit wurde massgebend beeinflusst durch das Ausknicken der Längsbewehrung an den Stützenenden, durch Schubversagen und Verankerungsbruch der Längsbewehrung. Das Verhalten und die Berechnung dieser Versagens- und Brucherscheinungen sowie die Massnahmen zur Erzielung eines guten Verformungsvermögens werden anhand der Resultate von 125 Prüfkörpern diskutiert.

Elastic-Postelastic Analysis of the Cyclic Behaviour of Reinforced Concrete Columns Taking Account of the Effort of Bond

Calcul élastique et post-élastique du comportement sous charge répétée de colonnes en béton armé, en tenant compte de la cohésion béton—acier

Elastisch-überelastische Berechnung des Verhaltens von Stahlbetonstützen unter wiederholter Belastung unter Berücksichtigung der Haftung

Yasuo HIGASHIBATA
Research Engineer
Takenaka Technical Research Laboratory
Tokyo, Japan

1. Introduction

In our countries subjected to earthquakes it is important that structures are capable of deforming in a ductile manner under the action of severe seismic motions. Recently,in the design of reinforced concrete frames it is necessary to consider the behavior of frames in the postelastic range,when researching the accurate response of the frames to the seismic motions. The accurate behavior of frames at the ultimate load for these aspects is dependent on grassping the accurate behavior of members in the elastic-postelastic range. The elastic-postelastic behavior of reinforced concrete columns under cyclic loading is discussed herein for the purpose of researching the accurate behavior of reinforced concrete frames under cyclic loading.

The elastic-postelastic analysis of the cyclic behavior of reinforced concrete columns is discussed herin in the process as;

1.Properties of concrete under cyclic stress in a member.
2.Properties of steel under cyclic stress.
3.Moment-curvature relation in the cross section of a member.
4.Longitudinal distribution of curvature.
5.The effect of bond.
6.Shear deformation.
7.Method of analysis.

And the experiment is done to investigate the general cyclic behavior of columns and to make sure the method of analysis.

The author propose that considering the effect of beam-column connection behavior under cyclic load,the analysis is capable to utilize for elastic-postelastic analysis of the cyclic behavior of the reinforced concrete frames.

2. Properties of concrete

Many equations for the stress-strain curve of concrete under uniaxial compression have been proposed in past years. Probably the most widely accepted curve in our countries is the proposed by Umemura(1) which consists of a e-function up to the maximum stress σ_B at a strain ε_B and down of the same function as shown in Fig1.

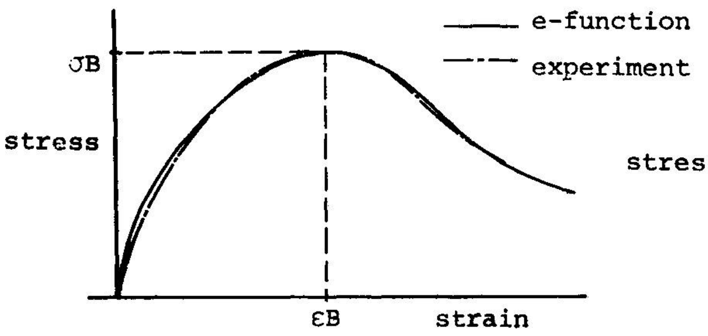

FIG1. e-FUNCTION CURVE

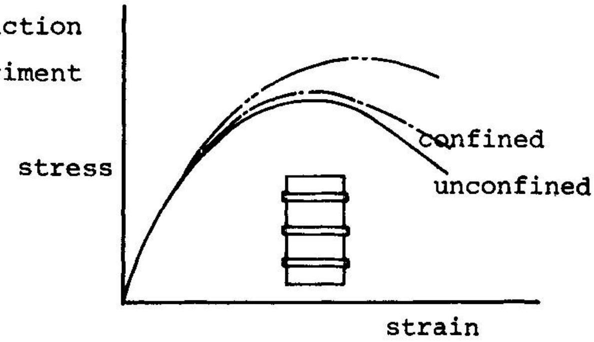

FIG2. CONFINED CONCRETE CURVE

Umemura's curve showed a little stress over the experimental value in initial range but is become widely used. Concrete which is restrained in the directions at right angles to the applied stress will be referred to as confined concrete. The test conducted by Hanajima(2) showed that both the strength and ductility of the concrete are greatly increased by such stress,as shown in Fig2. However,the tests of reinforced concrete members by many investigators in the past,showed that rectangular hoops do not confine the concrete as effectively as circular spirals.

On the basis of the experimental evidence it is proposed that the curve as shown in Fig3 is able to cover the cyclic stress-strain curve for confine concrete by rectangular hoops.

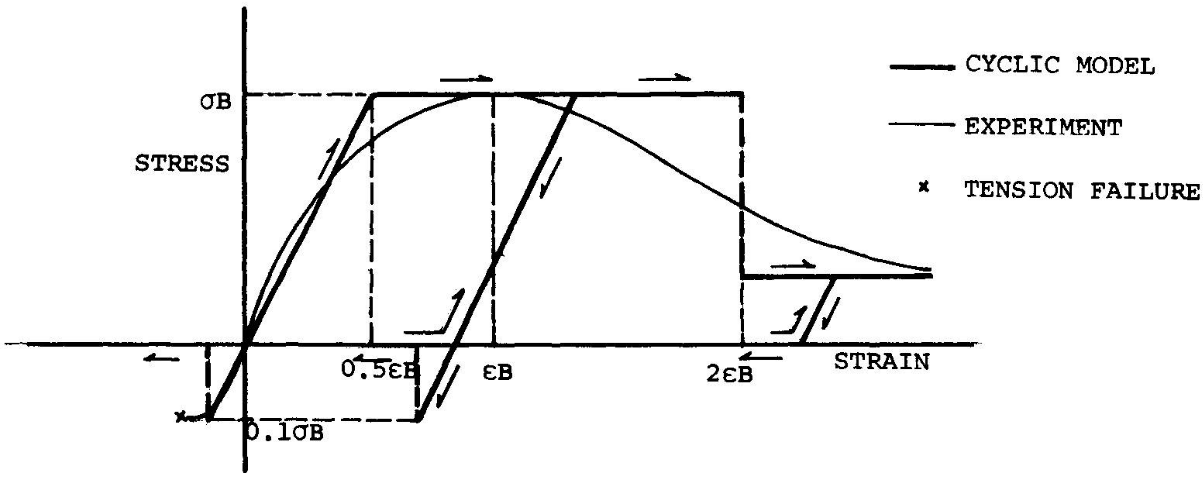

FIG3. PROPOSED STRESS-STRAIN CURVE OF CONCRETE

3. Properties of steel

The behavior of structural reinforcing steel under tensile loading has been extensively explored within both its elastic and inelastic range,but little information is available regarding its inelastic behavior under reversed loading. By reversing the graph paper between tensile and compressive testing,it was possible to obtain continuous graphs as shown in Fig4. In assessing the factors that are responsible for the difference between the virgin stress-strain curves and those obtained after previous cycles of inelastic loading,the following variables are relevant;(1)the virgin properties of the material;(2)the entire previous history of loading;and(3)the rate of straining.

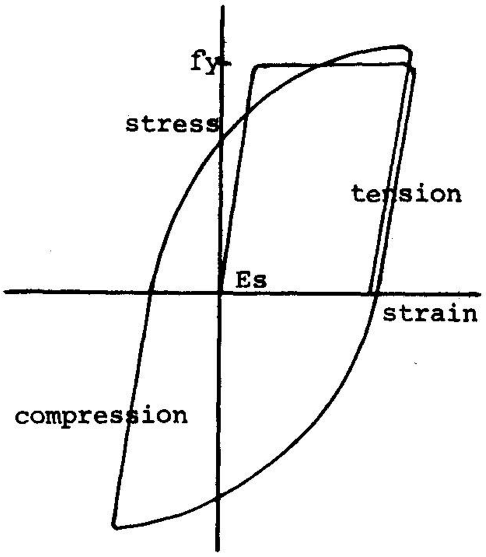

FIG4. EXPERIMENTAL CURVE

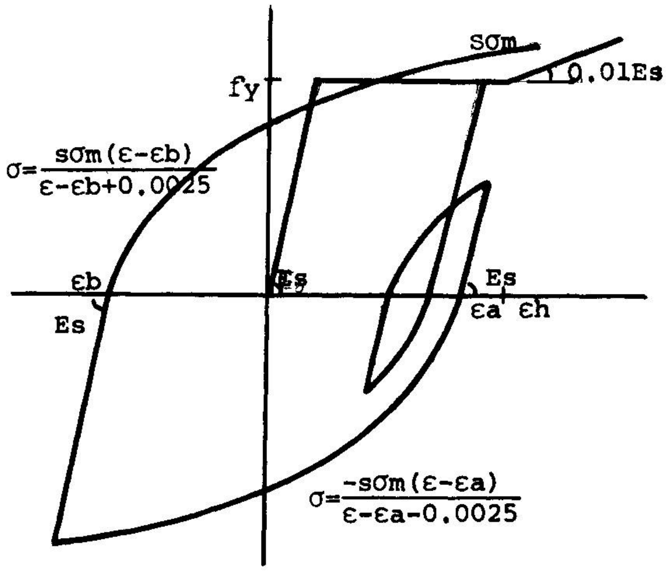

FIG5. PROPOSED CURVE OF STEEL

However,considering the state of existing columns,the influence of the plastic strain at previous reversal is being considered quantitatively,and proposed cyclic stress-strain curve for reinforcing steel is shown in Fig5.

4. Flexural strength and curvature analysis

In the analysis of sections for flexure the following assumptions will be made.

1.The longitudinal strain in the steel and concrete at the various section levels is directly proportional to the distance from the neutral axis.

2.The cyclic stress-strain curve for the steel and concrete have general shapes shown in Fig3,Fig5.

3.The 50 concrete blocks are taken in the section,and each block has the properties of concrete,as shown in Fig6.

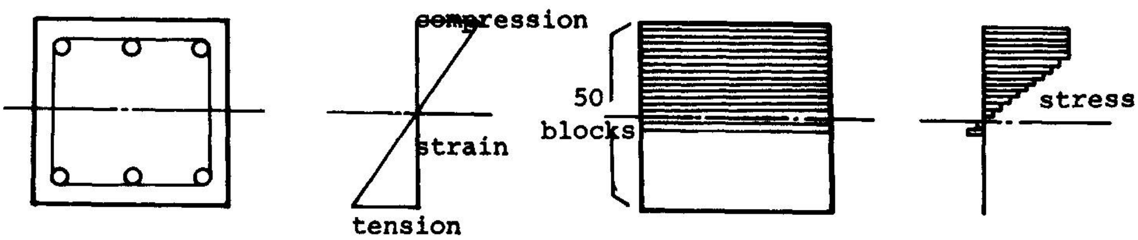

FIG.6 STRESS DISTRIBUTION OF CONCRETE BLOCKS

4.Cyclic behavior of the concrete blocks is shown in Fig7.

5.The equilibrium of forces in the section.

Fig8 shows some theoretical moment-curvature curves obtain for rectangular concrete columns sections with different amount of longgitudinal steel and axial stress,compared to the e-function theory.

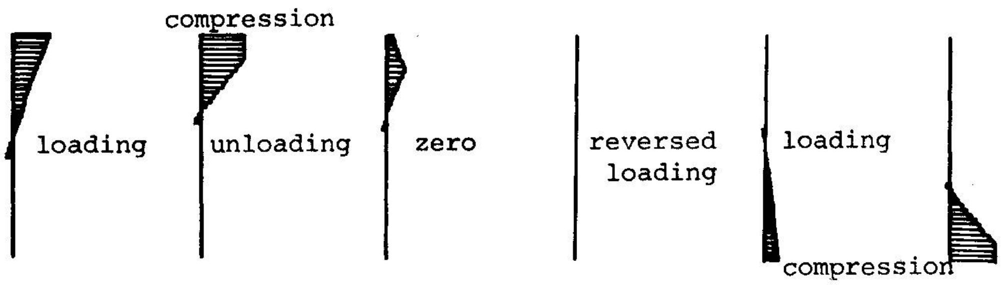

FIG.7 CYCLIC STRESS OF CONCRETE BLOCKS

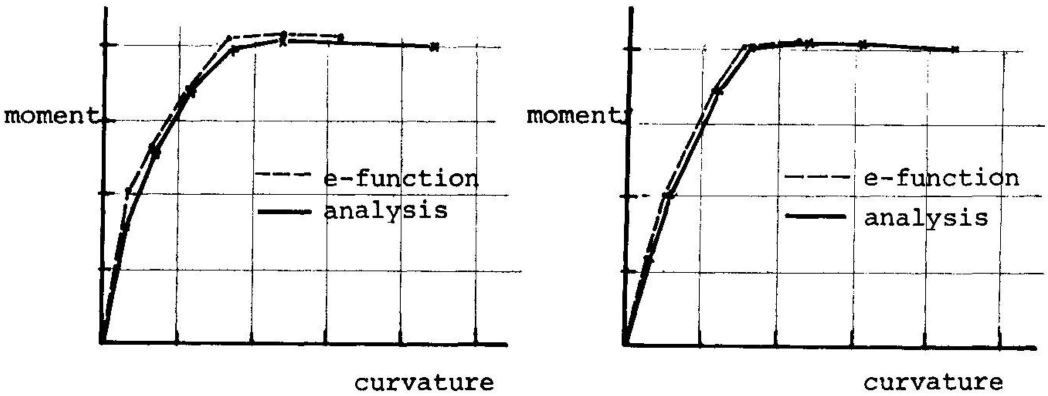

FIG.8 THEORETICAL MOMENT-CURVATURE RELATION

5. Distribution of curvature

By longitudinal distribution of curvature,the deformation of member due to bending moment canbe obtained. It is not good for obtaining the longitudinal distribution of corvature to use the moment-curvature relation of cross section because many sections have a considerable capacity for plastic rotation beyond the peak of the moment-curvature curve. Tests by many investigators in the past,have shown that such longitudinal distribution of curvature in reinforced concrete column canconsiderably obtained by simple model having a flexible zone at the end of member.

The simple model and the experimental distribution of curvature in reinforced concrete column testing by Kokusho(3) are shown in Fig9.

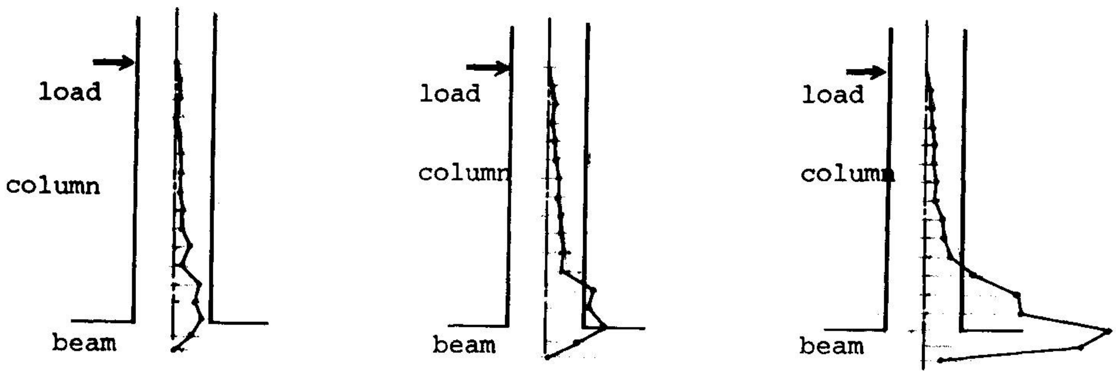

FIG.9 EXPERIMENTAL DISTRIBUTION OF CURVATURE

Proposed distribution considering the flexible zone of curvature is shown in Fig10.

6. The effect of bond

Maximum bond stress for concrete and steel due to form of reinforcing bar,concrete strength,concrete cover for reinforcement. While in the beam-column connection,a large shear force occurs during an earthquake and as a result large shear and bond stresses are produced in concrete and reinforcements. Test by Okita(4) showed the bond stress-slip curve under cyclic loading in Fig11.

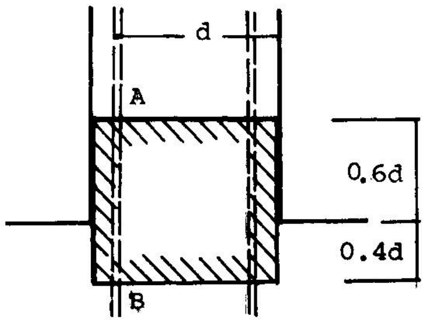

FIG10 FLEXIBLE ZONE

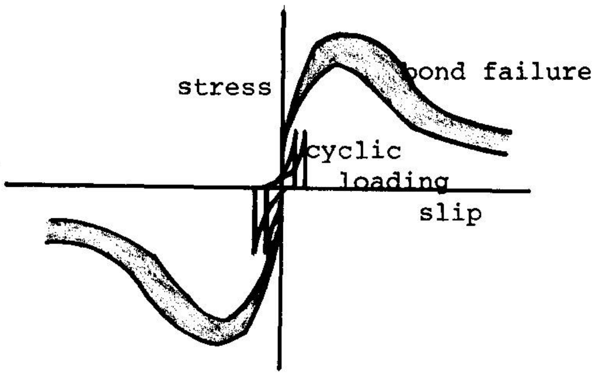

FIG.11 BOND STRESS-SLIP CURVE

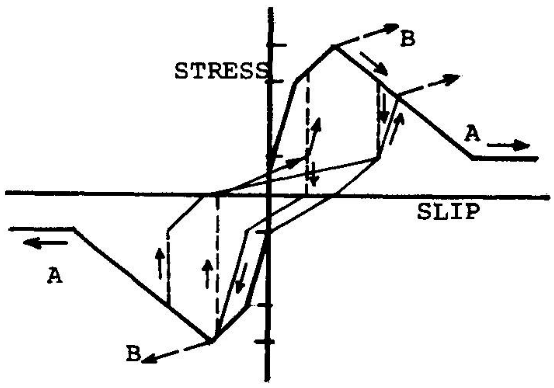

FIG.12 PROPOSED CYCLIC CURVE

The permissible bond stress along the reinforcement can be increased by making the surface of a bar rough or irregular.

In this research, considering of such deformed bars are generally used for longitudinal reinforcement. On the basis of the experimental and analytical evidence it is proposed that the curve bond stress-slip relation shown in Fig12,separating the cases of in column(A) and in pannel(B).

The average curvature of flexible zone due to bond slip is shown as follows.

$$1/\phi a=\frac{s1+s2-s3-s4}{f \times D}$$

Where f; length of the flexible zone,D; spacing of tension and compression reinforcement,s1 s4; bond slip to flexible zone.

The curvature due to bond effect is added to bending curvature.

7. Deformation due to shearing force

In reinforced concrete members, it is difficult to obtain the accuracy deformation due to shearing force. The auther propose the experimental method to obtain the deformation as follows.

In the experimental study of reinforced concrete columns, the deformation due to shearing force is regarded as the difference between the total measured deformation and the deformation calculated by the longitudinal distribution of the measured curvature including crack's width. The experimental results are shown in Fig13. In considering shear strength,the study by Arakawa(5) showed the average shear strength of reinforced concrete beams as follows. On the basis of the existing experimental evidence it is proposed that the curve shown in Fig14 gives a good representation of the shear stress-deformation relationship for general reinforced concrete column.

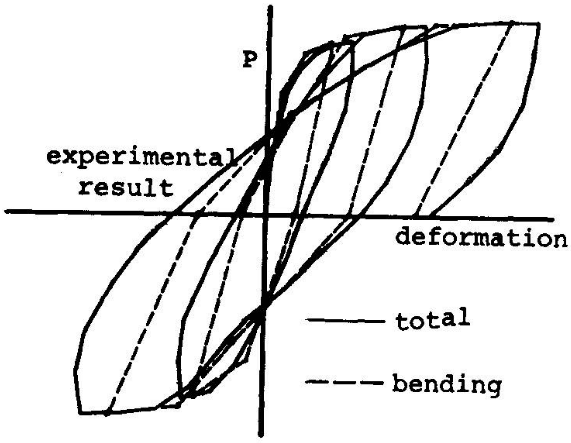

FIG.13 BENDING DEFORMATION

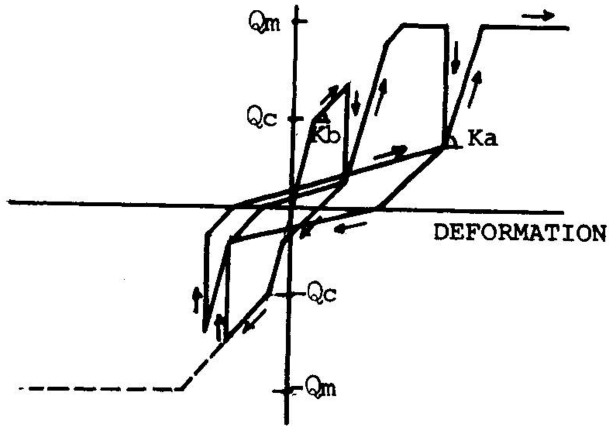

FIG.14 PROPOSED CYCLIC CURVE

8. Method of analysis

In the analysis developed in this study assumed that previous steps,a computer program was used embodying the step shown in Fig15.

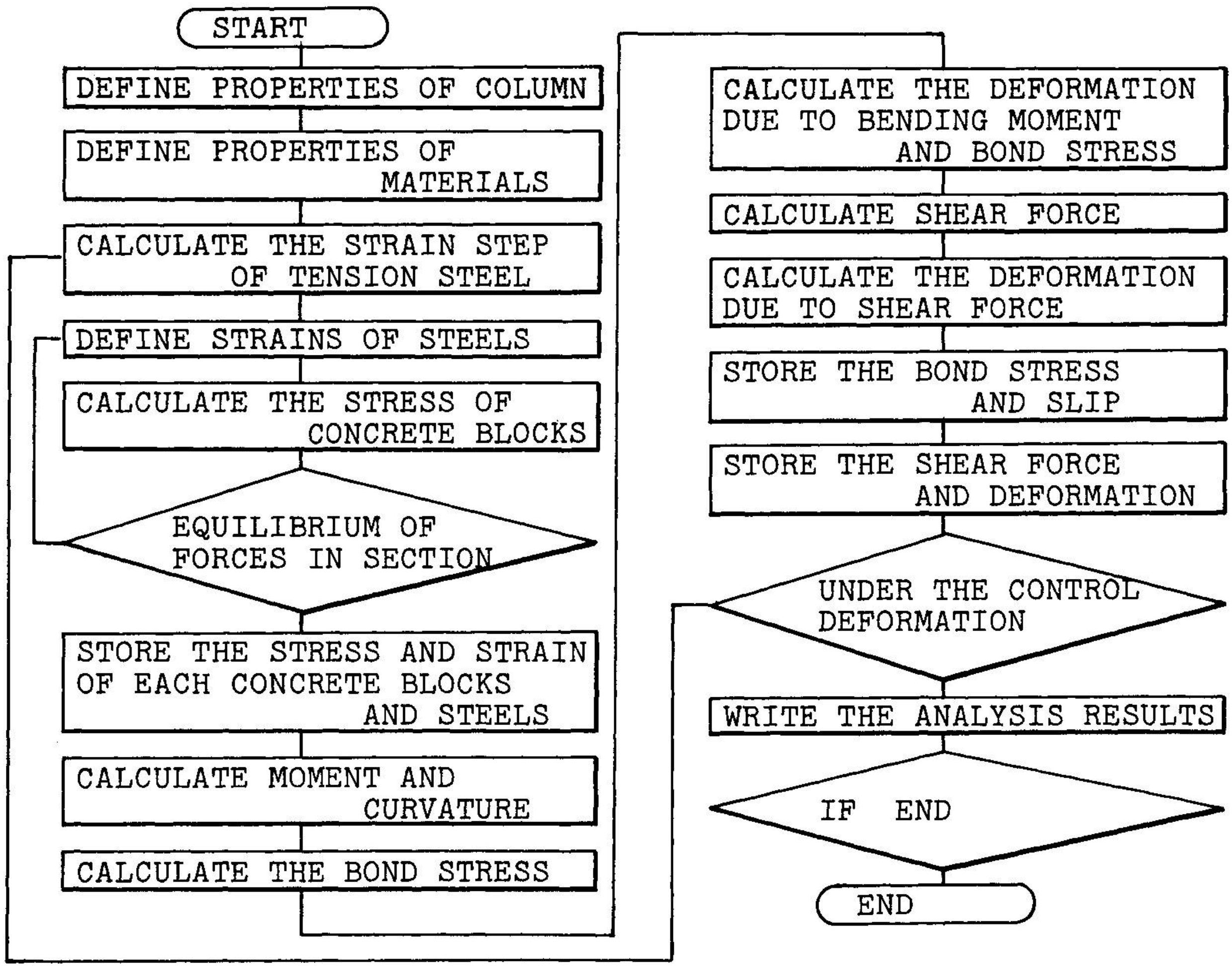

FIG. 15 ANALISIS PROGRAM FLOW

9. Results of analysis

The analysis described in this paper was compared to the results of test on 16 columns.

Experiment of columns ; In the test,the principal variables are the ratio of span to depth(a/D),the axial stress(σ0,in kg/cm), the amount of longitudinal tension steel (Pt,in %),and the shear steel(Pw,in %). The test setup shown in Fig16 consists of steel reaction frames which is anchored to the test floor,hydrauric jacks for lateral forces and reaction steel bars and a oil pressure jack for constant axial forces. The test specimens are anti-symmetrically and reverally loaded by two pairs of jacks to simulate the moment distribution in actual column subjected to lateral forces.

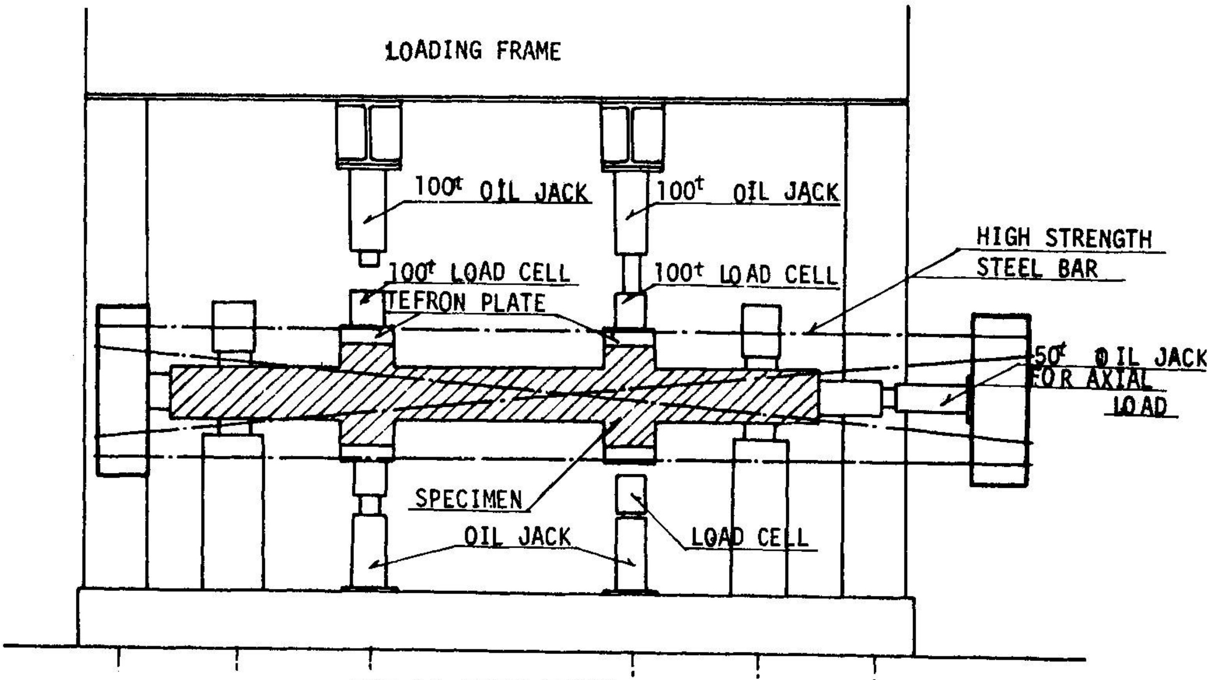

FIG.16 TEST SETUP

The typical results of load deformation curves compared with the results of the analysis are shown in Fig.17,Fig.18. The analytical results show a good agreement with the experimental results.

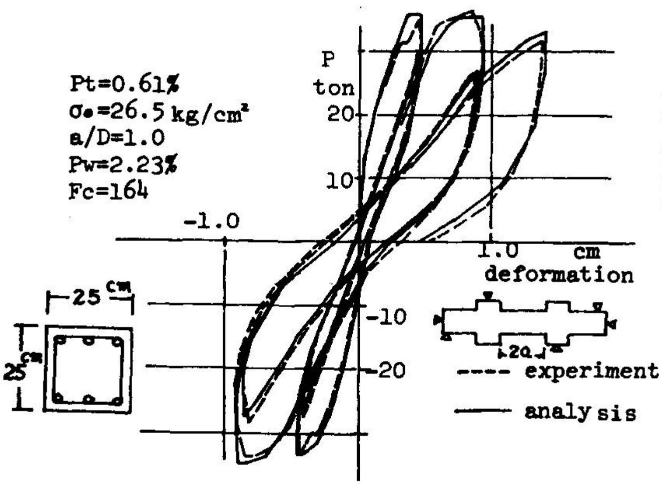

FIG.17 LOAD-DEFORMATION CURVE

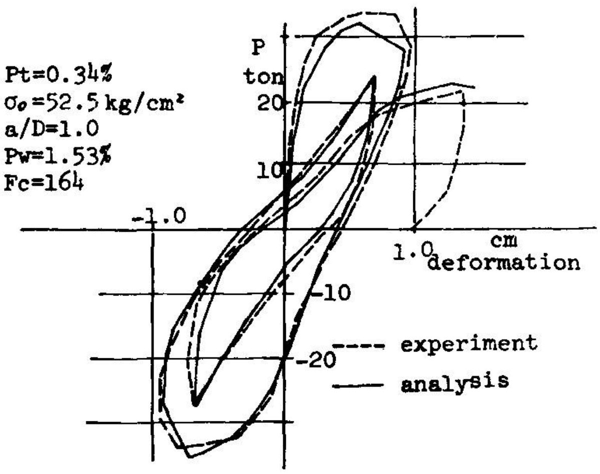

FIG.18 LOAD-DEFORMATION CURVE

10. Conclusions

The calculated load deformation characteristics of columns show a good agreement with the test results of reinforced concrete columns. The analysis is proposed to use the analysis of reinforced concrete frame directly. The author hope to propose the analysis of reinforced concrete frame in the other paper.

References

(1) A.I.J Standerd for Structural Calculation of Reinforced Concrete Structures, Architectural Institude of Japan,'71

(2)Kent.D.C, Park.R, "Flexural Members with Confined Concrete" A.S.C.E Structural div./July.'69

(3)Wight.J.K, Sozen.M.A, "Shear Strength Decay in Reinforced Concrete Columns Subjected to Large Deflection Reversals." Report on TheNational Science Foundation/ August,'73

(4)Morita.S, Kaku.T, "Yielding of Tensile Reinforcing Steel in Beams" Transactions of A.I.J /Oct.'66

(5)Tomii.M,Kawamura.Y, "Experimental Study on Bond Strength of Reinforcement of Beams and Columns" /Oct.'66

(6)Kokusho.S,Mazuzaki.Y"Elastic and Plastic Behavior of Reinforced Concrete Frame" Transactions of A.I.J /Oct.'67

SUMMARY

The elastic-postelastic behaviour of reinforced concrete columns under cyclic loading is discussed herein for the purpose of the analysis of reinforced concrete frames. In this paper, the elastic-postelastic analysis of the cyclic behaviour of reinforced concrete columns taking account of the effect of bond and the effect of shear force is proposed. The analytical results show a good agreement with the experimental results.

RESUME

On traite du comportement élastique et post-élastique de colonnes en béton armé soumises à une charge répétée, pour en déduire un calcul des cadres en béton armé. Dans ce rapport, on propose un calcul élastique et post-élastique du comportement sous charge répétée de colonnes en béton armé, en tenant compte de la cohésion entre l'armature et le béton, et de l'influence de l'effort tranchant. Les résultats analytiques concordent bien avec les résultats expérimentaux.

ZUSAMMENFASSUNG

Das elastisch-überelastische Verhalten von Stahlbetonstützen unter wiederholter Belastung wird – als Grundlage für die Berechnung von Stahlbetonrahmen – diskutiert. Im Beitrag wird eine elastisch-überelastische Berechnung des Verhaltens von Stahlbetonstützen unter wiederholter Belastung und unter Berücksichtigung der Haftung zwischen Beton und Bewehrung und der Querkraft vorgeschlagen. Die Berechnungsresultate zeigen gute Uebereinstimmung mit den Versuchsergebnissen.

IV

Shear Strength of Steel Reinforced Concrete (SRC) Columns

Résistance au cisaillement des colonnes en béton armé

Schubfestigkeit von Stahlbetonstützen

Koichi MINAMI
Lecturer
Osaka Institute of Technology
Osaka, Japan

Minoru WAKABAYASHI
Professor
Disaster Prevention Research Institute
Kyoto University
Kyoto, Japan

1. INTRODUCTION

Composite steel section and reinforced concrete structure which is called SRC structure has been widely used for buildings with more than 7 stories in Japan since these structures gave an excellent performance against The Kanto Earthquake of 1923. The first edition of the design specification for SRC system was published in 1958 by Architectural Institute of Japan and the revised edition was published in 1963. And now the third edition is being prepared in which the main part for revision is anticipated to be the design of columns under shear force. For this purpose a working group for the shear tests of SRC columns(Chairman is Dr. S. Takada) was formed in the SRC Sub-committee(Chairman is Dr. T. Naka) belonging to Architectural Institute of Japan. This paper presents an outline of the experiments conducted by the working group, and some results.

Very few experimental study on shear resistance of SRC columns had been conducted till recent years(1, 2). Recently some experimental works have been conducted by the authors(3), and the test program in the present paper is designed in reference to these recent works.

Forty two full scale SRC column specimens with full-web type, lattice and butten plate type open-web steel sections, and one ordinary reinforced concrete column specimen are tested under constant axial load and alternately repeated bending moment and shear. All specimens fail in shear. The shear capacities, failure modes, unloading characteristics in large deformation range, effect of cyclic loading on the shear resistance, and shapes of hysteresis curves are investigated.

2. TESTS

a. Test Plan: 3 types of the steel cross section are chosen for each specimen as shown in Fig. 1; full-web(F series), Lattice type open-web(L series) and butten plate type open-web(B series). The value of shear span ratio, h/D (h: column length, D: depth), is fixed to be 3 for all specimens except 3 specimens, for which h/D is selected to be 5 to investigate the effect of the shear span ratio. In Tables 1, 2 and 3, shown are the identification number for each specimen and the values of the experimental parameters. As the experimental parameters, selected for the specimens in F series are; flange thickness(t_f), web thickness(t_w), amount of main feinforcements(n, ϕ), spacing of web reinforcements(s), concrete strength(F_c), axial load ratio(N/N_0) and shear span ratio(h/D). N is the applied axial load, and N_0 is the maximum compressive strength of the cross section computed by summing the contributions from each components; concrete, steel, and main reinforcing bars. For L series, inclination angle of lattice plate(θ), lattice plate thickness(t_1), spacing of web reinforcement and axial load ratio are selected, and ratio of spacing of butten plate to depth of steel section(p), butten plate thickness(t_b), spacing of web reinforcements and axial load ratio are selected for B series. In order to compare the shear failure, a specimen of ordinary reinforced concrete column (No. 43) is included in the test plan.

b. Material Properties: Details of reinforced concrete portion of the cross section, dimensions and arrangement for reinforcing bars, and shapes and dimensions of steel portion are shown in Figs. 2, 3 and 4, respectively. For the main reinforcements and web reinforcements, deformed bars SD35(guaranteed yield stress: 3.5ton/cm^2) and round bars SR24(2.4ton/cm^2) with diameter of 4.5 mm are used, respectively. The steel portion for each specimen is built up by welding, from SS41 steel plates(2.4ton/cm^2). The used concrete is a mixture of ordinary Portland cement, coarse aggregates(river gravel, maximum size less than 10mm) and fine aggregates(river sand maximum size less than 2.5mm).

c. Loading Apparatus: The loading apparatus and principle are shown in Figs. 5 and 6, respectively. Detail of this apparatus is omitted in this paper, since it was already presented at 5WCEE(4). Data detecting system for the relative displacement between the column top and bottom, δ, is shown in Fig. 7. The chord rotation angle R is given by δ/h.

d. Loading Program: Figures 8(a) and (b) show the loading programs employed in the test, in which the cyclic loading is controlled by the prescribed amplitude of the chord rotation angle, R.

e. Axial Load: Shown in Fig. 9 are the results of the investigation on the intensity of the axial load in columns of the first story of the actually constructed, regular shaped steel reinforced concrete buildings. The values of the axial load ratio, N/N_0, in the column of the first story scatter in the range from 0.1 to 0.4, and the mean value is about 0.2. Based on Fig. 9, the axial load ratios in the test are determined.

3. TEST RESULTS

a. Crack Observation: In all specimens except the reinforced concrete column, the diagonal tension crack appears at the angle R of ±0.003rad., and the shear bond crack appears along the main reinforcement or the steel flange when the chord rotation angle, R, reaches to ±0.005 to ±0.01rad. In the process after the attainment of the maximum strength, the shear bond crack continues to grow to the whole length of the column, while the crack due to the diagonal tension stops to grow, as shown in Fig. 10.

The bare steel portions after the test are investigated by taking the concrete off. The local buckling of neither flange nor web plates is observed in F series, while the damage on the web of the open-web steel portion is quite severe, such as the fracture and buckling of lattice plates in L series, and the fracture of butten plates at the joint to the chord member in B series.

b. Hysteretic Characteristics: Some sample hysteretic relations between the applied shear force, Q, and the displacement, δ(or the chord rotation, R), obtained in the tests are shown in Figs. 11(a) to (c). Specimens in F series show stable, spindle-shaped hysteresis loops, and large energy absorption capacities. The maximum shear strength is attained under the loading controlled by R of $\pm$0.010 to $\pm$0.015rad and the rate of the strength reduction after that is slow. When R reaches to $\pm$0.03rad., the loop seems to converge to that of the bare steel portion. In case of specimens in L and B series, when R is $\pm$0.005rad. to $\pm$0.01rad., the maximum shear strength is attained, followed by the quick strength reduction, and the hysteresis loop is the reversed S-shaped. Particularly in B series, the energy absorption capacity is very small.

Figure 12 shows the strength reduction when the cyclic loading is applied on the specimen under a fixed value of the displacement amplitude. The strength reduction factor(the ratio of the maximum strength attained in each cycle of loading to the maximum strength in the first cycle under that amplitude) is taken for the ordinate, and the number of loading cycles is taken for the abscissa. Solid circles are the data in the positive loading, and open circles the negative loading. In general, the strength reduction factor converges to a certain value after 3 cycles of loading; about 80% in F series, about 70% in L series, and about 60% in B series.

c. Effects of Experimental Parameters: In Figs. 13(a) to (e), the sustained load and the chord rotation angle at the returning point in the first cycle of positive loading under each displacement amplitude are plotted in Q-R coordinates, with taking concrete strength, flange and web thicknesses, lattice and butten plate thicknesses, the amount of web reinforcement, and the axial load ratio as varying parameters. The shear strength increases with the increase of those parameters except the axial load ratio which seems not to affect much on the shear strength, as long as the present test results are concerned. It is interesting to note that in each of the figures straight lines with an nearly equal negative slope are obtained by connecting the data at the returning points after the attainment of the maximum shear strength.

4. DISCUSSIONS ON THE TEST RESULTS

For each specimen, the maximum shear strength $\tilde{Q}_{max}$(solid circle) in the whole history of loading, and the minimum shear strength $\tilde{Q}_{min}$(open circle) detected at the negative loading under R = $\pm$0.03rad., are plotted in Fig. 14, where $\tilde{Q}$ is equal to the sum of the applied shear force Q and NR/2 due to the secondary moment. Ratios of $\tilde{Q}_{max}$ and $\tilde{Q}_{min}$ to Q_{mo} are shown in Fig. 15, where Q_{mo} is computed from the maximum flexural strength of the cross section obtained by the method of superposition. The ratios of $\tilde{Q}_{max}/Q_{mo}$ are about 70% in F series, and about 50% in L and B series, and it is shown that all apecimens except one(No. 15) fail in shear. In Fig. 16, Q_{all} is compared with the maximum and minimum strengths, $\tilde{Q}_{max}$ and $\tilde{Q}_{min}$, of each specimen, where Q_{all} is the temporary allowable shear strength obtained from AIJ Standard published by Architectural Institute of Japan. In the figure, ${}_cQ$, ${}_rQ$ and ${}_sQ$ are contributions to Q_{all} from concrete, web reinforcement and steel web, and $Q_{Fc/15}$ is computed assuming that the maximum shear stress of concrete, τ is given by Fc/15(Fc: cylinder strength). The safety factor possessed by Q_{max} is about 1.4 in F series, and about 2.5 in L and B series, while the safety factor based on Q_{min} is less than 1.0 for some specimens in L and B series, although it is about 1.1 in F series. The effects of the experimental parameters, such as concrete strength, web thickness, lattice plate thickness, butten plate thickness, the amount of web reinforcement and the axial load are shown in Figs. 17(a) to (f), respectively. For the shear strength of the full-web type steel portion, $_{fs}Q_o$, the smaller value of the yield shear strength of the web, $_{fs}Q_{so}$, and $_{fs}Q_{mo}$ determined from the full plastic moment of the steel cross section, is taken. The smaller value of the shear strength based on the failure mechanism shown in Fig. 17(c)(or Fig. 17(d)), $_{ls}Q_{so}$(or $_{bs}Q_{so}$), and the shear strength based on the full plastic moment of the open-web steel cross section, $_{ls}Q_{mo}$ (or $_{bs}Q_{mo}$), it taken for the shear stегength of the open-web steel portion, $_{ls}Q_o$(or $_{bs}Q_o$). From Fig. 17(a), it is observed that the shear strength obtained in the test increases with the increase of the concrete strength, and that the slope of the experimental curve is approximately equal to that of a straight line $_cQ_o = F_c \cdot b \cdot {}_rd/15$(b: width of concrete section, $_rd$: distance between upper and lower main reinforcing bars). It seems from Figs. 17(b), (c) and (d) that the rates of increase of the shear strength is approximately equal to those of $_{fs}Q_o$, $_{ls}Q_o$ and $_{bs}Q_o$, respectively, all of which are computed neglecting the bond action between steel and concrete. A similar statement seems to be also adequate for the effect of the web reinforcement, $_rP_w \cdot {}_{rw}\sigma_y \cdot b \cdot {}_rd$, in Fig. 17(e), where $_rP_w$ is the web reinforcement ratio, and $_{rw}\sigma_y$ yield stress of the web reinforcing bar. On the other hand the axial load does not affect on the shear strength, as seen in Fig. 17(f). Since the maximum shear strength is determined by the shear bond failure in the present test series, the result is different from the previously reported one that the axial load affects on the shear strength of the specimen failing in the diagonal tension.

5. CONCLUSIVE REMARKS

As already indicated, the shear bond failure plays a key role to determine the behavior of the steel reinforced concrete column under the axial load and alternately repeated shear. It is urgently needed to carry out the theoretical analysis associated with the development of the adequate mathematical model which explains the failure mechanism observed in the test.

REFERENCES

1. Tsuboi, Y. and Wakabayashi, M.:STUDY ON STEEL REINFORCED CONCRETE STRUCTURES, PART 5 - TESTS ON COLUMNS SUBJECTED TO AXIAL FORCE AND SHEAR, Trans. Architectural Institute of Japan, No. 56, June 1957, p. 39(In Japanese).

2. Wakabayashi, M.:EXPERIMENTAL STUDY ON COMPOSITE STRUCTURE, Report of the Institute of Industrial Science, University of Tokyo, Vol. 6, No. 2, Serial No. 45, Dec. 1956(In Japanese).

3. Wakabayashi, M., Minami, K. and Nakamura, T.:EXPERIMENTAL STUDIES ON STEEL-REINFORCED CONCRETE COLUMNS UNDER CONSTANT AXIAL FORCE AND ALTERNATE REPEATED BENDING AND SHEAR, Annuals, Disaster Prevention Research Institute, Kyoto University, No. 15-B, April 1973, p. 69(In Japanese).

4. Hirosawa, M., Ozaki, M. and Wakabayashi, M.:EXPERIMENTAL STUDY ON LARGE MODELS OF REINFORCED CONCRETE COLUMNS, Preprint of 5WCEE, Rome, June 25-29, 1973, No. 96.

ACKNOWLEDGEMENT

Research work presented here was supported by The Kozai Club and Building Research Institute, Ministry of Construction, Japan. Test apparatus was designed in Building Research Institute, and test was separately conducted in the laboratories of the following steel makers; Kawasaki Steel Corporation, Kobe Steel Ltd., Nippon Kokan K.K., Nippon Steel Corporation, and Sumitomo Metal Industry Ltd. Authors wish to express sincere appreciations for their supports.

TABLES AND FIGURES

Table 1. Test Program for Series F.

No.	Specimen Name	tf (mm)	tw (mm)	n	ϕ (mm)	s (mm)	Fc (kg/cm²)	N/No
1	12F8 M1216 W100 C210 N1	12	8	12	16	100	210	0.1
2	12F8 M1216 W100 C210 N2	12	8	12	16	100	210	0.2
3	12F8 M1216 W100 C210 N3	12	8	12	16	100	210	0.3
4	12F8 M1216 W100 C210 N1*	12	8	12	16	100	210	0.1
5	12F8 M1216 W100 C210 N2*	12	8	12	16	100	210	0.2
6	12F8 M1216 W100 C210 N3*	12	8	12	16	100	210	0.3
7	12F6 M1216 W100 C210 N2	12	6	12	16	100	210	0.2
8	12F10 M1216 W100 C210 N2	12	10	12	16	100	210	0.2
9	8F6 M1216 W100 C210 N2	8	6	12	16	100	210	0.2
10	8F8 M1216 W100 C210 N2	8	8	12	16	100	210	0.2
11	8F10 M1216 W100 C210 N2	8	10	12	16	100	210	0.2
12	16F6 M1213 W100 C210 N2	16	6	12	13	100	210	0.2
13	16F8 M1213 W100 C210 N2	16	8	12	13	100	210	0.2
14	16F10 M1213 W100 C210 N2	16	10	12	13	100	210	0.2
15	12F8 M0413 W100 C210 N2	12	8	4	13	100	210	0.2
16	12F8 M1216 W150 C210 N2	12	8	12	16	150	210	0.2
17	12F8 M1216 W050 C210 N2	12	8	12	16	50	210	0.2
18	12F8 M1216 W025 C210 N2	12	8	12	16	25	210	0.2
19	12F8 M1216 W100 C250 N2	12	8	12	16	100	250	0.2
20	12F8 M1216 W100 C300 N2	12	8	12	16	100	300	0.2
21	12F8 M1216 W100 C350 N2	12	8	12	16	100	350	0.2

Table 2. Test Program for Series L.

No.	Specimen Name	θ (deg.)	tl (mm)	n	ϕ (mm)	s (mm)	Fc (kg/cm²)	N/No
22	45L8 M1216 W100 C210 N1	45	8	12	16	100	210	0.1
23	45L8 M1216 W100 C210 N2	45	8	12	16	100	210	0.2
24	45L8 M1216 W100 C210 N3	45	8	12	16	100	210	0.3
25	30L8 M1216 W100 C210 N1	30	8	12	16	100	210	0.1
26	30L8 M1216 W100 C210 N2	30	8	12	16	100	210	0.2
27	30L8 M1216 W100 C210 N3	30	8	12	16	100	210	0.3
28	45L6 M1216 W100 C210 N2	45	6	12	16	100	210	0.2
29	45L10 M1216 W100 C210 N2	45	10	12	16	100	210	0.2
30	45L8 M1216 W150 C210 N2	45	8	12	16	150	210	0.2
31	45L8 M1216 W050 C210 N2	45	8	12	16	50	210	0.2
32	45L8 M1216 W025 C210 N2	45	8	12	16	25	210	0.2

Table 3. Test Program for Series B.

No.	Specimen Name	p	tb (mm)	n	ϕ (mm)	s (mm)	Fc (kg/cm²)	N/No
33	75B8 M1216 W100 C210 N1	0.75	8	12	16	100	210	0.1
34	75B8 M1216 W100 C210 N2	0.75	8	12	16	100	210	0.2
35	75B8 M1216 W100 C210 N3	0.75	8	12	16	100	210	0.3
36	75B6 M1216 W100 C210 N2	0.75	6	12	16	100	210	0.2
37	75B10 M1216 W100 C210 N2	0.75	10	12	16	100	210	0.2
38	75B8 M1216 W150 C210 N2	0.75	8	12	16	150	210	0.2
39	75B8 M1216 W050 C210 N2	0.75	8	12	16	50	210	0.2
40	75B8 M1216 W025 C210 N2	0.75	8	12	16	25	210	0.2
41	90B8 M1216 W100 C210 N2	0.90	8	12	16	100	210	0.2
42	50B8 M1216 W100 C210 N2	0.50	8	12	16	100	210	0.2
43	M1816 W100 C210 N2			18	16	100	210	0.2

tf : Flange Thickness of Wide Flange Section
tw : Web Thickness of Wide Flange Section
tl : Lattice Plate Thickness
tb : Butten Plate Thickness
n : Number of Longitudinal Reinforcement
ϕ : Nominal Diameter of Longitudinal Reinforcement
s : Spacing of Web Reinforcement
Fc : Concrete Strength
N/No : Ratio of Axial Force to Ultimate Compressive Strength
θ : Angle of Inclination of Lattice Plate
p : Ratio of Spacing of Butten Plate to Depth of Steel Cross Section

* h/D = 5.

All dimensions shown in these tables are nominal.

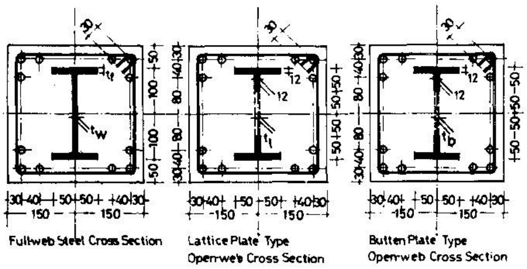

Fig. 1 Typical Column Cross Sections

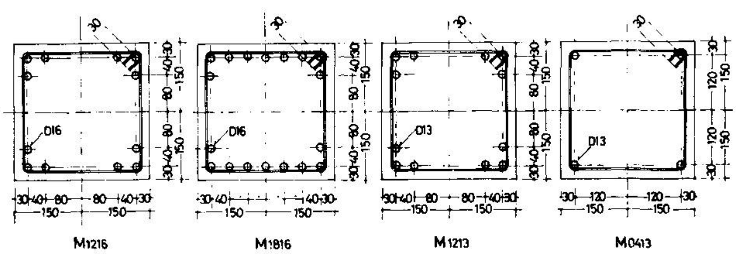

Fig. 2 Details of Reinforced Concrete Sections

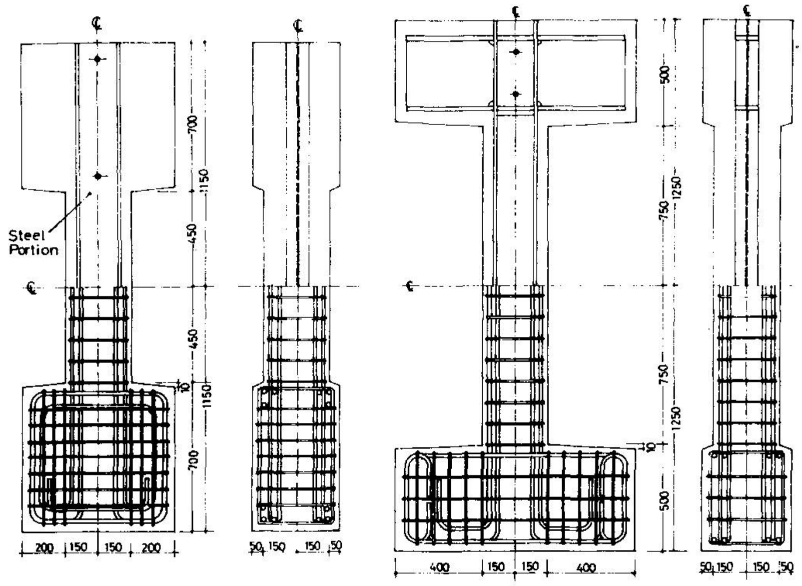

(a) h/D=3 (b) h/D=5

Fig. 3 Dimensions and arrangement of Reinforcements

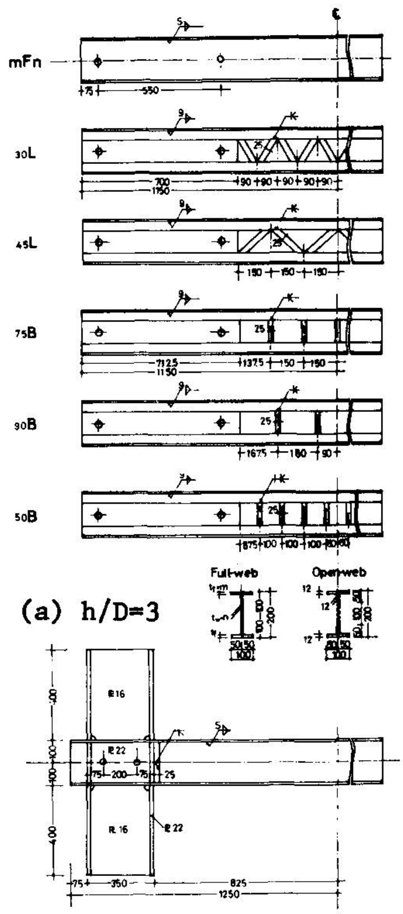

(a) h/D=3

(b) h/D=5

Fig. 4 Dimensions of Steel portion

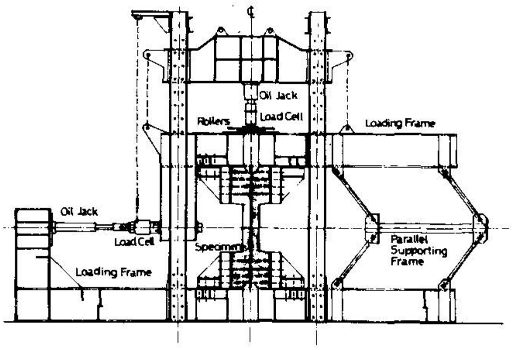

Fig. 5 Loading Apparatus

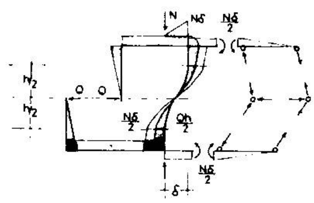

Fig. 6 Loading Principle

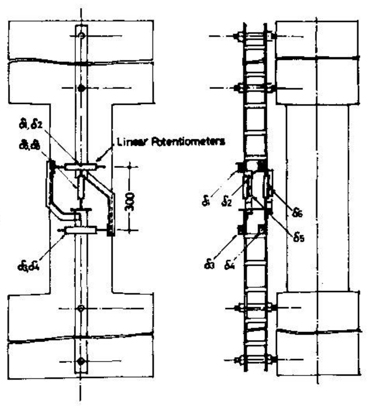

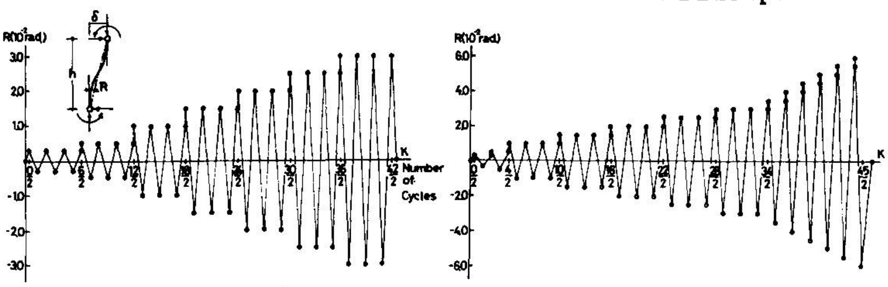

(a) h/D = 3 (b) h/D = 5

Fig. 8 Loading Program

Fig. 7 Data Detection System

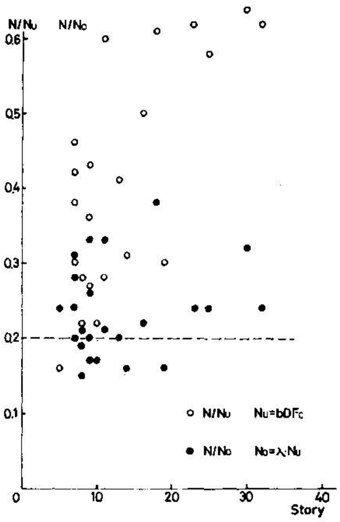

Fig. 9 Axial Loads in Columns

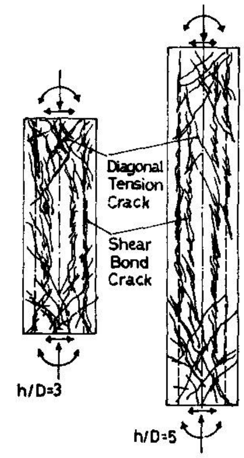

Fig. 10 Crack Observation

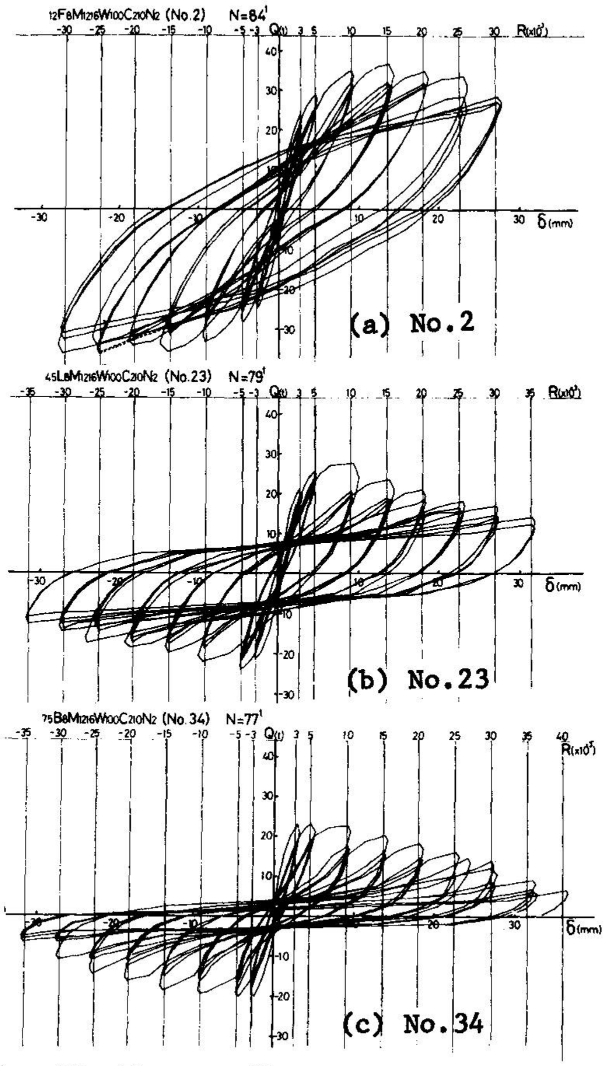

Fig. 11 Shear-Deflection Relationship

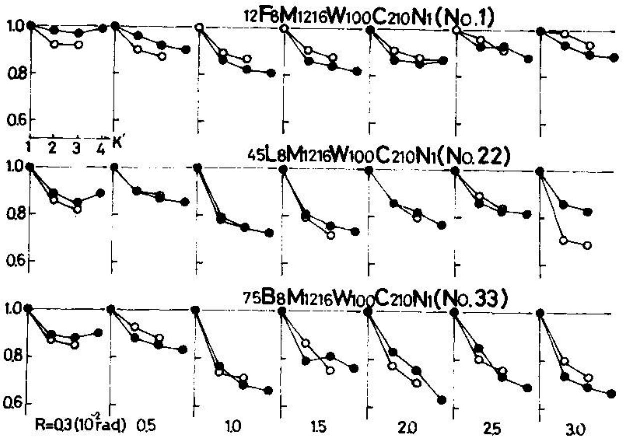

Fig. 12 Deterioration of Shear Strength

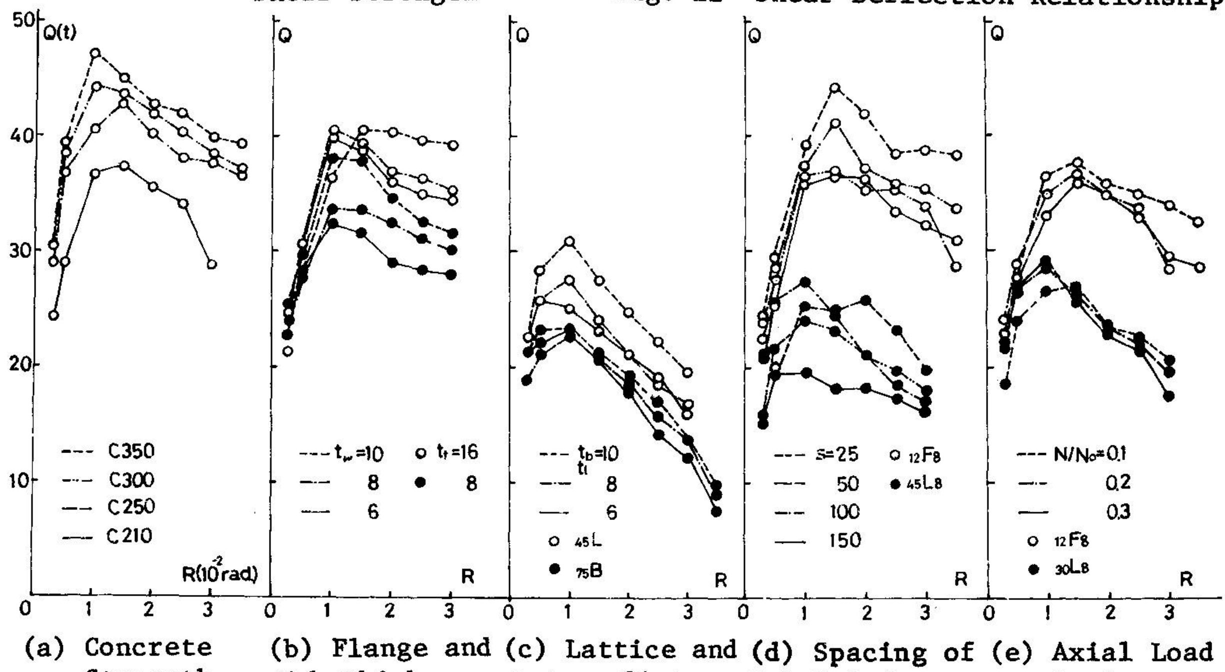

(a) Concrete Strength (b) Flange and Web Thickness (c) Lattice and Butten Plate Thickness (d) Spacing of Web Reinforcement (e) Axial Load Ratio

Fig. 12 Deterioration of Shear Strength

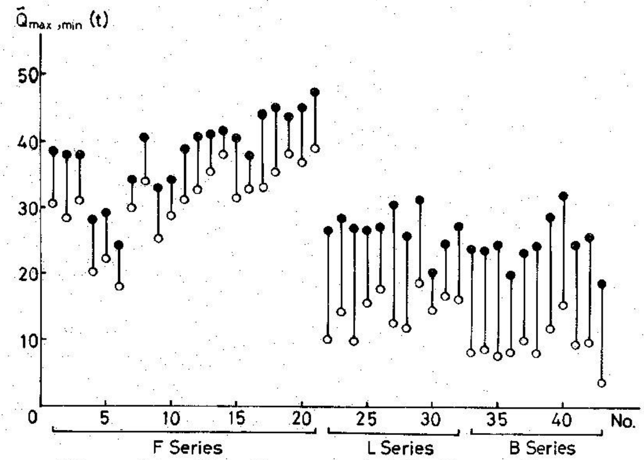

Fig. 14 Maximum and Minimum Shear

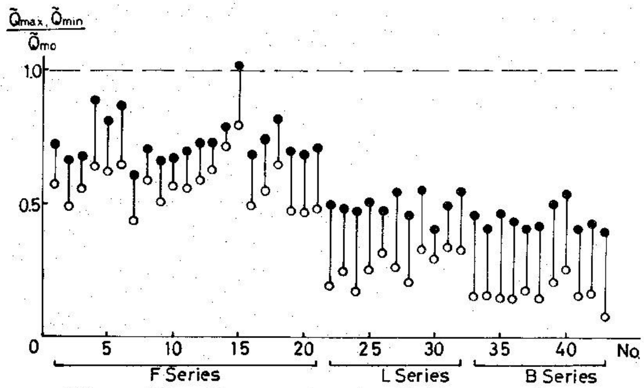

Fig. 15 Comparison of Strength

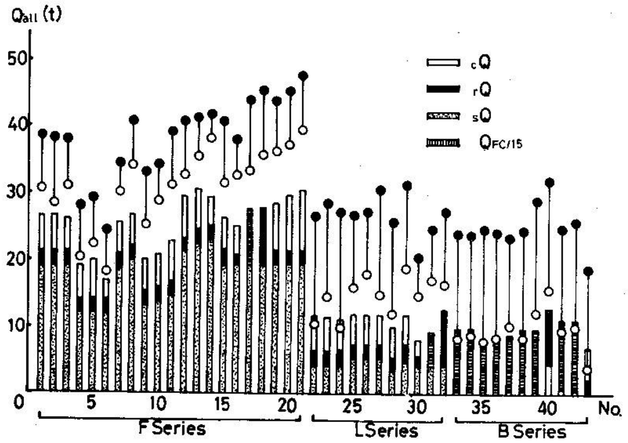

Fig. 16 Comparison of Measured and Allowable Shear Strength

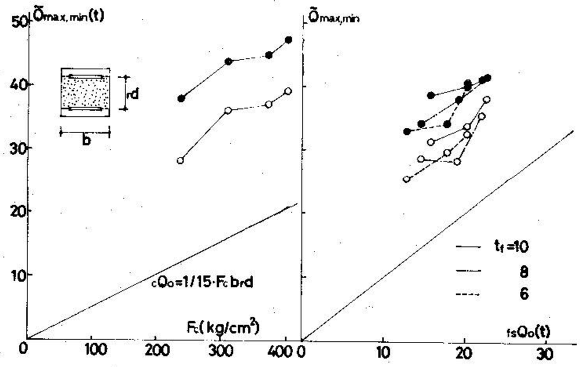

(a) Concrete Strength (b) Flange and Web Thickness

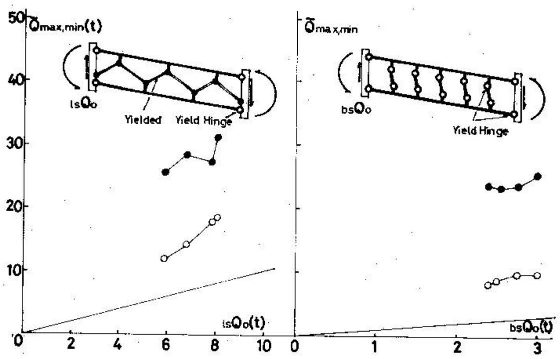

(c) Lattice Plate Thickness (d) Butten Plate Thickness

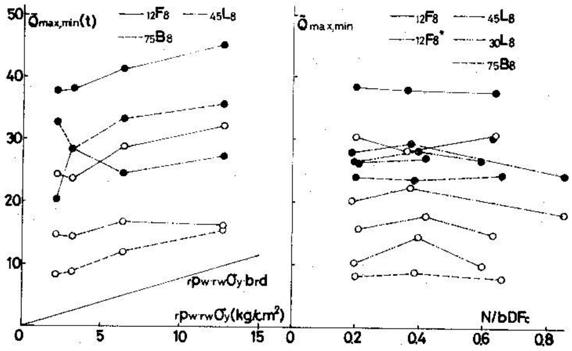

(e) Amount of Web Reinforcements (f) Axial Load

Fig. 17 Effects of Experimental Parameters

SUMMARY

A parametric experimental study is carried out on the shear strength of steel reinforced concrete (SRC) columns under constant axial load and alternately repeated bending and shear, using three types of steel sections; full-web type, lattice plate type open-web and butten plate type open-web. The effects of experimental parameters, such as axial load ratio, web plate thickness, spacing of web reinforcements, thickness of lattice and butten plates and concrete strength, on the shear strength and the hysteretic behavior of columns are discussed.

RESUME

On procède à une étude expérimentale de la résistance au cisaillement de colonnes en béton armé soumises à une force axiale constante et à une flexion et un cisaillement alternés; on utilise trois types de section pour l'armature. On discute l'influence des paramètres des essais, tels que grandeur de la force axiale, forme de l'armature et résistance du béton, sur la résistance au cisaillement et le comportement hystérétique des colonnes.

ZUSAMMENFASSUNG

Es wird eine experimentelle Untersuchung über den Einfluss verschiedener Parameter auf die Schubfestikeit von Stahlbetonstützen unter konstanter Normalkraft und abwechselnd wiederholter Beanspruchung auf Biegung und Schub durchgeführt. Hierbei werden drei Typen von Bewehrungs-Querschnitten untersucht. Die Wirkung des Versuchs-Parameter, wie z.B. die Grösse der Normalkraft, die Form der Bewehrung sowie die Betonfestigkeit auf die Schubfestigkeit und das Energieaufnahmevermögen der Stützen werden diskutiert.

Leere Seite
Blank page
Page vide

Strength of Laterally Loaded Reinforced Concrete Columns

Résistance des colonnes en béton armé soumises à une charge latérale

Tragfähigkeit seitlich belasteter Stahlbetonstützen

Wai F. CHEN
Associate Professor
Department of Civil Engineering
Fritz Engineering Laboratory
Lehigh University
Bethlehem, Pennsylvania, USA

Andrie C.T. CHEN
Design Engineer
Gannett, Flemming, Corddry and
Carpenter, Incorporated
Harrisburg, Pa., USA

INTRODUCTION: Most theoretical investigations on reinforced concrete beam-columns have been limited to beam-columns with no lateral loads [Fig. 1(b)]. This investigation was made to obtain solutions of a beam-column with a concentrated lateral load applied at mid-span [Fig. 1(a)]. In the analysis, the moment-curvature-thrust relationships are first established. These relationships are then approximated by appropriate mathematical expressions. Finally, the computer programs developed in Refs. [1] and [2] are modified and utilized to obtain solutions of the problems shown in Fig. 1. Non-dimensional interaction curves relating thrust, slenderness ratio, and lateral load for the maximum load carrying capacity of the reinforced concrete beam-columns are presented. The analytically obtained results are then compared with the prediction based on the empirical ACI formula (moment magnifier method) and good agreement is observed in most cases.

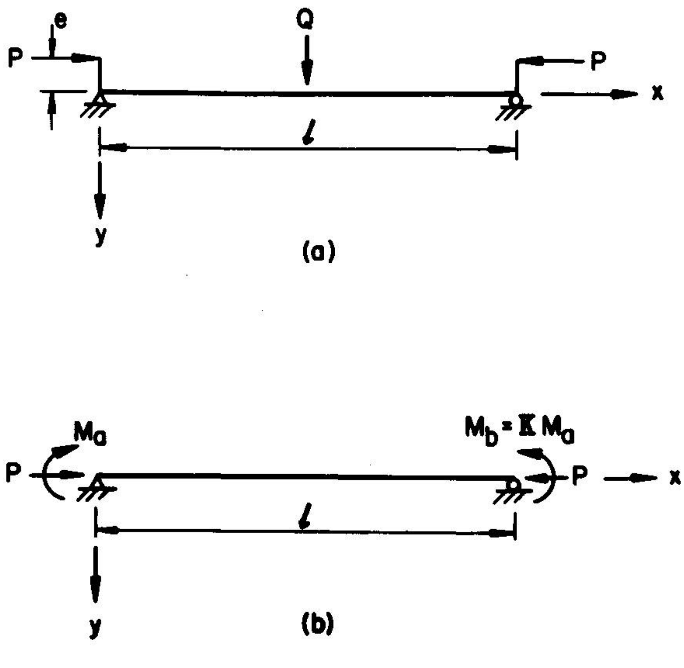

Fig. 1 Beam-Columns Studied in the Paper

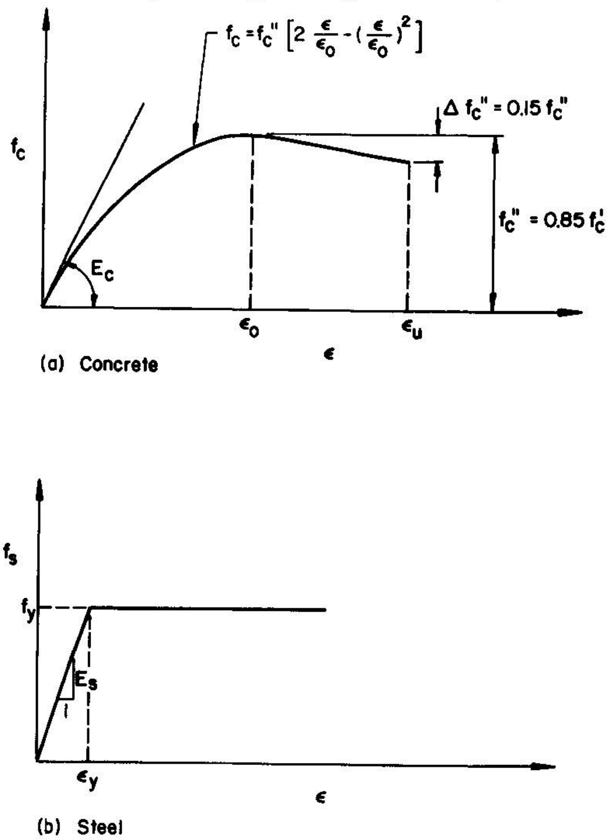

Fig. 2 Stress Strain Relationships used in the Paper

STATEMENT OF THE PROBLEM: It is assumed that the beam-column will fail in the plane of the loading only. The failure is either caused by excessive bending of the beam-column as a whole or by compressive crushing of the critical cross section because of the limited deformability of concrete in compression. The crushing strain ϵ_u used in the analysis is 0.004 in/in. For the case, Fig. 1(a), it is further assumed that the axial force P at the ends of the beam-column will be applied first and maintained at a constant value as the lateral load Q is continuously increased from zero to a maximum value and then allowed to drop off steadily beyond the maximum point. For the case, Fig. 1(b), proportional loading is assumed for M_a and M_b, i.e., $M_b = KM_a$.

MOMENT-CURVATURE-THRUST RELATIONSHIPS: Several widely accepted assumptions are adopted herein in obtaining the moment-curvature-thrust relationships of reinforced concrete sections. For the concrete, Hognestad's stress-strain relationship [3] in compression is used and its tensile strength is neglected, [Fig. 2(a)]. The initial modulus of elasticity for concrete is taken [3] as $E_c = 1{,}800{,}000 + 500\ f''_c$ in which $f''_c = 0.85\ f'_c$. For reinforcing steel, the stress-strain relationship is assumed to be linearly elastic-perfectly plastic, [Fig. 2(b)] and E_s is taken at 30,000,000 psi. The creep effects of both materials are neglected.

A symmetrically reinforced rectangular concrete cross section is considered herein (Fig. 3). Assuming linear strain distribution over the section, the corresponding stress distribution and thus the moment-curvature-thrust relationships of the section can be obtained. Details of the method and the computer program are described elsewhere [4].

It is convenient to introduce quantities so that the moment-curvature-thrust relationships and hence the basic differential equations may be written in a form more appropriate for computation. The nondimensional moment, curvature and thrust are

$$m = \frac{M}{M_B} \quad , \quad \varphi = \frac{\Phi}{\Phi_B} \quad , \quad p = \frac{P}{P_o} \tag{1}$$

in which M_B is the balanced moment which produces at ultimate strength, simultaneously, a strain of $\epsilon_u = 0.004$ in the extreme fiber of concrete and the strain $\epsilon_y = f_y/E_s$ at the first yield on the tension steel; Φ_B is the corresponding curvature. And P_o is defined as

$$P_o = f''_c\, A_c + A_s\, f_y \tag{2}$$

in which A_s = total steel area and A_c = concrete net area.

In general, the moment-curvature curve with a constant thrust for a reinforced concrete section can be separated into three regimes: first regime, the slope of the curve is nearly constant; second regime, the rate of change of the slope is relatively large, third regime, the rate of change of the slope is small and the moment asymptotically approached the maximum moment capacity m_{pc} of the cross section. The dimensionless maximum curvature is denoted by φ_{pc}.

Following the previous work [5,6], the actual moment-curvature-thrust relationships may be closely represented by the following three mathematical expressions:

In the first regime ($0 \leq \varphi \leq \varphi_1$)

$$m = a\varphi \tag{3}$$

In the second regime ($\varphi_1 \leq \varphi \leq \varphi_2$)

$$m = b - \frac{c}{\varphi^{1/2}} \quad (4)$$

In the third regime ($\varphi_2 \leq \varphi \leq \varphi_{pc}$)

$$m = m_{pc} - \frac{f}{\varphi^{2}} \quad (5)$$

where a, b, c, f, φ_1, φ_2, φ_{pc}, and m_{pc} may be treated as the arbitrary curve-fitting parameters. The parameters will be a function of axial force p only. These functions may be expressed as polynomials of p for a given cross section. The choice of the curve-fitting parameter functions to fit an actual m-φ-p curve is not as difficult as it would seem to be. A detailed procedure to guide the choice of these parameter functions is given in Ref. 6. The approximate equations (Eqs. 3, 4, and 5) and the actual moment-curvature curves for a section with a constant thrust are compared in Figs. 3 and 4. The actual moment-curvature curves (solid curves in the figures) are calculated for the following cross section and material properties: $d'/t = 0.1$, $A_s/bt = 0.04$, $f_y = 45$ ksi, and $f'_c = 3$ ksi where b, d' and t are defined in the inset of Fig. 3. Since the failure of a beam-column is usually controlled by the second and third regimes, it can be concluded that the approximate m-φ-p equations are sufficiently accurate for practical use.

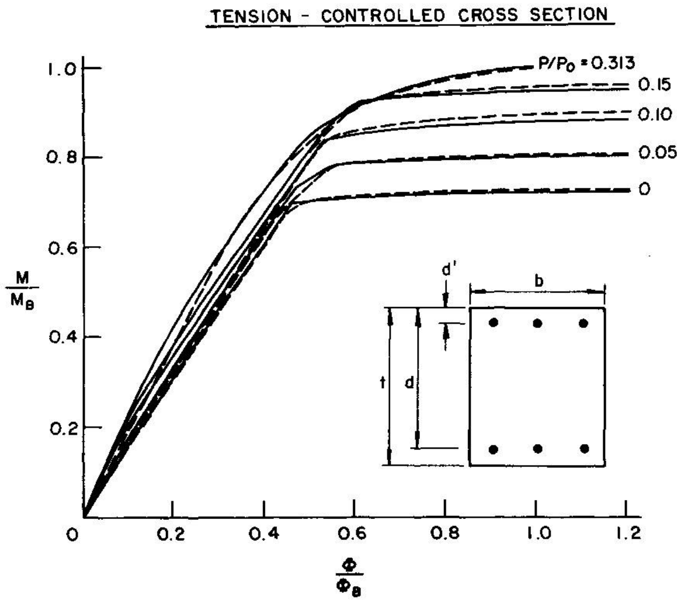

Fig. 3 Moment-Curvature-Thrust Relationships (Approximate Curves Shown Dashed)

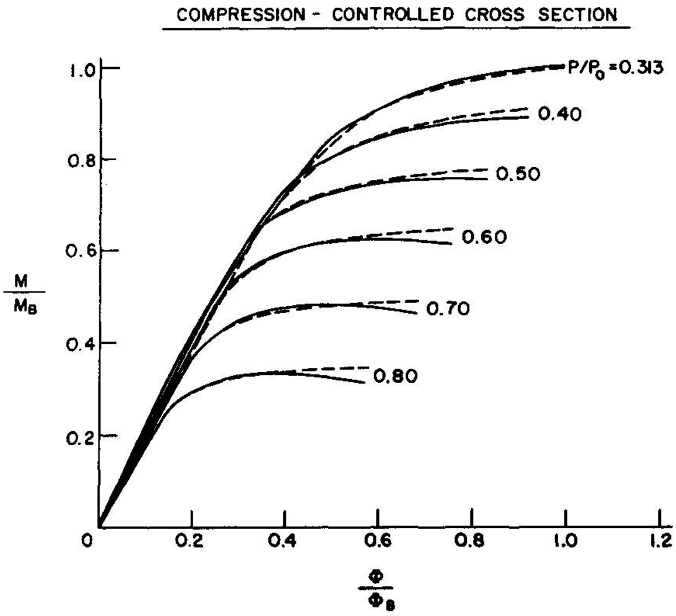

Fig. 4 Moment-Curvature-Thrust Relationships (Approximate Curves Shown Dashed)

NUMERICAL RESULTS: Using the approximate moment-curvature-thrust relationships, the basic differential equations of the beam-column are expressed in terms of curvature. The solutions to these differential equations with various boundary conditions are reported in Refs. [1] and [5].

A modified version of the program in Ref. [2] is used to solve the reinforced concrete beam-column problem as shown in the inset of Fig. 5. Computer programs are now available at Lehigh University. The results obtained directly from the program are the values of lateral load and the corresponding mid-span curvature (Fig. 5) The maximum lateral load, at which the beam-column will fail either by the instability of the beam-column or by the crushing of the mid-span cross section, is also indicated in the output of the program. By varying the beam-column length and the magnitude of the applied thrust, a series of maximum load interaction curves for combinations of axial force, P/P_o, and lateral load Q/Q_o, ($Q_o = 4\ M_B/\ell$) that can be safely supported by the reinforced concrete beam-column are obtained and plotted in Figs. 6 through 10, for the eccentricity ratios e/t = 0.0, 0.1, 0.3, 0.6 and 1.0, respectively.

The Column-Curvature-Curve method developed in Ref. [1] is utilized in the numerical solutions of the reinforced concrete beam-column shown in Figs. [11] and [12]. The interaction curves obtained are also compared in the figures with the results from Ref. 7, and good agreement is observed.

COMPARISON OF RESULTS WITH ACI MOMENT MAGNIFIER FORMULA: In designing reinforced concrete members carrying combined axial compression and bending moment, use is frequently made of the so-called moment magnifier method. According to the method, the influence of the second-order PΔ moment caused by the lateral deflection of a slender column on column strength is considered by multiplying the first-order moment M_o by the moment magnifier factor, δ. Formula recommended for estimating the magnification factor, δ is given in the 1971 ACI Building Code [8].

The general form of the formula which will be used in the comparison is Formula (10-5) given in Section 10 of the ACI Code. It takes the form

$$\delta = \frac{C_m}{1 - (P/P_c)} \tag{6}$$

where C_m = a coefficient depending on loading and support conditions to be taken as 1 and $P_c = \pi^2\ EI/\ell^2$ in which EI is computed by the approximate formula

$$EI = \frac{E_c\ I_g}{5} + E_s\ I_s \tag{7}$$

where I_g = moment of inertia of gross concrete section about the centroidal axis, neglecting the reinforcement, and I_s = moment of inertia of reinforcement about the centroidal axis of the member cross section.

The maximum loads determined by the ACI Formula (6) are compared in Figs. 6 to 10 with the numerical results obtained here. In general, the ACI Formula is seen to give good predictions for most cased investigated. For the case e/t = 0 (Fig. 6), the formula tends to underestimate the load carrying capacity for high slenderness ratio columns, especially in the high axial force range. For the case e/t= 0.1(Fig. 7), the formula gives an excellent prediction for all slenderness ratios considered. For the cases e/t = 0.3, 0.6 and 1.0 (Figs. 8, 9 and 10), the trend reverses and the formula tends to overestimate the load carrying capacity for low slenderness ratio columns, but the difference is usually small. It may be concluded from this study that the current ACI formula is valid not only in predicting the ultimate strengths of beam-columns without transverse loads but also in estimating the ultimate strength of laterally loaded beam-columns.

CONCLUSIONS: Ultimate strength of a laterally loaded reinforced concrete beam-column has been obtained. Nondimensional interaction curves relating thrust, slenderness ratio, and lateral load for the maximum load carrying capacity of the reinforced concrete beam-column are presented. The maximum lateral loads determined by the analytical method have been compared in Figs. 6 to 10 with ACI moment magnification formula. Results indicated that ultimate strength predicted by ACI is in good agreement with calculated theoretical values.

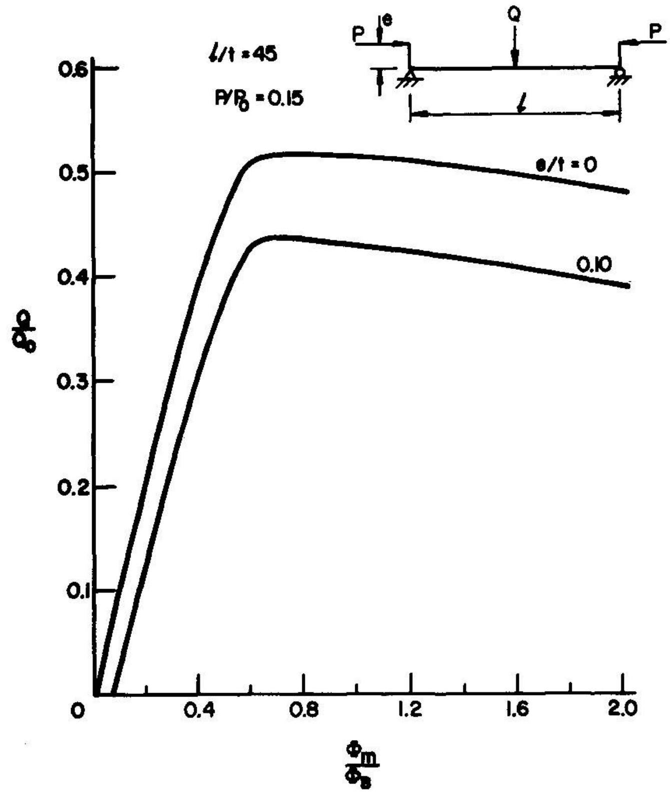

Fig. 5 Lateral Load vs. Mid-Section Curvature Curves

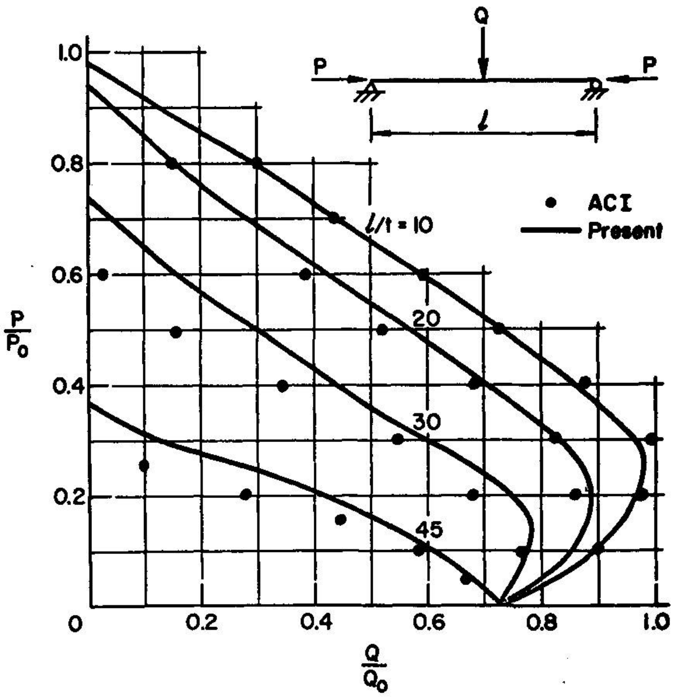

Fig. 6 Interaction Curves for Lateral Load vs. Thrust for e/t = 0

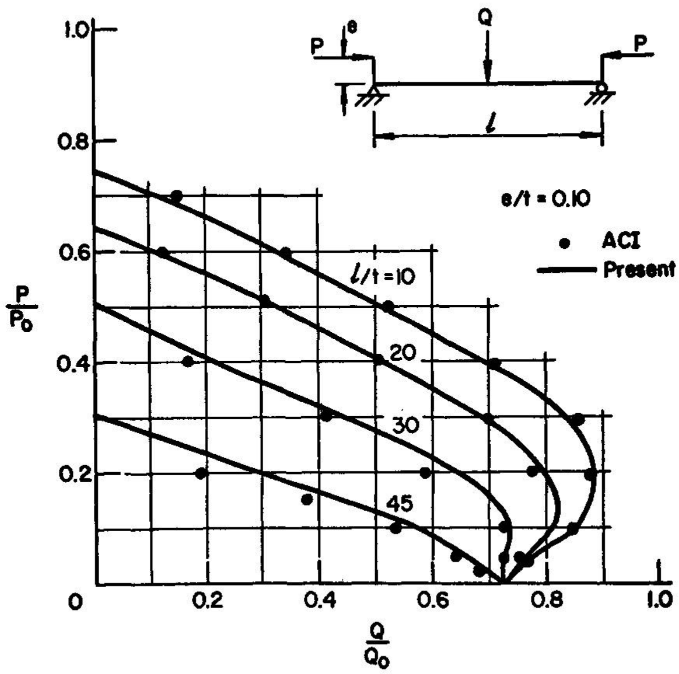

Fig. 7 Interaction Curves for Lateral Load vs. Thrust for e/t = 0.1

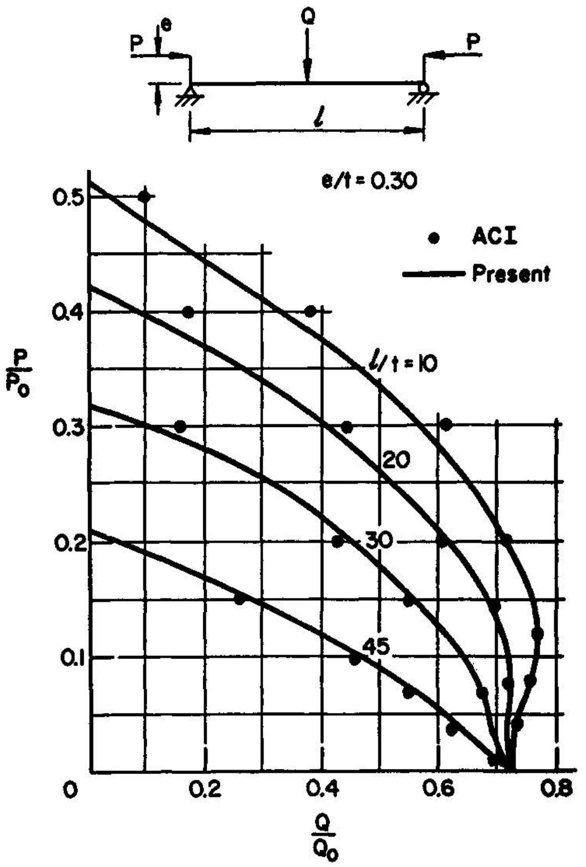

Fig. 8 Interaction Curves for Lateral Load vs. Thrust for e/t = 0.3

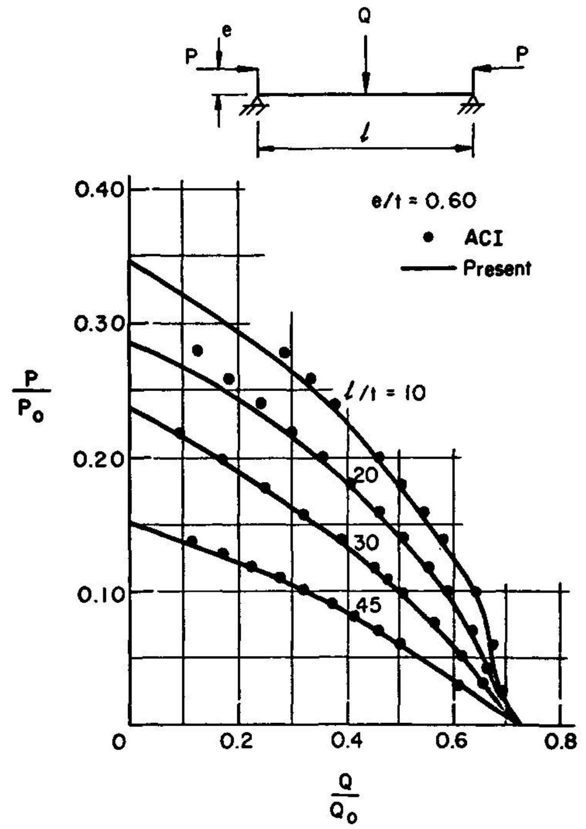

Fig. 9 Interaction Curves for Lateral Load vs. Thrust for e/t = 0.6

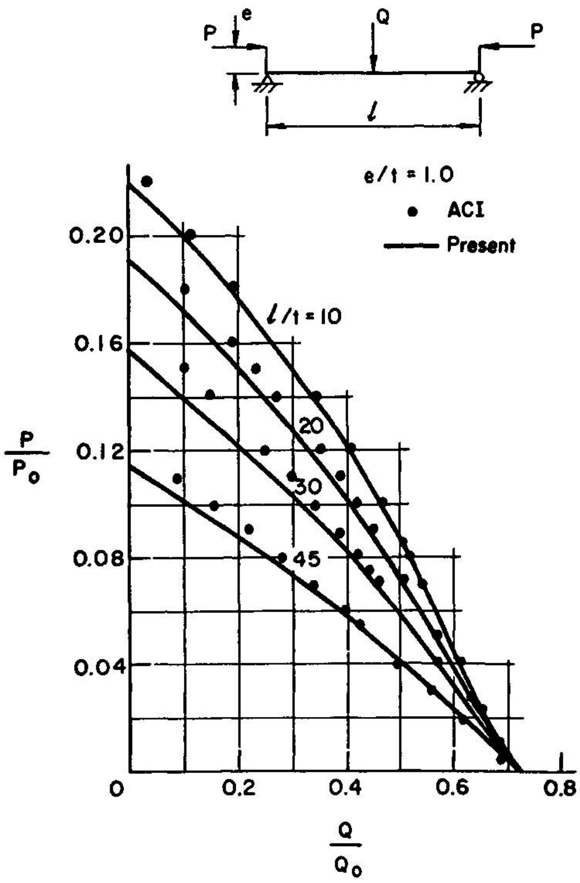

Fig. 10 Interaction Curves for Lateral Load vs. Thrust for e/t = 1.0

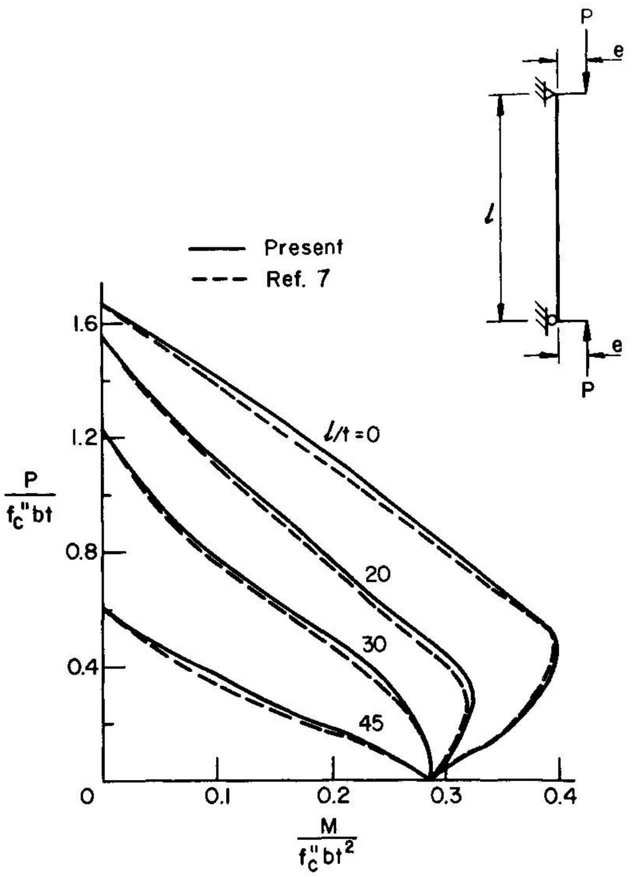

Fig. 11 Comparison of Interaction Curves --Equal End Eccentricities

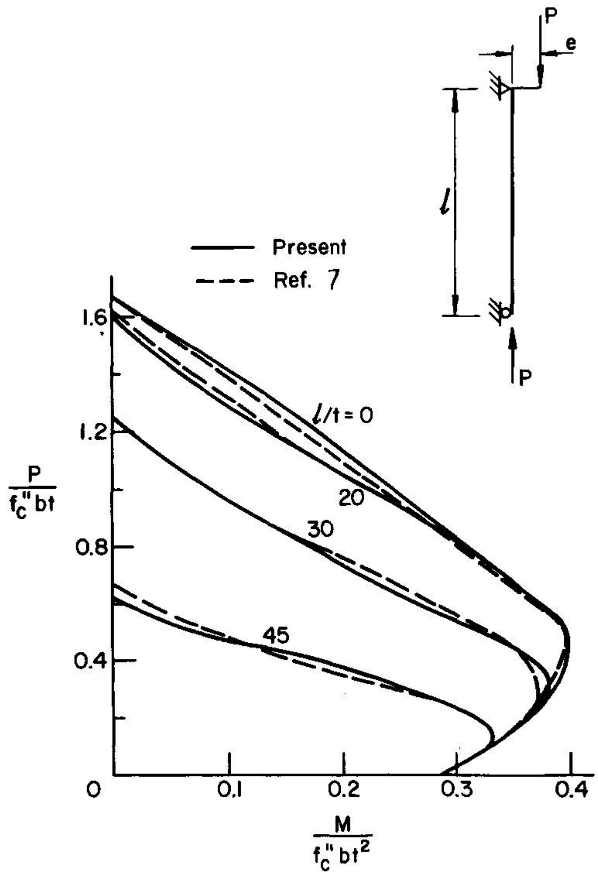

Fig. 12 Comparison of Interaction Curves--One End Eccentricity

REFERENCES:

1. Chen, W. F. and Atsuta, T., "Column Curvature Curve Method for Analysis of Beam-Columns", The Structural Engineer, The Journal of the Institute of Structural Engineers, London, England, Vol. 50, No. 6, June 1972, pp. 233-240.

2. Iyengar, S. N. and Chen, W. F., "Computer Program for an Inelastic Beam-Column Problem", Fritz Engineering Laboratory Report No. 331.7, Lehigh University, May 1970.

3. Hognestad, E. A., "A Study of Combined Bending and Axial Load in Reinforced Concrete Members", Bulletin No. 399, University of Illinois Engineering Experiment Station, Urbana, Ill., 1951.

4. Chen, A. C. T. and Chen, W. F., "Solutions to Various Reinforced Concrete Beam-Column Problems", Fritz Engineering Laboratory Report No. 370.2, September 1970, Lehigh University.

5. Chen, W. F., "General Solution of Inelastic Beam-Column Problems", Journal of the Engineering Mechanics Division, ASCE, Vol. 96, No. EM4, August 1970, pp. 421-441.

6. Chen, W. F., "Further Studies of Inelastic Beam-Column Problems", Journal of the Structural Division, ASCE, Vol. 97, No. ST2, February 1961, pp. 529-544.

7. Pfrang, E. O. and Siess, C. P., "Behavior of Restrained Reinforced Concrete Columns", Journal of the Structural Division, ASCE, Vol. 90, ST5, Proceeding Paper 4111, October 1964, pp. 113-136.

8. ACI Committee 318, "Building Code Requirements for Reinforced Concrete", (ACI 318-71), American Concrete Institute, Detroit, 1971.

SUMMARY

Analytical solutions are obtained for the maximum load carrying capacity of a reinforced concrete beam-column subject to combined axial thrust and a concentrated lateral load applied at mid-span. Numerical results are presented in the form of interaction curves relating axial thrust, lateral load and slenderness ratio. The analytically obtained results are compared with the prediction based on the empirical ACI formula and good agreement is observed in most cases.

RESUME

On obtient une solution analytique pour exprimer la charge ultime d'un système colonne-poutre en béton armé soumis à l'action conjuguée d'une force axiale et d'une charge latérale concentrée appliquée à mi-hauteur. On présente les résultats numériques sous forme de courbes d'interaction qui mettent en relation la force axiale, la charge latérale et l'élancement. On compare les résultats du calcul avec ceux obtenus par les formules empiriques ACI et on observe une bonne concordance dans la plupart des cas.

ZUSAMMENFASSUNG

Rechnerische Lösungen werden erhalten für die Tragfähigkeit von Balken-Stützen-Systemen unter der kombinierten Wirkung von Normalkraft und konzentrierter seitlicher Last in Feldmitte. Die numerischen Ergebnisse werden in Form von Interaktionsdiagrammen dargestellt, abhängig von Normalkraft, seitlicher Belastung und Schlankheit. Die rechnerisch erhaltenen Resultate werden mit den empirischen ACI-Formeln verglichen, wobei in den meisten Fällen gute Uebereinstimmung herrscht.

Ein baustatisches Verfahren zur Bestimmung der Traglasten ebener Druckbogen

A Practical Method for Determining the Load Capacity of Plane Arches under Compression

Un procédé pratique pour le calcul de la charge ultime des arcs plans comprimés

Helmut BOMHARD
Direktor der Dyckerhoff & Widmann AG
München, BRD

1. Einleitung

Das Traglastproblem des Druckbogens ist ein Durchschlagproblem mit oder ohne Gleichgewichtsverzweigung. Der für die Traglast ungünstige Durchschlagvorgang ist nur mit einer geometrisch nichtlinearen Theorie faßbar. Doch genügt für die numerische Traglastrechnung im Schlankheitsbereich, den die technischen Baubestimmungen erlauben (z.B. [1] [2]), die geometrisch linearisierte Theorie. Mit dieser bestimmte Traglasten sind dann nur mehr wenige Prozent größer als die Durchschlaglasten, wie Vergleichsrechnungen an 2-Gelenkbogen beweisen [3]. Bei Pfeilverhältnissen $f/l \geq 0{,}1$ kann außerdem die Achsdehnung ε_o unberücksichtigt bleiben.

Auf der Grundlage der geometrisch linearen Theorie wird ein leistungsfähiges und anschauliches Rechenverfahren großer Genauigkeit entwickelt, mit dem die Traglasten ebener Bogen ohne und mit Gleichgewichtsverzweigung schnell von Hand gerechnet werden können, und das mit den üblichen baustatischen Mitteln auskommt. Mit dem Verfahren ist das geometrisch linearisierte Traglastproblem sowohl näherungsweise als auch genau lösbar. Erfaßbar sind bei beliebiger Bogenform und frei wählbaren σ - ε -Beziehungen für Beton und Stahl nicht nur vertikale und horizontale Lasten, sondern auch Geometrieimperfektionen, Vor- und Eigendehnungszustände, eingeprägte Verschiebungen sowie Kriechverformungen.

In [4] ist das Verfahren dazu benutzt, den Einfluß unterschiedlicher Querschnittsformen (Rechteck und 2-Punktquerschnitt) und unterschiedlicher σ - ε -Diagramme von Beton (Normalbeton und Leichtbeton) zu studieren.

2. Voraussetzungen

a. Der Bogen ist eben und nur in seiner Ebene belastet. Ausweicherscheinungen senkrecht zur Bogenebene werden ausgeschlossen.
b. Die Bogenquerschnitte sind unverformbar. Die Schwerpunkte ihrer Betonflächen bilden die Bogenachse. Eine Hauptachse der Querschnitte liegt in der Bogenebene, im übrigen sind sie beliebig geformt.
c. Für die Querschnitte gilt die Bernoulli-Hypothese.
d. Die Anfangskrümmung ist so schwach, daß die Schnittgrößen-Verzerrungsbeziehungen des geraden Stabes gelten.
e. Die Lasten bleiben bei Verformung richtungstreu und ändern ihre Größe nicht.

3. Gleichgewicht

In den Gleichungen kennzeichnet der Zirkumflex die Werte des verformten Bogens.

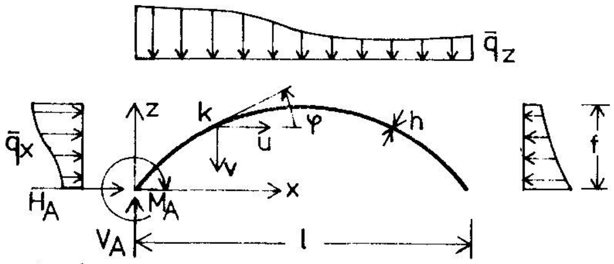

BILD 1
GEOMETRIE UND BELASTUNG

Belastung (Bild 1)

$$\tilde{q}_z d\tilde{s} = \tilde{q}_z(1+\varepsilon_o)\, ds = q_z\, ds = \bar{q}_z\, dx \quad (1a)$$

$$\tilde{q}_x d\tilde{s} = q_x(1+\varepsilon_o)\, ds = q_x\, ds = \bar{q}_x\, dz \quad (1b)$$

Bei $\varepsilon_o = 0$ ist jede Belastung mit einem einheitlichen Lastparameter beschreibbar, weil $\tilde{q}_z = q_z$ und $\tilde{q}_x = q_x$.

Moment und Normalkraft im Querschnitt k (Bild 1)

$$\tilde{M}_{ek} = M_k + V_k u_k + H_k v_k + \triangle M_A + \triangle V_A x_k - \triangle H_A z_k + \int_o^{x_k} \bar{q}_z u\, dx - \int_o^{z_k} \bar{q}_x v\, dz \quad (2a)$$

$$\tilde{N}_{ek} = N_k(1-\varepsilon_{ok}) + (V_k v_k' - H_k u_k')\cos\varphi_k - \triangle V_A \sin\varphi_k - \triangle H_A \cos\varphi_k \quad (2b)$$

Auf den rechten Gleichungsseiten ist der Zeiger e für "äußere Schnittgröße" der Übersichtlichkeit wegen weggelassen.

Es bedeuten: $$V_k = V_A - \int_o^{x_k} \bar{q}_z dx,\; H_k = H_A + \int_o^{z_k} \bar{q}_x dz, \text{ und} \quad (3)$$

$$\triangle M_A = \tilde{M}_A - M_A,\; \triangle V_A = \tilde{V}_A - V_A,\; \triangle H_A = \tilde{H}_A - H_A. \quad (4)$$

In (2) sind, im Sinne einer geometrisch linearen Theorie kleiner Verschiebungen, alle Glieder vernachlässigt, die Produkte von Verschiebungsgrößen enthalten (Abschnitt 10).

Die bezogenen Schnittgrößen m und n sind dimensionslos und parametrisiert: $$m = \frac{M}{A_c h f_c'}\,,\quad n = \frac{N}{A_c f_c'} \quad (5)$$

Der Einfachheit halber sind Ortszeiger k und Zirkumflex weggelassen.

4. Geometrie

Alle Geometriebeziehungen werden linearisiert. Damit gelten die üblichen baustatischen Methoden wie Arbeitsgleichung, Mohrsche Analogien usw.

5. Werkstoffgesetz

Beanspruchbarkeit (m,n) (Bild 2) und Verzerrungen (Stabkrümmung Kh und Achsdehnung ε_o) (Bild 3) eines Querschnitts gegebener Form und Bewehrung ($\omega = p\sigma_y/f_c'$, $\omega' = p'\sigma_y/f_c'$) werden festgelegt durch

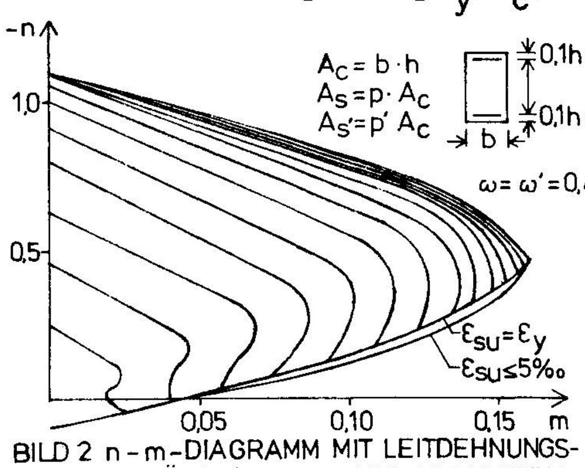

BILD 2 n-m-DIAGRAMM MIT LEITDEHNUNGSZUSTÄNDEN ε_{c1} = KONST. GERASTERT. RASTERABSTAND $\triangle\varepsilon_{c1} = 0{,}25‰$

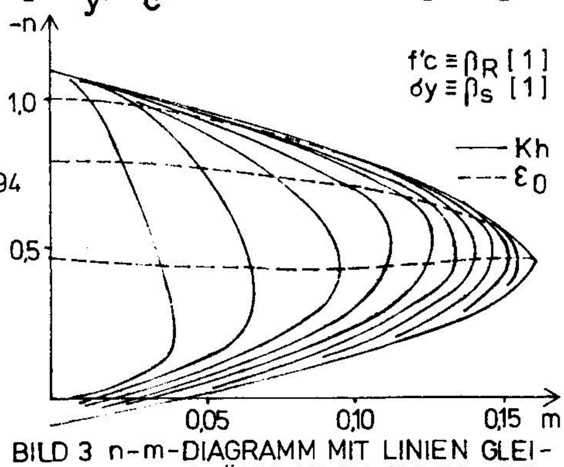

BILD 3 n-m-DIAGRAMM MIT LINIEN GLEICHER KRÜMMUNG Kh (0,5/1,0...5,0) U. ACHSDEHNUNG ε_0 (-0,5,-1,0...-2,0) die Spannungsdehnungslinien von Beton und Stahl sowie durch Dehnungsdiagramme, die angeben, wie weit die σ- ε-Linien ausgenutzt werden dürfen. Jedem Wertepaar m, n ist ein Wert Kh = Kh (m,n) und $\varepsilon_o = \varepsilon_o(m,n)$ eindeutig zugeordnet (s. Bild 3).

Für das Rechenverfahren wird das Interaktionsdiagramm (Bild 2) durch Interaktionslinien gerastert, die durch Variation der Größe der Leitdehnung ε_{c1} des gedrückten Querschnittsrandes erhalten werden. Die Linien bilden nichts anderes als Interaktionsdiagramme mit fiktiven Grenzdehnungen $\varepsilon_{cu\ fikt} = \varepsilon_{c1}$ = konst. Durch dieses Rastern, das mit einem Rechner keine Mühe bereitet, gelingt es, auch die Gleichgewichtszustände zu erfassen, bei denen der Bogen instabil wird, ohne Grenzdehnungen zu erreichen (Linien mit dn/dm = 0 in Bild 8). Meist genügt ein grober Raster.

Das Werkstoffverhalten wird für Kurzzeitlast elastisch vorausgesetzt. Die Traglast wird damit unabhängig von der Belastungsgeschichte.

6. Traglastberechnung mit einem angenommenen Krümmungsverlauf

Das Rechenverfahren ist innerhalb seiner Voraussetzungen auf beliebige Bogenformen und Belastungen anwendbar (Abschnitt 7). Es wird hier am Beispiel symmetrischer Bogen dargestellt, deren Achse bei $\varepsilon_o = 0$ Stützlinie einer symmetrischen Gleichlast $\bar{q}_{zs}$ ist, und die entweder einer antimetrischen Gleichlast $\bar{q}_{za} = \beta\bar{q}_{zs}$ oder einer symmetrischen Scheitellast $Q = \beta\bar{q}_{zs}l$ als Störlasten ausgesetzt sind (Bilder 4, 5, 6). Die Grundgedanken des Verfahrens kommen bei diesem einfachen Bogenmodell besonders klar zum Ausdruck, da es ohne großen formalen Aufwand behandelt werden kann. Der Rechengang ist bei Bedarf ohne weiteres auf allgemeinere Fälle übertragbar, wozu nicht mehr als die üblichen baustatischen Mittel benötigt werden (s. [3]). Wenn beispielsweise auch horizontale Störlasten $\bar{q}_x$ auftreten, müssen sie in die Rechnung einbezogen werden, da sie die Traglast verkleinern.

6.1 Iterationsgleichung für den 3-Gelenkbogen

Die kritische Ausweichform des flachen Bogens (etwa $f/l < 0{,}3$) ist symmetrisch (Bild 4). Dementsprechend sind symmetrische Störmomente M_k zu betrachten, wie sie von der Scheitellast Q erzeugt werden.

Aus einer symmetrischen Biegelinie (u_k, v_k) folgen symmetrische Verformungsmomente $\triangle M_k$. Glchg. (2a) läßt sich vereinfachen zu:

$$\tilde{M}_{ek} \simeq M_{k,\bar{q}_{zs}Q} + V_{k,\bar{q}_{zs}Q} \cdot u_k + H_{k,\bar{q}_{zs}Q} \cdot v_k - \triangle H_{A,\bar{q}_{zs}Q} \cdot z_k \qquad (6a)$$

Die Momente werden damit etwas zu groß, weil die vernachlässigten Glieder Anteile liefern, die abzuziehen wären. $\triangle V_A = 0$ aus Symmetriegründen. Bei der Normalkraft verschwinden an der Stelle des Größtmoments in sehr guter Näherung die Differentialquotienten u_k' und v_k'. (2b) läßt sich demnach vereinfachen zu

$$\tilde{N}_{ek} \simeq N_{k,\bar{q}_{zs}Q} - \triangle H_{A,\bar{q}_{zs}Q} \cdot \cos\varphi_k . \qquad (6b)$$

Aus $\tilde{M}_{eG} = 0$ für das Scheitelgelenk k = G folgt

$$\triangle H_{A,\bar{q}_{zs}Q} = \frac{H_{G,\bar{q}_{zs}Q} \cdot v_G}{f} \qquad (7)$$

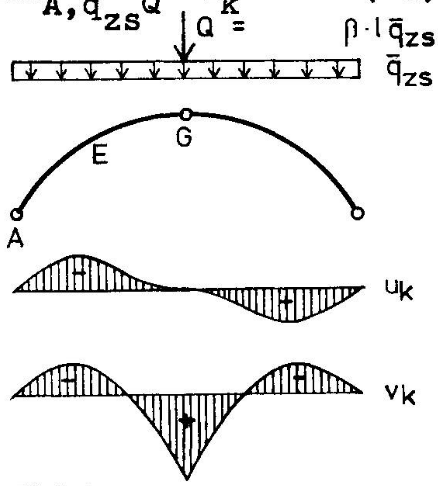

BILD 4
3-GELENKBOGEN ($f/l \simeq < 0{,}3$)

Bei bekanntem Krümmungsverlauf $\tilde{K}(x)$ können die Komponenten u_k, v_k des Verschiebungsvektors berechnet werden, beispielsweise mit der Arbeitsgleichung:

$$\frac{u_k}{h} = - \int_o^l \frac{\tilde{K}(x)}{\cos\varphi(x)} M_{H1}(x)dx = - C_{uk} \left(\frac{l}{h}\right)^2 \left(\frac{f}{l}\right) (\tilde{K}h)_E \tag{8a}$$

$$\frac{v_k}{h} = - \int_o^l \frac{\tilde{K}(x)}{\cos\varphi(x)} M_{V1}(x)dx = - C_{vk} \left(\frac{l}{h}\right)^2 (\tilde{K}h)_E \tag{8b}$$

Dabei bedeuten:

$\tilde{K}_E = - \tilde{M}_E/(\widehat{EI})_E$	Stabkrümmung an der Stelle k = E als Krümmungsparameter
M_{H1}, M_{V1}	Momente aus den virtuellen Einheitslasten H = 1 und V = 1 an der Stelle k
C_{uk}, C_{vk}	Verschiebungskonstanten für die Stelle k, abhängig von f(x) Glchg. (9)

Tatsächlich ist der Krümmungsverlauf unbekannt, er wird deshalb möglichst zutreffend angenommen:

$$\tilde{K}(x) = \tilde{K}_E\, f(x) \tag{9}$$

Die Ansatzfunktion f(x) (Abschnitt 6.4) muß bei symmetrischer Ausweichform ebenfalls symmetrisch sein.

Mit dem angenommenen Krümmungsverlauf (9) kann das Gleichgewicht zwischen äußeren (e) und inneren (r) Schnittgrößen nur an einer Stelle k genau erfüllt werden. Dafür wird die Stelle k = E des Größtmoments gewählt:

$$\max \tilde{M}_{eE} = M_{rE}, \quad \tilde{N}_{eE} = N_{rE} \tag{10}$$

An allen übrigen Stellen wird das Gleichgewicht Fehler aufweisen, deren Größe davon abhängt, wie gut der angenommene Krümmungsverlauf mit dem tatsächlichen übereinstimmt. Die Stelle E könnte iteriert werden, es genügt jedoch

$$E = l/4 \tag{11}$$

zu setzen. Damit werden aus (6) (7) (8) im l/4-Punkt:

$$\tilde{M}_{eE} \simeq - \frac{\bar{q}_{zs} l^2}{32} \left\{ 2\beta + 4(1+2\beta)\left(\frac{l}{h}\right)\left[2\left|C_{uE}\right|\left(\frac{f}{l}\right) + \left(\left|C_{vE}\right| + \frac{3}{4}\left|C_{vG}\right|\right)\left(\frac{f}{l}\right)\right](\tilde{K}h)_E \right\} \tag{12a}$$

$$\tilde{N}_{eE} \simeq - \frac{\bar{q}_{zs} l}{8} \; \frac{1+2\beta}{\cos\varphi_E} \left(\frac{l}{f}\right) \left[1 + \left|C_{vG}\right| \cos^2\varphi_E \left(\frac{f}{l}\right)\left(\frac{l}{h}\right)(\tilde{K}h)_E\right] \tag{12b}$$

Das Zusammenfassen von (12a) und (12b) ergibt nach einigem Rechnen eine parametrisierte Iterationsgleichung für das Wertetripel (n,m,Kh), wobei der Ortszeiger E nicht mehr angeschrieben ist, soweit keine Verwechslungsgefahr besteht ($Kh \equiv \tilde{K}h$):

$$|n| = \frac{4|m|}{\cos\varphi} \left(\frac{l}{f}\right)\left(\frac{h}{l}\right) \frac{1 + \left|C_{vG}\right| \cos^2\varphi \left(\frac{f}{l}\right)\left(\frac{l}{h}\right)|Kh|}{\frac{2\beta}{1+2\beta}\left\{1 + \frac{2(1+2\beta)}{\beta}\left(\frac{l}{h}\right)\left[2\left|C_{uE}\right|\left(\frac{f}{l}\right) + \left(\left|C_{vE}\right| + \frac{3}{4}\left|C_{vG}\right|\right)\left(\frac{f}{l}\right)\right]|Kh|\right\}} \tag{13}$$

Das Zählerglied mit C_{vG} ist vor allem bei flachen Bogen nicht mehr << 1 und deshalb nicht vernachlässigbar.

Die kritische Last schließlich folgt aus:

$$\frac{\bar{q}_{zs,cr}}{b\, f'_c} = 8 \cos\varphi \left(\frac{f}{l}\right)\left(\frac{h}{l}\right) \frac{1}{1 + \left|C_{vG}\right| \cos^2\varphi \left(\frac{f}{l}\right)\left(\frac{l}{h}\right)|Kh|} \; \frac{|n_{cr}|}{(1+2\beta)} \tag{14}$$

Dabei ist $b = A_c/h$ unabhängig von der Querschnittsform die Breite eines flächengleichen Rechteckquerschnitts der Höhe h.

Der steile 3-Gelenkbogen versagt wie der 2-Gelenkbogen, es gelten die für diesen entwickelten Gleichungen.

6.2 Iterationsgleichung für den 2-Gelenkbogen

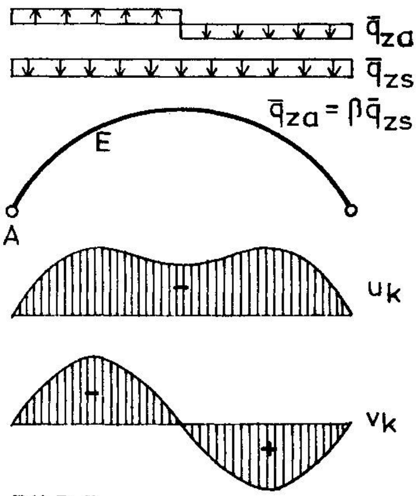

BILD 5
2-GELENKBOGEN UND
3-GELENKBOGEN (f/l ≈ > 0,3)

Die kritische Ausweichform ist antimetrisch (Bild 5). Zu betrachten sind demnach antimetrische Störmomente M_k. Bei der antimetrischen Biegelinie (u_k, v_k) entstehen zusätzlich Verformungsmomente ΔM_k, die aus $\bar q_{zs}$ antimetrisch, aus $\bar q_{za}$ symmetrisch verlaufen. Für das Tragvermögen entscheidend sind allein die antimetrischen Verformungsmomente, die sehr viel kleineren symmetrischen sind vernachlässigbar. Diese erreichen erst bei $\bar p_{xa} \neq 0$ und größerem f/l merkliche Größe. Bleibt außerdem der ebenfalls sehr kleine antimetrische Anteil $\Delta V_A x_k + \int_0^{x_k} \bar q_{zs} u \, dx$ unberücksichtigt, so werden Momente $\tilde M_{ek}$ erhalten, die etwas zu groß sind. Sie folgen aus (2a):

$$\tilde M_{ek} \simeq M_{k,\bar q_{za}} + V_{k,\bar q_{zs}} \cdot u_k + H_{k,\bar q_{zs}} \cdot v_k \qquad (15a)$$

Mit den beim 3-Gelenkbogen beschriebenen Vereinfachungen wird aus (2b):

$$\tilde N_{ek} \simeq N_{k,\bar q_{zs}\bar q_{za}} - \Delta V_{A,\bar q_{zs}\bar q_{za}} \cdot \sin\varphi_k, \qquad (15b)$$

wobei $$\Delta V_{A,\bar q_{zs}\bar q_{za}} = -\bar q_{zs} \int_0^l \frac{u}{l} \, dx \text{ ist.} \qquad (16)$$

Die Ansatzfunktion f(x) in (9) für die Stabkrümmung muß bei antimetrischer Ausweichform antimetrisch sein (Abschnitt 6.4). Sie genügt dann auch der Randbedingung $\tilde l = l$ mit $\Delta H_A = 0$.

Für die Stelle k = E = l/4 des Größtmoments werden mit (8)

$$\tilde M_{eE} \simeq -\frac{\bar q_{zs} l^2}{32} \left\{\beta + 4\left(\frac{l}{h}\right)\left[2\,|c_{uE}|\left(\frac{f}{l}\right) + |c_{vE}|\left(\frac{l}{f}\right)\right](\tilde K h)_E\right\} \qquad (17a)$$

$$\tilde N_{eE} \simeq -\frac{\bar q_{zs} l}{8\cos\varphi_E}\left(\frac{l}{f}\right)\left[1 + 4\frac{J}{l}\sin 2\varphi_E \left(\frac{l}{h}\right)\left(\frac{f}{l}\right)^2 (\tilde K h)_E\right] \qquad (17b)$$

In $\tilde N_{eE}$ ist eingesetzt, mit J als Kürzel für das Integral:

$$\Delta V_A = \bar q_{zs} \left(\frac{l}{h}\right)\left(\frac{f}{l}\right)(\tilde K h)_E \int_0^l c_u \, dx.$$

Die Iterationsgleichung wird nach einigem Rechnen ähnlich wie beim 3-Gelenkbogen erhalten:

$$|n| = \frac{4|m|}{\cos\varphi}\left(\frac{l}{f}\right)\left(\frac{h}{l}\right) \frac{1 + 4\frac{J}{l}\sin 2\varphi \left(\frac{l}{h}\right)\left(\frac{f}{l}\right)^2 |Kh|}{\beta + 4\left(\frac{l}{h}\right)\left[2\,|c_u|\left(\frac{f}{l}\right) + |c_v|\left(\frac{l}{f}\right)\right]|Kh|} \qquad (18)$$

Der Ortszeiger E ist nicht mehr angeschrieben. Das Zählerglied mit J ist stets << 1 und kann vernachlässigt werden. Dies bedeutet $\Delta V_A = 0$ in (15b) und (17b). (Lösungen enthält Bild 8.) Die kritische Last wird mit dieser Vereinfachung

$$\frac{\bar q_{zs,cr}}{b f'_c} = 8\cos\varphi\left(\frac{f}{l}\right)\left(\frac{h}{l}\right)|n_{cr}| \qquad (19)$$

6.3 Die Iterationsgleichungen für den gelenklosen Bogen

Wie beim 2-Gelenkbogen ist die Ausweichform antimetrisch (Bild 6). Die Momente und Normalkräfte lassen sich deshalb in gleicher Weise vereinfachen. Aus (2a) wird für die Momente:

$$\tilde{M}_{ek} \simeq M^{o}_{k,\bar{q}_{za}} + \tilde{M}_{A,\bar{q}_{za}} \left(1-2\frac{x}{l}\right) + V_{k,\bar{q}_{zs}} \cdot u_k + H_{k,\bar{q}_{zs}} \cdot v_k \qquad (20a)$$

(Der zu $\triangle M_A$ gehörende $\triangle V_A$-Anteil ist nicht vernachlässigbar, weil beide zusammen das Glied $\triangle M_A + \triangle V_{A,\triangle M_A} x_k = \triangle M_A \left(1-2\frac{x}{l}\right)$ bilden).

Die Normalkraft folgt aus (2b):

$$\tilde{N}_{ek} \simeq N^{o}_{k,\bar{q}_{zs}\bar{q}_{za}} + \frac{2\tilde{M}_{A,\bar{q}_{za}}}{l} \sin\varphi_k \qquad (20b)$$

Dabei sind M^o, N^o, V^o und H^o Werte des 2-Gelenkbogens, der als Hauptsystem benutzt wird, wobei $V \equiv V^o$ und $H \equiv H^o$, weil $M_{A,\bar{q}_{zs}} \equiv 0$.

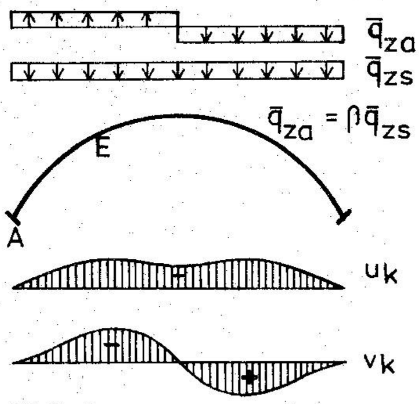

BILD 6
GELENKLOSER BOGEN

Die Ansatzfunktion für die Krümmung muß antimetrisch und durch wenigstens zwei Parameter festgelegt sein (s. Bild 7):

$$\tilde{K}(x) = \tilde{K}_A f_1(x) + \tilde{K}_E f(\tilde{K}_A / \tilde{K}_E)\, f_2(x) \qquad (21)$$

Sie erfüllt die Randbedingung $\tilde{l} = 1$. $\tilde{K}_A$ ist die Krümmung an der Einspannstelle $k = A$, $\tilde{K}_E$ an der Stelle $k = E$ des Größtmoments im Feld. Beide, $\tilde{K}_A$ und $\tilde{K}_E$, sind durch die Randbedingung "volle Einspannung" miteinander verknüpft:

$$\int_0^{l/2} \frac{K(x)}{\cos\varphi(x)} M_{M1}(x)\, dx = 0 \qquad (22a)$$

Die Integration liefert $(\tilde{K}h)_E = -c\,(\tilde{K}h)_A$. (22b)

$M_{M1} = 1\left(1 - 2\frac{x}{l}\right)$ ist das virtuelle Moment.

Mit den Krümmungsparametern $\tilde{K}_A$ und $\tilde{K}_E$ kann das Gleichgewicht an den beiden Bogenstellen A und E genau erfüllt werden. Dementsprechend wird ein System von zwei gekoppelten Iterationsgleichungen erhalten. Auch hier wird $E = l/4$ gesetzt.

Aus (20) folgen mit (8) die Schnittgrößen:

$$\tilde{M}_{eA} = - \tilde{K}_A\, (\widetilde{EI})_A \qquad (23a)$$

$$\tilde{N}_{eA} \simeq - \frac{\bar{q}_{zs}\, l}{8\cos\varphi_A} \left(\frac{l}{f}\right) \left[1 - \beta\left(\frac{f}{l}\right) \sin 2\varphi_A\right] + \frac{2\,\tilde{M}_A}{l} \sin\varphi_A \qquad (23b)$$

$$\tilde{M}_{eE} \simeq - \frac{\bar{q}_{zs}\, l^2}{32} \left\{ \beta + 4\left(\frac{l}{h}\right) \left[2\left|C_{uE}\right| \left(\frac{f}{l}\right) + \left|C_{vE}\right| \left(\frac{l}{f}\right)\right] (\tilde{K}h)_E \right\} + \frac{\tilde{M}_A}{2} \qquad (24a)$$

$$\tilde{N}_{eE} \simeq - \frac{\bar{q}_{zs}\, l}{8\cos\varphi_E} \left(\frac{l}{f}\right) + \frac{2\tilde{M}_A}{l} \sin\varphi_E \qquad (24b)$$

Die Verknüpfung von (23) und (24) ergibt nach einiger Rechnung zusammen mit (22b) das System der Iterationsgleichungen:

$$\left|n_E\right| = \frac{2}{\cos\varphi_E} \left(\frac{l}{f}\right)\left(\frac{h}{l}\right) \frac{2\left|m_E\right| + \left|m_A\right|}{\beta + 4\left(\frac{l}{h}\right)\left[\,2\left|C_{uE}\right|\left(\frac{f}{l}\right) + \left|C_{vE}\right|\left(\frac{l}{f}\right)\right] \left|Kh\right|_E} \pm 2\left|m_A\right|\left(\frac{h}{l}\right)\sin\varphi_E \qquad (25a)$$

$$\left|n_A\right| = \frac{\cos\varphi_E}{\cos\varphi_A} \left[\left|n_E\right| \mp 2\left|m_A\right| \left(\frac{h}{l}\right) \sin\varphi_E\right] \left[1 \pm \beta\left(\frac{f}{l}\right) \sin 2\varphi_A\right] \pm 2\left|m_A\right| \left(\frac{h}{l}\right)\sin\varphi_A \qquad (25b)$$

Die kritische Last wird:

$$\frac{\bar{q}_{zs,cr}}{b\, f'_c} = 8 \cos\varphi_E\left(\frac{f}{l}\right)\left(\frac{h}{l}\right) \left[\left|n_E\right| \mp 2\left|m_A\right| \left(\frac{h}{l}\right) \sin\varphi_E\right]_{cr} \qquad (26)$$

Aus (23) und (24) ergeben sich in den Iterationsgleichungen die unteren Vorzeichen. Sie entsprechen der Untersuchung der linken Bogenhälfte (s. Bild 6), oder anders gesagt, der Kombination der Momente mit den kleinsten Bogendruckkräften. Die oberen Vorzeichen gehören zur Untersuchung der rechten Bogenhälfte in der die Momente zusammen mit den größten Druckkräften auftreten. Maßgebend ist die Bogenhälfte, die das kleinste $\bar{q}_{zs,cr}$ liefert.

6.4 Ansatzfunktionen f(x) für die Stabkrümmung

Bei 3-Gelenk- und 2-Gelenkbogen liefert eine quadratische Ansatzfunktion (Bild 7)

$$f(x) = 8\,\frac{x}{l}\,(1 - 2\frac{x}{l}) \text{ mit } (x \leq l/2) \qquad (27)$$

meist sehr genaue Traglasten, die fast ausnahmslos etwas kleiner als die exakten Werte sind.

Bei gelenklosen Bogen gibt es dagegen keine einigermaßen einheitliche Ansatzfunktion, die den gesamten β- und f/l-Bereich erfassen würde. Sieht man aber von sehr kleinen Störungen - die meist nicht mehr im baupraktischen Bereich liegen - bei Bogen mit sehr kleinem f/l ab, so sind

$$f_1(x) = 1 - 2\frac{x}{l}\,, \quad f_2(x) = 8\frac{x}{l}\,(1 - 2\frac{x}{l}) \qquad (28)$$

$$f\,(\tilde{K}_A/\tilde{K}_E) = 1 + |\tilde{K}_A| \,/\, 2\,|\tilde{K}_E| \quad \text{für } (x \leq l/2)$$

brauchbare Ansätze (Bild 7).

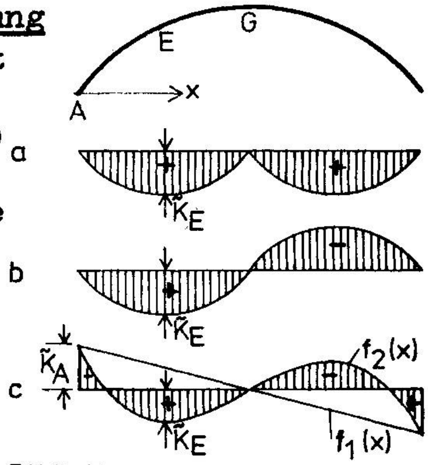

BILD 7
ANSATZFUNKTIONEN f(x)
a : 3 - GELENKBOGEN
b : 2 - GELENKBOGEN
c : GELENKLOSER BOGEN

Stetig gekrümmte Ansatzfunktionen wie (27) (28) vermögen die Stabkrümmung nur so lange zutreffend zu beschreiben, als Fließzonen fehlen, die auftreten, wenn die Stahldehnung auf der Zugseite die Streckgrenze überschreitet. Bei 3-Gelenk- und 2-Gelenkbogen sind solche Zonen nicht bedeutsam, weil deren Tragvermögen mit dem Erreichen der Streckgrenze der Zugbewehrung praktisch erschöpft ist. Bei gelenklosen Bogen aber, kann, besonders wenn sie gedrungen sind, die Last vielfach noch beträchtlich gesteigert werden, wenn an der Einspannstelle die Streckgrenzendehnung überschritten wird. Es breiten sich Fließzonen aus, im Grenzfall fließt die Zugbewehrung auch in den Viertelpunktbereichen. Mit den Ansätzen (28) lassen sich diese Tragreserven nicht erfassen. Das gelingt erst, wenn der Krümmungsverlauf iterativ verbessert und so den auftretenden Fließzonen angepaßt wird (Abschnitt 7).

6.5 Lösen der Iterationsgleichungen

Die Gleichungen werden für die einzelnen Leitdehnungszustände ε_{c1} = konst. gelöst, mit denen das n-m-Diagramm gerastert ist. Auf jeder Rasterlinie gibt es nur ein zusammengehöriges Wertetripel (n,m,Kh), das die Iterationsgleichung erfüllt. Dieses Tripel stellt einen Gleichgewichtszustand dar, der stabil, indifferent oder labil sein kann (s. Bild 8). Das Maximum der Verbindungslinie aller Gleichgewichtszustände ist die kritische Normalkraft n_{cr}, aus der die Traglast $\bar{q}_{zs,cr}$ berechnet werden kann.

Der Iterationsvorgang beim 3-Gelenk- und 2-Gelenkbogen bedarf keiner weiteren Erläuterung. Beim gelenklosen Bogen sind folgende Iterationsschritte nötig:

1. Leitdehnungszustand für Querschnitt A wählen
2. n_A schätzen, der Leitdehnungszustand liefert m_A, $(Kh)_A$
3. n_E aus (25b) rechnen, $(Kh)_E$ aus (22b)

4. n_E und $(Kh)_E$ zusammen ergeben m_E
5. n_E aus (25a) rechnen mit m_E, m_A und $(Kh)_E$
6. n_E-Identität prüfen

Iteration wiederholen bis die Identität erreicht ist.

Verzweigungslasten müssen mit sehr kleinem (Kh) berechnet werden, weil sie für infinitesimal kleine Verschiebungen definiert sind. Mit größerem (Kh) ist ein Lastabfall verbunden (s.Bild 8).

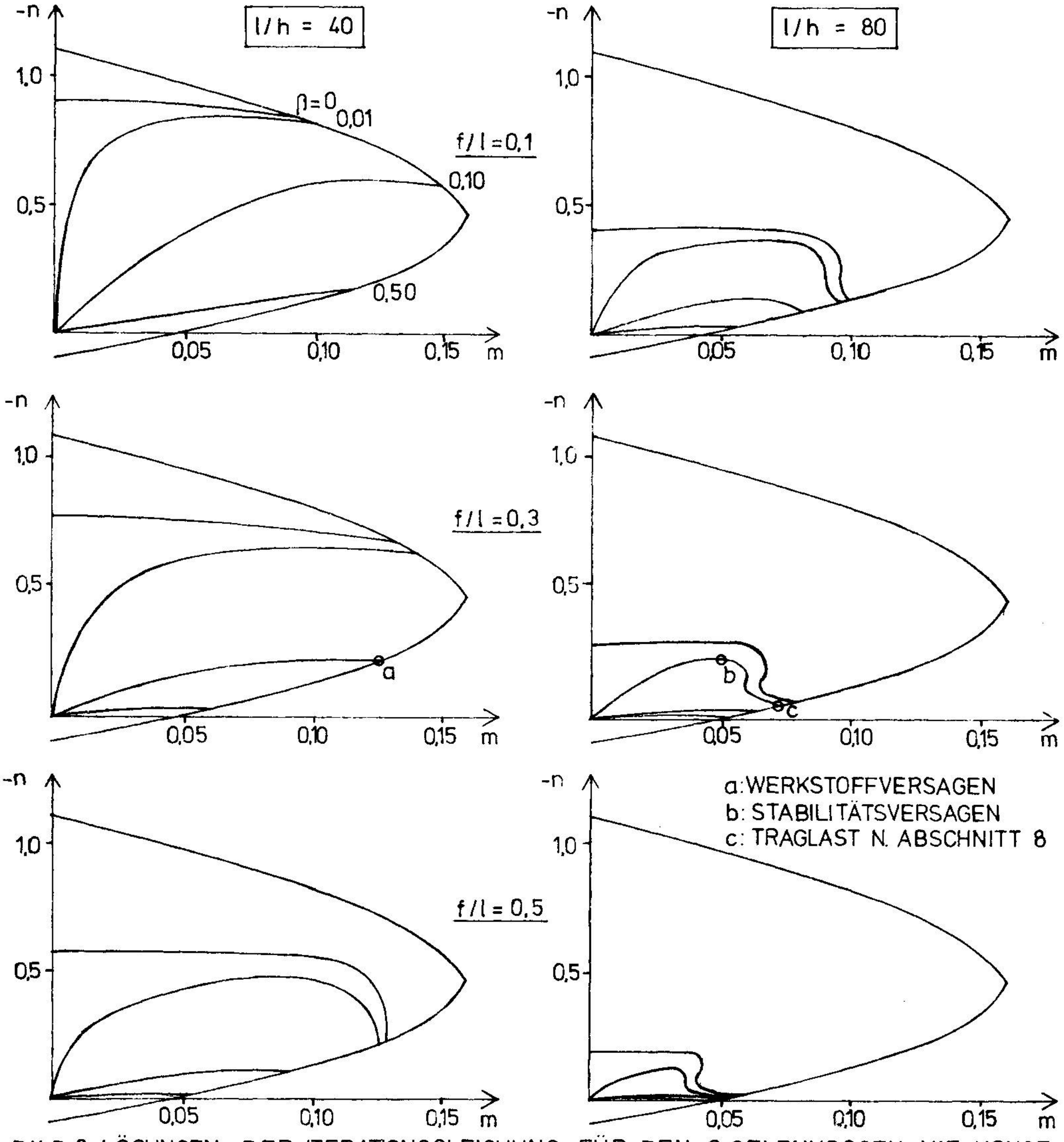

BILD 8 LÖSUNGEN DER ITERATIONSGLEICHUNG FÜR DEN 2-GELENKBOGEN MIT KONST. I-QUERSCHNITT UND $\omega = \omega' = 0{,}494$ FÜR DIE STÖRPARAMETER $\beta = 0/0{,}01/0{,}10/0{,}50$. σ-ε-DIAGRAMME BETON U. STAHL [1] BILD 13, 14, 15

7. Traglastberechnung mit iterativ verbessertem Krümmungsverlauf

Durch iteratives Verbessern des Krümmungsverlaufs kann das Traglastproblem exakt gelöst werden. Nachdem $(Kh)_{E,cr}$ und n_{cr} nach Abschnitt 6 bestimmt sind, ist eine Iteration mit folgenden Schritten nötig:

1. Biegelinien u und v rechnen.
2. mit den Biegelinienwerten $\tilde{M}_e$- und $\tilde{N}_e$-Verlauf rechnen.

3. aus $\tilde{M}_e = M_r$ und $\tilde{N}_e = N_r$ verbesserten $\tilde{K}$-Verlauf bestimmen
4. Einhalten der Randbedingungen prüfen. Wenn nötig $\tilde{M}_e$-, $\tilde{N}_e$- und $\tilde{K}$-Verlauf durch stat. unbest. Rechnung berichtigen.
5. Iterationsgleichung an den verbesserten und mit den Randbedingungen verträglichen $\tilde{K}$-Verlauf anpassen (C-Werte und ggf. verbesserte Stelle E) und lösen.

Iteration mit den verbesserten n_{cr}- und $(Kh)_{E,cr}$-Werten wiederholen, bis die Ergebnisse zweier Durchgänge ausreichend übereinstimmen. Die Konvergenz ist gut, meist reichen ein bis zwei Durchgänge aus.

Normalerweise genügen auch für diese Rechnung die Näherungsausdrücke des Abschnitts 6 für $\tilde{M}_{ek}$ und $\tilde{N}_{ek}$. Es wäre nicht schwierig, nur mühsam, die genauen Gleichungen (2) zu benutzen. Ebenso könnte die Achsdehnung ε_o in die Iteration einbezogen werden, was vor allem bei 3-Gelenkbogen mit $f/l < 0{,}1$ nötig sein kann.

Das Verfahren der iterativen Verbesserung soll nicht die Regel sein. Es ist vielmehr besonders zum Nachprüfen der Güte der $\tilde{K}$-Ansatzfunktion gedacht, wenn Querschnitt und Bewehrung veränderlich sind. Dazu genügt schon ein Iterationsdurchgang.

8. Traglastberechnung mit Grenzdehnungszuständen

Das ist die einfachste Art der Traglastrechnung. Sie arbeitet mit einem angenommenen Krümmungsverlauf (Abschnitt 6), verzichtet aber auf die Rasterung des n-m-Diagramms durch Leitdehnungszustände (Abschnitt 5) und löst die Iterationsgleichung nur für die Begrenzungslinie des Diagramms, also für Grenzdehnungszustände. Damit ist zwar die Bruchlast erfaßbar, nicht aber die vielfach beträchtlich höhere Traglast bei Stabilitätsversagen, das durch $dn/dm = 0$ gekennzeichnet ist (s. Bild 8).

9. Verallgemeinern der Ergebnisse

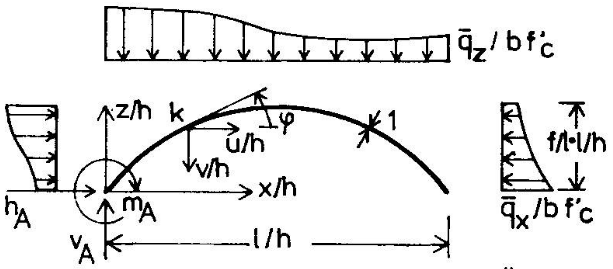

BILD 9 PARAMETRISIERTER BOGEN FÜR KONSTANTES A_c UND h.
$h_A = H_A / A_c f'_c$, $v_A = V_A / A_c f'_c$

Die für einen bestimmten Bogen gewonnenen Ergebnisse gelten für alle Bogen gleichen statischen Systems mit gleichen Geometrie-, Bewehrungs-, Werkstoff- und Lastparametern (Bild 9). Beispielsweise sind die Verschiebungen (8) u/h und v/h parametrisierte Verschiebungswerte und die krit. Lasten (14) (19) (26) q/bf'_c parametrisierte Lasten. Parametrisiert sind sie für konst. Querschnitt. Bei veränderlicher Querschnittshöhe und -fläche wäre grundsätzlich h durch h_o zu ersetzen, wenn h_o als Höhenparameter eingeführt wird, und außerdem in (8) $(Kh)_E$ durch $(Kh)_E \; h_o/h_E$ und in (14) (19) b durch $b_E \; h_E/h_o$, um einige Beispiele zu nennen.

10. Berücksichtigen des Einflusses nichtlinearer Geometrieglieder

Der Einfluß der nichtlinearen Geometrieglieder läßt sich durch Korrekturen Δu, Δv der Biegelinien u,v nach dem Gesetz

$$\Delta u' - \Delta v' z' + (\tfrac{1}{2} v'^2 + \varepsilon_o v' z')(1 + z'^2) = 0 \qquad (29)$$

abschätzen. Der Vergleich mit der linearisierten Verschiebungsbeziehung:

$$u' - v' z' - \varepsilon_o (1 + z'^2) = 0$$

zeigt, daß $(1/2\; v'^2 + \varepsilon_o v' z')$ als fiktive Achsdehnung gedeutet werden kann. Die Biegelinienkorrekturen Δu, Δv sind demnach in 1. Näherung nichts anderes als die horizontale bzw. vertikale Biegelinie aus einer fiktiven Dehnung

$$\varepsilon_{o\ fikt} = -\left(\frac{1}{2} v'^2 + \varepsilon_o v'z'\right) \qquad (30)$$

Auch sie sind demnach mit baustatischen Mitteln berechenbar.

Der Einfluß ist nur für den Grenzfall äußerst schlanker Bogen bedeutsam. Die Rechnung vermag lediglich das Einleiten des Durchschlags zu erfassen.

In Glchg.(2) sind die Glieder vernachlässigt, die Produkte von Verschiebungsgrößen enthalten, bei M_{ek}: $\triangle V_A u_k$ und $\triangle H_A v_k$.

SCHRIFTTUM

[1] DIN 1045, Ausgabe 1972

[2] Internationale CEB-FIP-Richtlinien, Ausgabe Juni 1970

[3] Bomhard, H.: "Verfahren zur Traglastberechnung ebener Druckbogen mit nichtlinear-elastischem Werkstoffgesetz und nichtlinearen Geometriebeziehungen". Dissertation TU München, 1974

[4] Bomhard, H.: "Versagensformen und -größen der Druck- und Zugbogen des Hallenbaus". Sicherheit von Betonbauten, Beiträge zur Arbeitstagung, Berlin 1973. Wiesbaden: Deutscher Beton-Verein E.V.

ZUSAMMENFASSUNG

Für ebene Druckbogen wird ein leistungsfähiges Handrechenverfahren beschrieben, das im gesamten Ausmittenbereich mit geringem Arbeitsaufwand sehr genaue Traglasten liefert. Das Verfahren arbeitet auf deterministischer Basis und kann mit unterschiedlichen Genauigkeitsansprüchen betrieben werden. Es führt bei iterativ verbesserter Stabkrümmung zur genauen Lösung des geometrisch linearisierten Traglastproblems. Das Problem wird so parametrisiert, dass die Ergebnisse bei gleichen Parametern allgemein gelten.

SUMMARY

An efficient manual computation method for plane compression arches is presented by which very accurate load carrying capacities can be evaluated for the whole eccentricity range with a comparatively small effort. The method works on a deterministic basis and can be applied to varying demands of accuracy. By iteratively improving the bar-curvature, it eventually leads to the accurate solution of the geometrically linearized problem. The problem is parametrizised thus that the results are generally applicable.

RESUME

Pour les arcs comprimés plans, on décrit un procédé pratique de calcul à la main, qui fournit en peu de temps les charges ultimes très précises dans toute la zone d'excentricité. Le procédé fonctionne sur une base déterministe et peut être appliqué avec n'importe quel degré de précision. En améliorant itérativement la courbure des barres, il peut conduire à la solution exacte du problème de charge ultime géométriquement linéarisé. Le problème repose sur des paramètres tels que les résultats sont toujours valables quand les paramètres sont égaux.

An Investigation on Concrete Columns with Special Reference to L and T Sections With and Without Diaphragms

Une étude sur les colonnes en béton, traitant spécialement des sections en L et en T avec et sans cloison transversale

Eine Untersuchung an Stahlbetonstützen unter besonderer Berücksichtigung von L- und T-förmigen Querschnitten mit und ohne Querschotten

S. BHATTACHARYAY B. CHATTOPADHYAY T.K. RAY P. SOM
Civil Engineering Department
Jadavpur University
India

1. INTRODUCTION:

Strength of columns having T and L shapes subject to biaxial bending is determined experimentally and compared with theoretical values of Hsu & Mirza (1). Efficiencies of T, L and rectangular column sections are also compared. Effect of end stiffening of T & L shaped columns by means of diaphragms has also been studied in the paper. One of the objects of this paper is to suggest a suitable method of design of non-rectangular column sections - T & L sections - for a practical designer's office using a desk calculator only.

2. PREPARATION OF THE SPECIMENS AND TESTING PROGRAMME:

Materials of the test specimens are ordinary portland cement, quarry sand & 6mm down (passing 6mm sieve size) crushed rock aggregates mixed in the proportion of 1:1.5:3 by weight with water cement ratio of 0.6. 6mm square black wire mesh with 0.6mm wire diameter, are used as reinforcement. Test specimens and concrete cylinders are cast with the same concrete and both cured under water.

Different shapes of specimens viz. T,L, rectangular and cruciform are prepared.Three sets of the test specimens are cast monolithically with end diaphragms of 6mm thickness to find the effect of diaphragm on column strength. Particulars of the specimens are given in Table 1. Length of each specimen is kept as 38.10 cm.

The first phase of the testing programme deals with uniform compressive load over the whole area and the second phase is conducted to study biaxial bending of the test specimens.

The stress strain curve of concrete is shown in Fig.1. The ultimate strain is recorded as 31×10^{-4}.

3. TEST RESULTS AND DISCUSSIONS:

3.1. Under uniform compression:

Total results are shown in Table 1.

3.1.1. Effect of shape:

Table 1 shows the ultimate load carried by different shapes. For equal concrete area, it is seen that a marked effect of shape on strength exists. T sections carry higher load than rectangular ones whereas L sections normally showed the lowest strength. T sections with wide flange or deep web and L sections with one leg much larger than the other behave as rectangular ones.

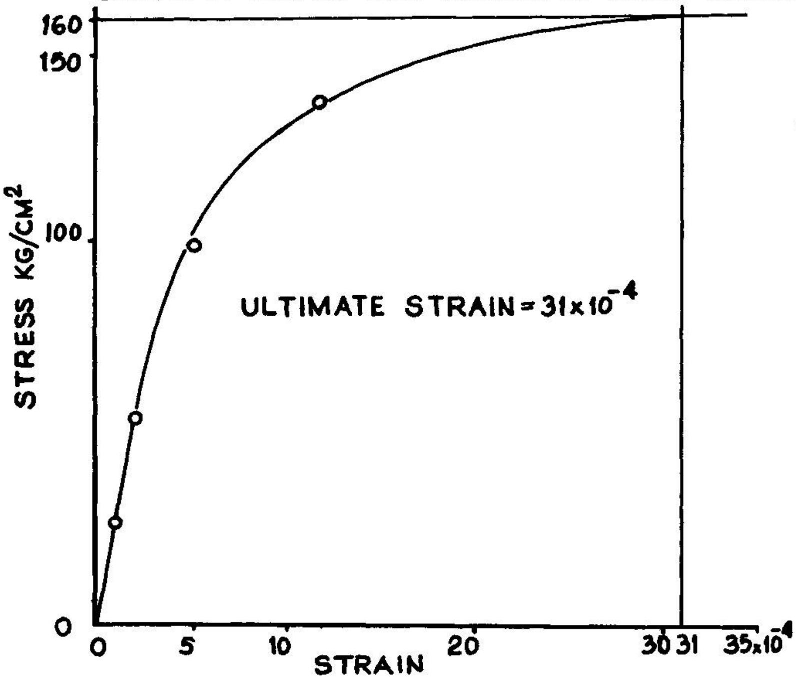

FIG.1. STRESS-STRAIN CURVE OF CONCRETE.

3.1.2. Effect of end Diaphragms:

In a building, the columns in each floor are always bounded by the slabs at the top and bottom. Keeping this in view columns (L & T sections) are tested with end diaphragms of 6mm thickness. Table 2 shows that columns with end diaphragms have carried more load than columns without diaphragms. From the present seires of tests (Table 2) it is seen that the percentage increase in strength is nearly 30 to 35.

TABLE.1. CYLINDER STRENGTH = 160 KG/CM²

P_c = LOAD AT FAILURE

P_A = CYLINDER ULTIMATE STRESS × AREA OF CROSS SECTION

SPECIMEN MARKING	SPECIMEN	a CM	b CM	t_1 CM	t_2 CM	CONC. AREA CM²	EQ STEEL AREA CM²	AVERAGE P_c tonne	P_c/P_A
A1	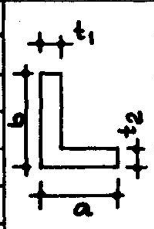	5·08	5·08	2·22	2·22	17·7	0·47	1·810	0·641
A2		7·62	7·62	2·22	2·22	29·0	0·86	2·750	0·595
A3		7·62	5·08	2·22	2·22	23·8	0·75	2·800	0·758
A4		5·08	5·08	3·17	3·17	22·6	0·43	2·370	0·660
A5		7·62	7·62	3·17	3·17	38·4	0·75	6·150	1·020
A6		7·62	5·08	3·17	3·17	30·3	0·55	3·780	0·780
A7		7·62	5·08	1·27	1·27	14·6	0·78	1·950	0·840

TABLE 1 (CONTD)

SPECIMEN MARKING	SPECIMEN	a CM	b CM	t_1 CM	t_2 CM	CONC AREA CM^2	EQ STEEL AREA CM^2	AVERAGE P_c tonne	P_c/P_A
T_1	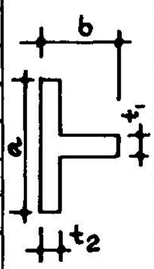	5·08	7·62	2·22	2·22	23·8	0·67	2·755	0·746
T_2		7·62	5·08	2·22	2·22	23·8	0·67	3·250	0·880
T_3		5·08	7·62	3·17	3·17	30·3	0·67	4·550	0·940
T_4		5·08	5·08	2·22	2·22	17·7	0·63	2·280	0·816
T_5		7·62	5·08	3·17	3·17	30·3	0·67	5·330	1·100
T_6		5·08	5·08	3·17	3·17	22·6	0·51	3·100	0·870
T_7		5·08	7·62	1·27	2·22	18·2	0·67	2·500	0·860
T_8		7·62	7·62	1·27	2·22	24·9	0·86	5·520	1·400
T_9		7·62	7·62	1·27	1·27	17·8	0·86	3·690	1·290
T_{10}		10·16	7·62	2·54	1·27	29·1	1·17	7·300	1·580
T_{11}		15·24	5·08	2·54	1·27	29·1	1·34	4·950	1·060
R_1	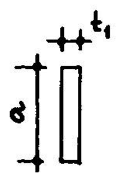	7·98	–	2·22	–	17·7	0·47	1·740	0·620
R_2		10·72	–	2·22	–	23·8	0·75	1·620	0·580
R_3		7·13	–	3·17	–	22·6	0·43	3·600	0·740
R_4		9·56	–	3·17	–	30·3	0·67	3·200	0·660
R_5		11·43	–	1·27	–	14·6	0·78	1·355	0·580
R_6		13·97	–	1·27	–	17·8	0·86	1·540	0·540

TABLE 2. DIMENSIONS ARE IN CM.

SPECIMEN MARKING		SPECIMEN	AVERAGE ULTIMATE LOAD tonne	PERCENT INCREASE IN LOAD FOR SPECIMENS WITH DIAPHRAGM
A_1	WITHOUT DIAPHRAGM	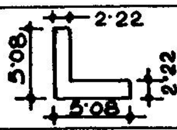	1·81	
A_{1S}	WITH DIAPHRAGM	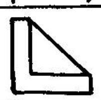	2·44	35·15
A_6	WITHOUT DIAPHRAGM	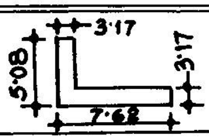	3·78	
A_{6S}	WITH DIAPHRAGM	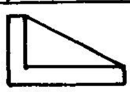	4·90	30·05
T_4	WITHOUT DIAPHRAGM	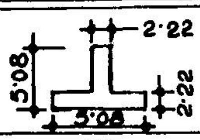	2·28	
T_{4S}	WITH DIAPHRAGM	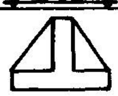	2·96	30·20

3.1.3. Effect of Slenderness ratio:

The ratio $l/r_{min.}$ being the most important design parameter in designing a column under uniform compression a plot of $l/r_{min.}$ against P_C/P_A for different shapes viz. T & L are shown in Fig.2 where P_C = Load at failure and P_A = cylinder ultimate stress X area of cross-section. From the curve it is observed that for a particular $l/r_{min.}$ ratio, T sections are about 30 to 40 percent more efficient than L sections.

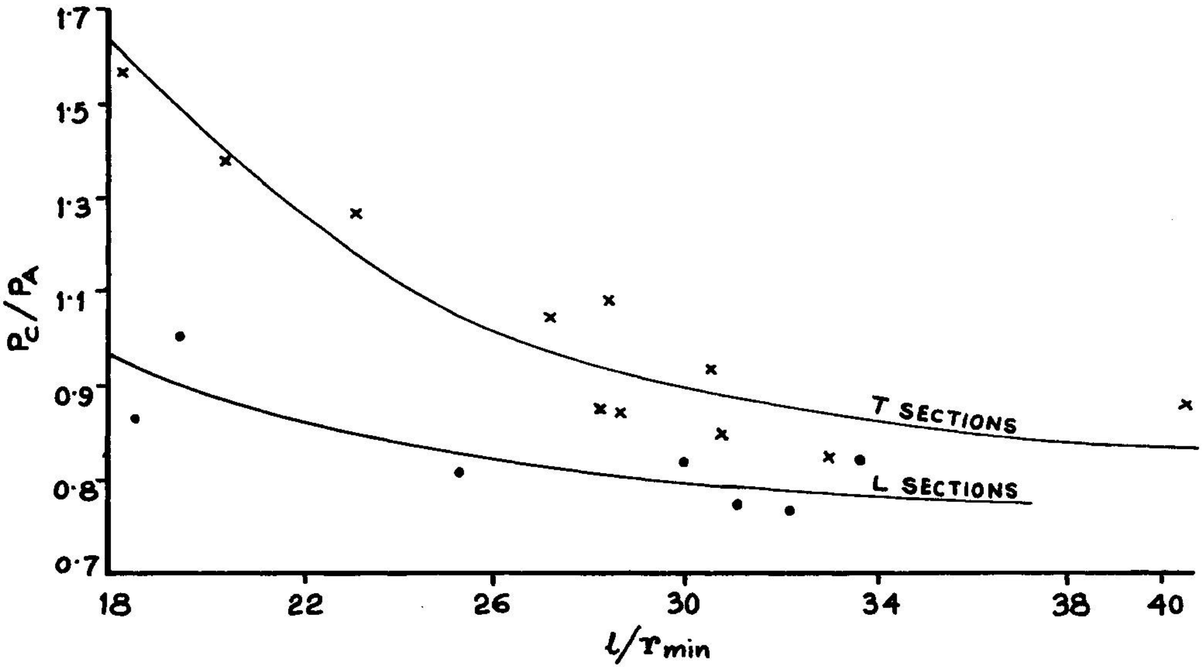

FIG.2 EFFECT OF l/r_{min} ON STRENGTH.

3.2. Bending Effect:

Specimens of different shapes viz. L, T. Cruciform were tested under bending and test results have been compared with the values obtained by the method of Hsu & Mirza (1) shown in Table 3.

TABLE. 3.

SPECIMEN MARKING	SPECIMEN	a CM	b CM	t_1 CM	t_2 CM	ECCENTRICITY(e) e_x CM	ECCENTRICITY(e) e_y CM	AVERAGE P_c (EXPT) tonne	AVERAGE P_c (THEO)[1] tonne
A_{1b}	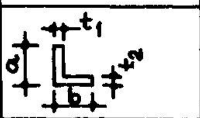	5·08	5·08	1·27	1·27	1·0	1·0	1·02	1·21
T_{1b}	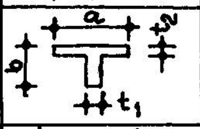	10·16	5·08	2·54	1·27	1·0	1·0	1·85	2·30
C_{1b}	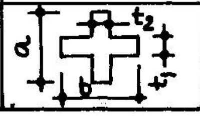	10·16	10·16	2·54	2·54	3·175	3·175	2·97	2·66

3.2.1. Theoretical Model:

The method of Hsu & Mirza is an iteration process based on Newton-Raphson technique where the axial load, moment in x & y directions have been expressed as functions of difect strain and curvatures in x & y directions as,

$$P = P(\phi_x, \phi_y, \epsilon_p)$$

$$M_x = M_x(\phi_x, \phi_y, \epsilon_p)$$

$$M_y = M_y(\phi_x, \phi_y, \epsilon_p)$$

The convergence of the calculated value at any cycle and the final value has been accelerated by using Taylor's expansion as,

$$P(c)-P(s) = u = -(\frac{\partial P(c)}{\partial \phi_x}\delta\phi_x + \frac{\partial P(c)}{\partial \phi_y}\delta\phi_y + \frac{\partial P(c)}{\partial \epsilon_p}\delta\epsilon_p)$$

$$M_x(c)-M_x(s) = v = -(\frac{\partial M_x(c)}{\partial \phi_x}\delta\phi_x + \frac{\partial M_x(c)}{\partial \phi_y}\delta\phi_y + \frac{\partial M_x(c)}{\partial \epsilon_p}\delta\epsilon_p)$$

$$M_y(c)-M_y(s) = w = -(\frac{\partial M_y(c)}{\partial \phi_x}\delta\phi_x + \frac{\partial M_y(c)}{\partial \phi_y}\delta\phi_y + \frac{\partial M_y(c)}{\partial \epsilon_p}\delta\epsilon_p)$$

where at any cycle y, iteration

$$P(c) = \sum_{k=1}^{n} (E_t)_k \, \epsilon_k \, a_k$$

$$M_x(c) = \sum_{k=1}^{n} (E_t)_k \, \epsilon_k \, a_k \, y_k$$

$$M_y(c) = \sum_{k=1}^{n} (E_t)_k \, \epsilon_k \, a_k \, x_k$$

the strain in kth element ϵ_k is given as

$$\epsilon_k = \epsilon_p + \phi_x y_k + \phi_y x_k$$

and $(E_t)_k$ = Tangent modulus at a given strain level.

As an example a T section has been shown here with element subdivisions in Fig. 3. A quadrilinear model of stress-strain curve has been considered as shown in Fig. 4 for the purpose of calculation. Tangent modulus of steel has been kept constant throughout because it is assumed that the strains in the steel will remain within the elastic limit. Fig. 5 giving the load values at successive iteration, shows that the process converges very rapidly. Practically iteration is not needed after the third cycle. The deviation between second and third cycle is very small and for practical purposes two iteration cycles are sufficient. The process is therefore, very much suitable in design office with only a desk calculator.

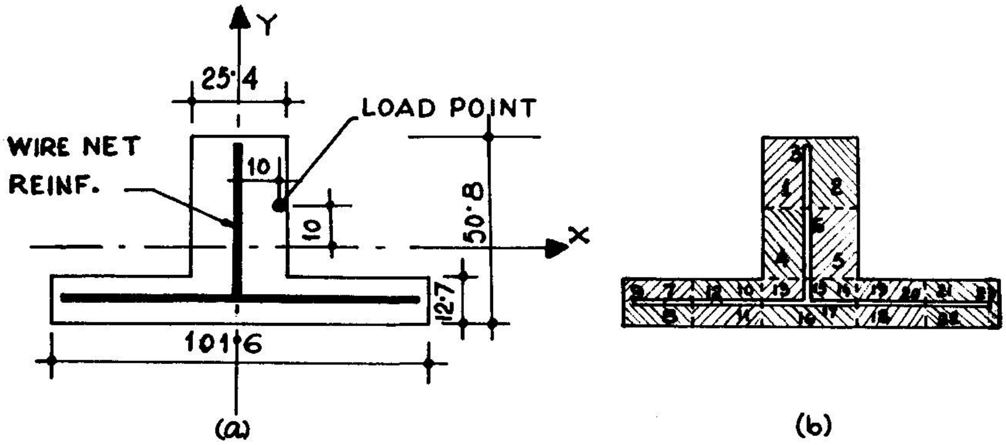

FIG.3 ELEMENT IDEALISATION.

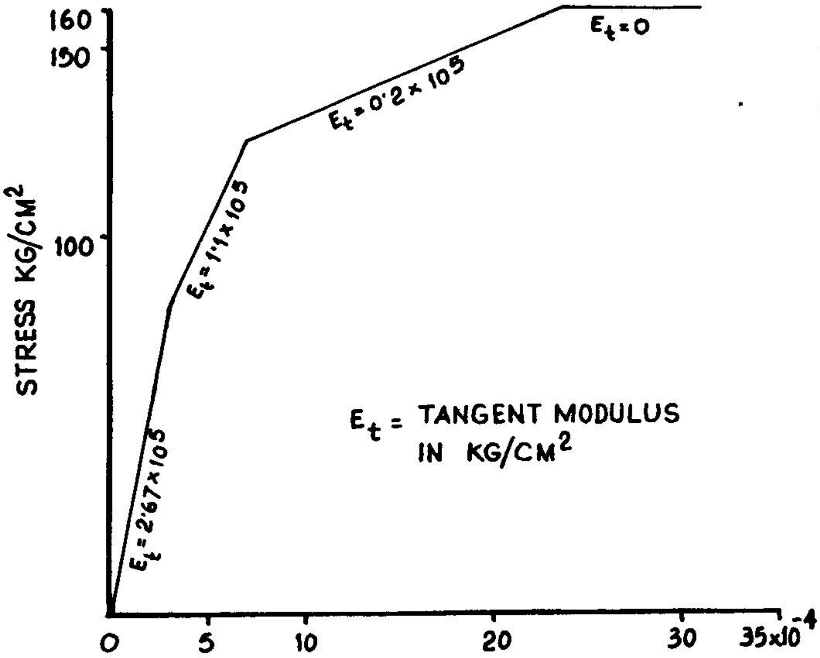

FIG. 4 IDEALISED QUADRI-LINEAR MODEL OF STRESS STRAIN CURVE OF CONCRETE(TAKEN FROM FIG.1)

From Table 3 it is observed that the method is fairly good in estimating the ultimate load of compression members under biaxial bending.

Fig. 6 shows the photograph of some of the specimens after test.

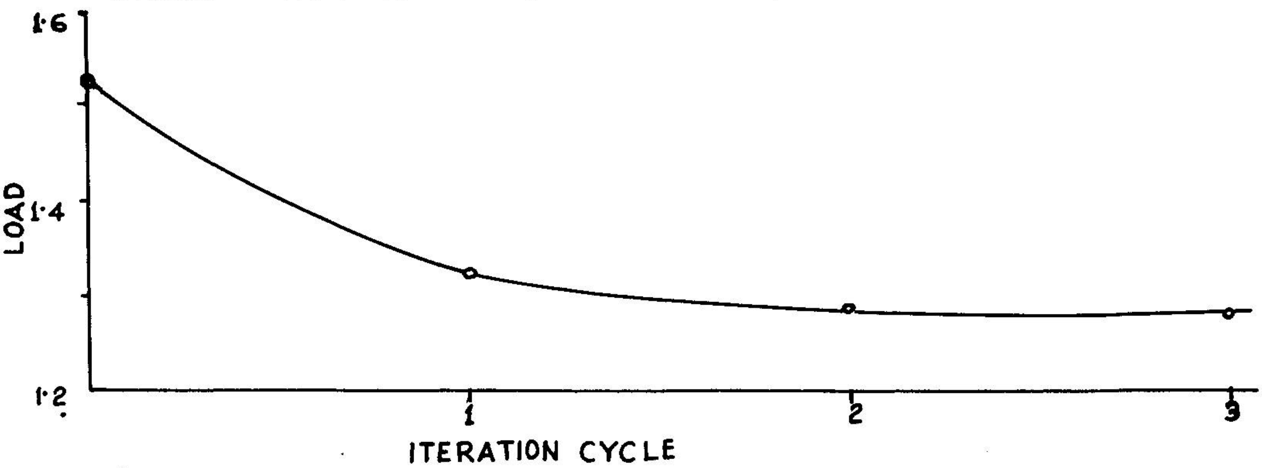

FIG.5 CONVERGENCE OF ITERATION PROCESS.

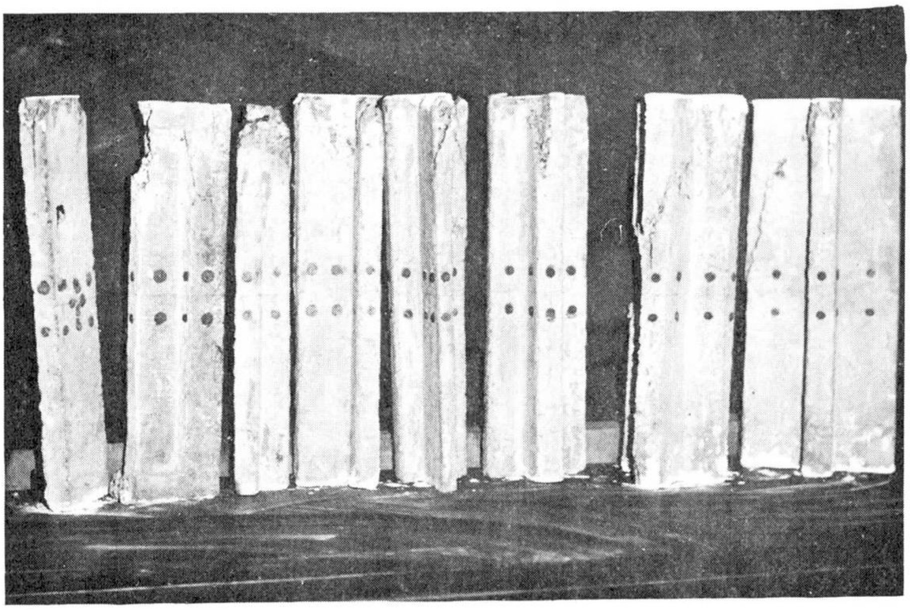

FIG.6 SOME OF THE SPECIMENS AFTER TEST

4. CONCLUSION:

Within the scope of the present series of experiments conclusions are,

1) T sections are about 30 to 40 percent more efficient than L sections.

2) Rectangular sections carry less load than T sections but more load than L sections.

3) The increase in column strength ranges from 30 to 35 percent for columns with end diaphragms in case of T and L sections.

4) The iteration procedure given by Hsu & Mirza (1) is a highly convergent one and is fairly good in estimating the ultimate load carrying capacity of compression members under biaxial bending.

5) In case of biaxial bending also, T sections carry more load than L sections.

REFERENCE:

1. Cheng-Tzu Hsu and M. Saeed Mirza "Structural Concrete - Biaxial Bending and Compression". Technical note, ASCE Vol.99 No. ST2 Feb. 1973.

SUMMARY

Strength of columns having T and L shapes subject to biaxial bending is determined experimentally and compared with theoretical values of Hsu & Mirza (1). Efficiencies of T, L and rectangular column section are also compared. Effect of end stiffening of T and L shaped columns by means of diaphragms has also been studied in the paper.

RESUME

On détermine expérimentalement la résistance des colonnes en forme de T et de L soumises à une flexion biaxiale, et on effectue une comparaison avec les valeurs théoriques de Hsu et Mirza (1). On compare également les colonnes à section en forme de T, de L, et de rectangle. Ce rapport étudie également l'influence d'un raidissage aux extrémités des colonnes en T et en L au moyen de cloisons transversales.

ZUSAMMENFASSUNG

Zahlenmässige Schätzungen für den Wert der grössten Druckstauchung von Beton bei der Bruchbeanspruchung von Stahlbeton-Stützenquerschnitten unter Einwirkung verschiedener Kombinationen von Normalkraft und Biegemomenten wurden vorgenommen. Die Ergebnisse zeigten, dass die grösste Druckstauchung durch eine Reihe von Faktoren, wie die Kombination von Normalkraft und Biegemoment, den Verlauf des Spannungs - Dehnungs - Diagramms von Beton, die Streckgrenze der Bewehrung, den Bewehrungsgehalt usw. beeinflusst wird.

IV

Additional Moments in Slender Prestressed Concrete Columns

Moments additionnels dans des colonnes élancées précontraintes

Zusatzmomente in schlanken Spannbetonstützen

R.D. STURROCK
BSc, MICE
Great Britain

Introduction

The derivation and application of the additional moment method for the design of slender R.C. columns is dealt with in a recent report by Cranston[1]. The report includes an extensive comparison between the design method and test data, and is shown to be suitable for a wide range of columns covering the principle variables. The present study was carried out in order to examine the suitability of applying the method directly to prestressed concrete columns. Similar comparisons between calculated and test results were made and differences in the trends relative to R.C. columns led to a closer study of the problem being carried out.

The additional moment expressions for the design of slender R.C. columns are given in Section 3.5 of the British Standards Code of Practice CP 110[2].

For long columns bent about the minor axis, the cross-section should be designed to resist the ultimate axial load N and a total moment given by

$$M_t = M_i + \frac{Nh}{1750} \left(\frac{l_e}{h}\right)^2 \times \left(1 - 0.0035 \frac{l_e}{h}\right) . \; K \qquad (1)$$

Where M_i is the maximum moment in the column due to ultimate loads, h is the overall depth of the cross-section in the plane of bending, l_e is the effective length, and K is an adjustment factor depending on N/N_{uz} where N_{uz} is the axial load capacity.

All tests reported and analyses carried out in this study were of pin-ended columns subject to loads acting at equal eccentricities with respect to both ends of the column. In such cases, $l_e = l_c$ where l_c is the clear height, and $M_i = N \times e_i$ where e_i is the initial eccentricity of load.

The test series used in the comparisons are reported in references 3, 4 and 5, and the results listed in Table 1. Details of the method used for calculating the failure loads are given in the appendix to this report.

A histogram of $(N_u)_{Test}/(N_u)_{Calc}$ is shown in Figure 1(b), and includes all the test cases analysed. In Figure 1(a) the corresponding histogram for pinned R.C. columns abstracted from reference (1) is shown. There is insufficient data available for the significance of individual parameters to be observed clearly, but the results did indicate somewhat different trends to those shown by the R.C.

column study. In general, the reported test work was not sufficiently detailed for study, and a series of computer analyses was therefore carried out. All combinations of the parameters listed in Table 2 were considered, but only one grade of concrete and one grade and percentage of steel used in the analyses.

Slenderness ratio	$- l/h$	20	30	40
Initial eccentricity	e_i/h	0.5	0.2	0.5
Level of prestress	f_{cp}/f_{cu}	0	0.15	0.3

Table 2

$f_{cu} = 40\ N/mm^2$

$f_{pu} = 1700\ N/mm^2$

$\frac{Aps}{bh} = 0.01$

Where

f_{cu} is the characteristic cube strength

f_{pu} is the characteristic strength of the prestressing tendons

f_{cp} is the compressive stress in the concrete due to prestress

Aps is the area of the prestressing tendons

The stress strain curves assumed in the analyses were those given in Figures 1 and 3 of reference (2) with γ taken as 1.0 in each case, and the modulus of elasticity of the tendons assumed to be 200 KN/mm^2. The computer programme used was essentially the same as that used in the R.C. column study, and full details are given in reference (6).

The computer analyses have merely been used to augment the information available on tests reported, for the effects of the various parameters may be observed without the inherent variability of laboratory testing obscuring the trends. The histogram of the results from the analyses is given in Figure 1(c) and it may be seen that the distribution is similar to that of Figure 1(b) but with a lower mean value.

The main differences between the histograms shown in Figure 1 are the lower mean value for the prestressed columns, and the percentage of the population values below 0.95. For the R.C. columns, there are 7% below, and for the P.S.C. columns, 17%. There are basically two reasons for these differences, both related, and being functions of the level of prestress and the additional moment philosophy.

In order to understand these effects, it is necessary to consider the basic additional moment expression, the derivation of which is covered in detail in reference (1).

Essentially, the method depends upon forecasting the deflection of the column at ultimate conditions, and this is assumed to be given by:

$$a_u = l_e^2/10r_u \qquad (2)$$

Where

a_u is the maximum deflection corresponding to material failure conditions.

$1/r_u$ is the corresponding curvature.

CP 110 assumes $1/r_u = K \times (1/r)_{bal}$ Where $(1/r)_{bal}$ is the curvature at 'balanced' conditions on the cross-section, and K is defined as $(N_{uz} - N)/(N_{uz} - N_{bal}) \leqslant 1.0$.

$(1/r)_{bal}$ is taken $(\varepsilon_{uc} + f_y{}^*/E_s - l_e/50000h)/h$ and fixed values of ε_{uc}, the ultimate strain in the concrete in compression, and $f_y{}^*/E_s$, the yield strain of the steel, of 0.00375 and 0.002 respectively give

$$(1/r)_{bal} = \frac{1 - 0.0035\ le/h}{175h}$$

Substituting the above in equation (2) yields the additional deflection or eccentricity implied in equation (1).

If the above criterion is applied to a P.S.C. section, then the value of 0.002 adopted for the steel yield strain will obviously be inappropriate. The corresponding condition in a P.S.C. section should, therefore, take into account the actual yield strain of the tendons, and also the prestrain applied. The corresponding strain diagram, due to loading at the balance point is shown in Figure 2.

The effect of ε_{pc} may be neglected as being insignificant relative to 0.00375 and, in analogy with R.C. formula, a value of 0.008 for ε_y may be assumed to cover the likely range of prestressing steels used. Hence, a modified expression for $(1/r)_{bal}$ is given by

$$(1/r)_{bal} = (0.00375 + 0.008 - \varepsilon_{ps} - l_e/50000h)/h \qquad (4)$$

Figure 3 shows the variation in the ratio of a_u for a prestressed section to a_u for reinforced section against level of prestress. It is apparent that for the low levels of prestress the R.C. expression considerably underestimates the deflection at ultimate.

Using the modified expression above, the test columns and the computer 'tests' were re-analysed, and the new histograms are shown in Figure 4. There are now less than 2% of the values below 0.95, and the mean value is close to that obtained from the R.C. column study.

Although the modified formula improves the results it was noticed that there was still a significant decrease in the value of $(N_u)_{Test}/(N_u)_{Calc}$ as the level of prestress was increased. For example, Figure 5 (a) shows some of the values obtained from the tests reported in reference 3 and Figure 5 (b) the results obtained from the computer analyses. It was also observed that the $(N_u)_{Test}/(N_u)_{Calc}$ values decreased with increasing eccentricity and increased with increasing slenderness. The reason for these trends is essentially a function of the strength based failure criterion that is assumed in the additional moment method. In the case of a slender column loaded axially or with small eccentricity, the failure mode is that of instability and, in general, the design method results in a conservative estimate of the failure load. This behaviour is illustrated in Figure 6 in which the effects of prestress, slenderness and eccentricity on the load - maximum moment curves are shown.

Also plotted on the figures are the load versus total moment lines as calculated from the additional moment expression.

The effects of initial eccentricity and slenderness produce the marked skewness of the histogram shown in Figure 1 (a). The additional effect of prestress which tends to inhibit instability failures may be observed in the reduced skewness of Figure 4 relative to Figure 1 (a). It may be concluded therefore, that provided the modified expression is used, the additional moment method may be applied to P.S.C. columns, and will in general result in a rather better forecast of the failure load than in the case R.C. columns.

The skewness of the histograms in Figures 1 and 4 could be eliminated by introducing an alternative failure criterion for slender columns with low levels of prestress and loaded at small eccentricities. Mikhailov(7) tackles this aspect by proposing a failure criterion based on first cracking. Analysis on this basis gives $(N_u)_{Test}/(N_u)_{Calc}$ results close to unity for the conditions outlined above, but is not applicable over the whole range of parameters.

There is a further consideration in that the additional moment method makes an implicit allowance for long term effects in the calculation of the deflection at ultimate. If an alternative failure criterion such as outlined above were adopted, the possibility of creep buckling failures at reduced load levels would have to be explicitly taken into account. Since the additional moment method is generally conservative - albeit unnecessarily so in some cases - it seems unwarranted to introduce a dual failure criterion. In particular, the interaction of the three main parameters makes it very difficult to set limits on the values of these parameters in order to define the transition from one failure criterion to the other.

Appendix - Calculation of failure loads

The various test series considered are given in Table 1, all results having been reduced to a common basis in S.I. Units. The interaction diagrams giving the section strengths for each individual cross-section were produced by a computer program using the stress strain curves given in Figures 1 and 3 of reference 2. Where cylinder strengths were given in the reported test work, the cube strength has been assumed to be 1.25 times the quoted values. The failure loads are obtained by the intersection of the load versus total moment line with the interaction diagram, taking account of the reduction factor K.

References

(1) CRANSTON, W.B. Analysis and Design of Reinforced Concrete Columns - Research Report 20, Cement and Concrete Association, London 1972.

(2) British Standards Code of Practice CP 110 (Part 1). The Structural Use of Concrete. 1972.

(3) ARONI, S. Slender Prestressed Concrete Columns. Journal of the Structural Division, Proceedings of the American Society of Civil Engineers, Volume 94, No. ST4. April 1968.

(4) BROWN, H.R. and HALL, A.S. Tests on Slender Prestressed Concrete Columns - Paper No. 8, Symposium on Reinforced Concrete Columns. American Concrete Institute Special Publication SP-13. 1966.

(5) LIPSON, S.L. Experimental Investigation of Buckling of Slender Prestressed Columns. Rilem International Symposium. Buenos Aires, Argentina, September 1971.

(6) CRANSTON, W.B. A computer Method for the Analysis of Restrained Columns. Technical Report TRA 402, Cement and Concrete Association. London 1967.

(7) MIKHAILOV, V.V. Design of Slender Prestressed Concrete Columns Based on Stability Criteria, P.C.I. Journal, Sept/Oct 1972.

TABLE 1

ARONI[3]

Test column	100 ρ	f_{cu} N/mm^2	f_{pu} N/mm^2	l/h	e_i/h	$\frac{f_{cp}}{f_{cu}}$	$(N_u)_{Test}$ kN	$(N_{uz})_{Calc}$ kN	$(N_{bal})_{Calc}$ kN	$(N_u)_{Calc}$ kN	$\frac{(N_u)_{Test}}{(N_u)_{Calc}}$
A1 20c 3	2.03	49	1730	20	1.98	0.208	11.8	137	8.3	9.8	1.21
A1 30a 3				30	0.124	0.208	46.4	137	8.3	37.8	1.24
A1 40b 3				40	0.743	0.208	13.8	137	8.3	12.9	1.07
A2 20b 5				20	0.743	0.32	22.8	112	-10.8	21.1	1.08
A2 30c 5				30	1.98	0.32	8.8	112	-10.8	8.2	1.07
A2 40a 5				40	0.124	0.32	26.4	112	-10.8	25.6	1.03
B1 20a 1				20	0.124	0.072	83.7	166	35	61.2	1.37
B1 30b 1				30	0.743	0.072	17.3	166	35	15.8	1.10
B1 40c 1				40	1.98	0.072	7.3	166	35	7.1	1.03
B2 20b 3				20	0.743	0.2	21.7	139	9.7	21.5	1.01
B2 30c 3				30	1.98	0.2	8.7	139	9.7	8.4	1.04
B2 40c 3				40	0.124	0.2	26.6	139	9.7	21.5	1.23
C1 20c 1				20	1.98	0.08	12.0	164	33	9.4	1.27
C1 30a 1				30	0.124	0.08	51.9	164	33	30.0	1.73
C1 40b 1				40	0.743	0.072	11.9	166	35	11.5	1.03
C2 20a 3				20	0.124	0.2	56.9	139	9.7	64.0	0.89
C2 30b 3				30	0.743	0.192	17.6	140	11	16.7	1.05
C2 40c 3				40	1.98	0.192	7.2	140	11	6.9	1.03
D1 20c 5				20	1.98	0.336	12.5	109	-17	9.3	1.35
D1 30b 5				30	0.743	0.336	20.1	109	-17	17.3	1.16
D1 40a 5				40	0.124	0.336	26.3	109	-17	25.8	1.02
D2 20b 3				20	0.743	0.2	24.8	139	9.7	21.5	1.15
D2 30b 3				30	0.743	0.2	18.9	139	9.7	17.1	1.10
D2 40b 3				40	0.743	0.2	13.0	139	9.7	12.8	1.02
E1 20a 5				20	0.124	0.336	58.3	112	-10.8	55.1	1.06
E1 30b 5				30	0.743	0.336	19.3	109	-17.0	17.3	1.14
E1 40c 5				40	1.98	0.336	8.4	109	-17.0	7.5	1.12
E2 20b 1				20	0.743	0.072	22.6	166	35	20.7	1.10
E2 30c 1				30	1.98	0.08	8.9	164	33	8.1	1.10
E2 40a 1				40	0.124	0.072	29.8	166	35	17.4	1.71
F1 20b 1				20	0.743	0.08	24.8	164	33	21.1	1.17
F1 30b 1				30	0.743	0.072	16.5	166	35	16.1	1.02
F1 40b 1				40	0.743	0.072	11.1	166	35	11.5	0.97
F2 20b 5				20	0.743	0.32	23.6	112	-10.8	21.1	1.12
F2 30a 5				30	0.124	0.32	42.8	112	-10.8	40.1	1.07
F2 40b 5				40	0.743	0.32	13.4	112	-10.8	13.7	0.98

BROWN AND HALL[4]

A1	2.09	35.9	1558	33	0.04	0.019	56	145	32.6	21.3	2.63
A2					0.045		53.2			21.1	2.53
A3					0.13		33.5			19.1	1.75
A4					0.25		22.1			17.0	1.30
A5					0.75		12.0			10.9	1.10
A6					1.965		7.9			6.5	1.21
B1		42.0			0.01	0.182	64.2	130	10.4	32.5	1.98
B2					0.11		43.0			27.3	1.58
B3					0.165		37.8			24.4	1.55
B4					0.305		25.8			20.4	1.27
B5					0.815		13.9			13.0	1.07
B6					1.960		8.0			7.3	1.10
C1		40.3			0.05	0.26	53.4	113	-0.8	31.0	1.72
C2					0.11		46.7			29.0	1.61
C3					0.15		40.0			26.4	1.51
C4					0.285		31.3			21.4	1.46
C5					0.875		15.1			12.8	1.18
C6					1.97		7.9			6.9	1.15

TABLE 1 continued

BROWN AND HALL[4] continued

Test column	100 ρ	f_{cu} N/mm²	f_{pu} N/mm²	l/h	e_i/h	$\frac{f_{cp}}{f_{cu}}$	$(N_u)_{Test}$ kN	$(N_{uz})_{Calc}$ kN	$(N_{bal})_{Calc}$ kN	$(N_u)_{Calc}$ kN	$\frac{(N_u)_{Test}}{(N_u)_{Calc}}$
D1	2.09	39.0	1558	33	0.025	0.382	57.8	89.5	-20.6	35.8	1.61
D2					0.13		6.7			27.8	1.68
D3					0.285		33.4			21.9	1.52
D4					0.42		26.4			18.4	1.43
D5					0.82		17.5			12.7	1.38
D6					1.995		8.9			6.6	1.34
E1					-0.015	0.471	67.4	73.3	-30.0	36.3	1.86
E2					0.055		57.7			30.1	1.92
E3					0.15		44.5			24.6	1.81
E4					0.35		32.1			18.3	1.75
E5					0.885		18.4			11.7	1.57
E6					2.18		9.3			5.9	1.59
LIPSON[5]											
A1	0.23	75.6	1724	40	0.102	0.03	165	773	115	48.7	3.39
A2	0.23	77.3			0.177	0.029	90	790	119	45.0	2.00
B1	0.45	63.8			0.041	0.069	210	638	43.4	64.4	3.27
C1	0.60	56.1			0.081	0.103	175	551	-5.0	74.4	2.35
C2	0.60	61.1			0.050	0.095	246	602	4.8	78.3	3.15
C3	0.60	66.0			0.121	0.088	153	653	14.4	78.3	1.95
C4	0.60	75.6			0.103	0.077	190	753	33.1	82.8	2.30
C5	0.60	77.3			0.037	0.075	246	770	36.2	84.7	2.91
D1	0.91	75.6			0.077	0.116	214	735	-34.5	108.7	1.96
D2	0.91	63.7			0.035	0.138	231	611	-58.0	102.0	2.27
D3	0.91	77.3			0.058	0.114	239	752	-31.6	110.5	2.16
E1	1.20	62.8			0.032	0.184	244	584	-123	126.7	1.92
E2	1.20	57.5			0.080	0.201	165	529	-133	119.6	1.38
COMPUTER ANALYSES											
1 a	1.00	40	1700	20	0.05	0	204	335	-10.3	114	1.42
1 b						0.15	167	272	-16.1	176	0.95
1 c						0.3	127	207	13.5	146	0.87
2 a					0.2	0	109	335	-10.3	85	1.29
2 b						0.15	110	272	-16.1	104	1.06
2 c						0.3	92	207	13.5	99	0.93
3 a					0.5	0	50	335	-10.3	52	0.97
3 b						0.15	58	272	-16.1	60	0.98
3 c						0.3	57	207	13.5	59	0.96
4 a				30	0.05	0	149	335	-10.3	51	2.91
4 b						0.15	128	272	-16.1	72	1.79
4 c						0.3	100	207	13.5	102	0.98
5 a					0.2	0	66	335	-10.3	43	1.52
5 b						0.15	84	272	-16.1	60	1.41
5 c						0.3	72	207	13.5	71	1.02
6 a					0.5	0	31	335	-10.3	33	0.93
6 b						0.15	45	272	-16.1	41	1.10
6 c						0.3	46	207	13.5	45	1.01
7 a				40	0.05	0	103	335	-10.3	28	3.70
7 b						0.15	96	272	-16.1	42	2.30
7 c						0.3	77	207	13.5	59	1.30
8 a					0.2	0	41	335	-10.3	26	1.59
8 b						0.15	63	272	-16.1	36	1.74
8 c						0.3	57	207	13.5	47	1.22
9 a					0.5	0	20	335	-10.3	22	0.93
9 b						0.15	36	272	-16.1	29	1.25
9 c						0.3	38	207	13.5	34	1.10

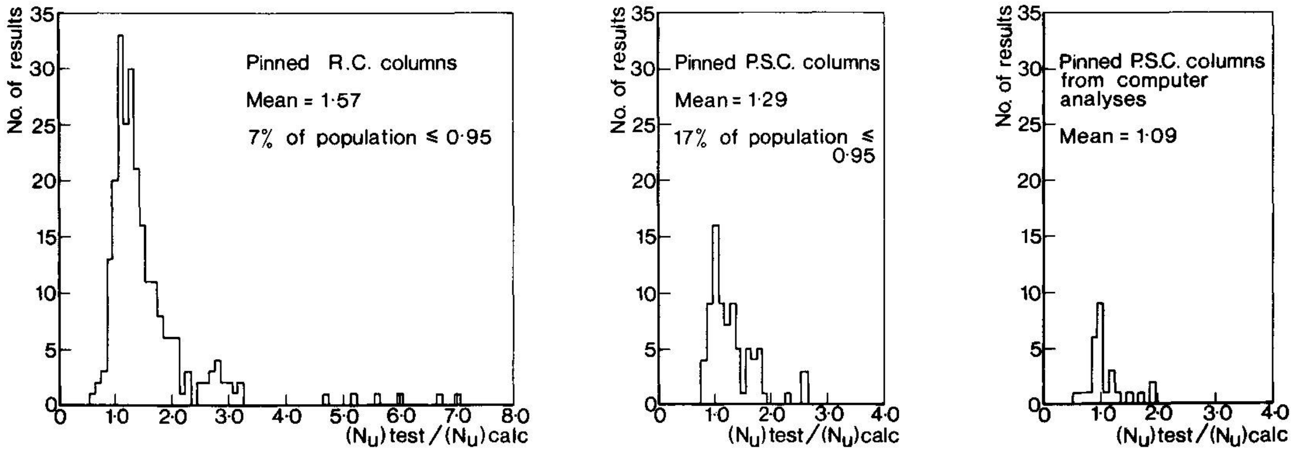

1(a) 1(b) 1(c)

FIGURE 1 (N_u) TEST/ (N_u) CALC USING ADDITIONAL MOMENT EXPRESSION FOR R.C. SECTIONS

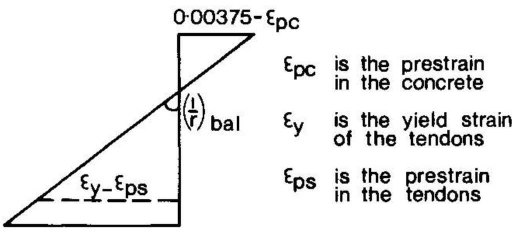

FIGURE 2 STRAIN PROFILE ACROSS SECTION AT THE "BALANCE POINT"

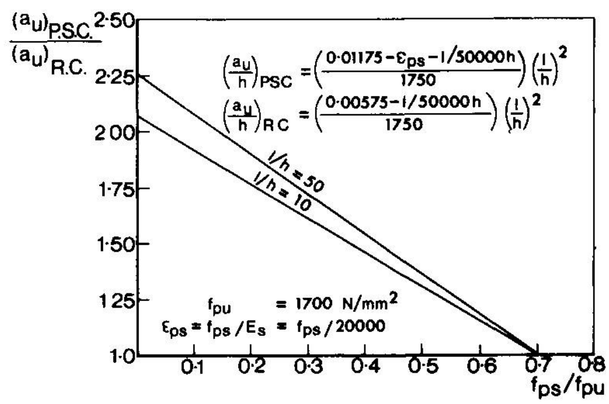

FIGURE 3 EFFECT OF PRESTRESS ON ULTIMATE DEFLECTION

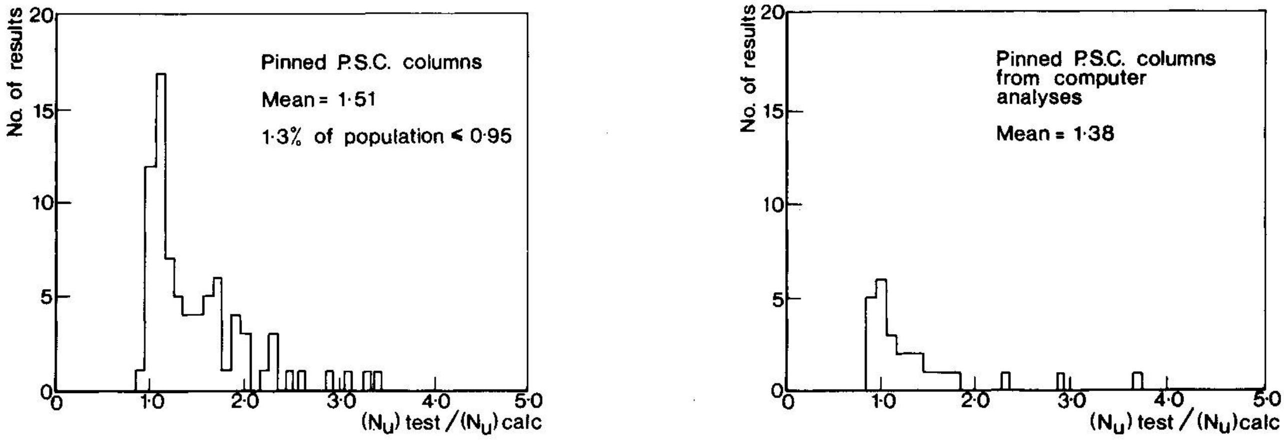

4(a) 4(b)

FIGURE 4 (N_u) TEST/ (N_u) CALC USING MODIFIED ADDITIONAL MOMENT EXPRESSION

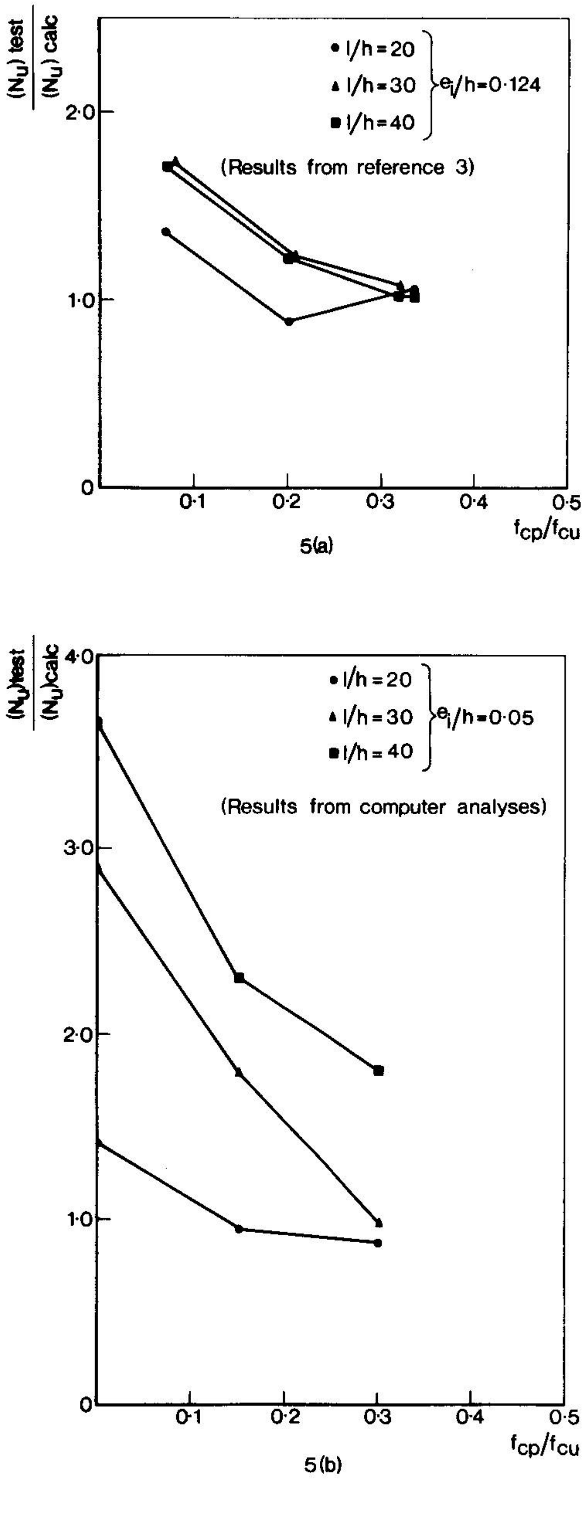

FIGURE 5 EFFECT OF PRESTRESS ON (N_U)TEST / (N_U)CALC

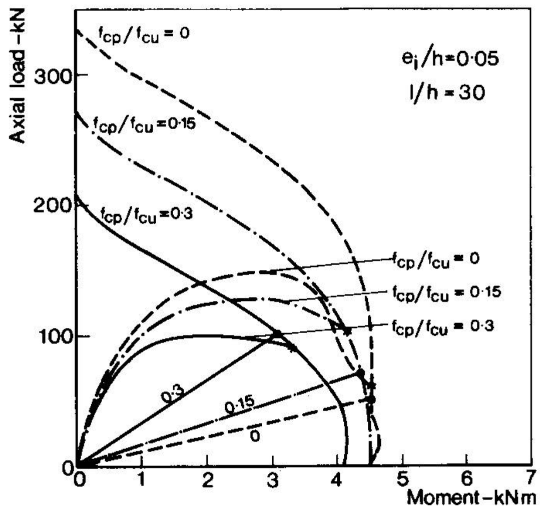

FIGURE 6A EFFECT OF PRESTRESS ON LOAD v MAXIMUM MOMENT

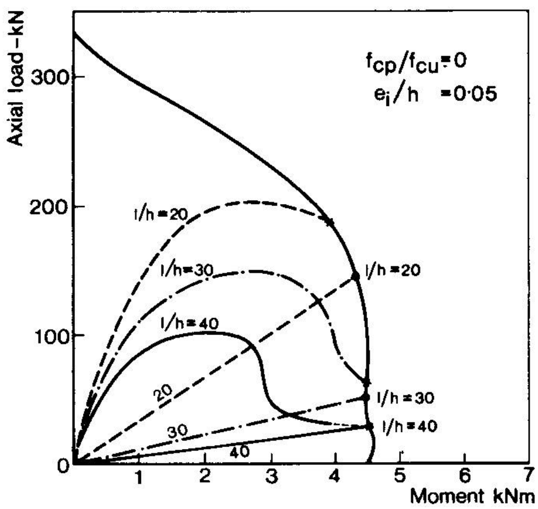

FIGURE 6B EFFECT OF SLENDERNESS ON LOAD v MAXIMUM MOMENT

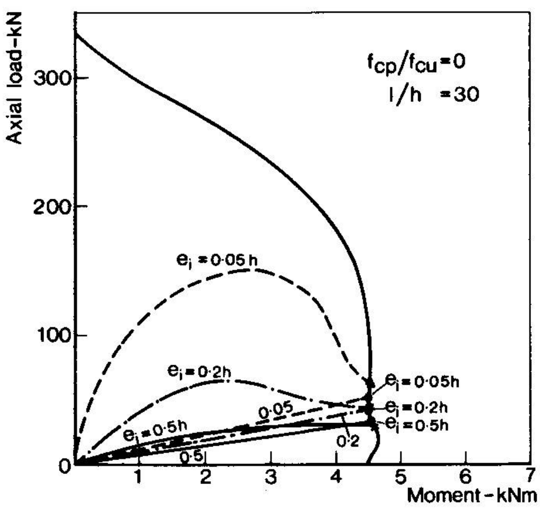

FIGURE 6C EFFECT OF INITIAL ECCENTRICITY ON LOAD v MAXIMUM MOMENT

SUMMARY

A comparison between calculated and test failure loads of prestressed concrete columns is presented. The calculated values were obtained by applying the additional moment method as derived for R.C. columns to the prestressed concrete columns in the test work reported. The comparisons showed somewhat different trends relative to R.C. columns and a series of computer analyses was carried out in order to study more closely the reasons for these differences. The behaviour of prestressed columns as influenced by slenderness, initial eccentricity of loading and level of prestress is discussed and recommendations for design proposed.

RESUME

La contribution présente une comparaison entre les charges ultimes calculées et celles constatées à l'essai, pour les colonnes précontraintes en béton armé. Les valeurs calculées ont été obtenues en appliquant aux colonnes précontraintes la méthode des moments additionnels des colonnes en béton armé. Les comparaisons ont montré des tendances assez différentes de celles des colonnes en béton armé; une série d'analyses par ordinateur ont été exécutées en vue d'étudier de plus près les raisons de ces différences. On a discuté le comportement de colonnes précontraintes sous l'influence de l'élancement, de l'excentricité initiale à la charge et du degré de précontrainte, et on propose des recommandations pour le dimensionnement.

ZUSAMMENFASSUNG

Der vorstehende Bericht behandelt einen Vergleich zwischen berechneten und Versuchsbruchlasten vorgespannter Stahlbetonstützen. Die berechneten Werte für die dem Versuch unterworfenen Spannbetonstützen ergeben sich nach der für Stahlbetonstützen hergeleiteten Methode der Zusatzmomente. Die Vergleiche zeigen ein im Vergleich zu Stahlbetonstützen unterschiedliches Verhalten; eine Reihe von Computerberechnungen wurde durchgeführt, um die Ursachen für diese Abweichungen genauer zu untersuchen. Das Verhalten vorgespannter Stützen unter dem Einfluss von Schlankheit, Anfangsexzentrizität und Grad der Vorspannung wird diskutiert und Empfehlungen für die Bemessung gegeben.

Leere Seite
Blank page
Page vide

Bemessung von Stahlbeton-Fertigteilstützenstössen

Detailing of Precast Columns Reinforcement Near the Joints

Dimensionnement des raccords de colonnes préfabriquées en béton armé

Bernd BRANDT Horst G. SCHÄFER
TH Darmstadt, BRD

1. Einleitung

Im Hochhausbau dienen Fertigteilstützen vorwiegend zur Übertragung reiner Druck-Normalkräfte. Im Stoßbereich muß der Traganteil der Längsbewehrung und des eventuell abplatzenden Betonmantels von der Kernquerschnittsfläche mit übernommen werden. Dadurch treten sowohl erhöhte Betondruckbeanspruchungen als auch Spaltzugkräfte auf, die eine Querbewehrung erfordern, um die Tragfähigkeit einer ungestoßenen Stütze zu erreichen.

Im vorliegenden Bericht sollen für Stützen mit Kreis- und Quadratquerschnitt, die zentrisch belastet und nicht knickgefährdet sind, Bemessungsdiagramme zur Ermittlung der Querbewehrung im Stoßbereich angegeben werden.

2. Mörtelfuge

Versuche zur Ausbildung und Tragfähigkeit von Stützenstößen mit dünnen Mörtelfugen haben gezeigt, daß primär nicht die Mörtelfuge für die Tragfähigkeit des Stoßes verantwortlich ist, sondern die konstruktive Durchbildung des Stützenfußes [1 bis 3] .

Bei einer satt verfüllten, dünnen Fuge ($d/c \geqq 7$) behindern die an die Fuge anschließenden Fertigteile durch Reibungskräfte eine Querdehnung des Mörtels. Diese Querdehnungsbehinderung erhöht die Tragfähigkeit des Fugenmörtels, da sich ein dreiaxialer Spannungszustand einstellt. Bei verdeckten Fugen wird die Querdehnung zusätzlich durch den umgebenden Deckenbeton behindert, so daß theoretisch sogar eine Sandfüllung zur Lastübertragung ausreichen würde. Aufgrund der oben genannten Versuche reicht es aus, wenn die Güte des Fugenmaterials der Güte des Stützenbetons entspricht.

3. Einfache Modelle zur Herleitung von Bemessungsformeln

3.1 Prinzip der Lastabtragung

Im Bereich des Stützenfußes müssen die Traganteile der Längsbewehrung F_s und des Betonmantels F_m in den Stützenkern umgelenkt werden. Die gesamte umzulenkende Kraft F^* beträgt:

$$F^* = F_s + F_m = A_s \cdot \beta_{0.2} + A_m \cdot \beta_R \qquad (1)$$

Der Lastanteil F_s wird im Einleitungsbereich über Haft- und Scherkräfte an die Bewehrungsstäbe abgegeben. Für die weiteren Überlegungen wird als Länge des Lasteinleitungsbereiches, die durch eine erhöhte Querbewehrung verkürzt werden kann [4], näherungsweise die Stützendicke d, mindestens jedoch 30 cm, angesetzt.

Versuche zeigen [5], daß die Kraft in der Längsbewehrung vom Ende an (z = 0) sehr rasch anwächst und sich der Verlauf recht gut durch einen Kreis beschreiben läßt. Das Verhältnis der örtlichen Betonüberlastung F'(z) zum rechnerischen Stahltraganteil F_s beträgt also angenähert:

$$\frac{F'(z)}{F_s} = 1 - \sqrt{\frac{z}{d}\left(2 - \frac{z}{d}\right)} \qquad (2)$$

Der Einfachheit halber wird für den Traganteil F_m des Betonmantels näherungsweise die gleiche Gesetzmäßigkeit zugrunde gelegt. Die gesamte betondruckerhöhende Belastung ergibt sich durch Summation über die Länge des Lasteinleitungsbereiches zu 0.215 F*.

Der Traganteil F_m des Betonmantels hängt von der Dicke und Lage der Fuge ab. Bei "freien" Fugen, die ober- oder unterhalb der Deckenscheibe liegen, wird angenommen, daß die Fuge um eine halbe Fugendicke (c/2) ausplatzen kann, mindestens jedoch um das Maß h'. Bei "verdeckten" Fugen, die innerhalb der Deckenscheibe liegen, ist die Dicke des Betonmantels immer mit h' anzusetzen.

Die Querbewehrung hat im Lasteinleitungsbereich also folgende Aufgaben zu erfüllen:

- Wirksame Behinderung der Querdehnung; dadurch erreicht man eine Verkürzung des Lasteinleitungsbereiches <u>und</u> die Ausbildung eines dreiaxialen Spannungszustandes. Dieser ermöglicht die Aufnahme der erhöhten Betondruckbeanspruchungen.
- Aufnahme von Spaltzugkräften, die durch Umlenkung der Kräfte der Längsbewehrung und des Betonmantels in den Kernbereich der Stütze entstehen.

3.2 Ermittlung der Querbewehrung für Stützen mit Kreisquerschnitt

3.2.1 Aktivierung der dreiaxialen Festigkeit des Betons

Die Wendelbewehrung soll die Querdehnung des Betons wirksam behindern, so daß die dreiaxiale Festigkeit des Betons aktiviert wird. Dadurch kann der Kernbeton erheblich über die Prismenfestigkeit hinaus beansprucht werden, ehe der Bruch eintritt. Die Ringzugkraft Z_μ zur Behinderung der Querdehnung beträgt in Anlehnung an [6] mit einem mittleren Beiwert $\gamma = 1.7$:

$$Z_\mu = \frac{0.215\ F^*}{\gamma \pi} = 0.040\ F^* \qquad (3)$$

Die dazu erforderliche Querbewehrung wäre entsprechend dem Kraftverlauf in den Längsstäben etwa im unteren Drittel des Lasteinleitungsbereiches anzuordnen.

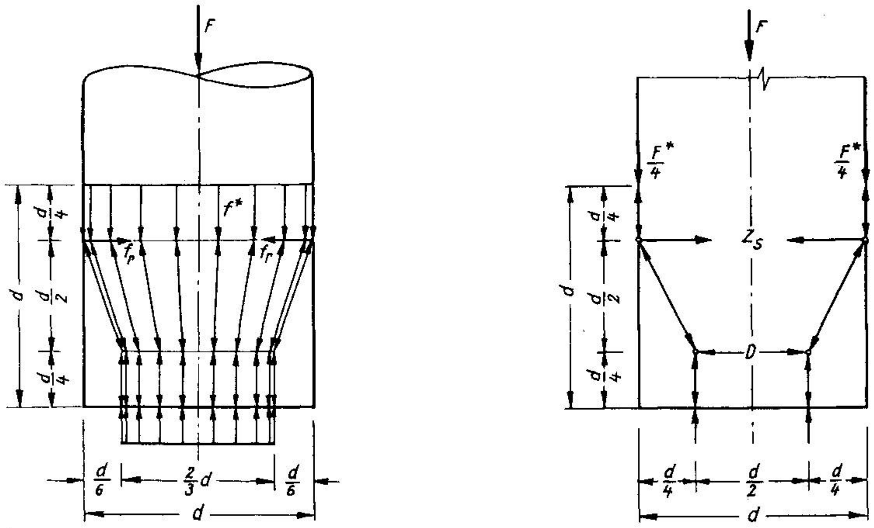

a) Kreisquerschnitt b) Quadratquerschnitt

Bild 1: Fachwerkmodell zur Ermittlung der Spaltzugkräfte im Stützenfuß

3.2.2 Aufnahme der Spaltzugkräfte

Der Lastanteil $F_c - F_m$ wird von der Mörtelfuge in der Kernquerschnittsfläche A_n übertragen, ohne daß Spaltzugkräfte entstehen. Der Umlenkkräfte erzeugende Lastanteil F* wird vereinfachend über den äußeren Umfang der Stütze als Linienlast f* "verschmiert" angenommen.

Die Querzugkräfte können anschaulich und genügend genau mit dem Gedankenmodell eines Fachwerks ermittelt werden (Bild 1a). Das Fachwerk wird in den Störbereich, dessen Länge etwa dem Stützendurchmesser entspricht, so hineingelegt, daß Lage und Neigung der Fachwerkstäbe in groben Zügen dem Trajektorienverlauf angepaßt sind [7] . Zur Verteilung der Pressungen in der Fuge wird aufgrund der Ergebnisse einer Vergleichsrechnung mit Hilfe der Finite-Element-Methode eine gleichmäßige Spannungsverteilung angenommen [8] .

Wie aus Bild 1a zu ersehen ist, erhält man unter Vernachlässigung der unterschiedlichen Stützen- und Fugendurchmesser aus der Lastumlenkung eine radial gerichtete Kraft $f_r = f^*/3$; diese bewirkt eine Ringzugkraft Z_s:

$$Z_s = \frac{F^*}{6\pi} = 0.053\ F^* \qquad (4)$$

3.3.2 Ermittlung der Querbewehrung für Stützen mit Quadratquerschnitt

Das räumliche Kräftespiel in Stützen mit Quadratquerschnitt kann näherungsweise durch eine getrennte Betrachtung der x- und y-Richtung erfaßt werden (Bild 1b). Es entstehen dann axial gerichtete Zugkräfte $Z_x = Z_y$.

Mit Hilfe der bereits erwähnten einfachen Modelle erhält man als Zugkräfte analog zu den Gln (3) und (4):

$$Z_{\mu x} = Z_{\mu y} = \frac{0.215\ F^*}{2\gamma} = 0.063\ F^* \qquad (5)$$

$$Z_{sx} = Z_{sy} = F^*/8 = 0.125\ F^* \qquad (6)$$

Die Ermittlung der Spaltzugkräfte mit Hilfe eines Fachwerkmodells wurde durch Rechnungen an einem Scheibenmodell überprüft. Dabei wurden die Zugspannungen sowohl mit der Finite-Element-Methode als auch auf analytischem Wege bestimmt [8]. Der Vergleich ergab eine befriedigende Übereinstimmung für die Größe der Spaltzugkräfte. Abweichungen in der Lage der resultierenden Kräfte sind von untergeordneter Bedeutung, da man aus konstruktiven Gründen ohnehin eine gleichmäßig verteilte Querbewehrung anstreben wird. Dies bietet sich auch deshalb an, weil die Spaltzugbewehrung vorwiegend im oberen Teil und die "Umschnürungsbewehrung" im wesentlichen im unteren Teil des Einleitungsbereiches anzuordnen wäre.

Für Institutsbauten der Technischen Hochschule Darmstadt [1] und ein Verwaltungsgebäude im Olympischen Dorf in München [2] wurde die Tragfähigkeit von Fertigteil-Stützenstößen in Versuchen überprüft. Eine Nachrechnung mit Hilfe der hier mitgeteilten Formeln ergab eine gute Übereinstimmung [8].

3.4 Bemessungsvorschlag

Während die gesamte Ringzugkraft bei einer Stütze mit Kreisquerschnitt gemäß den Gln (3) und (4)

$$Z_t = 0.040\ F^* + 0.053\ F^* = 0.093\ F^* \cong \frac{F^*}{10} \qquad (7)$$

beträgt, ergibt sich bei einer Stütze mit Quadratquerschnitt als gesamte Querzugkraft in einem Axialschnitt gemäß den Gln (5) und (6)

$$Z_t = 0.063\ F^* + 0.125\ F^* = 0.188\ F^* \cong \frac{F^*}{5} \qquad (8)$$

Die zur Aufnahme der Ringzugkräfte erforderliche Wendelbewehrung schneidet einen Längsschnitt durch die Stützenachse an zwei Stellen. Wird die gesamte geschnittene Bewehrung mit A_t bezeichnet, kann man zur Bemessung kreisförmiger und quadratischer Stützenstöße die gleichen Formeln und Diagramme benutzen.

Die für die Bemessung angesetzte Stahlspannung sollte im Hinblick auf die Verformungen nicht zu hoch gewählt werden. Es wird vorgeschlagen, die Bruchzugkräfte mit $\beta_{0.2}$ aufzunehmen und als Sicherheitsfaktor $\gamma = 2.1$ anzusetzen. Die erforderliche Querbewehrung A_t folgt mit Gl (1) zu

$$A_t = A_{t1} + A_{t2} = \frac{A_s}{5} + \frac{A_m}{5} \frac{\beta_R}{\beta_{0.2}} \qquad (9)$$

Bezieht man die erforderliche Bewehrung auf die Betonquerschnittsfläche A_c, dann erhält man für den erforderlichen Bewehrungsgrad:

$$\mu_t = \mu_{t1} + \mu_{t2} = \frac{1}{5}\mu_1 + \frac{1}{5} \frac{A_m}{A_c} \frac{\beta_R}{\beta_{0.2}} \qquad (10)$$

Gl (10) kann in einem Diagramm dargestellt werden. Bild 2 zeigt ein solches Diagramm für in der BRD übliche Werkstoffe.

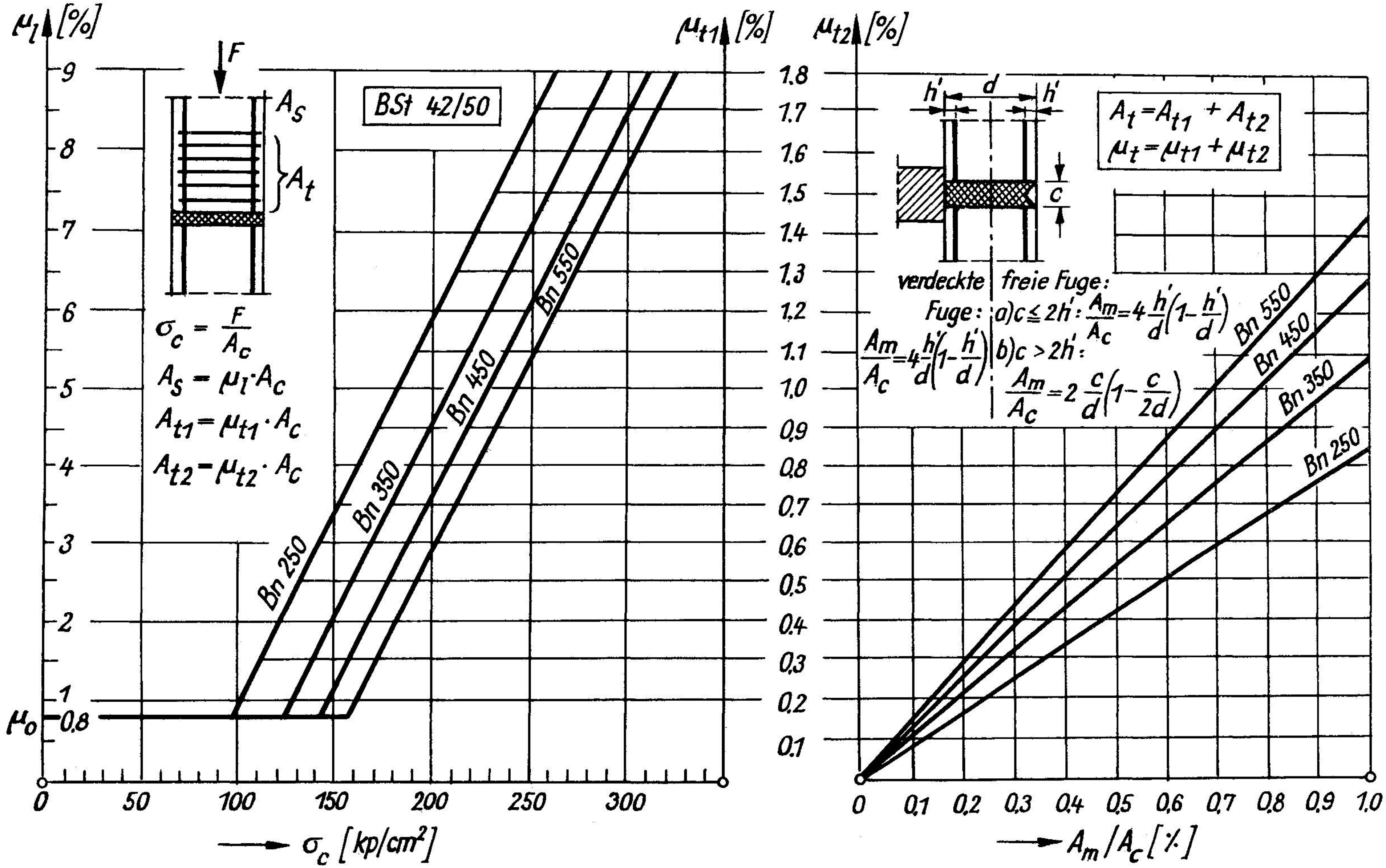

Bild 2: Bemessungsdiagramme für Stützen und Stützenstöße mit Kreis- und Quadratquerschnitt

4. Konstruktive Durchbildung

Die erforderliche Querbewehrung wird bei Stützen mit Kreisquerschnitt als Wendel eingelegt, bei Stützen mit Quadratquerschnitt als engmaschige Orthogonalbewehrung. Dabei wird die sofortige Lastaufnahme an den Stabenden durch Bügelecken oder angeschweißte Querstäbe gewährleistet.

Im Lasteinleitungsbereich sollte eine Mindestquerbewehrung im Hinblick auf die Betondruckerhöhung und die Spaltzugkräfte eingehalten werden. Dafür wird vorgeschlagen:

$$\min \mu_t = 0.6 \frac{50}{d\ [\mathrm{cm}]} \geq 0.6\ [\%] \qquad (11)$$

Bild 3 zeigt Vorschläge für die Anordnung der Mindestquerbewehrung bei Stützen mit Quadratquerschnitt. Eine Mindestquerbewehrung, die über die normale Verbügelung hinausgeht, kann entfallen, wenn der Kernbeton in der Lage ist, die gesamte Stützenlast allein aufzunehmen.

Ist aus statischen Gründen eine geringere Anzahl von Längsbewehrungsstäben erforderlich als in den Skizzen angegeben, so sind im Lasteinleitungsbereich zusätzliche Längsstäbe vom gleichen Durchmesser der Bügelbewehrung anzuordnen. Nur bei einer solchen kubischen Anordnung der Bewehrung kann der vorhandene räumliche Spannungszustand optimal durch Bewehrung abgedeckt werden. Für Stützen mit Kreisquerschnitt ist die Wendelbewehrung die beste Lösung.

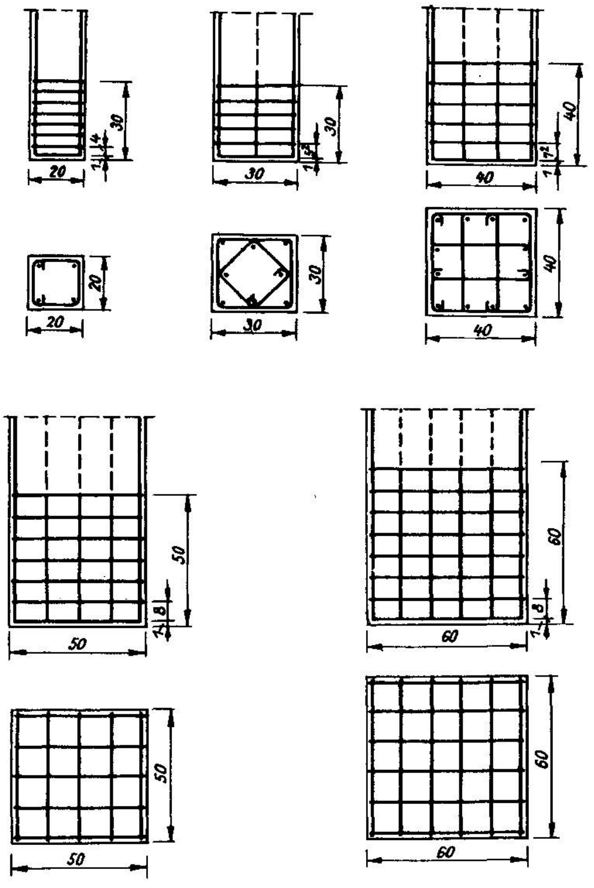

a) d ≤ 40 cm:

Bügel oder geschweißte Netze

b) d > 40 cm:

Geschweißte Netze

Bild 3: Vorschlag für eine Mindestquerbewehrung für Stützen mit Quadratquerschnitt (Bügeldurchmesser 8 mm)

Bezeichnungen

d	= Stützendicke	[cm]
c	= Fugendicke	[cm]
h'	= Betonüberdeckung der Längsbewehrung	[cm]
A_c	= Fläche des Stützenquerschnitts	[cm^2]
A_n	= Kernquerschnittsfläche der Fuge	[cm^2]
A_m	= $A_c - A_n$ = Querschnittsfläche des Betonmantels	[cm^2]
A_s	= erforderliche Längsbewehrung	[cm^2]
A_t	= erforderliche Querbewehrung in einem Längsschnitt mit der Länge d durch die Stützenachse	[cm^2]
$\beta_{0.2}$	= Stahlspannung bei einer Dehnung von 0.2 %	[kp/cm^2]
β_R	= Rechenwert der Betonfestigkeit	[kp/cm^2]
F_s	= Traganteil der Längsbewehrung	[kp]
F_c	= Traganteil des Stützenbetons	[kp]
F_m	= Traganteil des Betonmantels	[kp]
F^*	= $F_s + F_m$ = Umlenkkräfte erzeugender Lastanteil der Stütze	[kp]
f^*	= $F^*/\pi d$ = Umlenkkräfte erzeugender Lastanteil der kreisförmigen Stütze	[kp/cm]
Z_μ	= Zugkraftanteil infolge Querdehnungsbehinderung	[kp]
Z_s	= Zugkraftanteil infolge Lastumlenkung	[kp]
Z_t	= $Z_\mu + Z_s$ = Ringzugkraft bei kreisförmigen Stützen, Querzugkraft bei quadratischen Stützen	[kp]
f_r	= Radialkraft infolge Lastumlenkung bei der kreisförmigen Stütze	[kp/cm]
ν	= 2.1 = Sicherheitsbeiwert	[-]
μ_l	= $A_s/A_c \cdot 100$ = Längsbewehrungsgrad	[%]
μ_t	= $A_t/A_c \cdot 100$ = Querbewehrungsgrad	[%]

Literatur

[1] Weigler, H., u. J. Nicolay: Prüfung von Fertigteil-Stützenstößen auf ihre Tragfähigkeit. Technische Hochschule Darmstadt, Institut für Massivbau, Prüfungsbericht Nr. 568.66 vom 15.8.1966.

[2] Zimmermann, W., u. H. Dieterle: Belastungsversuche an gestoßenen Stützen. Otto-Graf-Institut an der Technischen Hochschule Stuttgart, Prüfungsbericht Nr. S 11659 vom 25.3.1970.

[3] Stiller, M.: Die Bemessung von Mörtelfugen. Betonstein-Zeitung 1970, S. 366/69.

[4] Leonhardt, F., u. K.-T. Teichen: Druck-Stöße von Bewehrungsstäben und Stahlbetonstützen mit hochfestem Stahl St 90. Deutscher Ausschuß für Stahlbeton Heft 222. Berlin: Verlag von Wilhelm Ernst & Sohn 1972.

[5] Franz, G., M. Sommer u. W. Eisenbiegler: Lasteintragung in die Bewehrung von Stahlbetondruckgliedern. Universität Karlsruhe (TH), Institut für Beton und Stahlbeton. Bericht für das AIF-Forschungsvorhaben Nr. 1689 vom 1.7.1970.

[6] Müller, K.F.: Beitrag zur Berechnung der Tragfähigkeit wendelbewehrter Stahlbetonsäulen. CEB, Bulletin d'information, Nr. 69, 1968.

[7] Leonhardt, F.: Spannbeton für die Praxis. Berlin: Verlag von Wilhelm Ernst & Sohn 1962.

[8] Brandt, B., u. H.G. Schäfer: Verbindung von Stahlbetonfertigteilstützen. Technische Hochschule Darmstadt, Forschungsberichte der Arbeitsgruppe Massivbau, Nr. 12, 1973.

ZUSAMMENFASSUNG

Im Fertigteilbau erfordert die Ausbildung der Stützenstösse in statistischer und konstruktiver Hinsicht besondere Sorgfalt. Durch Versuche kann nachgewiesen werden, dass es ausreicht, wenn die Güte des Fugenmaterials der Güte des Stützenbetons entspricht. Im Lasteinleitungsbereich von Stützen mit Kreisquerschnitt ist eine Wendelbewehrung zur Erhöhung der Betondruckfestigkeit und zur Aufnahme der Spaltzugkräfte vorzusehen, bei Stützen mit Quadratquerschnitt eine gleichmässig verteilte, kubische Bewehrung. Für die erforderliche Bewehrung werden einfache Formeln, Bemessungsdiagramme und Vorschläge zur konstruktiven Durchbildung angegeben.

SUMMARY

Detailing of precast column reinforcement near the joints requires special accuracy. Tests have shown that it is sufficient, when the quality of the joint mortar corresponds to the concrete of the columns. In the joint region of circular columns a spiral reinforcement is needed for increasing the compression-strength and against the splitting forces; for square columns a uniformly distributed cubic reinforcement is recommended. Simple formulas, design charts and suggestions for the layout of the reinforcement are given.

RESUME

Dans la préfabrication, la conception des raccords de colonnes requiert un soin particulier du point de vue statique et constructif. Les essais montrent que la qualité du matériel de raccord correspondant à celle du béton de la colonne est suffisante. Dans la zone d'introduction des efforts, il faut prévoir pour des sections circulaires une armature en spirale qui augmente la résistance à la compression du béton et qui reprend les forces de traction fissurantes, et pour les sections carrées une armature cubique régulièrement répartie. On donne des formules simples, des diagrammes de dimensionnement et des conseils constructifs relatifs à l'armature nécessaire.